

Investigation of cement substitution by blends of calcined clays and limestone

THÈSE N° 6001 (2013)

PRÉSENTÉE LE 3 DÉCEMBRE 2013

À LA FACULTÉ DES SCIENCES ET TECHNIQUES DE L'INGÉNIEUR
LABORATOIRE DES MATÉRIAUX DE CONSTRUCTION
PROGRAMME DOCTORAL EN SCIENCE ET GÉNIE DES MATÉRIAUX

ÉCOLE POLYTECHNIQUE FÉDÉRALE DE LAUSANNE

POUR L'OBTENTION DU GRADE DE DOCTEUR ÈS SCIENCES

PAR

Mathieu ANTONI

acceptée sur proposition du jury:

Prof. A. Fontcuberta i Morral, présidente du jury
Prof. K. Scrivener, directrice de thèse
Dr P. Bowen, rapporteur
Prof. D. Herfort, rapporteur
Prof. M. Thomas, rapporteur



ÉCOLE POLYTECHNIQUE
FÉDÉRALE DE LAUSANNE

Suisse
2013

ABSTRACT

This thesis investigates the replacement of Portland cement by addition of high amounts of calcined clays and limestone. Such ternary blends can become more ecological and economical binders to answer the worldwide housing shortage.

It could be demonstrated that up to 60% of cement could be replaced by such combined addition of pure metakaolin and limestone with acceptable compressive strengths after 7 and 28 days. With natural clays, with about 50% kaolinite content, cement can still be replaced by 45% with mixtures of calcined clays and limestone without significantly impairing strength development.

The good compressive strengths obtained at 7 and 28 days have been explained by the synergetic formation of carboaluminates phases and the porosity refinement. The aluminates from the metakaolin react together with the carbonates from the limestone and calcium hydroxide, from cement hydration and could be confirmed by thermodynamic calculations. The synergetic reaction could be optimized by carefully adjusting the sulfate content and controlling the alkali content of the cement.

The durability aspects of these novel blends were studied. The STADIUM[®] multiionic transport model has been used and successfully adapted to the specificities of our materials. The ternary blends have very low ionic diffusion coefficients, more than one order of magnitude lower than Portland cement. These explain the good resistance to chloride ingress observed in ponding tests.

Carbonation resistance was also investigated. The first results tend to demonstrate that the ternary blends have somewhat lower carbonation resistance than Portland cement, due to the lower Portlandite content. However, in the short term investigated here, performance in natural carbonation condition is still good. Accelerated carbonation leads to the formation of aragonite rather than calcite in the blended system. The different densities of these polymorphs means that the porosity after carbonation will be higher in the accelerated conditions than in natural carbonation. Considering that the rate of carbonation in the long term is determined by the diffusion through the carbonated structure, this indicates that accelerated tests are likely to overestimate long term rates of carbonation.

Keywords: Ternary blends, carboaluminates synergy, calcined clays, limestone, durability, STADIUM, chloride penetration, carbonation

RÉSUMÉ

La substitution du ciment par des additions combinées d'argiles calcinées et de poudre de calcaire permet d'obtenir d'excellentes propriétés mécaniques. De tels ciments ternaires répondent tout à fait à la demande de bétons de plus en plus écologiques et économiques, notamment pour parer au besoin mondial de logements.

Avec des métakaolins, de très bon résultats mécaniques ont été obtenus pour mêmes pour des taux de substitution du ciment allant jusqu'à 60%. Il a pu aussi être démontré qu'avec des argiles naturelles contenant 50% de kaolins les propriétés mécaniques étaient maintenues pour des substitutions jusqu'à 45%. Ces découvertes permettent d'imaginer que de tels mélanges ternaires peuvent être développés et disséminés aisément car de tels gisements d'argile à bas coûts sont très répandus.

Dès 7 jours, des propriétés mécaniques similaires à des ciments Portland sont obtenues avec ces ciments ternaires. Elles peuvent être expliquées à la fois par un affinement de la porosité ainsi que par la formation d'hydrates de carbo-aluminates de calcium par réaction en synergie des aluminates provenant des métakaolins, des ions carbonates, du calcaire et de l'hydroxyde de calcium issu de la réaction du ciment. La synergie de la réaction a été confirmée par calcul thermodynamique et optimisée en ajustant précisément la quantité de sulfate et d'alcalins du ciment.

La durabilité de ces mélanges ternaires a aussi été étudiée. Le modèle STADIUM de transport multi-ionique a pu être adapté afin de répondre aux spécificités de notre ciment ternaire. Les propriétés de transport ionique ont ainsi été caractérisées, démontrant une excellente perméabilité des mélanges ternaires, inférieure d'un ordre de grandeur à celle de ciments Portland. Cela explique également la très bonne résistance à la pénétration des chlorures qui a pu être observée.

Enfin, il a été procédé à l'étude préliminaire de la résistance à la carbonatation. La carbonatation accélérée semble favoriser la formation d'aragonite au lieu de calcite. Cela provoque une augmentation de la porosité en carbonation accélérée par rapport à la carbonatation naturelle due à la différence de densité entre ces deux polymorphes.

Les premiers résultats démontrent une résistance en carbonatation des ciments ternaires Portland-argiles calcinées-poudre de calcaire légèrement moindre à celle des ciments Portland, toutefois les performances en carbonatation naturelle semblent satisfaisantes.

Mots clefs : Ciments ternaires, synergie, carboaluminates, argiles calcinées, calcaire, durabilité STADIUM, pénétration des chlorures, carbonatation

ZUSAMMENFASSUNG

In dieser Dissertation wurde der teilweise Ersatz von Zement durch eine Mischung aus kalziniertem Ton und Kalkpulver untersucht. Solch ein Dreikomponentenzement kann die Forderung nach einem immer ökologischeren und wirtschaftlicher hergestellten Beton, gerade auch im Hinblick auf den aktuellen Wohnungsmangel in Entwicklungsländer, wo Zementersatzrohstoffe nicht immer verfügbar sind, erfüllen.

Es konnte gezeigt werden, dass bei einem Ersatz von bis zu 60 Gewichts-% Zement durch eine Mischung von kalziniertes Kaolin und Kalkpulver, zulässige Druckfestigkeiten nach 7 und nach 28 Tagen erzielt werden. Wird eine Mischung aus kalziniertem Ton mit nur 50% Kaolingehalt und 15% Kalk verwendet, kann immer noch 45 % Zement ersetzt werden, ohne dass die Festigkeitsentwicklung wesentlich beeinträchtigt wird. Ein solcher Ersatz ist vielversprechend, da zahlreiche günstige Tonbestände mit vergleichbarem Kaolininhalt auf der Welt existieren.

Die sehr guten Druckeigenschaften konnten durch die synergetische Herausbildung von Karboaluminatphasen und durch die Porenverfeinerung erklärt werden. Die Aluminate des kalzinierten Tons reagieren mit den Karbonaten aus dem Kalk und dem Kalziumhydroxyd aus der Zementhydratation. Zur Validierung der Beobachtungen wurde außerdem eine thermodynamische Modellierung durchgeführt. Diese bestätigte die synergetische Reaktion und zeigte darüber hinaus, dass die Reaktion durch eine Anpassung des Sulfatgehalts und eine präzise Kontrolle des Alkaligehalts im Zement optimiert werden kann.

Des Weiteren wurde die Beständigkeit des Dreikomponentenzement analysiert. Hierzu wurde das STADIUM multiionische Transportmodell modifiziert, um die Karboaluminatphasen und die Strätlingitephasen zu berücksichtigen. Die Diffusionseigenschaften wurden bestimmt. Dabei zeigte sich, dass die Permeabilität des Dreikomponentenzement um eine Größenordnung kleiner ist als die von Portlandzement, was den sehr guten Widerstand gegen Chloreintritt erklärt, welcher auch experimentell beobachtet wurde.

Schließlich wurde der Widerstand gegen Karbonatisierung untersucht. Erste Ergebnisse zeigen, dass der Karbonatisierungswiderstand des Dreikomponentenzement geringfügig niedriger ist, als der des Portlandzement. Die beschleunigte Karbonatisierung scheint die Bildung von Aragonit an Stelle von

Kalzit zu begünstigen. Dies führt wiederum, aufgrund des Dichteunterschieds zwischen beiden Polymorphen, zu einer höheren Porosität im Vergleich zur normalen Karbonatisierung.

Stichwörter: Dreikomponentenzement, Karboaluminat Synergie, Kalzinierte Ton, Kalkpulver, Beständigkeit , STADIUM, Chloreintritt, , Karbonatisierung

RESUMEN

Esta tesis se ocupa de la fabricación de materiales de construcción basada en un cemento ternario con sustitución del cemento Portland por adición combinada de arcilla calcinada y cal. Este cemento puede ser una alternativa viable ecológicamente y económicamente para responder a la demanda creciente de viviendas, especialmente en los países en vía de desarrollo.

Fue demostrado que la sustitución de hasta 60% en peso del cemento Portland por la adición combinada de 40% de metakaolin y 20% de caliza fina permite obtener más del 90% de la resistencia mecánica a 7 días de curado y se mantiene a edades más elevadas. Similarmente, se pudo demostrar que 45% de sustitución por 30% de una arcilla calcinada con solo 50% de contenido en caolinita y 15% de cal también da resultados aceptables. Es muy prometedor teniendo en cuenta que existen numerosos yacimientos con similar contenido de caolinita e accesibles a bajo costo.

Los buenos resultados de resistencia a la compresión se pueden explicar por el refinamiento de la estructura de los poros y la formación sinérgica de carboaluminatos. Esa reacción ocurre entre los aluminatos de la caolinita, los carbonatos de la cal y el hidróxido de calcio resultante de la hidratación del cemento. La robustez de la reacción sinérgica fue también confirmada a través de la modelación termodinámica, y la optimización del sistema fue realizada a través del ajuste del contenido de sulfato y de álcali del cemento.

Las propiedades de transporte de ese cemento ternario fueron también estudiadas. El modelo de transporte multiionico "STADIUM" fue adaptado a nuestro cemento y aplicado. Demostró que la difusión iónica se redujo en un factor de orden 12 en comparación del cemento Portland. Esos resultados están en acuerdo con la resistencia al ingreso de cloruros considerablemente mejor observada con los sistemas ternarios.

Finalmente los primeros resultados del estudio preliminar de carbonatación demuestran una resistencia a la carbonatación ligeramente inferior de los sistemas ternarios en comparación a los sistemas Portland, relacionada a la ausencia de Portlandita. La carbonatación acelerada parece provocar la formación preferencial de Aragonito en vez de Calcita.

Eso provoca un aumento de los poros en carbonatación acelerada en comparación a la carbonatación natural, debido a la diferencia de densidad entre esos dos polimorfos e induce una sobrestimación de la carbonatación de los cementos mezclados en condiciones aceleradas.

Palabra clave: Cemento ternario, arcilla calcinada, caliza, sinergia, carboaluminatos, durabilidad, STADIUM, ingreso de cloruros, carbonatación

REMERCIEMENTS

Arrivé au bout de cette aventure qu'est le doctorat, il est temps de jeter un regard en arrière et d'apprécier le chemin parcouru. Cette thèse s'inscrit dans un projet qui a unit deux visions différentes mais complémentaires, avec la motivation de développer des matériaux de construction abordables et aussi respectueux de l'environnement que possible. Ces deux visions sont celles d'une part, du Prof. Karen Scrivener, qui m'a donné sa confiance, son soutien et m'a guidé tout au long de la thèse. Je l'en remercie profondément. L'autre vision est celle du Professeur Fernando Martirena, avec toujours son optimisme légendaire, son enthousiasme et ses idées innovantes pour faire avancer les choses, même en vivant à Cuba ! Merci Fernando !

Et c'est avec beaucoup de fierté que j'observe les applications réelles en cours, et les développements futurs prometteurs, notamment en Inde, de ce projet que nous avons lancé et qui n'en finit plus de grandir. Surtout lorsque je repense à mon premier séjour de 2004 à Cuba, au passage de l'ouragan Ivan, à la vie à « l' Hotelito », aux allers retours en vélo « Flying Pigeon », aux verres de lait de vaches de Dopico, à la difficulté de trouver un tracteur, du pétrole pour simplement chercher les matériaux nécessaires aux premières expériences !

Cette thèse est aussi le fruit d'un travail collaboratif soutenu avec mes collègues cubains. Tout au long de ces quatre années sont successivement venus à Lausanne ; Rances, Ruben, Adrian, Leng, Fidel, Yanisleidy. Nous avons pu travailler ensemble intensément, gracias a Ustedes ! Je remercie également sincèrement Pierre Henocq, dont le séjour au laboratoire m'aura été d'une aide précieuse pour avancer dans l'utilisation du protocole de migration et de Stadium. Je remercie aussi Ruben Snellings, qui m'a guidé plus d'une fois dans le monde de l'analyse Rietveld ainsi que pour tous ses conseils précieux. Merci aussi à Barbara Lothenbach de l'EMPA pour la thermodynamique et l'utilisation de GEMS.

Le travail d'un laboratoire dépend beaucoup de ses différents membres, je me dois de remercier mon ami Lionel, qui gère avec maestria son labo et est toujours prêt à filer un coup de main ou... boire un café ;-) Merci par la même occasion à Mr Vuillemin, à Jean et Tonio, à Carlos du LTP et Elena du groupe CEL. Tous les étudiants que j'ai supervisé pendant cette thèse dans le cadre d'un projet de bachelor (Dominik), de master (Leili) ou de diplôme (John !), de même que Betty (et Felix) pour

son aide au laboratoire sont aussi chaleureusement remerciés pour leur motivation et leur engagement.

Je remercie bien évidemment aussi tous mes collègues de boulot ou de promo, pour la bonne humeur communicative qui émane de ce labo et toutes les aides que j'ai pu recevoir : Christophe, Théo, Patrick, Shashank, Vanessa, Alex, Alain, Quang Hui, Aditya, Cédric, Hui, Cheng, Bizzo, Mo, Amélie, Elise, Berta, Hadi, Cyrille. Un merci spécial à mes collègues et amis du bureau MXG239: Olga, John et Arnaud !

Je remercie également Sandra, Anne-Sandra et Maude pour leur aide avec les tâches administratives, et dieu sait que c'est un boulot difficile lorsque ça touche à Cuba ;-)

J'aimerais aussi dire un remerciement particulier pour les membres du Jury de thèse : Prof. Anna Fontcuberta i Morral qui a présidé le jury et Dr Paul Bowen, Prof. Mike Thomas et Dr. Duncan Herfort en tant qu'experts.

D'un point de vue plus personnel, j'adresse mes remerciements à mes coéquipiers et amis du LUC Rugby, c'est toujours un plaisir immense de se retrouver sur et en dehors du terrain avec vous et c'était une soupape de décompression incroyable. Je remercie aussi mes amis JB, Rémi, Sébastien, Adrien, Jojo, Romin et Oliv, pour leur attention et leur amitié. Un immense merci à ma famille et plus particulièrement à mes parents, toujours présents, leur soutien sans faille et leur amour a fait de moi ce que je suis et cet accomplissement est certainement aussi le leur. Finalement, je remercie mon épouse, mon amour et à la fois ma meilleure amie, qui partage ma vie depuis maintenant bientôt 6 ans, Daiky : merci pour ta patience et ton amour inconditionnel au quotidien, tu m'as donné la force d'achever cette étape !

CONTENT

Abstract.....	II
Résumé	IV
Zusammenfassung	VI
Resumen	VIII
Remerciements.....	X
Content	XII
Glossary	XIX
List of Tables.....	XXII
List of Figures.....	XXIV
Chapter 1 : Introduction.....	1
1.1. <i>Context of the thesis</i>	1
1.2. <i>Objectives of the thesis</i>	3
Chapter 2 : State of the Art	6
2.1. <i>Calcined clays as supplementary cementitious materials (SCMs)</i>	6
2.1.1. The different main clay types and their activation.....	6
2.1.2. Reactivity and calcination process.....	10
2.2. <i>Basics of cement hydration</i>	13
2.2.1. Portland cement	13
2.2.2. Blended cements with SCMs	15

2.2.3.	Synergy of the carboaluminates reaction.....	16
2.3.	<i>Influence of calcined clays on durability</i>	17
2.4.	<i>Summary and open questions</i>	20
Chapter 3	: Materials and methods	21
3.1.	<i>Materials</i>	21
3.1.1.	Cements.....	21
3.1.2.	Clays.....	22
3.1.3.	Compositions studied for carbonation	24
3.1.4.	compositions studied for chloride resistance.....	26
3.2.	<i>Methods</i>	28
3.2.1.	Strength testing	28
3.2.2.	Hydration Stop.....	28
3.2.3.	Thermogravimetry analysis	29
3.2.4.	Mercury intrusion Porosimetry	29
3.2.5.	X-Ray diffraction	29
3.2.6.	Isothermal calorimetry	29
3.3.	<i>Carbonation</i>	30
3.3.1.	mortar fabrication	30
3.3.2.	Paste fabrication & sample preparation.....	30
3.3.3.	Characterization techniques.....	31
3.4.	<i>Chloride Resistance</i>	35

3.4.1.	Grinding and acidic dissolution.....	35
3.4.2.	chloride binding isotherms: experimental procedure.....	36
Chapter 4	Article: Cement substitution by blends of metakaolin and limestone.....	37
4.1.	<i>Introduction.....</i>	38
4.2.	<i>Experimental procedure.....</i>	39
4.3.	<i>Results.....</i>	42
4.3.1.	Mechanical strength.....	42
4.3.2.	Characterization of pozzolanic reaction by Thermogravimetric Analysis.....	44
4.3.3.	X-Ray Diffraction.....	47
4.3.4.	Estimation of Degree of reaction of MK by Mass balance calculations.....	48
4.3.5.	Thermodynamic modelling.....	52
4.3.6.	Porosity.....	55
4.3.7.	Gypsum adjustment.....	56
4.4.	<i>Conclusions.....</i>	60
Chapter 5	: Strength of blends with natural calcined clays.....	62
5.1.	<i>Introduction.....</i>	62
5.2.	<i>Reinvestigation of Fernandez's results.....</i>	63
5.3.	<i>Investigation of some key parameters.....</i>	66
5.3.1.	Alkali content.....	66
5.3.2.	Fineness effect.....	71
5.3.3.	Varying Limestone / Calcined clays ratio.....	73

5.3.4.	Influence of mixed clays	74
5.4.	<i>Series 3: Blends produced in Cuba</i>	76
5.4.1.	Mechanical performance.....	76
5.4.2.	Evolution of paste samples.....	79
5.5.	<i>Series 4: Blends with natural calcined clays produced in lausanne</i>	82
5.6.	<i>Effect of the calcination process</i>	85
5.6.1.	Static calcination.....	86
5.6.2.	Flash calcination	87
5.6.3.	Comparison flash and static calcination	92
5.7.	<i>Summary and outlook</i>	93
Chapter 6	: Carbonation of ternary blends of cement, calcined clays and limestone.....	95
6.1.	<i>Mechanisms of carbonation</i>	96
6.2.	<i>Accelerated carbonation test and CO₂ level</i>	101
6.3.	<i>Calcium carbonate polymorphs</i>	104
6.4.	<i>Overview of current work</i>	106
6.4.1.	Thermodynamic modelling of carbonation	106
6.5.	<i>Experimental details</i>	110
6.6.	<i>Paste results</i>	110
6.6.1.	Natural carbonation.....	110
6.6.2.	Accelerated carbonation with 3% CO ₂ on pastes	114
6.6.3.	Summary and comparison between normal and accelerated carbonation in pastes...	121

6.7.	<i>Mortar results</i>	123
6.7.1.	Mortars natural carbonation	123
6.7.2.	Accelerated carbonation 10% CO ₂ on mortars	125
6.7.3.	Carbonation and Strength	127
6.7.4.	Comparison of the studies on mortars	129
6.8.	<i>Summary and discussion</i>	130
6.9.	<i>Conclusions</i>	132
Chapter 7	: Chloride resistance and transport properties	135
7.1.	<i>State of the art</i>	135
7.1.1.	Chloride induced corrosion	135
7.1.2.	Chloride bearing phases	135
7.1.3.	Effect of SCMs	138
7.2.	<i>Outline of experimental work</i>	143
7.3.	<i>Materials</i>	144
7.4.	<i>Ponding experiments</i>	144
7.4.1.	Experimental procedures	144
7.4.2.	Results	146
7.5.	<i>Chloride binding isotherms</i>	164
7.5.1.	Experimental procedure	164
7.5.2.	Results	164
7.6.	<i>Chloride migration test: the simco rcpt modified procedure</i>	169

7.6.1.	Experimental set-up.....	169
7.6.2.	Modelling, theoretical background	170
7.6.3.	Current results	172
7.7.	<i>Modelling chloride migration: inverse tortuosity and diffusion coefficient calculation</i>	<i>177</i>
7.7.1.	results of preliminary series	177
7.7.2.	Series 2, 28d.....	180
7.7.3.	Series 2, 110d.....	184
7.8.	<i>Discussion.....</i>	<i>184</i>
7.8.1.	Phase assemblage calculations.....	184
7.8.2.	Effect of blending and curing time	186
7.8.3.	Comparison with formation factor	186
7.9.	<i>Conclusions and outlook</i>	<i>188</i>
Chapter 8	: Conclusions and outlook	191
8.1.	<i>Conclusions.....</i>	<i>191</i>
8.2.	<i>Outlook:.....</i>	<i>193</i>
Chapter 9	Bibliography	197
Chapter 10	: Annexes	206
10.1.	<i>Chloride figures.....</i>	<i>206</i>
10.2.	<i>Formation factor, Snyder.....</i>	<i>212</i>
10.3.	<i>Stadium</i>	<i>214</i>
10.3.1.	Description	214

10.3.2.	Discussion.....	215
10.3.1.	Additional figures	219
	Curriculum Vitae.....	223

GLOSSARY

Cement notation:

C= CaO

S=SiO₂

H=H₂O

A=Al₂O₃

F=Fe₂O₃

Š=SO₃

N=Na₂O

K=K₂O

M=MgO

C̄= CO₂

C̄=Cl

This leads to the following abbreviations for anhydrous and hydrates phases:

C₃S 3CaO. SiO₂ Tricalcium silicate

C₂S 2CaO. SiO₂ Dicalcium silicate

C₄AF 4CaO. Al₂O₃. Fe₂O₃ Ferrite

C₃A 3CaO. Al₂O₃ Tricalcium aluminate

CŠH₂ CaSO₄. 2 H₂O Gypsum

C̄C̄ CaCO₃ Calcium carbonate

XIX

CH	Ca(OH) ₂ Calcium hydroxide
C-S-H	CaO. SiO ₂ . H ₂ O Calcium silicate hydrate, unknown exact composition
C-A-S-H	CaO. Al ₂ O ₃ . SiO ₂ . H ₂ O Calcium silicate aluminate hydrate, unknown exact composition
C ₃ A. (C \bar{S}) ₃ .H ₃₂	3CaO. Al ₂ O ₃ . 3CaSO ₄ . 32H ₂ O Ettringite (Ettr)
AFm phases:	
C ₃ A. C \bar{S} .H ₁₂	3CaO. Al ₂ O ₃ . CaSO ₄ . 12H ₂ O Tricalcium monosulfo aluminate (MS)
C ₃ A. (C \bar{C}) _{0.5} H _{11.5}	3CaO. Al ₂ O ₃ . 0.5Ca(OH) ₂ . 0.5 CaCO ₃ . 11.5H ₂ O Hemicarboaluminate (HC)
C ₃ A.C \bar{C} H ₁₁	3CaO Al ₂ O ₃ . CaCO ₃ . 11H ₂ O Monocarboaluminate (MC)
C ₃ A.CC ₂ .H ₁₀	3CaO. Al ₂ O ₃ . CaCl ₂ . 12H ₂ O Friedel salt
C ₃ A(C \bar{S}) _{0.5} (CaC ₂) _{0.5} H ₁₁	3CaO·Al ₂ O ₃ ·1/2CaSO ₄ ·1/2CaCl ₂ ·11H ₂ O Kuzel's salt
C ₂ ASH ₈	2CaO. Al ₂ O ₃ . SiO ₂ . 8H ₂ O Strätlingite (or gehlenite hydrate)

PC: (Ordinary) Portland Cement

MK= pure metakaolin (AS₂ in cement notation)

LS= limestone

Y-Bxx= Blend with combined addition of calcined clays:limestone powder at 2:1 weight ratio, using clay Y for a total substitution of xx wt% of cement.

FC = Flash Calcined

XRD: X-Ray Diffraction

TGA: Thermogravimetric Analysis

XX

DTG: Derivative Thermogravimetry

DTA: Differential Thermal Analysis

DSC: Differential Scanning Calorimetry

SEM: Scanning Electron Microscopy

EDX analysis: Energy Dispersive X-Ray analysis (or EDS)

EDS: Energy Dispersive Spectroscopy

NMR: Nuclear Magnetic Resonance

BSE: Backscattered Electron

PSD: Particle Size Distribution

BET: Brunauer Emmet Teller (theory for specific surface measurements)

MIP Mercury Intrusion Porosimetry

LIST OF TABLES

Table 1.1: Description of the different sub-projects of the joint research programme “Production of activated clays for low cost building materials in developing countries”	3
Table 2.1: Characteristics of clay minerals of most abundance, from [8].....	8
Table 3.1: XRF Composition of all cements used in the thesis.....	21
Table 3.2: Presentation of the main characteristics of the calcined clays used during the thesis.....	23
Table 3.3: Summary of carbonation experiments carried out (“Clay30” is a blend with 30% of one of the calcined clays, see Section 3.1.3)	24
Table 3.4: Composition submitted to accelerated carbonation test with 10% CO ₂ :.....	25
Table 3.5: List of mortar compositions submitted to normal carbonation:.....	25
Table 3.6:Composition of the samples prepared to measure compressive strength with and without carbonation.	26
Table 3.7 Compositions studied in series 1a tested for chloride resistance (Chapter 7).....	26
Table 3.8: Compositions studied in series 2 tested for chloride resistance (Chapter 7).....	27
Table 3.9: Phase assemblage of the paste used for chloride binding isotherm as obtained by Rietveld refinement.....	27
Table 3.10: List of Rietveld references used.....	34
Table 4.1 : Chemical composition of the main components given by X-Ray Fluorescence, left part and crystalline composition by Rietveld of the cement, on the right.	39
Table 4.2 : Formulations of the blends “B” as well as the quartz references “Ref”	40
Table 4.3: The calculated reacted fractions of metakaolin (top) and calcium carbonate (bottom), based on the hypothesis of formation of hemicarboaluminate and C-A-S-H gel based on the Portlandite consumption measured by Thermogravimetry Analysis.....	50
Table 5.1: Summary table of all samples reported in this chapter.	63
Table 5.2: Compressive strength absolute values, for 0.55 and 0.8% Na ₂ O _{eq}	68
Table 5.3: Description of the clays used in Series 3,	77
Table 5.4: Description of the clays used in serie 4	82
Table 5.5: Metakaolin content calculated from TGA measurement, 1 st batch of Pontezuela clay, Series 5.....	88
Table 5.6: Metakaolin content calculated from TGA measurement, 2 nd batch of clay, series 6.....	92
Table 6.1: Carbonation rates obtained in accelerated carbonation using 3% CO ₂	115

Table 6.2: Summarizing table for MIP results in non-carbonated and carbonated zones.....	121
Table 6.3: Carbonation rates calculated for the different mortars samples and conditions in mm/square root(year).....	129
Table 7.1: Compositions studied in chloride chapter.....	144
Table 7.2: Summary of properties of the different mixtures, Preliminary series	179
Table 7.3: Summary of properties of the different mixtures, Series 2 at 28days	180
Table 7.4: Summary of properties of the different mixtures, Serie 2 at 110days.....	184
Table 7.5: Comparison of phase assemblage obtained by Rietveld and used as input for the best fit of current in migration test, 28 days	185
Table 7.6: Summary of D_{OH} coefficients estimated with Stadium after migration tests.....	186
Table 7.7: Summary of initial resistivity values, formation factor and D_{OH} calculated by formation factor method during migration tests:.....	187
Table 10.1: Total chloride content, normalized by weight of mortar.	206
Table 10.2: Total chloride content, normalized by weight of anhydrous cement present in the mortar.	206
Table 10.3: Values at 25°C of D_i^0 in diluted solutions.....	215

LIST OF FIGURES

Figure 2.1: (a): Silicon in tetrahedral position, (b): Silica sheet,[21]	7
Figure 2.2: (a): Aluminium in octahedral position, (b): Alumina sheet,[19].....	7
Figure 2.3: Structural pattern of clay minerals [22]	8
Figure 2.4: Structures of kaolinite (a), illite (b) and montmorillonite (c) (adapted from Grim[7])	9
Figure 2.5: Schematic representation of kaolinite dehydroxylation producing increased disorder in the alumina sheet [27]	10
Figure 2.6: ²⁷ Al NMR spectra of kaolinite, illite and montmorillonite and their respective calcined products at 600 and 800°C [8].....	11
Figure 2.7: Phase stability predicted by thermodynamic in C3A-portlandite system for for varying amount of carbonate (CO ₂ /Al ₂ O ₃) and sulfate (SO ₃ /Al ₂ O ₃) content at 25°C, from [57].....	16
Figure 2.8: Compressive strength, in MPa at 28 days in blends of 70% PC and 30% calcined clay-limestone mix reported as a function of the clay/(clay+limestone) weight ratio [58]	17
Figure 3.1: Time derivative of the mass loss as a function of the increasing temperature obtained by TGA analysis of the raw clay samples.....	22
Figure 3.2: Picture of the experimental set-up used for carbonation.....	32
Figure 4.1: Particle size distribution of the raw materials measured by Laser Granulometry.....	40
Figure 4.2: Compressive strength of blends mortars at 1, 7, 28 and 90 days.....	42
Figures 4.3 a) et b): Compressive strength of blends normalized to the strength of pure PC (a) and to the quartz reference (b) mortars at 1, 7, 28 and 90 days.	44
Figure 4.4: Evolution of the CH content (determined from TGA mass loss) normalized to the PC content in the paste.	44
Figures 4.5: Time derivative of the mass loss as a function of the increasing temperature obtained by TGA analysis of samples at 90days.....	46
Figure 4.6: XRD patterns for PC, MK30, LS15, and MK-B45 at 1, 7, 28 and 90 days.	48
Figure 4.7: Graphical treatment of EDS points analysis obtained on a B45 300d old paste, Al/Ca ratio is plotted as a function of Si/Ca ratio (in atomic percentage).....	49
Figures 4.8: Metakaolin (a) and limestone (b) reactivities calculated by mass balance.....	51
Figure 4.9 a) et b) : Thermodynamic simulations of the phase assemblage with increasing substitution of cement by our 2 :1 metakaolin :limestone blend.	53

Figure 4.10: Compressive strength at 90 days represented as a function of its corresponding porosity calculated by GEMS.	54
Figure 4.11 : Cumulated porosity as a function of pore entry radius at 28 days obtained by Mercury Intrusion Porosimetry.....	55
Figure 4.12 : Isothermal calorimetry curves of the blends pastes (water/binder ratio 0.4) until 40 hours.....	56
Figure 4.13: Evolution of the mechanical strength of Blends systems at 45% substitution as a function of the gypsum added at all ages.....	57
Figure 4.14 : Isothermal calorimetric curves plotted for Blends systems at 45% substitution with different gypsum contents	58
Figures 4.15 : Evolution of phases obtained by Rietveld refinement of in-situ XRD during the first 24h of hydration for B45 (top) and B45 + 1.5wt% gypsum (bottom).	59
Figure 5.1: Compressive strengths obtained during Rodrigo Fernandez PhD work [8]	64
Figure 5.2: XRD Diffractograms for the Cuban clay calcined at 600 and 800°C with cement from series 2. Both carboaluminates peak are present in considerable amount after 28 days curing at 30°C[8]. .	65
Figure 5.3: Plot of the relative compressive strength obtained at 1, 7 and 28 days as a function of the equivalent alkali content of cement in blends containing 30% pure metakaolin.....	66
Figure 5.4: Strengths relative to PC3 at 2 different alkali contents for various blends (series 6).....	67
Figure 5.5: Heat released normalized by mass of cement for pastes with 30% calcined clays and different alkali addition at 20°C.....	69
Figure 5.6 Cumulated heat released over 6 days normalized by weight of anhydrous cement for pastes at 20°C.....	70
Figure 5.7: Relative compressive strengths obtained for MK-B45 blends with different amounts of gypsum (from previous chapter) and sodium sulfate, pointing out the crucial role of sulfate and alkali adjustment to optimize early age strength.....	71
Figure 5.8: Heat flow monitored by isothermal calorimetry at 20°C to observe the effect of Na ₂ SO ₄ addition.	71
Figure 5.9: Relative compressive strength at 1, 7 and 28 days for different limestone sizes.....	72
Figure 5.10: Relative compressive strength to PC for varying metakaolin: limestone ratios.	73
Figure 5.11: XRD Diffractograms for B45 blends made with varying metakaolin to limestone ratio. ..	74
Figure 5.12: The relative compressive strengths in comparison with PC4 reference are plot for different mixed clays (30% cement substitution, mortars cured at 30°C).....	75

Figure 5.13: Compressive strengths obtained with B45 blends at 3, 7 and 28 days. Quartz filler and different fineness of Metakaolin have been used in order to decompose the contribution to strength development of the different fraction.	78
Figure 5.14: Compressive strength for Cuban formulations normalized to pure OPC.....	79
Figure 5.15: XRD patterns for all Cuban blends at 7 and 28 days	80
Figure 5.16: Evolution of the CH content of Cuban pastes (determined from TGA mass loss) normalized to the OPC content in the paste.....	81
Figure 5.17: Relative strength to reference PC obtained with 3 different clays: metakaolin of Burgess (MK), Argicem from Argeco (Ar) with 40% kaolinite and	83
Figures 5.18: Portlandite content obtained at 1, 7 and 28 days for the 3 different blends made in series 4 with 3 clays containing varying kaolinite content.....	85
Figure 5.19: Example description of the temperature profiles in static and flash calcination processes.	86
Figure 5.20: Graphical representation of the remaining non dehydroxylated fraction of the clay after flash calcination at the Fumel flash calcination prototype as a function of the temperature measured at the end of the main calcination tube. Dehydroxylation is linearly improved with increasing temperature.	88
Figure 5.21: X-Ray diffractograms of Pontezuela clay as a function of flash calcination conditions. At the bottom in grey is represented the raw material, increasing temperatures given towards the top.	89
Figure 5.22: Differential Scanning calorimetry of the raw and flash calcined materials in different conditions given as a function of temperature, Fumel calcination.....	90
Figure 5.23: Particle size distribution of the clays measured by laser granulometry.	90
Figure 5.24: Relative compressive strengths compared with PC1 obtained for different flash calcination conditions carried out in Fumel for the first flash calcination trial (30% cement substitution). Series 5.....	91
Figure 5.25: Relative compressive strengths obtained with the second batch of Pontezuela clay calcined in Havana, series 6.....	92
Figure 6.1: Comparison of corrosion rate and carbonation as a function of relative humidity (derived from [107, 108]) and for different concrete.....	95
Figure 6.2: Variation of pH pore solution as a function of imposed Ca/Si ratio of synthetic C-S-H gel, from Sugiyama[113].	97
Figure 6.3 Linear relationship between carbonation depth and air permeability (from Dhir [116])....	99

Figure 6.4: The ratio of the carbonation of fly ash concrete over the carbonation of Portland cement concrete is plotted as a function of exposure time. [117], [118].....	100
Figure 6.5: Carbonation depth at 10 years, for varying fly ash content and curing time[118]......	101
Figure 6.6: Diversity of the accelerated carbonation procedures depending on each country[124].	102
Figure 6.7: Effect of the CO ₂ content of the carbonation atmosphere on Si coordination analysed by ²⁹ Si MAS NMR [126].....	103
Figure 6.8: Reduction of porosity accounted for C-S-H carbonation, normalized by mole of C-S-H for Portland cement as a function of CO ₂ atmospheric level, by Thiery [127]	104
Figures 6.9. Pore size distribution by Mercury Intrusion Porosimetry as a function of CO ₂ content during carbonation for Portland cement (left) and Slag cement (50% slags) (right) [128].....	104
Figure 6.10: Plot of the volume variation of the cementitious phases as well as pH as a function of increasing CO ₂ , both normalized for 100g of initial anhydrous cement. Anhydrous phases are considered inert and neglected.....	108
Figure 6.11: Plot of the volume variation of the cementitious phases as well as pH as a function of increasing CO ₂ , both normalized for 100g of B45.....	109
Figure 6.12: Carbonation penetration depth obtained by phenolphthalein test after 8 months of natural carbonation test on paste samples.....	110
Figures 6.13 a) b) c) & d): These graphs represent the semi-quantitative variation of crystalline phases as a function of the depth from the exposed surface to carbonation, for respectively PC, MK30, B45 and B45-K50. Red lines correspond to the phenolphthalein front experimentally observed.	113
Figure 6.14: Carbonation profiles obtained by phenolphthalein test in accelerated carbonation test using 3% CO ₂ on paste samples.....	115
Figure 6.15: Carbonation depth measured by phenolphthalein as a function of PC content	116
Figure 6.16 a) b) c) & d): Semi-quantitative quantification of crystalline phases of respectively PC, MK30, B45 and B45-K50 after accelerated carbonation as a function of the depth from the exposed surface to carbonation. Red lines correspond to the phenolphthalein front experimentally observed.	118
Figure 6.17: Cumulated MIP curves obtained in non-carbonated zones (left) and carbonated zones (right) after accelerated carbonation with 3% CO ₂	120
Figure 6.18: Carbonation penetration depth as a function of square root of time obtained by phenolphthalein test after 18 and 24 months of natural carbonation test on mortar samples (left) and picture of the carbonation depth by phenolphthalein spray after 24 months (right).	124

Figure 6.19: Carbonation depths represented as a function of PC content of the blend for natural carbonation.	125
Figure 6.20: Carbonation depths obtained by phenolphthalein test after 6 weeks of accelerated carbonation test with 10% CO ₂	126
Figure 6.21: Carbonation depths represented as a function of PC content. The linear variation, independently from the composition of the rest of the cementitious binder is observable, at any age.	127
Figure 6.22: Carbonation depths represented as a function of initial metakaolin content of the blend, approximating carbonatable content equal to the PC content.	127
Figure 6.23: Compressive strengths obtained for full carbonation and without any carbonation for the serie of accelerated carbonation carried out with 10% CO ₂ . Samples fully carbonated had systematically higher strength after carbonation; however the strength gain upon carbonation is decreasing with increasing blending.	128
Figure 6.24: Carbonated depth as a function of carbonatable content plotted all together.	129
Figure 7.1: Example of best-fit possible with Freundlich & Langmuir isotherms for a cement paste at water/cement ratio 0.5. Freundlich isotherm gives the best fit (from[164]).	138
Figure 7.2: Maximum Friedel peak intensity by XRD plot as a function of the bound chloride measured by chloride binding isotherm [164].	139
Figure 7.3: Bound chloride (for 3M NaCl) obtained by chloride binding isotherm measurement plot as a function of the alumina content of the binder, water/binder ratio 0.5, Temperature 23°C [164]. ..	139
Figure 7.4: Bound chloride plotted as function of free chloride concentration for 3 different ratios MK/Lime ratios [165].	140
Figure 7.5: XRD Diffractograms obtained for MK12 sample after chloride binding experiment for various NaCl concentrations [165].	141
Figure 7.6: Chloride binding values atpH13.5 by chloride binding isotherm as a function of Al ₂ O ₃ binder content. Empty and filled symbols stands for systems with and without limestone, respectively.....	142
Figure 7.7: Examples of reproducibility trials of chloride quantification for ponding experiments with composition B45 (top) and MK30 (bottom). The biggest standard deviation +/-0.06 wt% was found in the layer exposed to the solution that is more subject to local heterogeneity.....	145
Figure 7.8: Total chloride content measured by acidic dissolution for 30% of cement substitution by calcined clays with varying kaolinite content.....	147

Figure 7.9: Total chloride content measured by acidic dissolution for 45% of cement substitution blends by combined addition of 30% calcined clays with varying kaolinite content and 15% limestone.	148
Figure 7.10: Total chloride contents as a function of the depth from the outer layer exposed to the ponding solution. On the left all the samples containing pure metakaolin are given while samples with the Pontezuela calcined clay are given on the right.	149
Figure 7.11: Representation of the total chloride content as a function of Al_2O_3 content in the outer layer in contact with the ponding solution.	150
Figure 7.12: X-Ray Diffractograms obtained after 2 years Ponding for OPC. The number corresponds to the layer number, starting from surface in contact with ponding solution.	150
Figure 7.13: Hydrates phase assemblage evolution observed by semi-quantitative Rietveld analysis for PC1 after 2 years ponding.	151
Figure 7.14: X-Ray Diffractograms obtained after 2 years Ponding for MK30.....	152
Figure 7.15: Hydrates phase assemblage evolution observed by semi-quantitative Rietveld analysis for MK30 after 2 years ponding.	153
Figure 7.16: X-Ray Diffractograms obtained after 2 years Ponding for MKB45.....	154
Figure 7.17: Hydrates phase assemblage evolution observed by semi-quantitative Rietveld analysis for MKB45 after 2 years ponding.	154
Figure 7.18: Hydrates phase assemblage evolution observed by semi-quantitative Rietveld analysis for MKB15, MKB22 and MKB30 after 2 years ponding.....	156
Figure 7.19: Cl/Ca atomic ration as a function of Si/Ca atomic ration for PC, MK30 and MKB45 within the first 2.5 mm thickness, corresponding to layer 1.....	158
Figure 7.20: Cl/Ca atomic ration as a function of depth for MK30. Layer 1 has been take in the first 2.5 mm, layer 4 around 9.25mm and 5 at 11.25mm.	159
Figure 7.21: Al/Ca atomic ration as a function of depth for MK30. Layer 1 has been take in the first 2.5 mm, layer 4 around 8.75mm and 5 at 11.25mm.	160
Figure 7.22: Cl/Ca atomic ration as a function of depth for MK30. Layer 1 has been take in the first 2.5 mm, layer 2 around 3.75mm and 4 at 8.75mm.	161
Figure 7.23: Al/Ca atomic ratio as a function of depth for MKB45. Layer 1 has been take around 1.25 mm deep, layer 2 around 3.75mm and 4 at 8.75mm.	162
Figure 7.24: Chloride binding isotherm with Freundlich isotherm best fit for PC2, MK30, MKB15 and MKB45. The total chloride content normalized by dried weight of binder is given as a function of free chloride concentration.	165

Figure 7.25: Semi quantitative phase assemblage obtained for PC2 (a), MKB15 (b), MK30 (c) and MKB45 (d) respectively after 13 weeks of chloride binding experiment with 0.1; 0.3; 0.5; 0.7 and 1 M NaCl solution.	168
Figure 7.26. Schematic representation of the migration test (Stadium [®])	170
Figure 7.27. Current evolution during migration test for the three different samples	173
Figure 7.28: Chloride downstream concentrations monitored during the migration test and quantified by chromatography	174
Figure 7.29. Chloride profiles of the PC, MK30, and PontB45 after applying 10V during 14 days	174
Figure 7.30: Current evolution for all samples during the migration test carried out for samples cured 28d. These current values have been obtained for an applied voltage of 30V for MK30, MKB45 and MKB15, 10V for PC and 20V for PontB15 and PontB45.	177
Figure 7.31. Simulations of the current evolution during the migration test for PC and MK30.....	178
Figure 7.32. Simulations of the current evolution during the migration test for OPC and B45.....	178
Figures 7.33: Current values in mA obtained by migration test and given as a function of time in hours. Best fit obtained with the corresponding D_{OH^-} value calculated for each composition are also given for each composition studied in this serie.....	183
Figure 7.34: Comparison of Diffusion Coefficient obtained with Stadium and Formation factor calculations at 28 and 110 days.	187
Figures 10.1: X-Ray Diffractograms obtained after 2 years Ponding for MKB15, MKB22 and MKB30208	
Figures 10.2: X-Ray Diffractograms obtained after 2 years Ponding for Pont15 & Pont30	208
Figure 10.3: X-Ray Diffractograms obtained after 2 years Ponding for PontB45.....	209
Figures 10.4: X-Ray Diffractograms obtained after 2 years ponding for PontB15, PontB22 and PontB30	211
Figure 10.5: X-Ray Diffractograms obtained after 2 years Ponding for Ar30.....	211
Figure 10.6: X-Ray Diffractograms obtained after 2 years Ponding for ArB45.....	212
Figure 10.7: Chloride downstream concentration measured values and obtained for the model for the PC sample, 28 days old during migration test.....	216
Figure 10.8: Effect of alkalinity and hydroxyls concentration on initial current slope during migration test.....	218
Figure 10.9: Effect of porosity on initial level of current during migration test	218
Figure 10.10: Effect of different AFm content on current evolution during migration test	219
Figure 10.11: Current evolution monitored for series 2 and 110d curing during migration test	220
Figure 10.12: Current values with best model obtained by Stadium, migration tests at 110d	222

Chapter 1 : INTRODUCTION

1.1. CONTEXT OF THE THESIS

Shortage of building materials is a critical issue in developing countries. Worldwide about 1 billion people live in urban slums [1]. Housing shortage worldwide was estimated in 2010 above 428 million units. In Cuba for example, the housing shortage is estimated above 800 000 houses and the figures are similar in almost every developing country [2]. Concrete is well suited to meet these huge demands, although cement, the central ingredient is often disproportionately expensive in developing countries.

The environmental impact of concrete can be attributed to the enormous amount of cement produced each year, about $1.7 \cdot 10^9$ tonne. Production of 1 ton of concrete requires indeed about 0.08 to 0.32 tonnes CO_2 depending on cement type, strength and durability class [3, 4]. The major part of the CO_2 embodied in concrete originates from the cement. This explains that the cement industry is responsible for about 5-8% of the global man-made CO_2 emissions. On average 0.8-0.9 tonne CO_2 is emitted for the production of 1 tonne of cement [5]. 40-50% of the CO_2 emissions, originate from the heating of the cement kiln up to around 1450°C and from grinding and transportation to a lesser extent. The other 50-60% of the total amount of CO_2 originates from the decarbonation (calcination) of calcium carbonate decomposing to calcium oxide (see equation 1-1), thereby liberating CO_2 . The raw meal used to produce cement clinker consist of about 75-79% of calcium carbonate, which is added in the form of limestone and/or marl [6].



A promising option for lowering costs and environmental impact of concrete is to use blended cements which reduce the clinker content in the cement by replacing it with supplementary cementitious materials (SCMs).

Common SCMs such as fly ashes or slags are not available everywhere, especially in the developing world. The calcination of clay deposits, spread throughout the earth crust, therefore have interesting potential as SCMs .

From 2004 a collaboration has been established between Universidad Las Villas of Santa Clara, Cuba and the Laboratory of Materials of Construction (LMC) in EPFL, Lausanne Switzerland to develop the use of SCM in order to produce low cost materials with low embodied CO₂.

Prof. Martirena developed in Cuba a wide expertise in the development of eco-materials for construction. He collaborates with his team of CIDEM, namely the Centre for Research & Development of Structures and Materials and EcoSur, an international NGO network mostly based in South America.

This first phase, carried out by Rodrigo Fernandez at LMC [8], together with Adrian Alujas, Rances Castillo and Juan Dopico in Santa Clara intended to produce pozzolan from Solid Fuel Blocks, where clayey materials were intimately mixed with biomass and fired. Although promising, Solid Fuel Blocks technology had to be abandoned. The temperature control during firing was too difficult. It resulted in low reactivity of the residual ashes. In addition, the calcination of the organic materials was incomplete and this non-burnt material was detrimental to the development of proper construction materials.

The project was therefore reoriented in the direction of the more central study of the different clays as supplementary cementitious materials (SCM's). The main outcomes of this first phase can be summarized as following:

- Optimal calcination temperature of the each main clay group (kaolinite, montmorillonite and illite) were identified
- When substituting 30% of cement by properly calcined clay, mortars made with calcined kaolinite demonstrates the best results and give higher strength than Portland Cement (PC) reference. Montmorillonite also shows interesting reactivity and strength contribution, Illite is the least reactive clay.
- A natural clay from Cuba with 40% kaolinite was investigated and also demonstrated good results, with compressive strengths at 28 days similar to the PC reference.

Based on these results a second phase of the project was started, with the aim of further

investigating and optimizing blends of cement and calcined clays. The flash calcination process was also identified as another promising route to clay production. This is the calcination of powdered (ground) material by introduction in a tube where flux of hot gases circulates at controlled temperature. It has been claimed to give similar or better strength to calcined clays [9, 10] with processing time limited to some seconds compared to hours for static calcination. It can also have advantages in term of energy intensity.

1.2. OBJECTIVES OF THE THESIS

The thesis is part of a the second phase of the joint research programme “Production of activated clays for low cost building materials in developing countries” with the CIDEM, from University of Santa Clara in Cuba and also the CETER (Centre for Studies for Technologies for Renewable Energy) from the University of La Habana, Cuba. It was again funded by the Swiss National Science Foundation (SNSF) with the intention of promoting research in cooperation with developing countries. It started in September 2009. The project is divided into 4 different projects listed here in Table 1-1:

Table 1.1: Description of the different sub-projects of the joint research programme “Production of activated clays for low cost building materials in developing countries”

	Name	Location	Position	Candidate Background	Project description
Sub-project 1	Leng M. Vizcaino	UCLV, Santa Clara, Cuba	PhD student	Civil Engineering	Development of low carbon cement in Cuba with blends of calcined clays and limestone
Sub-project 2	Yanisleidy Oquendo	UCLV, Santa Clara, Cuba	PhD student	Inorganic chemistry	Chemical characterization of flash calcined clay
Sub-project 3	Mathieu Antoni	EPFL, Lausanne, Switzerland	PhD student	Materials science	Investigation of cement substitution by blends of calcined clays and limestone
Sub-project 4	Andy Rodriguez	CETER, Havana, Cuba	PhD student	Mechanics	Energetic optimization of the Clay Activation Unit

During the first year, the construction of a flash calcination prototype was carried out. The expertise on the calcination was brought by CETER and the support was given in Lausanne for the connections with experts and producers in Europe. A visit to Prof. Salvador was made and a contact was established with the company Argeco Développement [11] that has built an industrial flash calcination unit based on the development work of Salvador.

With the budget allocated for the building of the Clay Activation Unit (CAU), it was decided to design a CAU with a modest capacity of producing 100 grams per hour in order to assess the optimal calcining parameters. All parts were sourced and purchased in France or Switzerland, and were shipped to Havana. The CAU has been assembled during the second semester 2010 and operation started in January 2011.

Considering the long time required to design, ship and reassemble the CAU in Havana, it was decided to look at other aspects of calcined clay reactivity. The study of the literature (chapter 2) proved there was some encouraging studies on the effect of limestone addition to Portland cement and their interactions with aluminates phases [12, 13]. It was decided to investigate the combined addition of calcined clays and limestone.

With the first very promising results obtained early 2010, the objectives of the thesis progressively shifted from the initial focus on the flash calcination to prioritize the combined addition of calcined clays and limestone. It has been identified that this blended cement with calcined clays and limestone could compete with cements for general purpose and the thesis objectives have been reoriented with this aim in mind.

- The first objective was to fully characterize the strength development, the hydration products and the microstructure of the blends and compare them with the thermodynamic predictions. This work has been already published and is reproduced as chapter 4 of this thesis.

- The second objective was to confirm these results with different natural clays and the clays obtained by flash calcination. The different parameters that affect the reactivity of natural clays and the robustness of the ternary blends were assessed and optimizations were performed. This is given in chapter 5.
- The next objectives considering the high replacement rate were to assess their durability. For general purpose cements, the most important durability issue is corrosion of reinforced concrete structure. Therefore the two associated and most critical aspects were selected. Firstly the carbonation resistance, because carbonation can decrease pH, depassivates rebars and induces corrosion. It is the subject of chapter 6.
- The other selected topic was the chloride resistance, studied in chapter 7. Chloride can induce corrosion; it is the main threat for reinforced concrete structures. Chloride ions can be present in high concentration in industrial or urban zones, in soils and above all in marine and coastal area. In countries where winter conditions are harsh intensive use of de-icing salts is also made.
- The final chapter (8) gives the conclusions and suggestions for further work

The overall outline of the thesis is finally summarized here:

- Chapter 1: Introduction
- Chapter 2: State of the art
- Chapter 3: Materials and methods
- Chapter 4: Article: Cement substitution by combined addition of metakaolin and limestone
- Chapter 5: Factors affecting the strength when using calcined clays
- Chapter 6: Carbonation of ternary blends cement-calcined clays-limestone
- Chapter 7: Chloride resistance of ternary blends cement-calcined clays-limestone
- Chapter 8: Conclusion and outlook
- Chapter 9: Bibliography
- Chapter 10: Annexes

Chapter 2 : STATE OF THE ART

2.1. CALCINED CLAYS AS SUPPLEMENTARY CEMENTITIOUS MATERIALS (SCMs)

The use of calcined clays to substitute cement has already a large history. In the early 1950's Mielenz et al [14, 15] investigated the calcination of pozzolan and their possible use for concrete application in the US.

Metakaolin's first report of use as supplementary cementitious material (SCM) for the construction came in the 1960's in Brazil in Jupia dam, in replacement of 30% of cement by volume [16]. In India, Ramachadran also mentions at the same period the use of finely ground calcined clays, from Shivalik Hills, locally named *surkhi*, for the construction of Bhakra Dam in India [17]. Industrial use of calcined clay for cement replacement has already been established but overall remains marginal compared to other SCMs such as fly ashes or slags.

Clays are unique among the supplementary cementitious materials because of their worldwide availability; they are distributed throughout the world in the earth crust. As an example, US kaolin total resources are estimated over 1 billion tons, and up to 5 billion tons when considering discoloured and sandy clay reserves [18].

2.1.1. THE DIFFERENT MAIN CLAY TYPES AND THEIR ACTIVATION

Clay minerals originate from the weathering of silicate minerals in rocks (feldspar, micas, etc...). They are classified as phyllosilicates that usually occur in particle sizes of $2\mu\text{m}$ or less. But such a size classification is too imprecise. Some clays are also of larger particle size and non-clay minerals may occur in particles considerably less than 2mm in diameter.

Crystal structure and chemical composition are what really differentiates clays from non-clay minerals as they define their characteristic physical properties such as plasticity [19, 20].

Clay particles are made up of several tens or even hundreds of layers, whose structure is a combination of silica and alumina sheets. As can be seen in Figure 2.1, a silica sheet is composed of silicon atoms in tetrahedral coordination, where three of the four oxygens in each tetrahedron are shared to form a hexagonal net. Alumina sheets, as represented in Figure 2.2, are composed of aluminium atoms in octahedral coordination with oxygens or hydroxyls.

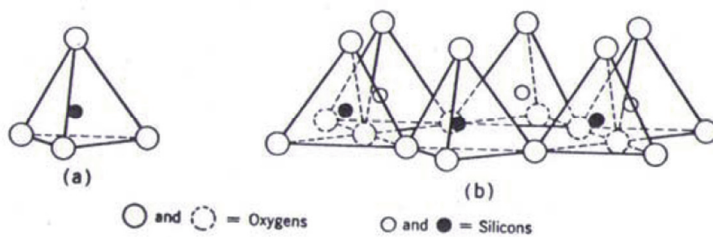


Figure 2.1: (a): Silicon in tetrahedral position, (b): Silica sheet,[21]

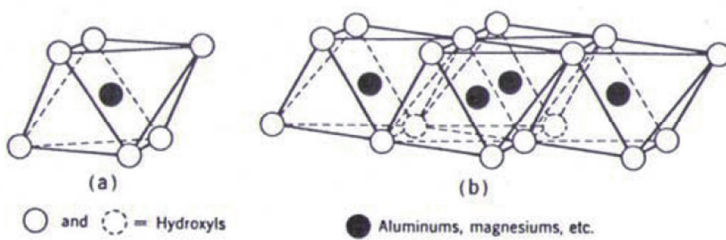


Figure 2.2: (a): Aluminium in octahedral position, (b): Alumina sheet,[19]

The aluminosilicate minerals represent 74% of the earth's crust and they represent therefore a very interesting candidate for construction materials since they are available almost everywhere.

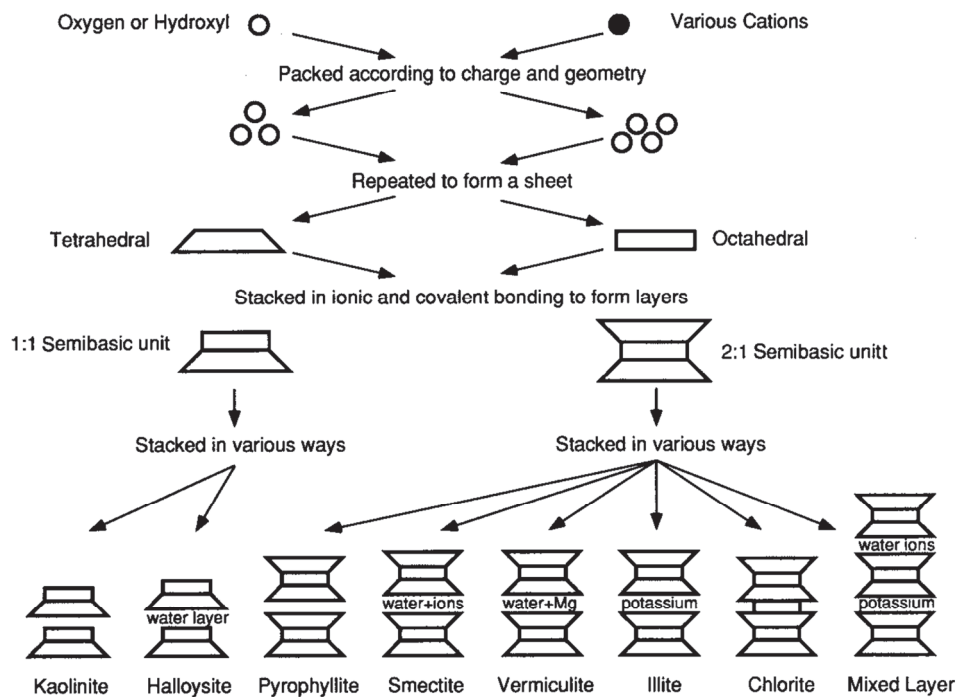


Figure 2.3: Structural pattern of clay minerals [22]

Different clay mineral groups are characterized by the stacking arrangements of sheets and the manner in which successive two-or three-sheet layers are held together[22]. The three clay types of major abundance are kaolinite, illite and montmorillonite (smectite). The structure of these clays is shown in Figure 2.4 and their average description is presented in Table 2.1.

Table 2.1: Characteristics of clay minerals of most abundance, from [8]

Name	Group	Crystal system	Ideal Formula ²	Isomorphous substitution	Interlayer Bond	Basal spacing
Kaolinite	1:1	Triclinic	$Al_2Si_2O_5(OH)_4$	Very little	O-OH, strong	7.2 Å
Illite	2:1	Monoclinic	$(Si_4)(Al,Mg,Fe)_{2,3}O_{10}(OH)_2 \cdot (K,H_2O)$	Some Si by Al, balanced by K between layers	K ions, strong	10 Å
Montmorillonite	2:1	Monoclinic	$Na_{0.33}(Al_{1.67}Mg_{0.33})Si_4O_{10}(OH)_2 \cdot n(H_2O)$	Mg for Al	O-O, very weak, expanding lattice	> 9.6 Å

Kaolinite belongs to the 1:1 layer group, while montmorillonite and illite belong to the 2:1 layer group. Note that more than one type of clay mineral is usually found in most soils. In addition, isomorphous substitutions are very common in this type of sheet. Various cations (Mg^{2+} , Fe^{2+} , Fe^{3+} , Mn^{2+}) can substitute for Al^{3+} . Also, interstratification of two or more layer types can occur within a single particle, so that clay complexity is very large. The diversity of the clay structures is represented in the Figure 2.3.

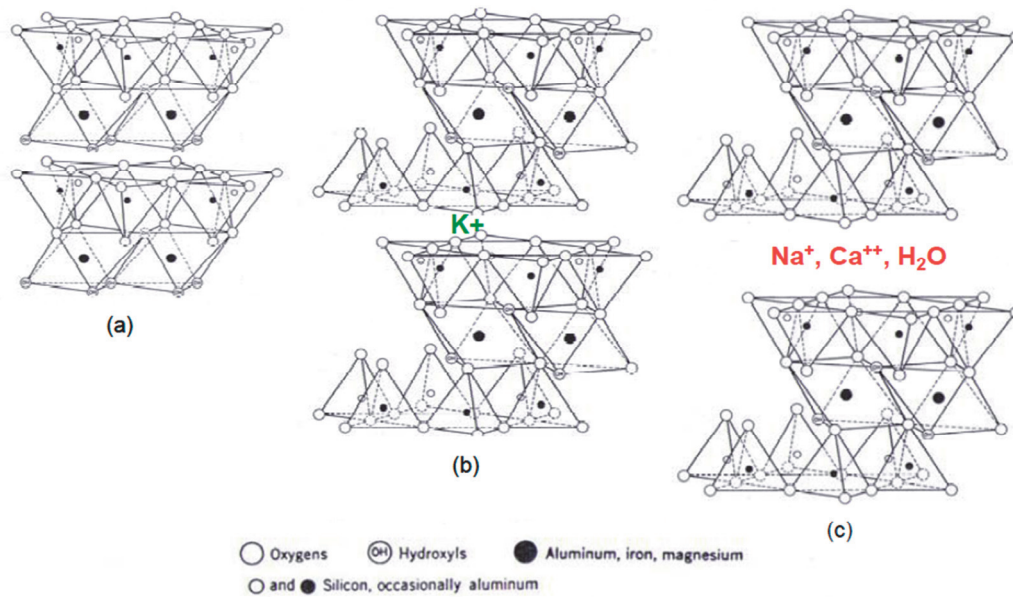


Figure 2.4: Structures of kaolinite (a), illite (b) and montmorillonite (c) (adapted from Grim[7])

Mineral particles of the kaolinite subgroup consist of the basic unit stacked in the c direction (see Figure 2.4). The bonding between successive layers is both by Van der Waals forces and hydrogen bonds. The bonding is sufficiently strong that there is no interlayer swelling in the presence of water. The basal spacing in the c direction $d(001)$ is 7.2 Å. Well-crystallised particles of kaolinite generally occur in the form of hexagonal plates (lateral dimensions in the range 0.1 to 4 µm; thickness from 0.05 to 2 µm).

A recent study using density functional modelling from White and co-workers [23] proposed a refined kaolinite structure in accordance with vibrational spectra obtained by inelastic neutron scattering. The structure could be related with decent approximation to an experiment structure resolved by Rietveld refinement by Bish [24]. But kaolinite natural origin makes it a complex material

with a structure that can significantly vary depending on isomorphic substitution and structural defects [25].

2.1.2. REACTIVITY AND CALCINATION PROCESS

2.1.2.1. THERMAL ACTIVATION

Clays can be thermally activated by heating to a given temperature in order to remove structural water [26], this phenomenon is called the dehydroxylation. In the case of kaolinite, the removal of these hydroxyl groups leads the clay to a state of more structural disorder that is a metastable state; called metakaolin, see Figure 2.5:

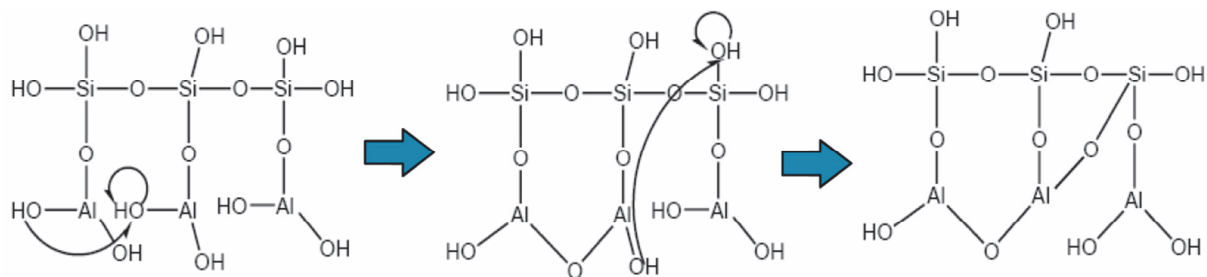


Figure 2.5: Schematic representation of kaolinite dehydroxylation producing increased disorder in the alumina sheet [27]

MAS NMR (Magic Angle Spinning Nuclear magnetic resonance) is an interesting technique to determine the chemical environment of the aluminium or silicon atoms and quantify the different atomic coordination. ^{27}Al NMR spectra of kaolinite, illite and montmorillonite and their respective calcined products at 600 and 800°C are shown in Figure 2.6 [8].

The raw kaolinite shows only $\text{Al}^{[VI]}$, for Al exist only in octahedral position while montmorillonite and illite show both $\text{Al}^{[IV]}$ & $\text{Al}^{[VI]}$, because Al exist in these clay both in octahedral position and substituting Si in tetrahedral positions.

Various authors have already investigated the evolution of kaolinite upon heating by ^{27}Al NMR: Sanz & coworkers [28], Rocha & Klinowski [34], more recently Fernandez [29] all coincide that 4-coordinated aluminium ($\text{Al}^{[IV]}$) and $\text{Al}^{[V]}$ appears at the expense of $\text{Al}^{[VI]}$ when the dehydroxylation takes place.

Montmorillonite shows a similar behaviour upon heating but Al^[IV] largely dominates after dehydroxylation. No clear sign of Al^[IV] could be detected in montmorillonite, although broadening of the Al^[IV] peaks to the right at 800°C could suggest the presence of this type of coordination. Illite is similar to montmorillonite. A gradual shift from Al^[VI] to Al^[IV] with increasing temperature is also observed. It is a clear sign of dehydroxylation as OH groups in a clayey structure are originally bound to aluminium.

Note also that montmorillonite or illite are swelling clays, but they lose their swelling properties after dehydroxylation, making them also potentially suitable for use in concrete.

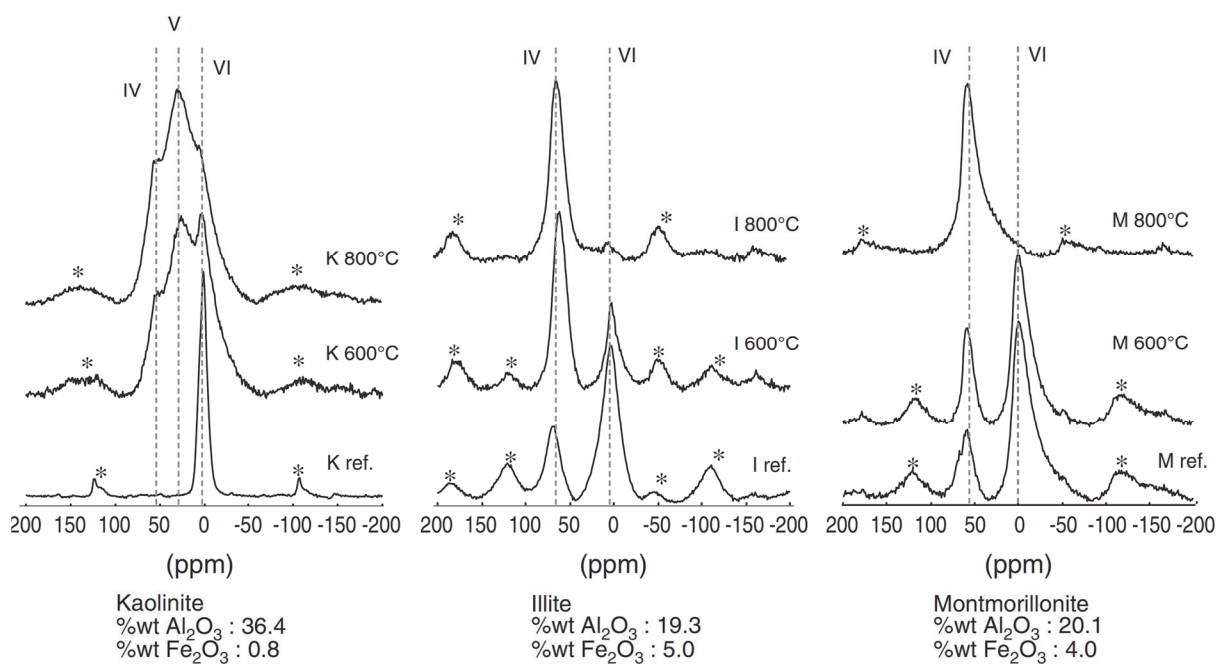


Figure 2.6: ²⁷Al NMR spectra of kaolinite, illite and montmorillonite and their respective calcined products at 600 and 800°C [8]

More recently, White and co-workers [30, 31] presented studies solving metakaolin structure combining density functional theory and pair distribution function analysis. According to their results, metakaolin structure still retains the 1: 1 layering inherent of the original kaolinite, but the alumina layers are locally buckled. Their results are in good accordance with the previous ²⁷Al NMR results, but in addition to 4, 5 and 6 coordinated Al they could also show the presence of a small percentage of three-coordinated aluminium.

2.1.2.2. REACTIVITY OF CLAYS

He and co-workers [32-37] evaluated the optimum activation temperature of different standard clayey materials and assessed the reactivity of the calcined clays when mixed with lime or cement. They concluded that kaolin had the highest pozzolanic activity, followed by Ca-montmorillonite. The rest of the materials could be considered of low or average pozzolanic activity even when calcined at their optimum activation temperature. These results are in accordance with earlier work of Mielenz [15].

It is also confirmed in the review done by Sabir [38] demonstrating that kaolin has the highest potential for pozzolanic activity among the studied clays. The work of Sabir, together with the other review of Siddique [39] or Fernandez [8] reported considerable number of publications. They all define varying optimal activation temperature being in the 650 – 800 °C range, depending on its purity and companion minerals, characterization method, etc...

The degree of dehydroxylation α , defined as the remaining kaolinite fraction divided by the initial kaolinite fraction, measured by Thermo Gravimetry Analysis (TGA) or Different Thermal Analysis (DTA) remains the best indicator of optimal calcination. Bich [40] studied reactivity of metakaolin-lime paste for three different kaolinite calcined in 9 different conditions. She reported that best reactivity was obtained for degree of dehydroxylation superior to 95%, also dispersion of results was high and results were influenced by crystallinity of the clay.

Fernandez and co-workers in their recent publication [8] have studied by various techniques the behaviour in pastes and in mortars of blends containing 30% of calcined clays. They confirmed that blends with metakaolin gave the best results. By relating MAS-NMR, TGA and X-Ray Diffraction (XRD) investigation of the calcined clays to the strength obtained as well as the portlandite consumption by TGA they related the higher reactivity of metakaolin to the high content of aluminium in kaolinite and the formation of highly reactive Al^{IV} after calcination.

When looking at the use of natural calcined clays, numerous other studies related the performance of calcined clays in term of reactivity or contribution to strength development to their kaolinite content [41-43], but studies with kaolinitic clays containing modest or low content of kaolinite are rare [44, 45].

Fernandez [8] reported excellent strength development for mortars with 30% substitution of cement by a clay with 40% kaolinite, reaching similar strength to the Portland reference without substitution at 7 and 28 days.

The effect of flash calcination on pozzolanic reactivity was investigated by Salvador [46], who showed that reactivity can be slightly increased by reducing the residence time from hours (soak-calcination) to a few seconds in a pilot flash calcining plant. Flash-calcined products revealed structural properties different from soak-calcined products. Flash calcination is reviewed more in detail in Chapter 5, section 5.6. Cadoret and co-workers [47] have published in 2004 a patent claiming better pozzolanic reactivity for kaolin activated by flash calcination associated with high temperature grinding. But no data, further work or application were later reported to support this finding.

2.2. BASICS OF CEMENT HYDRATION

2.2.1. PORTLAND CEMENT

Portland cement (PC) is produced by calcining finely ground raw meal consisting of mainly limestone, and to a lesser degree marl, clay or even shale, at about 1450°C in a rotary kiln. The material obtained after calcination is called clinker. The clinker is cooled rapidly, blended with gypsum and subsequently ground to a fine powder.

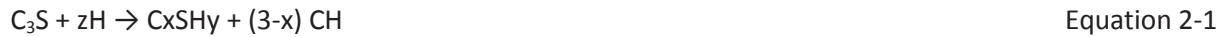
Average oxide composition of Portland clinker is CaO (60-70%), SiO₂ (18-22%), Al₂O₃ (4-6%) and Fe₂O₃ (2-4%). These oxides are the main constituents of clinker (about 95%). The remaining 5% includes MgO, K₂O, Na₂O, SO₃, TiO₂, and Mn₂O₃.

This average Portland clinker composition corresponds in term of the different mineralogical phases of the clinker to [48]:

• Alite	3CaO-SiO ₂	(C ₃ S)	55-65%
• Belite	2CaO-SiO ₂	(C ₂ S)	15-25%
• Aluminate	3CaO-Al ₂ O ₃	(C ₃ A)	8-14%

- Ferrite or brownmillerite $4\text{CaO} \cdot \text{Al}_2\text{O}_3 \cdot \text{Fe}_2\text{O}_3$ (C4AF) 8-12%

Alite and belite react with water to form C-S-H gel and CH according to respectively equation 2-1 & equation 2-2:



and $z = y+3-x$ for alite and $z = y+2-x$ for belite; z typically falls in the range 3-4.

Alite is the first of the silicate phase to react during the first days of hydration and accounts for the majority of the strength development during the first 7 to 28 days. Belite reacts slower and mostly contributes to the strength development after 28 days.

The aluminate phase reacts with water and gypsum to form ettringite (Ettr.) (Equation 2-3). Within the first day the gypsum gets depleted and the ettringite starts to react with the remaining aluminate to form calcium monosulfoaluminate (also referred to as monosulfate, MS) as described by Equation 2-4.



The hydration of the ferrite phase is comparable with the hydration of the aluminate phases. The Al in ettringite and monosulfate can be partly replaced by Fe. The phases derived from pure monosulfate and pure ettringite with partial substitution of Al by Fe, and SO_4^{2-} by other ions are referred to, respectively as the AFm and AFt phases (for alumina-ferric oxide, monosulfate & alumina-ferric oxide trisulfate respectively).

The clinker contains alkalis, easy soluble or incorporated in the clinker phases. This together with the formation of CH results in a high pH pore solution in the hydrated paste.

2.2.2. BLENDED CEMENTS WITH SCMS

In conventional cement pore solution, metakaolin is attacked by the hydroxyl ions and dissolves according to Equation 2-5. The dissolution is favoured by a high alkalinity.



In the pore solution they can react with Ca^{2+} and OH^- ions and precipitate as C-S-H and strätlingite (C_2ASH_8). Equation 2-6 corresponding to the latter reaction is often presented in the literature as follow:



In reality as aluminium concentration in solution increases aluminium incorporation into C-A-S-H also increases [49] and the equation should be equilibrated accordingly.

Strätlingite will eventually precipitate only after aluminium incorporation capacity of C-A-S-H is exceeded. Other calcium aluminate phases such as C_3AH_6 or C_4AH_{13} can theoretically also precipitate [50] and are indeed reported for MK-lime pastes [51-54]. However in modern cements, the sulfate and/or carbonate content are usually high enough to precipitate ettringite, monosulfoaluminate and carboaluminates (see Figure 2.7) and these calcium aluminate phases don't precipitate.

When replacing cement, metakaolin will also have two opposite influences on the early hydration of cement. Because it hardly reacts during the first day of hydration, it provokes a dilution effect, as any SCM does. It impacts negatively the strength development, especially during the first 24 hours. The effect is more pronounced with increasing substitution rate. On the other hand, due to its fineness it accelerates the hydration of the cementitious phases by providing considerable extra surfaces for heterogeneous nucleation. [48]

2.2.3. SYNERGY OF THE CARBOALUMINATES REACTION

With the improvement of the thermodynamic database, Matschei and co-workers have established that limestone additions up to around 5% can react with cement [12, 55, 56]. Calcium monocarboaluminate and hemicarboaluminate are formed instead of monosulphoaluminate, which in turn releases sulfate to form ettringite. Figure 2.7 presents the thermodynamic phase stability prediction depending on sulfate and carbonate addition for systems of C₃A and portlandite.

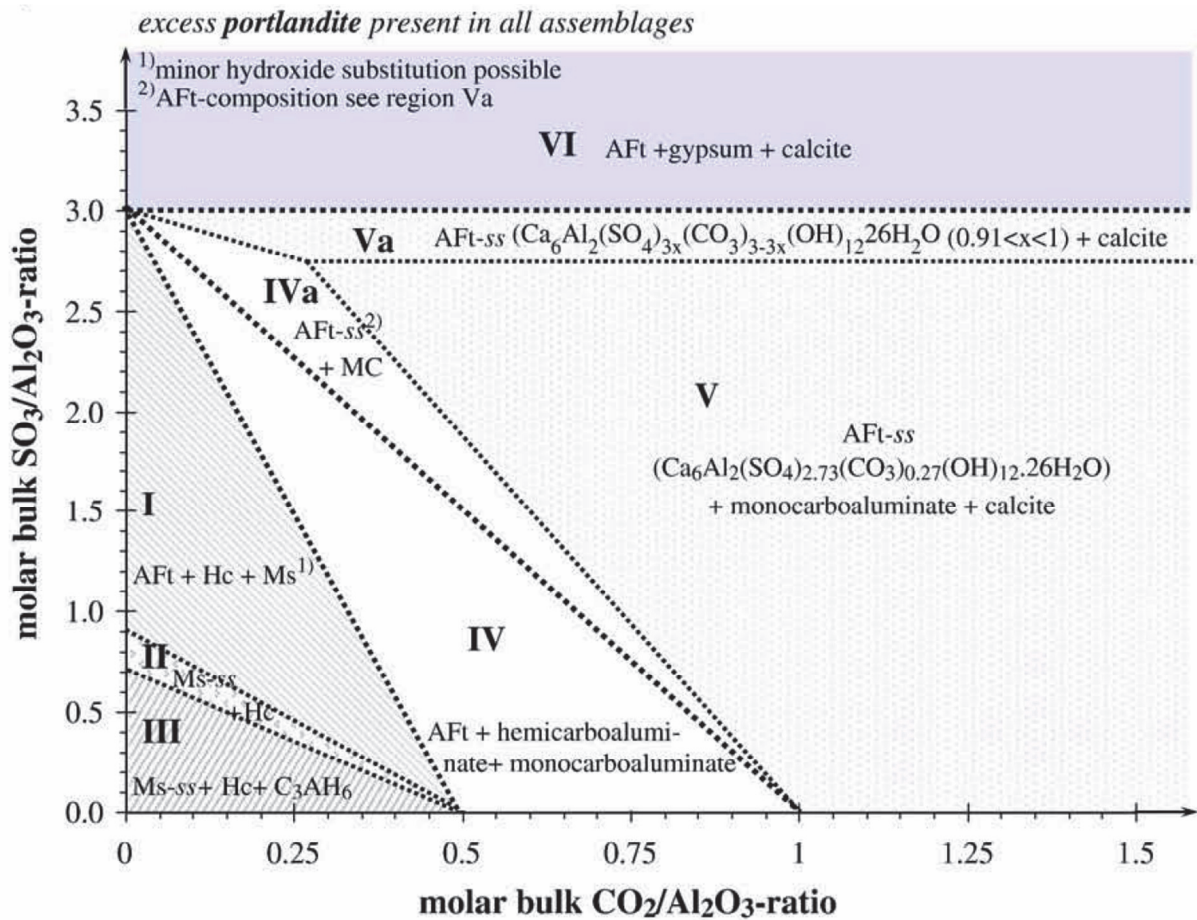


Figure 2.7: Phase stability predicted by thermodynamic in C₃A-portlandite system for for varying amount of carbonate (CO₂/Al₂O₃) and sulfate (SO₃/Al₂O₃) content at 25°C, from [57].

Damidot and co-workers [58] have also reported in 2011, using thermodynamic calculations, the possibilities to apply this fundamental finding to real systems(see also Chapter 4, 4.1). In particular in this publication, compressive strength results obtained at 28 days are reported for 30% substitution

of cement by combined addition of limestone and metakaolin or calcined smectite (reproduced in Figure 2.8). They have observed an optimum strength for 66% calcined clay and 33% limestone, for both clays. But blends with metakaolin showed strength higher than Portland reference, with calcined smectite slightly lower. An industrial patent also claims excellent strength development for ternary blends of cement, calcined clays and limestone [59].

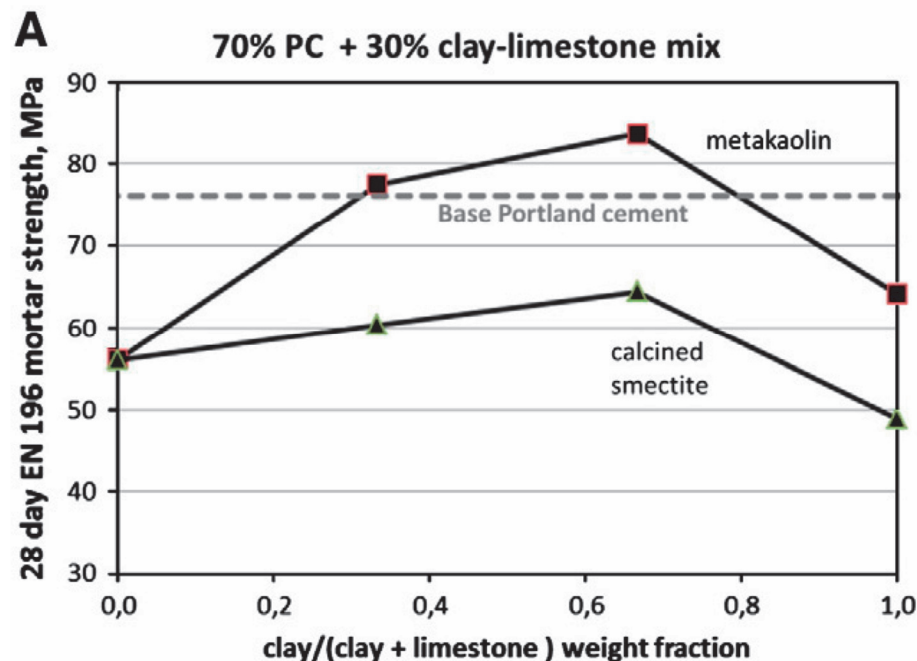


Figure 2.8: Compressive strength, in MPa at 28 days in blends of 70% PC and 30% calcined clay-limestone mix reported as a function of the clay/(clay+limestone) weight ratio [58]

2.3. INFLUENCE OF CALCINED CLAYS ON DURABILITY

The review of the resistance to carbonation and to chloride of systems including calcined clays is given in Chapter 6 and 7, respectively.

Durability of a material is not an intrinsic property but related to the exposure and environmental conditions. Many of the durability issues involve either ingress of aggressive ions or leaching of ions to the outside. One can distinguish different types of durability problems occurring in cementitious materials.

Durability issues are hence much related to the movement of ions in the cementitious matrix and therefore transport properties of the material play a major role in all durability issues and can be characterized experimentally.

The use of calcined clays is overall beneficial for the durability of concrete. Like for other SCMs the improved durability is linked to the porosity refinement produced by the pozzolanic reaction. Sabir's [38] and Siddique's [39] reviews of the use of metakaolin as SCMs report abundant examples from the literature of porosity reduction measured by Mercury Intrusion Porosimetry (MIP) or reduced water absorption, related to the reduction of the capillary porosity. But most of these studies investigate 10 to 20% substitution only.

Concerning other durability threats, sulfate attack has been reported by Ramlochan et al [60] to be reduced with high addition of metakaolin, independently of C_3A content and cement containing 25% of metakaolin was classed as high sulfate resistant cement according to ASTM C1012-89. They also found out that the higher the metakaolin content, the better the sulfate resistance. Al-Akhras et al [61] reported furthermore a considerably lower compressive strength loss due to sulfate attack after 6 months ponding in 5% Na_2SO_4 solution.

Other type of sulfate attack involving calcium carbonate causes formation of thaumasite, $CaSiO_3 \cdot CaSO_4 \cdot CaCO_3 \cdot 15H_2O$. It has been documented as being deleterious and damaging at lower temperature, especially below 15°C but some field cases above 20°C have been found [62].

Few experiments have been done to test the effect of metakaolin on thaumasite formation, but Skaropoulou et al reported an improving [63] effect of metakaolin incorporation compared to OPC or other mineral admixture, for 24 months of exposure to 1.8% $MgSO_4$ solution at 5°C. The improving effect was comparable to the effect obtained with slags or natural pozzolana. In comparison, limestone cement alone showed mass loss, visible deterioration and compressive strength decay after 24 months indicating deterioration of the C-S-H matrix. Some authors relate the improvement of thaumasite resistance to the change in CSH composition (enrichment in Al, longer CSH chains). Bellmann & Starck identified that C(-A)-S-H gel with low Ca/Si (1.1) ratios better resisting thaumasite attack than those with Ca/Si ratio of 1.7 [64].

In another paper [65] they underline the role of calcium hydroxide, that can be a reactant in the formation of thaumasite and stabilizes high Ca/Si ratio C(-A)-S-H. These different arguments make metakaolin a good candidate for increasing thaumasite resistance of concrete.

However combined addition of metakaolin and limestone should be studied more in detail since limestone cement has been showed to have very low resistance to thaumasite attack, while phase assemblage and C(-A)-S-H composition of such blended cement are closer to pozzolanic blended cements.

ASR has been shown to be highly reduced with as low as 10% of metakaolin addition [66]. Already in 1982 Saad et al have shown that 30% and 50% cement replacement by metakaolin could suppress expansion due to ASR [16], basing themselves upon the example of use of calcined clays in Jupia dam (Brazil) in the 60's. Recently, Chappex et al could demonstrate that it is probably related to reduction of silicate dissolution due to aluminium absorption on the surface, as well the as the alkali reduction induced.

2.4. SUMMARY AND OPEN QUESTIONS

The review of the existing literature confirms that metakaolin is the clay that behaves the better, as a pozzolan, among the different calcined clays. It is related to the significant presence of reactive Al^[VI] atoms created during dehydroxylation.

Studies on calcination have reported that the best temperature for kaolinitic clays is usually between 600 and 850°C and can be optimized for each unique clay deposit. Flash calcination seems an interesting option and needs to be further studied.

Mixed or natural clays have been rarely studied, but the study of Fernandez showed strength results similar to PC for 30% replacement with a clay containing only 40% kaolinite. The use of such inexpensive clays is very promising and should be investigated more in detail.

The scientific basis of the synergy of the carboaluminates reaction is established, promising results have been shown for 30% replacement. It requires more work to look at higher substitution level. The use of lower grade clay should also be considered here.

Durability of systems containing calcined clays is overall good. But levels of substitution are mainly limited to 20% and complementary investigations should be done for higher substitution levels.

Overall the review of the literature demonstrates that little has been done on the subject. It underlines the novelty of the concept of ternary blends of cement calcined clays and limestone and the need for a work investigating the potentialities of this promising binder that could set the basis for further developments and applications.

Chapter 3 : MATERIALS AND METHODS

3.1. MATERIALS

3.1.1. CEMENTS

XRF compositions and quantifications of the main oxides as well as calcite content of all cements used during the thesis are summarized in Table 3.1. The limestone used, Durcal 15 commercial product from Omya with $D_{v50}=15$ microns, is pure limestone. Gypsum for sulfate adjustment was reagent grade powder.

Table 3.1: XRF Composition of all cements used in the thesis

Oxides [wt%]	PC1	PC2	PC3	PC4	PC5	PC6	PC7
SiO ₂	21.01	20.60	19.80	21.22	22.03	21.03	19.30
Al ₂ O ₃	4.63	5.60	4.60	4.50	4.85	5.01	5.10
Fe ₂ O ₃	2.60	2.40	3.51	2.93	3.23	2.54	2.97
CaO	64.18	63.40	64.67	62.13	60.58	63.45	61.93
MgO	1.82	1.60	1.36	2.08	1.65	2.05	2.47
SO ₃	2.78	2.90	2.81	2.93	3.00	3.01	2.69
Na ₂ O	0.20	0.20	0.14	0.33	0.30	0.26	0.31
K ₂ O	0.94	0.70	0.66	0.33	0.62	1.02	0.85
Mn ₂ O ₃				0.00	0.08		
MnO	0.03		0.10	0.08		0.04	0.04
TiO ₂	0.14		0.16	0.20	0.25		
Others	0.41	0.47	0.66	0.38	0.10	0.24	0.53
LOI	1.26	2.13	1.54	2.99	3.31	1.34	3.81
Total	100.00	100.00	99.99	100.10	100.00	100.00	100.00
Alkalies [wt%] (Na ₂ O) _{eq}	0.82	0.66	0.58	0.55	0.71	0.93	0.87
	PC1	PC2	PC3	PC4	PC5	PC6	PC7
Strength class	32.5	32.5	42.5	32.5	32.5	52.5	42.5
C ₃ S	59.6	55.0	62.9	58.30	60.23	66.2	60.4
C ₂ S	15.7	13.9	8.7	9.63	12.17	14.1	12.1
C ₄ AF	7.5	6.5	12.7	8.70	10.74	10.6	11.5
C ₃ A	6.2	10.3	5.6	5.8	2.68	3.7	6.0
CaCO ₃	0.6	3.5	1.5	6.5	5.0	0.0	4.1

3.1.2. CLAYS

A summary of the different clays that have been used during the thesis is given in Table 3.2. MK is the Optipozz product from Burgess, U.S.A. Ar is the Argicem product from Argeco, France and Mani, Cu and Pont are three natural clays from Cuba. K and M are pure kaolinite (46 E 0995) and montmorillonite (bentonite, 46 E 0435) from Wards. Model clays KQ, MQ and KMQ were created by mixing, respectively, 45% pure kaolinite K and 55% fine quartz K50, 45% montmorillonite M and 55% quartz and 45% K, 45% M and 10% quartz.

The quartz K50 composition is pure quartz from Bernasconi AG, Switzerland, with SiO₂ content of about 99%, with a very fine PSD, Dv50=3.4, Dv10=0.6 and Dv90=11.5 microns.

In the Figure 3.1 the derivative of the TGA for the different clays are plotted as a function of temperature. It confirms that all clays reach full dehydroxylation before 800°C.

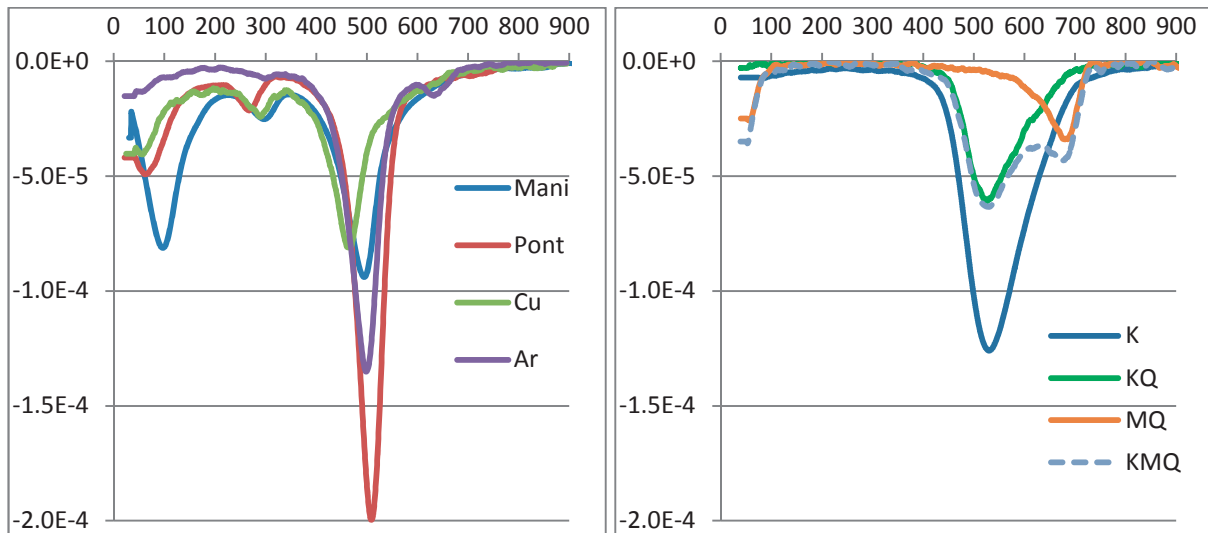


Figure 3.1: Time derivative of the mass loss as a function of the increasing temperature obtained by TGA analysis of the raw clay samples

The curve of the mixed model clay KMQ with the same kaolinite content as KQ and the same montmorillonite content than MQ can clearly be deconvoluted in its two contributing elements.

Table 3.2: Presentation of the main characteristics of the calcined clays used during the thesis

	MK	Ar	Mani	Cu	Pont**	K	M
BET [m^2g^{-1}]	7.6	11.4	28.2	11.8	31.9	26.2	31
d_{10} [μm]	0.4	2.6	1.1	1.0	1.2	0.3	0.6
d_{50} [μm]	2.3	35.5	29.0	16.1	27.5	4.88	2.98
d_{90} [μm]	16.1	119.4	169.7	224.1	170.7	23	30
Origin	USA	France	Cuba	Cuba	Cuba	Wards	Wards
Activation	Flash calcination	Flash calcination	Static calcination	Static calcination	Flash & Static calcination	Static calcination	Static calcination
Time	N/A	Few seconds	1h	1h		1h	1h
Temperature	N/A	750°C	800°C	800°C		800°C	800°C
Est. kaolinite content [wt%]	~ pure	40%	40%	28%	50%	80%	80% montmorillonite
XRF composition							
Oxides [% weight]	MK	Ar	Mani	Cu*	Pont**	K	M
SiO₂	50.62	72.47	48.33		45.71	48.00	63.15
Al₂O₃	46.91	20.80	26.63		28.04	36.40	20.09
Fe₂O₃	0.38	2.26	11.31		21.49	0.85	3.96
CaO	0.02	0.97	1.48		0.14	0.14	1.15
MgO	0.09	0.17	2.90		0.82	0.11	2.27
SO₃	0.08	0.17	0.06		0.27	0.03	0.51
Na₂O	0.28	0.08	2.22		0.17	0.02	2.22
K₂O	0.18	0.27	1.20		0.54	0.48	0.54
TiO₂	1.29	1.02	0.00		0.70	0.01	0.02
Others	0.16	0.00	3.66		0.32	0.00	0.00
LOI	0.00	1.78	2.20		1.80	13.41	5.90
Total	100.00	100.00	99.99		100.00	99.44	99.81
Alkalies % (Na₂O)_{eq}	0.39	0.26	3.01			0.53	0.33

*Cu clay has basically the same composition as Mani, with a slightly higher SiO₂ content because Mani is the same clay after a clay enrichment process, by deflocculation and sedimentation of the coarser quartz particles [8].

**For Pontezuela Chapter 5 details the different batches and the different calcination processes that have been carried out

3.1.3. COMPOSITIONS STUDIED FOR CARBONATION

3.1.3.1. EXPERIMENTAL PROTOCOLS

All details of sample preparation and experimental protocols are given in section 3.3.

Different carbonation experiments were carried out. The experimental details are compiled in Table 3.3. All samples, mortars and pastes, were cast at water/binder ratio 0.5. Preconditioning and carbonation experiments were run in the lab, at constant temperature, 22+/-1°C.

Table 3.3: Summary of carbonation experiments carried out (“Clay30” is a blend with 30% of one of the calcined clays, see Section 3.1.3)

Carbonation		Cement	Curing	Conditioning	Carbonation conditions	Duration	Blends investigated	Clays
Natural	Paste	PC4	28d	Until constant weight, 53%RH	0.03% CO ₂	32 weeks	Clay 30, Blend45	MK
Accelerated					3% CO ₂ , 53%RH			
Natural	Mortar	PC5	360d & 7d	/	0.03% CO ₂	2 years	PC, B15, B45	Cu, Ar, Pont, Mk
Accelerated		PC1	170d	28d, Ventilated oven at 50°C	10% CO ₂ , 53%RH	6 weeks	PC, Clay30, Blend45	Cu, Ar, Mk

3.1.3.2. MATERIALS

The exact compositions of the materials studied in this chapter are given in the Materials section 3.1.1 & 3.1.2.

3.1.3.2.1. PASTES

These materials were studied in natural (0.04%) and accelerated carbonation with 3% CO₂.

PC4	MK30	MK-B45	B45-K50
-----	------	--------	---------

3.1.3.2.2. MORTARS

One preliminary test of accelerated carbonation was carried out with the compositions given in

Table 3.4. We decided to follow an adapted version of the recommendation from AFREM [67] and developed by LCPC in Paris.

Table 3.4: Composition submitted to accelerated carbonation test with 10% CO₂:

PC1	MK30	MKB45	Pont30	PontB45	Ar30	ArB45	Cu30	CuB45
-----	------	-------	--------	---------	------	-------	------	-------

The test was carried out with samples that were previously cured for 28 days, used to monitor drying shrinkage during 100 days and then resaturated. After discussion with M. Thiery who helped develop the test, it was decided to adapt the preconditioning and leave the samples 1 month instead of 2 weeks (as in the AFREM recommendations) in the oven at 50°C to improve the drying and homogenization of the relative humidity profile within the samples and use 10% CO₂ instead of 50%. After acquisition and analysis of the results, and with a closer look to the literature, the validity of such highly accelerated tests was considered questionable and underlined the need for carbonation data in atmospheric CO₂ conditions. Due to lack of time and the evolution of the project, it was decided to use samples already available, and only add two samples PontB45 and PontB60 cured for 7 days to compare with samples cured in conditions closer to reality on site.

The following compositions were studied:

Table 3.5: List of mortar compositions submitted to normal carbonation:

PC5	Ref15	Ref45	ArB15	ArB45	CuB15	CuB45	Pont B45	PontB45 7d curing	PontB60 7d curing
-----	-------	-------	-------	-------	-------	-------	----------	-------------------	-------------------

These samples were stored in lab cupboards and neither the relative humidity nor the CO₂ atmospheric content were controlled, but they can be estimated to be 40-70 HR% and 0.04% respectively.

3.1.3.3. SERIES FOR COMPRESSIVE STRENGTH

This set of experiments was launched with the aim of studying the compressive strength of mortar bars with and without complete carbonation of the samples. The compositions studied are shown in Table 3.6:

Table 3.6: Composition of the samples prepared to measure compressive strength with and without carbonation.

	PC1	MK-B15	Mk-B22	MK-B30	FCPont-B15 ¹⁾	FCPont-B22	FCPont-B30
Clinker [%]	100	85	78	70	85	78	70
Metakaolin [%]	0	10	15	20	5	7.5	10
Other/filler [%]		0	0	0	5	7.5	10
Limestone [%]	0	5	7	10	5	7	10

¹⁾ Note that FC means Flash Calcination, this series of material has been calcined in Fumel, with $T_{\max}=750^{\circ}\text{C}$ (see 5.6)

For these systems three samples of each composition were subjected to the same accelerated carbonation without any wrapping during 6 weeks until constant weight was reached. In another glove box free of CO_2 but with the same relative humidity, 3 other samples of each same composition were kept. The fully carbonated samples did not show any remaining non-carbonated core after phenolphthalein test, while the samples that remained in the CO_2 free glove box showed no sign of carbonation.

3.1.4. COMPOSITIONS STUDIED FOR CHLORIDE RESISTANCE

The compositions of Series 1a & b are given in Table 3.7:

Table 3.7 Compositions studied in series 1a tested for chloride resistance (Chapter 7)

	PC1	MK-30	MK-B45	FCPont-30 ¹⁾	FCPont-B45	Ar-30	Ar-B45
Clinker [%]	100	70	55	70	55	70	55
Metakaolin [%]	0	30	30	15	15	11.9	11.9
Other/filler [%] ²⁾		0	0	15	15	18	18
Limestone[%]	0	0	15	0	15	0	15
	PC1	MK-B15	Mk-B22	MK-B30	FCPont-B15	FCPont-B22	FCPont-B30
Clinker [%]	100	85	78	70	85	78	70
Metakaolin [%]	0	10	15	20	5	7.5	10
Other/filler [%]		0	0	0	5	7.5	10
Limestone[%]	0	5	7	10	5	7	10

¹⁾ Note that FC means Flash Calcination, this series of material has been calcined in Fumel, with $T_{max}=750^{\circ}C$ (see 5.6)

²⁾ "Other/filler" corresponds to the non-reactive fraction of the natural clay, it is mostly quartz and hematite

The Series 2 with cement PC3 combines experiments of binding isotherms and migration tests with the STADIUM protocol. Details of the compositions are given in Table 3.8. The preliminary series each contain three samples: pure PC2, MK30 and PontB45. The sulfate was adjusted by adding 2%wt of gypsum.

Table 3.8: Compositions studied in series 2 tested for chloride resistance (Chapter 7)

	PC3	MK-B15	MK-30	MK-B45	Pont-B15	Pont-B45
Clinker [%]	100	85	70	55	85	55
Metakaolin [%]	0	10	30	30	5	15
Other/filler [%]		0	0	0	5	15
Limestone[%]	0	5	0	15	5	15

The composition of the pastes at 28 days, immediately prior to the chloride binding isotherm start is shown in Table 3.9.

Table 3.9: Phase assemblage of the paste used for chloride binding isotherm as obtained by Rietveld refinement

	Anhyd	Calcite	CH	Ettringite	Monosulfo	Monocarbo	Hemicarbo	Strätlingite	Amorphous
PC2	12.2%	0.0%	19.8%	3.4%	5.1%	0.1%	0.5%	0.0%	58.9%
MKB15	11.7%	1.0%	9.8%	5.3%	4.0%	1.2%	4.6%	0.0%	62.5%
MK30	9.5%	1.5%	1.1%	2.4%	3.7%	0.7%	0.0%	11.3%	69.9%
MKB45	8.1%	7.2%	0.8%	6.0%	0.5%	1.0%	4.3%	3.0%	69.1%

Anhyd is the sum of the remaining C_3S , C_2S and C_4AF anhydrous phases, amorphous contains mostly C-A-S-H gel and unreacted metakaolin.

3.2. METHODS

Mortars were cast at a water/binder ratio of 0.5 with standard sand according to EN-197-1 and pastes at a water/binder ratio of 0.4¹. Pastes were mixed at 2000 rpm with a metal propeller and usually 100g of paste (for B45 39.29 g of cement was mixed with 10.71 g. of limestone, 21.43g of calcined clays and 28-57g. of water) were mixed in a plastic vessel. Anhydrous binder was homogenized before water with superplasticizer was added.

Coupled substitutions of MK and LS were always made in the weight ratio 2:1 unless otherwise specified. These blends are always labelled as “x-Byy”, x being the clay name and yy the level of cement substitution.

The workability was adjusted when necessary using the Rheobuild 5500 superplasticizer (up to 3 wt% of binder for pastes and 2wt% for mortars. At these dosages there was no significant impact on the hydration kinetics).

3.2.1. STRENGTH TESTING

Flexural and compressive strength measurements were carried out on mortars at 1, 7, 28 and 90 days on 3 prisms of 120 × 40 × 40 mm and 6 prisms of 40 × 40 mm section respectively according to EN-197-1.

3.2.2. HYDRATION STOP

Hydration of paste samples was stopped by immersion of ca. 3 to 5 mm thick slices for seven days or more in 200 mL isopropanol and further vacuum drying during at least 7 days.

¹ Due to the higher porosity in the Interfacial Transition Zone around aggregate particles; a w/c ratio of 0.4 in paste is roughly equivalent to the paste phase of concrete with w/c = 0,5 68. Scrivener, K.L., A.K. Crumbie, and P. Laugesen, *The Interfacial Transition Zone (ITZ) Between Cement Paste and Aggregate in Concrete*. Interface Science, 2004. **12**(4): p. 411-421.

3.2.3. THERMOGRAVIMETRY ANALYSIS

Thermogravimetric measurements on paste samples of about 40 mg of pieces crushed in an agate mortar were done with a Mettler-Toledo TGA/SDTA 851 balance using a 10 °C/min ramp from 30 °C to 900 °C under a 30 ml/min flow of N₂.

3.2.4. MERCURY INTRUSION POROSIMETRY

Mercury intrusion porosimetry (MIP) data from mortars were obtained with POROTEC GmbH PASCAL 140 and PASCAL 440 instruments up to a maximum pressure of 400 MPa.

For pastes, samples of 1.5 g were used while mortars, samples of 3 g were used in order to take in account for the lower paste content. Samples were systematically broken into pieces of approximately 3x3x3 mm, according to an internal optimization protocol and the tests were replicated at least once.

3.2.5. X-RAY DIFFRACTION

Standard XRD measurements on pastes were carried out with a Panalytical X'Pert Pro MPD diffractometer in a θ - θ configuration using CuK α source ($\lambda=1.54 \text{ \AA}$) with a fixed divergence slit size of 0.5°. Samples were scanned on a rotating stage between 4 and 65 [$^{\circ}2\theta$] using an X'Celerator detector with a step size of 0.0167 $^{\circ}2\theta$ and a time per step of 30s. Rietveld analyses were carried out on in-situ hydrating samples (pastes with water/binder ratio 0.4) covered with 25 μm Kapton foil and using the external standard method, with Rutile as standard reference.

For the investigation of the mortars powder obtained by grinding after ponding, scanning was reduced from 4 to 30 [$^{\circ}2\theta$], the step size divided by 2 and time per step extended to 60s to improve the signal/noise ratio.

3.2.6. ISOTHERMAL CALORIMETRY

The heat of reaction of the pastes at 20 °C was measured with an isothermal calorimeter (TAM Air from TA instruments). It consists of 8 parallel twin measurement channels maintained at a constant temperature: one from the sample, the other for the reference sample. Reference samples were

prepared using deionised water weighed in order to have the same heat capacity than the paste sample. Cumulative curves are always plotted starting from the lowest point of the dormant period to get rid of mixing and dissolution heat.

3.3. CARBONATION

3.3.1. MORTAR FABRICATION

16x4x4 Mortars bars were cast according to EN-197-1 standard procedure with normalized sand (except microconcrete for natural carbonation made in Cuba, where graded limestone aggregates has been used, see Section 6.7.1) and water/binder ratio of 0.5. In both case, superplasticizer was used, up to 2 wt% binder to maintain satisfactory workability. Samples were demoulded at 24h and kept above 90% RH until needed.

3.3.2. PASTE FABRICATION & SAMPLE PREPARATION

Pastes samples were cast at water/binder ratio 0.5 for 2 minutes at 2000 rpm and sealed. During the first 24 hours the samples were placed on a mechanical wheel turning at 6 rpm to prevent inhomogeneity or bleeding. They were then cured for 28 days in a chamber kept above 90% RH.

All samples were wrapped with two layers of an alumina adhesive tape in order to have unidirectional carbonation. Carbonation depths were measured by spraying 0.1 wt. % phenolphthalein solution in ethanol on freshly fractured surfaces. Every value is an average of a minimum of 6 measurements and most of the samples were duplicated.

Paste cylinders after being fractured, were put back together in order to cut slices of approximately 3 mm thickness and analyse them by XRD & Rietveld refinement directly after having been cut, according to the XRD procedure (3.3.3.3). After hydration was stopped by solvent exchange with isopropanol, which was later on removed by vacuum pumping, thermogravimetry analyses and MIP experiments were conducted on the same slices (3.2.4).

3.3.3. CHARACTERIZATION TECHNIQUES

3.3.3.1. CARBONATION

For pastes, preconditioning until constant weight was carried out in a glove box at constant RH. Saturated solutions with magnesium nitrate $\text{MgNO}_3 \cdot 6\text{H}_2\text{O}$ maintained RH at 53%. Preconditioning was stopped when the daily relative mass change reached 0.01%; it took for example 85 days for the paste samples.

For accelerated carbonation at 10% CO_2 , the preconditioning was carried out by drying in a circulating oven at 50°C for 28 days. Weight changes were not monitored.

3.3.3.2. CARBONATION CONDITIONS

Natural carbonation was obtained by storing the mortar bars in a closed cupboard in the laboratory, temperatures varying from 20 to 23°C and relative humidity not controlled. In the preliminary test, conditions were better controlled; samples were kept in a ventilated room with relative humidity at 70% +/- 2% and 22°C.

For accelerated carbonation, the experimental set-up is illustrated in the Figure 3.2 below. Constant flow of premixed gas at fixed CO_2 concentration from the gas bottle is fed into the glove box, where constant humidity, maintained at 53%, is provided by the saturated $\text{MgNO}_3 \cdot 6\text{H}_2\text{O}$ solution. The gas flow is adjusted with a gas manometer. The gas is pre-humidified in a gas bubbler containing the same saturated $\text{MgNO}_3 \cdot 6\text{H}_2\text{O}$ solution before the inlet. Another bubbler is placed at the outlet to ensure constant a constant flow through the carbonation chamber. Air movement is ensured inside the glove box by a fan.

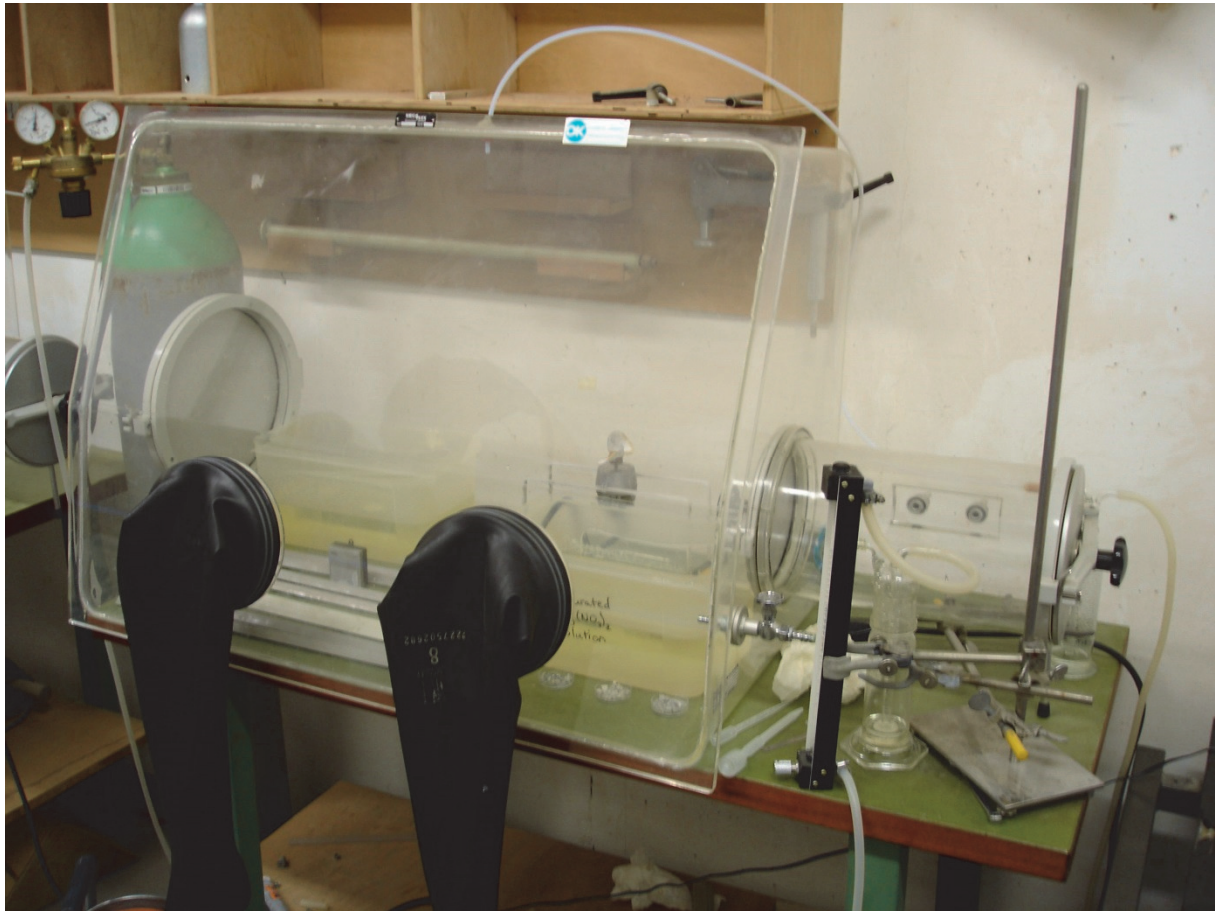


Figure 3.2: Picture of the experimental set-up used for carbonation.

3.3.3.3. RIETVELD ANALYSIS

Paste slices of approximately 3 mm thickness were analysed by XRD directly after having been cut, according to the X-Ray Diffraction procedure explained in Section 3.2.5. Rietveld refinement was performed using Highscore Plus X'Pert 3.0. Metakaolin is essentially X-Ray amorphous and cannot be revealed by such a Rietveld refinement. Similarly, silica gel and amorphous calcium carbonate precipitating during carbonation are also not detectable by XRD. They are all included into an amorphous content that could be quantified by the external method [69], using a Rutile reference to measure the scale factor [70]. For samples which hydration was stopped with isopropanol, the water content was determined with TGA to correct the quantification using the Mass Attenuation Coefficient (MAC) ratio.

The different sulfate bearing phases and the C_3A , C_4AF crystalline anhydrous cement phases were first refined and fixed based on the anhydrous material after SAM extraction (Salicylic Acid/Methanol Extraction) to dissolve alite belite and free lime [71]. Alite, belite and $CaCO_3$, $MgCO_3$, MgO can then be refined and based on the anhydrous cement. These phases become also fixed. In hydrated samples only their intensity factors and the Caglioti Width W Left factor are allowed to vary. Background was determined with the polynomial method with a minimum of 6 refinement coefficients.

The common cement hydrates used in section 4.3.7, namely ettringite, monocarboaluminate, hemicarboaluminate, monosulfoaluminate and calcium hydroxide, have been selected as control phases. In addition, strätlingite [72] and a C-S-H background derived by Renaudin [73] from [74] has been used. For the carbonation phases, vaterite from Le Bail [75](amcsd code 0019141) has been used, in accordance with the PDF 00-033-0268 Vaterite reference model, although its exact crystallography is still under debate among the researchers [76]. For aragonite the model of Caspi (ICSD #170225, [77]) has been taken. All the phases are summarized in Table 3.10:

Table 3.10: List of Rietveld references used

Phase	Chemical Formula	Crystal system	ICSD Reference	Author / Bibliographic reference
Alite	Ca ₃ SiO ₅	Monodinic/M3	94742	de la Torre et al., 2002
Belite	Ca ₂ SiO ₄	Monodinic/β	79550	Tsurumi et al., 1994
Tricalcium aluminate	Ca ₃ Al ₂ O ₆	Cubic	1841	Mondal et al., 1975
Tricalcium aluminate	Ca ₈ .5NaAl ₆ O ₁₈	Orthorhombic	1880	Nishi et al., 1975
Ferrite	Ca ₂ AlFeO ₅	Orthorhombic	9197	Coleville et al., 1971
Lime	CaO	Cubic	75785	Huang et al., 1994
Periclase	MgO	Cubic	104844	Taylor, 1984
Gypsum	CaSO ₄ ·2H ₂ O	Monodinic	2059	Cole et al., 1974
Hemihydrate	CaSO ₄ ·0.5H ₂ O	Monodinic	73263	Abreil et al., 1993
Anhydrite	CaSO ₄	Orthorhombic	40043	Hawthorne et al., 1975
Arcanite	K ₂ SO ₄	Orthorhombic	2827	McGinnety, 1972
Bassanite	CaSO ₄ ·0.6H ₂ O	Monodinic	69061	Bezou
Portlandite	Ca(OH) ₂	Rhombohedral	15471	Petch, 1961
Ettringite	C ₃ A(C ₂ S) ₃ H ₃ 2	Hexagonal P	16045	Goetz-Neunhoefffer et al., 2006
Monosulfate	C ₄ A ₁ S ₁ H ₁ 2	Hexagonal	100138	Allmann, 1977
Monocarboaluminate	C ₄ AC ₁ H ₁ 1	Triclinic P	59327	Francois et al., 1998
Hemicarboaluminate	C ₄ AC _{0.5} H ₁ 1.5	Rhombohedral	PDF041-0221	Runcevski & Dinnebier 2012
Calcium Silicate Hydrate	Ca _{1.5} SiO ₃ ·5xH ₂ O	Unknown		Renaudin 2009
Calcite	CaCO ₃	Rhombohedral	79674	Wartchow, 1989
Vaterite	CaCO ₃	Hexagonal	amcsd 0019141	LeBail 2011
Aragonite	CaCO ₃	Orthorhombic	PDF 00-033-0268	
Strätlingite	C ₂ AS ₂ H ₈	Rhombohedral	Caspi ICSD 170225	Pokroy 2006
			ICSD - 69413	Rinaldi 1989

3.4. CHLORIDE RESISTANCE

16x4x4 cm mortar bars at water/binder ratio 0.5 were prepared with the standard protocol used for compressive strength measurements and described above in Section 3.3.1. After 28 days of curing at 90% RH at room temperature, samples were rectified on one 16x4cm face (removal of about 1mm by polishing) and all the other faces carefully coated by 2 to 3 successive paraffin layers to prevent any leaching. Mortar samples were immersed in a NaCl 0.5 M ponding solution at 23°C +/-1°C with only one surface in contact with the solution so that the chloride penetration is unidirectional. It follows the ASTM ponding method [78]. The ponding experiment lasted over 2 years, without renewal of solution.

Pastes were prepared according to standard paste preparation procedure (section 3.2)

3.4.1. GRINDING AND ACIDIC DISSOLUTION

Sample grinding was carried out with mechanical grinding equipment with rotating iron blades of 3 cm diameter. The depth is controlled, so that successive layers of 2500 +/- 50 microns are ground perpendicularly to the migration direction. This corresponds approximately to 5 grams of powdered material for a saturated standard mortar that is carefully collected and kept in sealed plastic container.

Samples were dried until their weight remained constant in an oven at 110°C. They were then weighed and submitted to acidic dissolution in 100 mL volume of 6M HNO₃ for at least 12 hours. A sample was extracted and analysed by chromatography for Cl⁻ concentration with a DIONEX ICS – 3000 and its automated sampler AS40. This equipment has optimal accuracy for a range of 0.8mg/l - 40.0mg/l of chlorine so that samples were diluted as required to improve measurement accuracy. The high nitric acid content did not impair the measurement although it was sometimes necessary to dilute 2 or 3 times to enhance the chromatography peak resolution and precision. Sample measurement is automatized but quantification is carried out manually by determining background level and the area under the peak on the software Chromeleon Xpress always by the same technician.

3.4.2. CHLORIDE BINDING ISOTHERMS: EXPERIMENTAL PROCEDURE

Water/binder ratio was kept constant at 0.5, and 2 different curing times were investigated. Materials studied were the same as in Series 2 for the migration test, but were cast only as pastes.

At the end of the curing period the pastes were de-moulded and cut into 3 mm thick discs. The sliced samples were then vacuum-dried for three days in a desiccator containing silica gel and soda lime. The dried samples were transferred to a glove box containing soda lime to remove carbon dioxide from the air, and kept at 11% RH for a month. After storage, the 3-mm thick discs were broken into small fragments and samples, weighing approximately 5 g, were placed in 25-mL plastic bottles under vacuum for 2 h. The bottles were then filled with approximately 100 mL of NaCl solution using 5 different concentrations (0.1, 0.3, 0.5, 0.7, 1.0 M), sealed and stored at 23 ± 1 °C. 0.50 w/cm. Samples were stored for 20 weeks but solution concentrations were checked after 6 and 13 weeks. 20 weeks were sufficient to ensure that equilibrium was reached between the pore solution of the samples and the host solution. The host solutions were then analysed for chloride concentration by chromatography.

Chapter 4 ARTICLE: CEMENT SUBSTITUTION BY BLENDS OF METAKAOLIN AND LIMESTONE

Article published in Cement and Concrete Research, 42 (2012), p.1579-1589 [79]

¹Antoni M. ^{2*}, ¹Rossen J., ²F. Martirena, ¹Scrivener K.

¹ EPFL-STI-IMX— Laboratoires des Matériaux de Construction, Station12, CH-1015 Lausanne, Switzerland, ³CIDEM-UCLV, Universidad Las Villas, Santa Clara, Cuba

Abstract

This study investigates the coupled substitution of metakaolin and limestone in Portland cement (PC). The mechanical properties were studied in mortars and the microstructural development in pastes by X-Ray diffraction, Thermogravimetry analysis, Mercury Intrusion Porosimetry and Isothermal Calorimetry. It is shown that 45% of substitution by 30% of metakaolin and 15% of limestone gives better mechanical properties at 7 and 28 days than the 100% PC reference. Our results show that calcium carbonate reacts with alumina from the metakaolin, forming supplementary AFm phases and stabilizing ettringite. Using simple mass balance calculations derived from thermogravimetry results, we also present the thermodynamic simulation for the system, which agrees fairly well with the experimental observations.

It is shown that gypsum addition should be carefully balanced when using calcined clays because it considerably influences the early age strength by controlling the very rapid reaction of aluminates.

Keywords: calcined clays, limestone, cement substitution, ternary blend

² **Corresponding author: Email: mathieu.antoni@epfl.ch Tel +41216936758, Fax +41216935800**

4.1. INTRODUCTION

Supplementary cementitious materials (SCM's) are now commonly used to reduce the clinker factor of cements. However above a threshold substitution of about 30%, these materials reduce the mechanical properties, particularly at early age. The availability of commonly used industrial by-products such as fly ash and blast furnace-blast slags is locally imbalanced and the amounts produced are much less than the worldwide production of cement. Consequently, alternative sources of SCM's such as calcined clays are of interest. Kaolinitic clays are widely available in the earth's crust, and a heat treatment between 600 and 800°C of such clays leads to the dehydroxylation of the crystalline structure of kaolinite to give metakaolin [37, 80]. Metakaolin demonstrates excellent pozzolanic properties [7, 29, 38, 81]. The reactivity of metakaolin has been linked to its content of penta-coordinated aluminium ions that are formed during the dehydroxylation process [29, 82, 83].

Fine limestone is also commonly added to cement and it is established that limestone additions up to around 5% can react with cement and enhance most properties [12, 55, 56]. Calcium monocarboaluminate and hemicarboaluminate are formed instead of monosulphoaluminate, which leaves more sulfate to form ettringite. Damidot, et al. have also shown in a recent paper [58] with thermodynamic calculations that the increase in solid volume in a ternary blend cement-limestone-pozzolan when replacing limestone by pozzolan can be related to the reactive aluminous content of the pozzolan. In this sense, the use of metakaolin is interesting because of its high reactive aluminate content.

In this study we investigate the properties of blends with coupled additions of metakaolin and limestone, with the idea that the extra alumina provided by the metakaolin will react with more limestone, allowing good properties to be maintained to higher levels of substitution. There are already reports of such an approach for ternary PC limestone blends with blast furnace slag, fly ash and natural pozzolans [84-88], some improvement of mechanical properties and durability were observed at 28 or 90 days, but none of these studies explained the chemistry underlying these results. More recently De Weert et al. [89] and Moesgaard et al [90] report a synergetic increase of the mechanical properties fly ash and limestone to Portland cement and similarly for calcium aluminosilicate glass powder and limestone to Portland cement.

They related this synergy to the formation of carboaluminates phases; they found hemicarboaluminate from early age that is progressively converted into monocarboaluminate after 90 days.

4.2. EXPERIMENTAL PROCEDURE

The stoichiometric formation of monocarboaluminate hydrate (MC) was considered: one mole of metakaolin reacts with one mole of calcium carbonate in the presence of excess calcium ions in aqueous solution to give one mole of MC (Equation 4-1). This corresponds to an addition with a weight ratio of 2:1 metakaolin: limestone.



A Portland cement (PC) containing only trace amounts of limestone was used. The limestone powder (LS) was Durcal 15 from Omya Switzerland. Highly purity Optipozz Metakaolin (MK) produced by flash calcination by Burgess (USA) was used. Details of their chemical composition, size distributions and Rietveld refinement composition normalized to the total crystalline content for OPC are given in Table 4.1 and Figure 4.1.

Table 4.1 : Chemical composition of the main components given by X-Ray Fluorescence, left part and crystalline composition by Rietveld of the cement, on the right.

Oxides	PC	"MK"	"LS"		
SiO ₂	21.01	50.62	0.04	C ₃ S	62.1%
Al ₂ O ₃	4.63	46.91	0.06	C ₂ S	15.2%
Fe ₂ O ₃	2.60	0.38	0.05	C ₃ A cubic	3.9%
CaO	64.18	0.02	56.53	C ₃ A ortho	2.5%
MgO	1.82	0.09	0.10	C ₄ AF	6.2%
SO ₃	2.78	0.08	/	Anhydrite	1.8%
Na ₂ O	0.20	0.28	0.04	Hemihydrate	2.3%
K ₂ O	0.94	0.18	0.04	Aphtitalite	0.5%
TiO ₂	0.14	1.29	0.03	Syngenite	2.7%
Others	0.44	0.16	0.02	Periclase	0.5%
LOI	1.26	0.00	43.09	Dolomite	1.5%
Total	100.0	100.00	100.00	Calcite	0.5%
				Quartz	0.3%

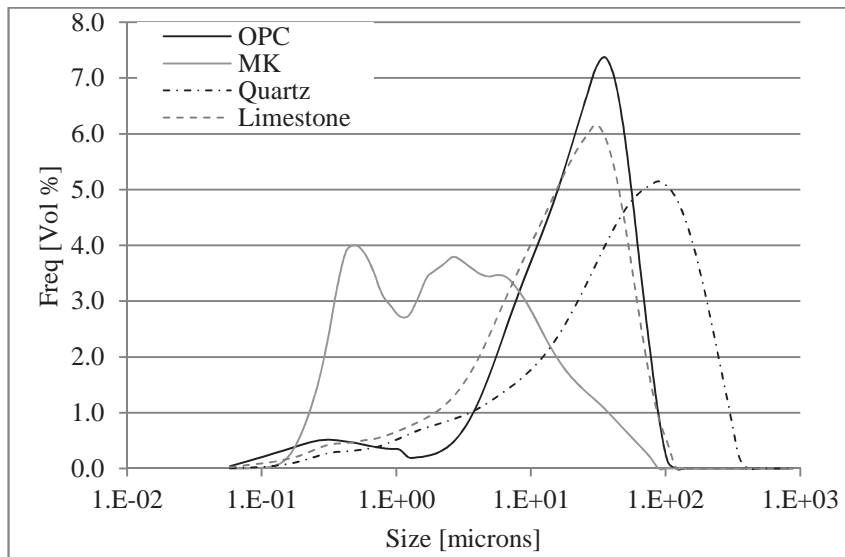


Figure 4.1: Particle size distribution of the raw materials measured by Laser Granulometry.

The formulations investigated are given in Table 4.2. Mortars were cast at a water/binder ratio of 0.5 with standard sand according to EN-197-1 and pastes at a water/binder ratio of 0.4³. Coupled substitutions of MK and LS were made in the weight ratio 2:1.

Table 4.2 : Formulations of the blends “B” as well as the quartz references “Ref”

	Cement [%]	Limestone [%]	Metakaolin [%]	Quartz [%]
PC	100	0	0	0
Ref15	85	0	0	15
Ref30	70	0	0	30
Ref45	55	0	0	45
Ref60	40	0	0	60
LS15	85	15	0	0
MK30	70	0	30	0
B15	85	5	10	0
B30	70	10	20	0
B45	55	15	30	0
B60	40	20	40	0

The coupled substitutions – “blends” – were made at a total level of substitution of 15, 30, 45 and 60%. For comparison, substitutions of just limestone at 15% and just Metakaolin at 30% were made; corresponding to the amounts of these materials in the 45% blend. Blends with quartz powder were made at levels of 15, 30, 45 and 60% to provide a comparison with inert filler. The workability was adjusted when necessary using Rheobuild 5500 superplasticizer (up to 3 wt% of binder for pastes and 2wt% for mortars. At these dosages there was no significant impact on the hydration kinetics).

Flexural and compressive strength measurements were carried out on mortars at 1, 7, 28 and 90 days on 3 prisms of 120 × 40 × 40 mm and 6 prisms of 40 × 40 mm section respectively according to EN-197-1. Hydration of paste samples was stopped by immersion of ca. 5 mm thick slices for seven days or more in isopropanol and further vacuum drying during at least 3 days. Thermogravimetric measurements on paste samples of about 40 mg of pieces crushed in an agate mortar were done with a Mettler-Toledo TGA/SDTA 851 balance using a 10°C/min ramp from 30°C to 900°C under a 30 ml/min flow of N₂. Mercury intrusion porosimetry (MIP) data from mortars were obtained with POROTEC GmbH PASCAL 140 and PASCAL 440 instruments up to a maximum pressure of 400 MPa. X-Ray Diffraction (XRD) measurements were carried out on pastes with a Panalytical X’Pert Pro MPD diffractometer in a θ - θ configuration using CuK α source ($\lambda=1.54 \text{ \AA}$) with a fixed divergence slit size of 0.5°. Samples were scanned on a rotating stage between 4 and 65 [$^{\circ}2\theta$] using an X’Celerator detector with a step size of 0.0167 $^{\circ}2\theta$ and a time per step of 30s. Rietveld analysis were carried out on in-situ hydrating samples (pastes with water/binder ratio 0.4) covered with 25 μm Kapton foil and using the external standard method, with Rutile as standard reference.

Scanning Electron Microscopy (SEM) results were obtained on a FEI Quanta 200 SEM equipped with a tungsten filament. It was operated at 15 kV. The detector is a Bruker AXS XFlash® Detector 4030 (with an active surface of 30 mm²) at a take-off angle of 35°C, i.e. an optimal working distance of 12.5 mm. The included Esprit software allows us to define a number of counts rather than only a counting time. This enables us to compare statistically equivalent points even if the filament source may show slight variations in current. A preset list of elements (O, Na, Mg, Al, Si, P, S, Cl, K, Ca, Ti, Fe) is inputted for identification. Automatic background correction and a standardless “Series Fit” fitting of peaks are used before each point analysis is quantified using the $\phi(\rho z)$ matrix correction scheme with standards. Normalisation by the pseudo beam current is done by measuring X-ray peak intensities from a copper film placed on the metallic sample holder. About 200 EDS points were chosen to look for C-A-S-H zones and determine their composition.

The X-ray interaction volume at the acceleration voltage used (15kV) is about 1 μm . While the C-A-S-H grey level is recognizable in OPC, the dense and homogeneous intermixing with fine metakaolin, carboaluminates and strätlingite explain the considerably higher dispersion of the points in blends containing metakaolin.

4.3. RESULTS

4.3.1. MECHANICAL STRENGTH

Compressive strengths values are given in Figure 4.2 and relative compressive strengths compared to PC and quartz references are given in Figures 4.3. The 15% blend B15 has higher strength than the 100% PC reference at all ages. The other blends have lower strengths at one day, but the 30% and 45% blends show higher strength with respect to PC at 7 and 28 days. Even the 60% blend has 93% of the PC strength at 28 days (330% of the 60% reference with inert filler).

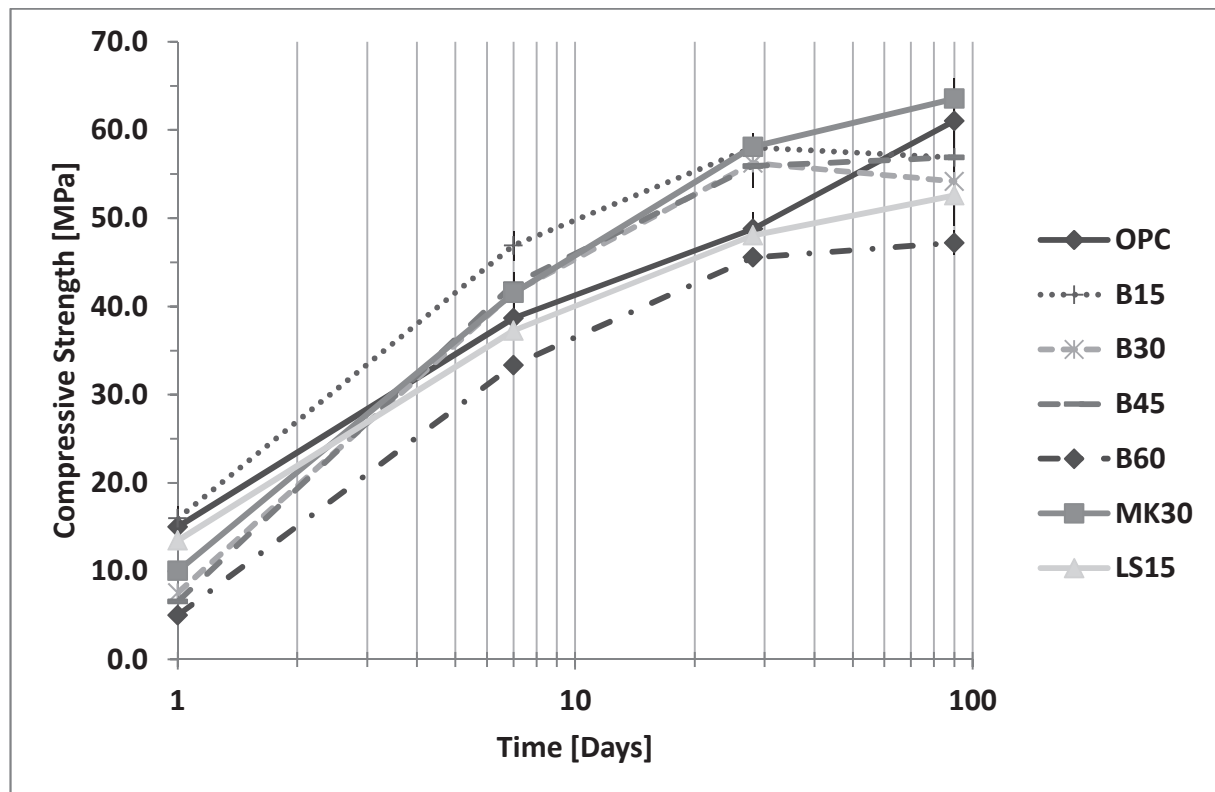
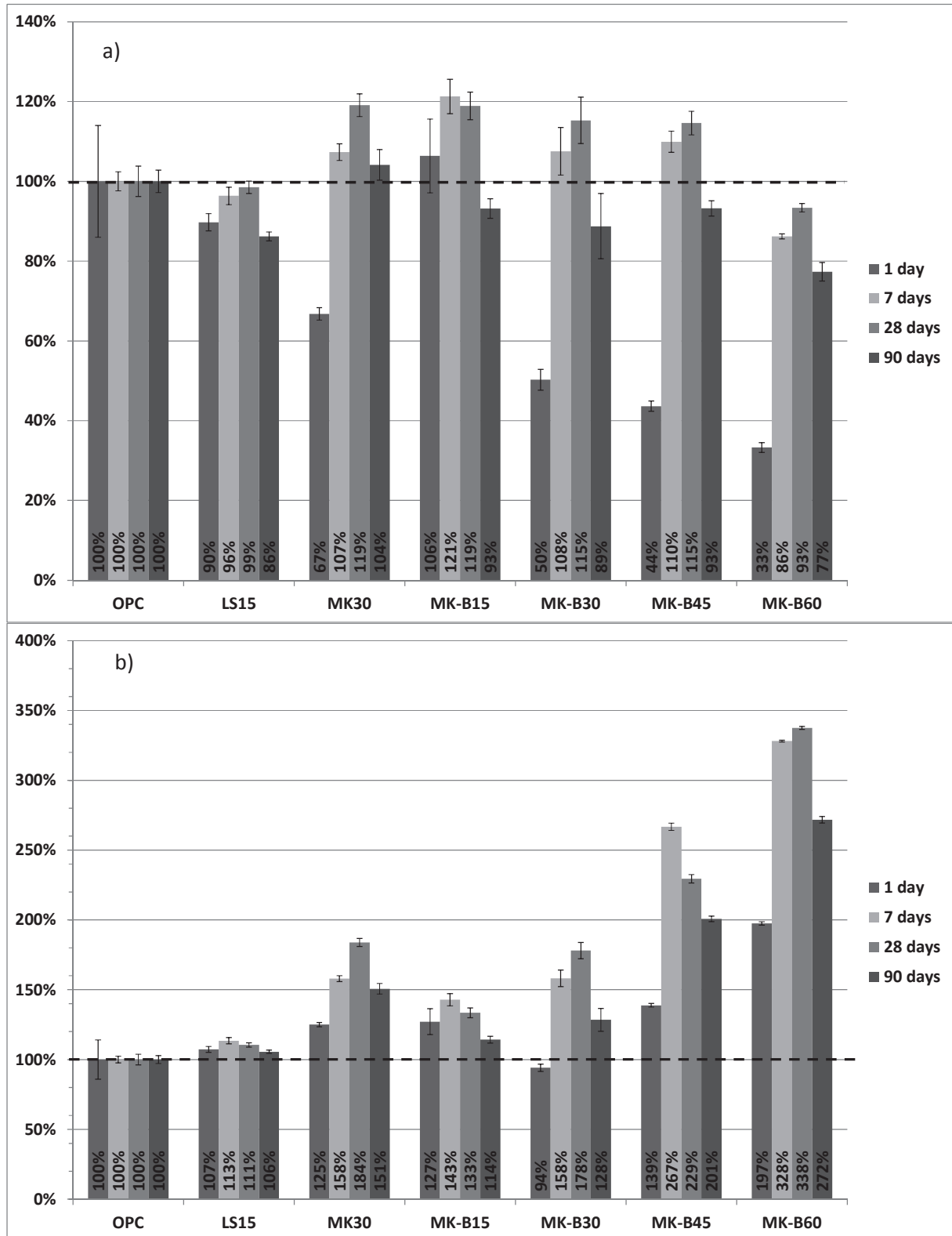


Figure 4.2: Compressive strength of blends mortars at 1, 7, 28 and 90 days.

Flexural strengths (not shown) globally follow the same trends as compressive strengths. All blends, including the 60% blend, show higher or similar bending strength with respect to the pure PC at 7, 28 and 90 days.



Figures 4.3 a) et b): Compressive strength of blends normalized to the strength of pure PC (a) and to the quartz reference (b) mortars at 1, 7, 28 and 90 days.

4.3.2. CHARACTERIZATION OF POZZOLANIC REACTION BY THERMOGRAVIMETRIC ANALYSIS

The evolution of calcium hydroxide for all blends and references is shown in Figure 4.4. The tangent method was used to quantify Portlandite from the dehydration peak between 450 and 600 °C and expressed per unit weight of original anhydrous cement as proposed by Marsh and Day [91]. There is no sign of any pozzolanic activity for the limestone blend (L15) and the quartz references.

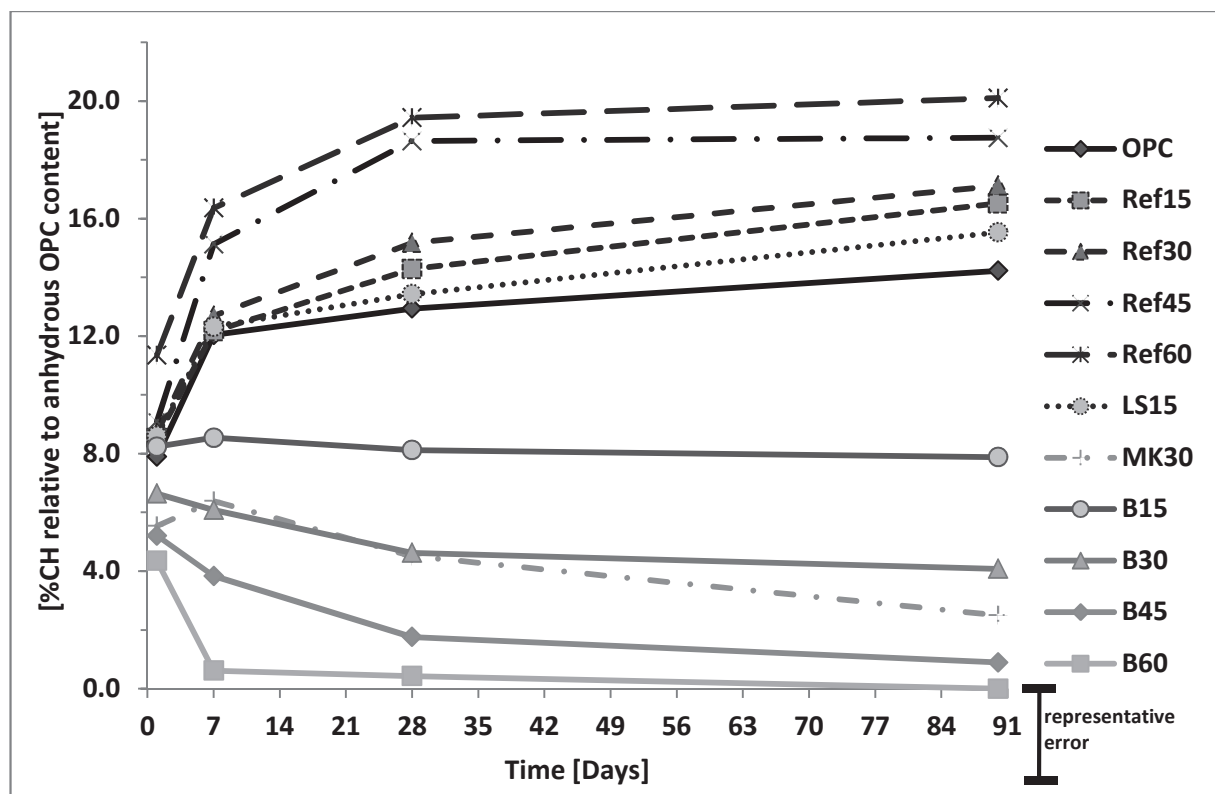
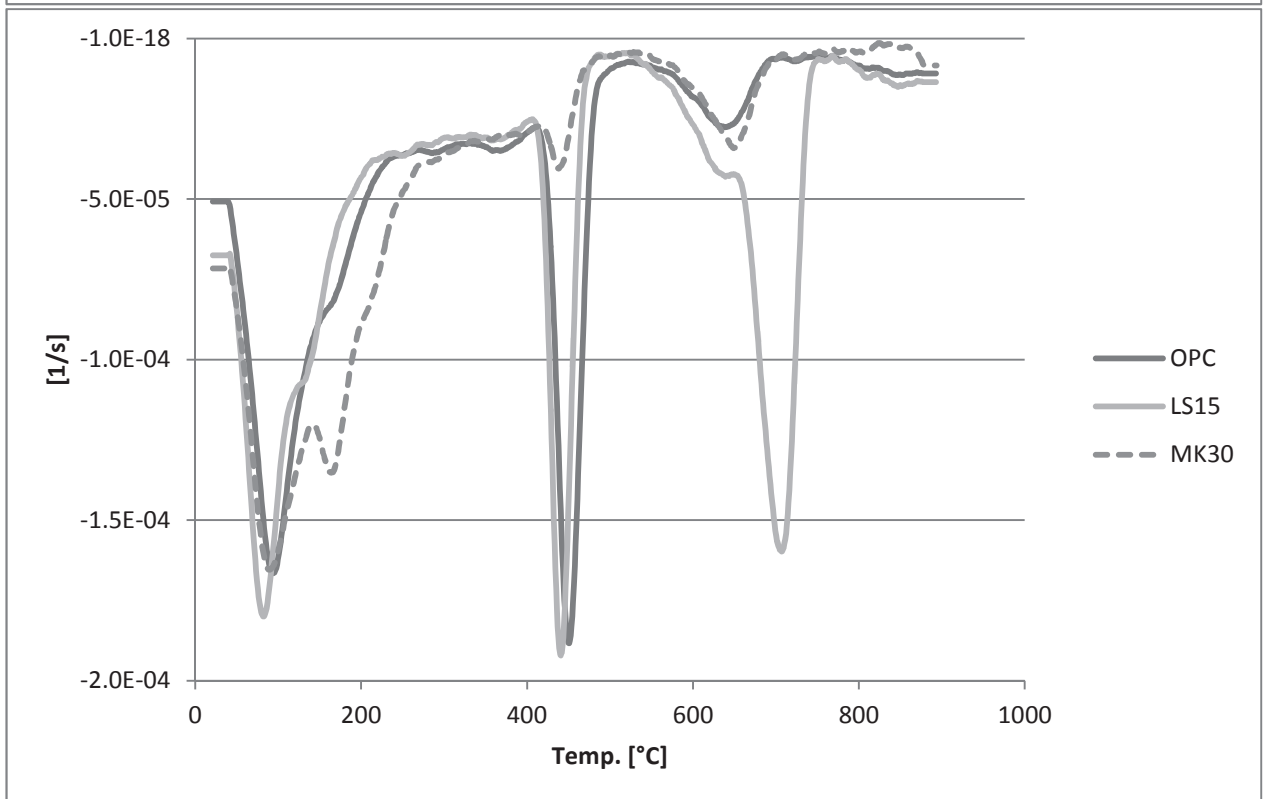
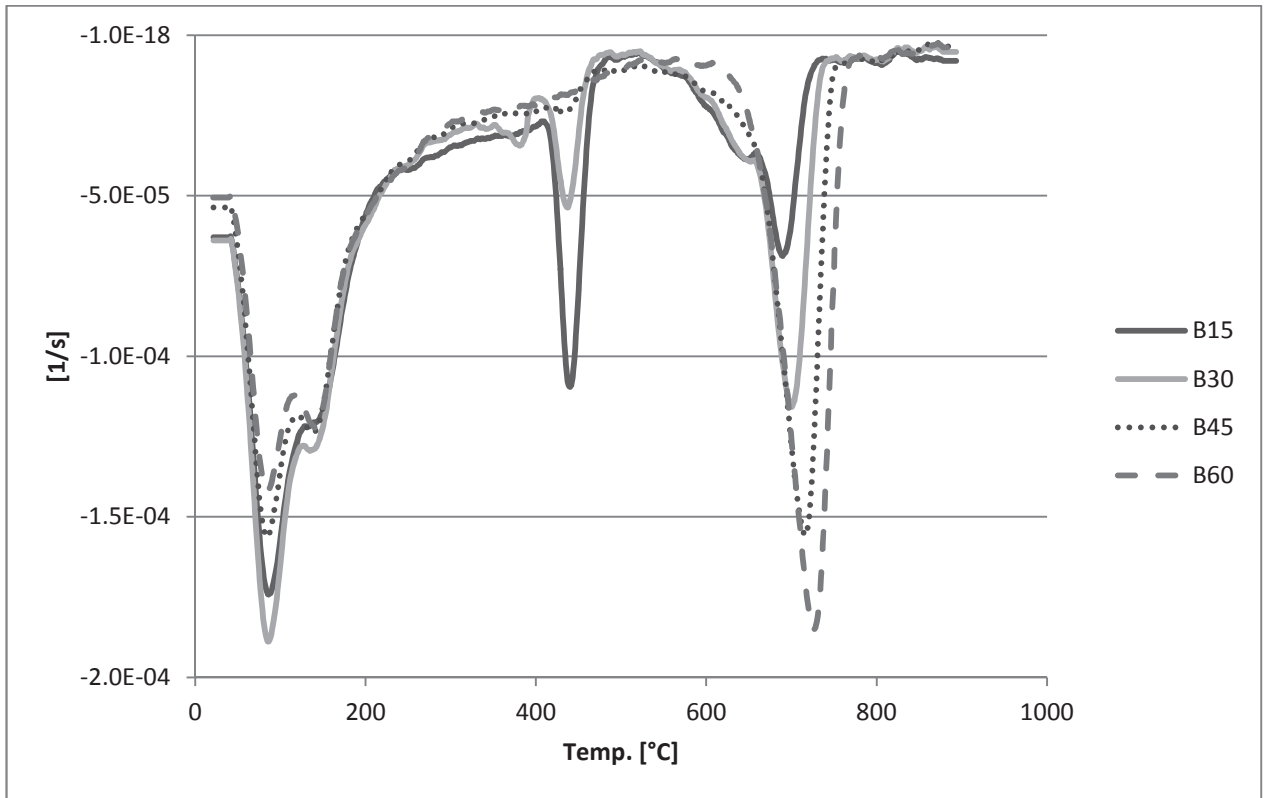


Figure 4.4: Evolution of the CH content (determined from TGA mass loss) normalized to the PC content in the paste.

In fact all these samples show a higher amount of Portlandite relative to the pure PC samples at the same age due to the so-called “filler” effect where the degree of reaction of the clinker phases is enhanced due to the extra space available for the hydrates [92]. The system with 30% metakaolin and all the blends of MK and LS, show significant reduction in the amount of calcium hydroxide even as early as 1 day. The higher the substitution rate, the stronger is the relative decrease in CH content.

In the 60% blend there is nearly total consumption of CH after only 7 days, which might be expected to limit later strength development in this blend. It is also interesting to compare B45 with the MK30 blend containing the same amount of metakaolin. The B45 system shows stronger consumption of calcium hydroxide after 1 day than MK30.

Figures 4.5 show the derivative of the mass loss as a function of temperature by TGA for all samples at 90 days. The total consumption of Portlandite by pozzolanic reaction is confirmed for MK30, B45 and B60. With curing time, there is also a growing peak with maximum around 140°C for B45 and 180°C for MK30 respectively. It is possible to assign these peaks to the presence of carboaluminates and strätlingite respectively. The peaks above 600°C are due to decarbonation, mainly from the non-reacted calcite in the case of LS15 and the blends but also to some carbonation by atmospheric CO₂ as well as reaction of isopropanol with C-S-H, as reported by Beaudoin et al [93].



Figures 4.5: Time derivative of the mass loss as a function of the increasing temperature obtained by TGA analysis of samples at 90days.

4.3.3. X-RAY DIFFRACTION

The XRD patterns (Figure 4.6) for the PC system show the formation of ettringite, monosulfoaluminate and a growing quantity of Portlandite. In the MK30 system (containing only metakaolin) there are ettringite and strätlingite at 7, 28 days and 90 days as well as monosulfoaluminate, along with less Portlandite. The limestone-PC blend (LS15) shows the formation of hemicarboaluminate from 7 days and monocarboaluminate from 28 days instead of monosulfoaluminate. In the B45 blend, which contains 15% of LS and 30% of MK, the formation of ettringite is enhanced in a similar manner, but there is a larger and increasing amount of hemicarboaluminate from 1 day throughout the period of study.

While in PC Ettringite and Monosulfoaluminate (Ms) hydrate form, MK addition leads to the formation of Strätlingite (Strät) and reduction of the Portlandite peak (CH). With Limestone addition in both LS15 and Blends systems, formation of Hemicarboaluminate (Hc) and later on Monocarboaluminate (Mc) are observed.

XRD data show also the development of the main crystalline alumina containing hydrate phases for all the blends. In the pure PC the amount of monosulphoaluminate grows over time. Some appears in the blends at 1 day but later on disappears. With increasing blending there is the formation of increasing amounts of hemicarboaluminate and ettringite at all ages. Ettringite increases with time for all blends, but seems to level off around 7 days. Hemicarboaluminate increases with time, for B30 and B45, while for B15 and B60 it seems to plateau at 28 days (however, due to the possibility of preferential orientation for these phases, these trends are only qualitative). Monocarboaluminate only starts to increase significantly after 28 days in the LS15 system, in the blends there is a low amount of this phase even at 90 days. It is interesting to note the persistent presence of the metastable hemicarboaluminate, while a significant quantity of unreacted calcite remains in the blends. It is possibly due to its relative coarse grain size distribution. Strätlingite is detected in both MK30 and B45 from 28 and 7 days respectively, also in presence of portlandite, meaning there are some chemical inhomogeneities over the sample.

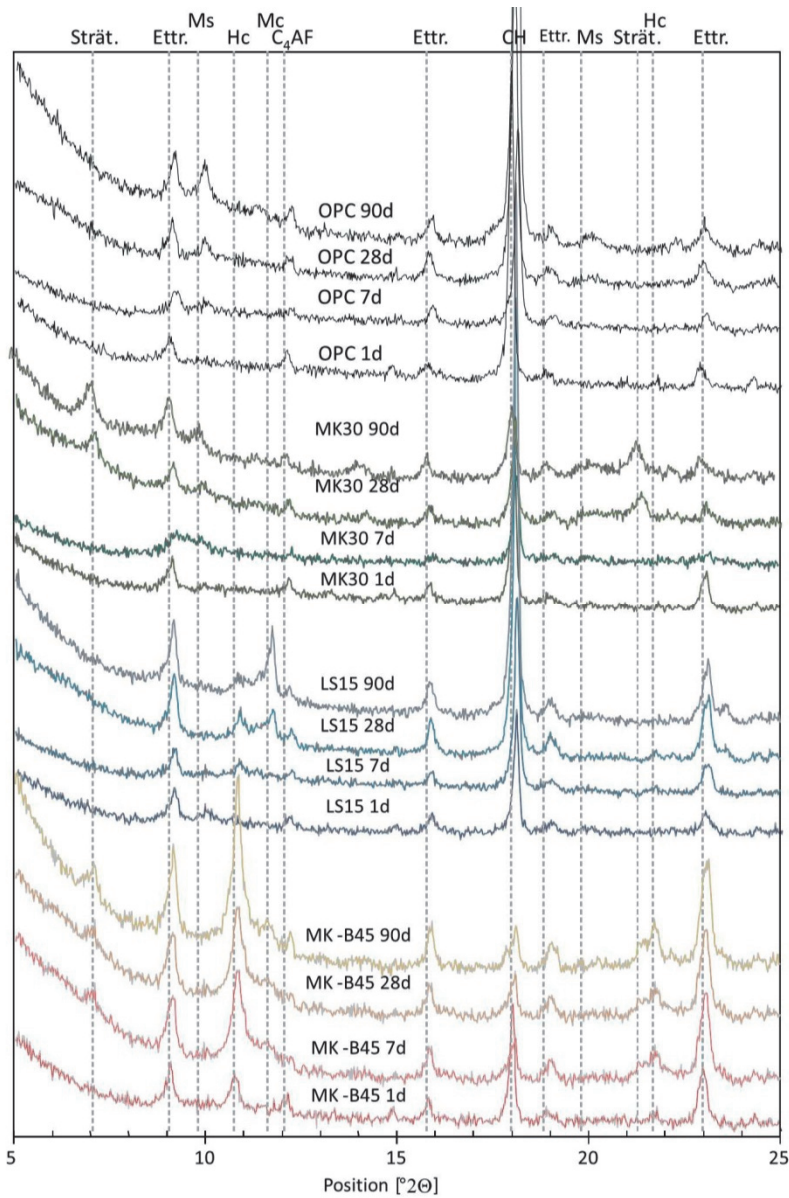


Figure 4.6: XRD patterns for PC, MK30, LS15, and MK-B45 at 1, 7, 28 and 90 days.

4.3.4. ESTIMATION OF DEGREE OF REACTION OF MK BY MASS BALANCE CALCULATIONS

To estimate the degree of reaction of the metakaolin simplified mass balance calculations were made based on Portlandite consumption by thermogravimetric analysis. For the metakaolin substituted sample, the difference between the Portlandite present in the equivalent quartz

reference (to take account of the filler effect) and the blend was considered to have reacted with metakaolin to produce C-A-S-H gel. For the blends, metakaolin was assumed to react with calcium carbonate and Portlandite to form hemicarboaluminate AFm and C-A-S-H gel.

Figure 4.7 shows the EDS microanalyses plotted as Al/Ca ratio against of Si/Ca (atomic %) ratio for B45 and OPC aged 300 days. due to the high level of intermixing with strätlingite, ettringite and metakaolin, it was difficult to determine the composition of the C-A-S-H gel for the calculations. This was taken as $(C_{1.67}A_{0.27}SiH_x)$.

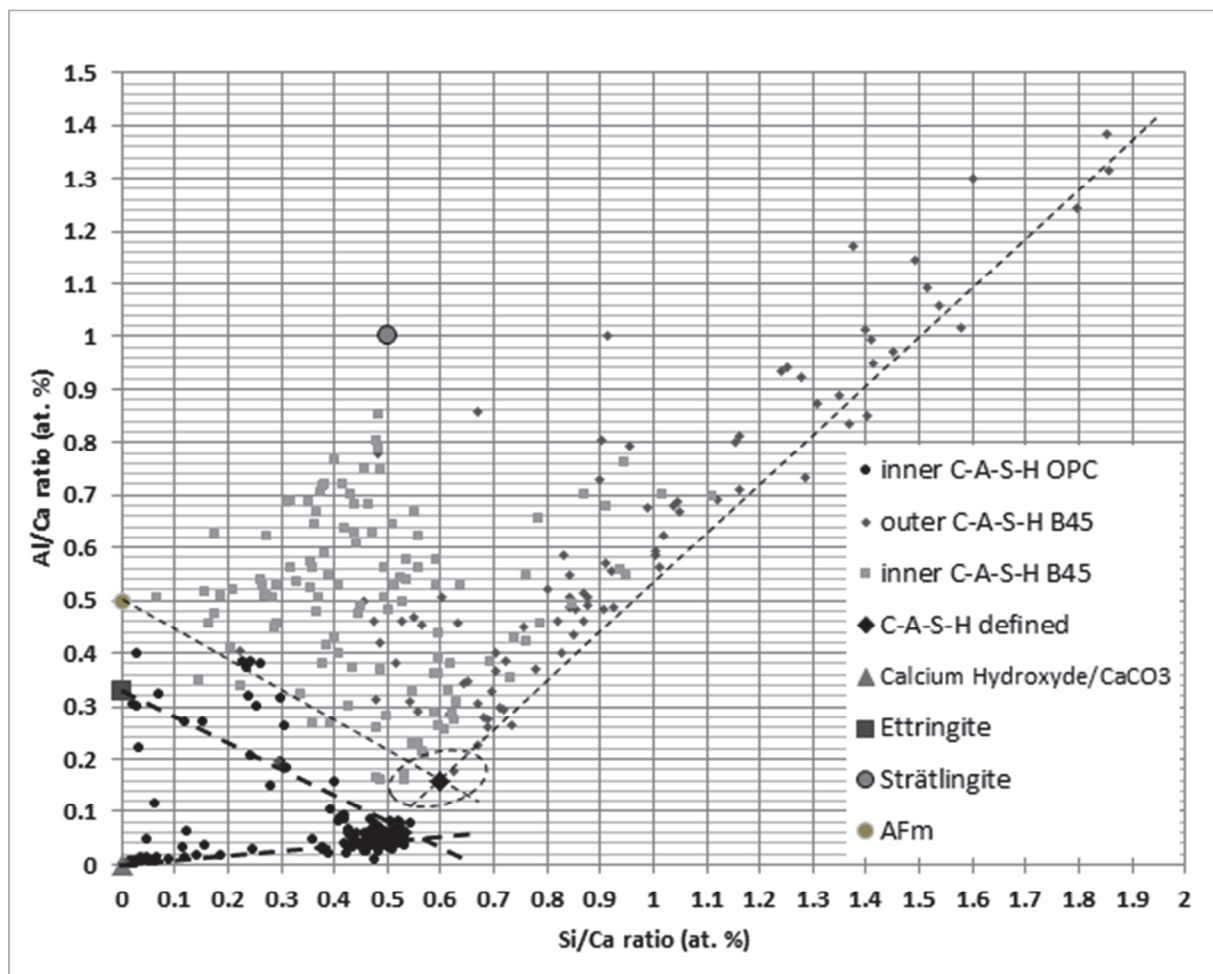


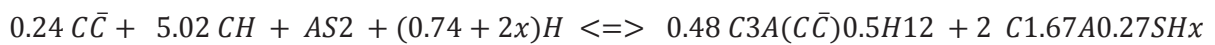
Figure 4.7: Graphical treatment of EDS points analysis obtained on a B45 300d old paste, Al/Ca ratio is plotted as a function of Si/Ca ratio (in atomic percentage).

The dotted lines join C-A-S-H with ettringite and with ettringite and form the lower limits in term of Al/Ca ratio of the cloud of measured points. The C-A-S-H composition in the blend lies within the dotted circle but cannot be precisely defined. The chosen C-A-S-H composition for mass balance

calculations is represented. For comparison inner C-A-S-H of OPC are given, where intermixing with Portlandite and AFm/Aft is observable.

The figure also indicates a shift in the composition of the C-S-H between the plain OPC system and the systems containing additions, similar to that widely observed in systems containing pozzolanic materials [92]. This indicates that some calcium for the reaction may come from the C-S-H. However, given the approximate nature of the calculation, the number of assumptions already made and the uncertainty of the EDS analyses, it was decided not to include this in the calculations.

The formula taken for the reaction of metakaolin (AS₂) is:



The main error in this calculation (Table 4.3 and Figures 4.8) is the fact that strätlingite formation was ignored. Strätlingite was observed by XRD in blends B30, B45, B60 after 7 or 28 days and remained present even after 300d.

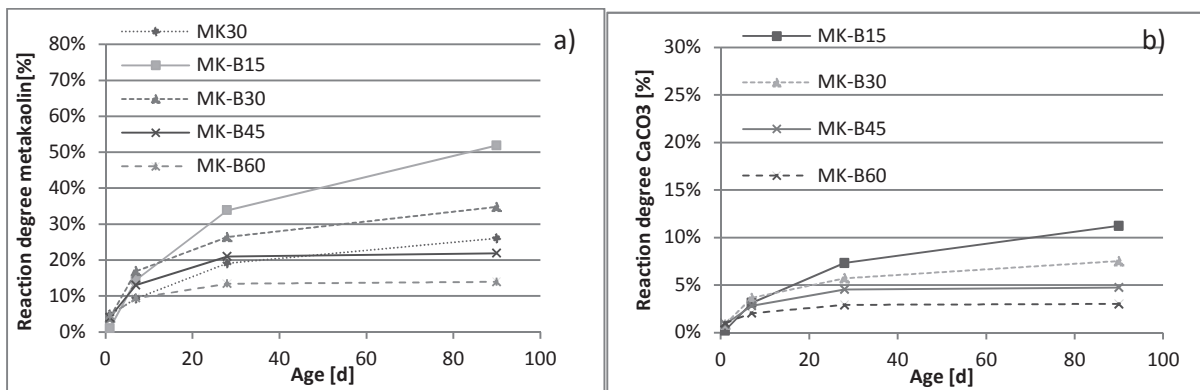
Table 4.3: The calculated reacted fractions of metakaolin (top) and calcium carbonate (bottom), based on the hypothesis of formation of hemicarboaluminate and C-A-S-H gel based on the Portlandite consumption measured by Thermogravimetry Analysis.

metakaolin reacted fraction					
	MK30	MK-B15	MK-B30	MK-B45	MK-B60
1	5%	1%	4%	4%	5%
7	9%	14%	17%	13%	9%
28	19%	34%	26%	21%	13%
90	26%	52%	35%	22%	14%

CaCO ₃ reacted fraction				
	MK-B15	MK-B30	MK-B45	MK-B60
1	0.2%	0.9%	0.9%	1.0%
7	3.1%	3.7%	2.8%	2.0%
28	7.3%	5.7%	4.6%	2.9%
90	11%	7.5%	4.7%	3.0%

This means that the degree of reaction of the metakaolin is underestimated as strätlingite formation only consumes 3.7 moles of calcium hydroxide per mole of metakaolin as opposed to 5-6 moles for the formation of C-A-S-H and hemicarboaluminate. Other errors may be introduced by the fact that metakaolin has a finer particle size than the quartz filler, so the extra Portlandite produced by filler effect may be underestimated, although the effect of filler size has been found to be minor after 3 days [94] and by the assumption that only hemicarboaluminate is formed, as monocarboaluminate consumes more calcite. Although a decrease in the peak from the decomposition of calcite was also observed, this could not be quantified reliably, due to variations in the small degrees of carbonation of the pastes and the storage in isopropanol.

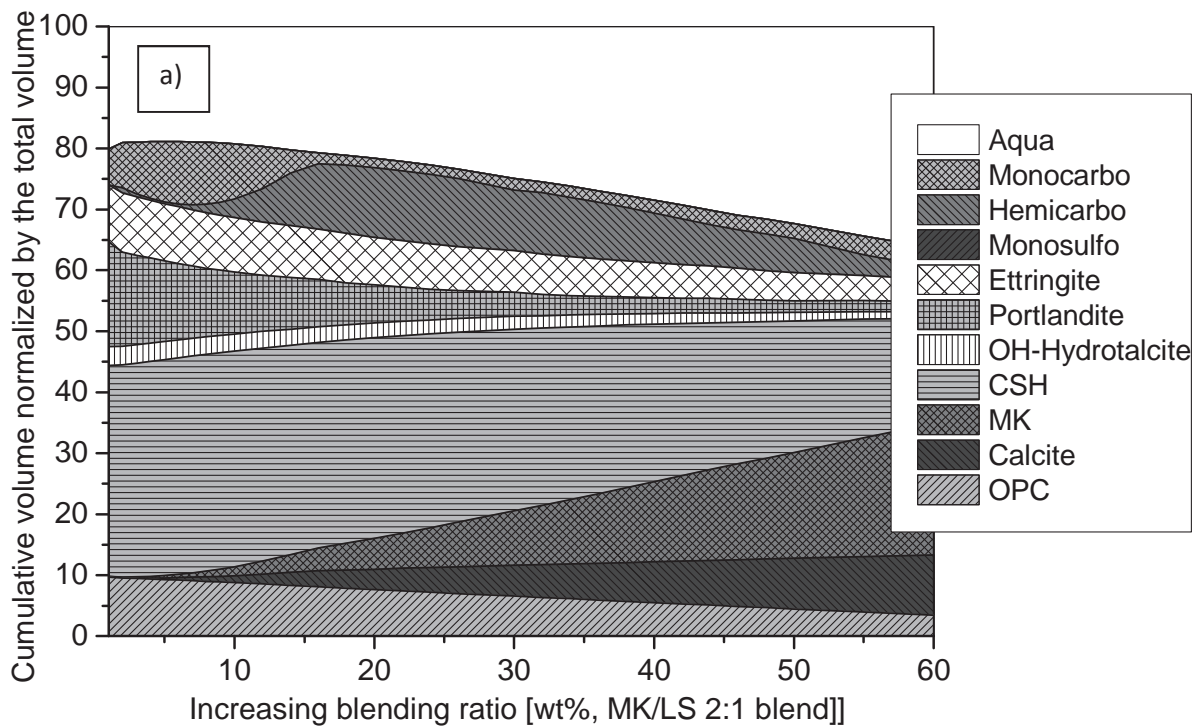
The mass balance calculations in Table 4.3 and Figures 4.8 show the degree of reaction of metakaolin, increases with time, reaching a maximum value of 52% for B15 at 90 days. The degree of reaction increases with blending at 1 day but decreases at all later ages, although this is thought to be misleading due to the important amount of strätlingite formed in the blends with higher levels of substitution. The combined addition of limestone in B45 shows a similar degree of reaction of metakaolin to MK30 at 1 day, then enhanced metakaolin reactivity at 7 and 28 days. The MK30 and the blend have similar degrees of reaction at 90 days, when the strätlingite error is considered. The low degree of reaction in the B60 blend suggests a limitation to the reaction due to Portlandite exhaustion.



Figures 4.8: Metakaolin (a) and limestone (b) reactivities calculated by mass balance

4.3.5. THERMODYNAMIC MODELLING

Thermodynamic modelling was carried out using the Gibbs free Energy Minimization program GEMS [95]. The effect of increasing cement substitution by blending at the chosen 2:1 weight ratio metakaolin:limestone was studied. The C-S-H composition was amended to take account of the calcium to silica ratio and aluminium incorporation measured by EDS analysis as described above. Si-hydrogarnet, goethite and hematite were excluded because they do not precipitate for kinetic reasons at 20°C. The exact chemical compositions of the raw materials used (Table 4.1) was taken as input in the GEMS program. The C-A-S-H gel molar volume in GEMS are taken from the work of Kulik et al [96], the value does not include gel porosity and was not adjusted for the aluminium incorporation as there are no data available to account for it. The data are shown as volumes relative to the total volume considered (for 100g of blend) to take account of the different densities of the components. The plot, Figure 4.9 a), assumes the degree of reaction of cement as 80%, and the degree of reaction of metakaolin and limestone calculated (Table 4.3). The phase assemblages agree qualitatively with the experimental observations, except for the absence of strätlingite which is not predicted to form in the thermodynamic calculation.



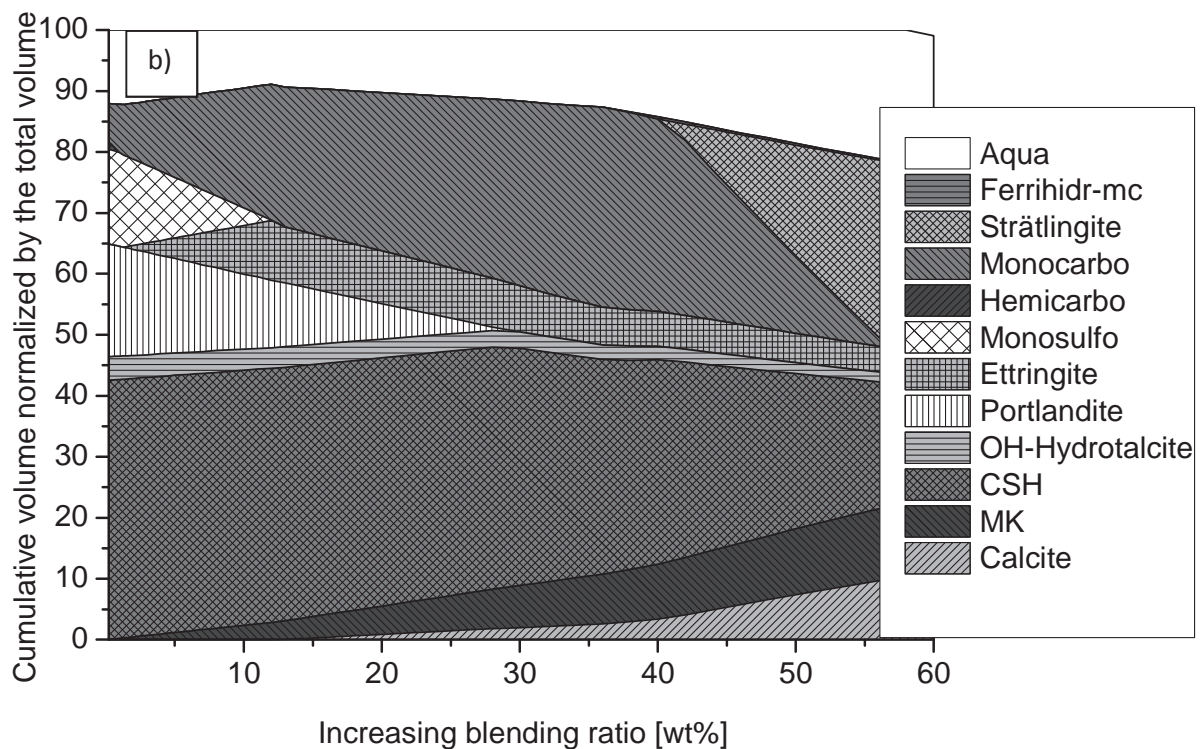


Figure 4.9 a) et b) : Thermodynamic simulations of the phase assemblage with increasing substitution of cement by our 2 :1 metakaolin :limestone blend.

The total cumulative volume of solid products is represented as a function of increasing blending percentage. In the first figure the reactivities of limestone and metakaolin obtained from mass balance calculations in the hypothesis of formation of hemicarboaluminate and real $C_{1.67}A_{0.27}SH_x$ are used, while in the second the limestone is let freely reacting and metakaolin fixed at 50% reactivity. PC was supposed to react at 80% in case a) and 100% in case b).

For comparison, the b) scenario is shown where the degree of reaction the cement is 100% and that of metakaolin is kept constant at 50%. Limestone is allowed to react freely. This version shows the appearance of strätlingite from 40% blending and the disappearance of Portlandite above 30% blending. This suggests that the degree of reaction of the metakaolin may indeed be underestimated. This second version shows only monocarboaluminate in contrast to hemi and monocarboaluminate in the first graph.

Regarding the solid volume, in the first version (calculated degrees of reaction) this remains roughly constant up to about 20% blending and then decreases slowly to about 80% of the pure PC at 60% blending. In the second case (100% PC reaction, 50% MK) it increases up to 3% and then decreases to about 90% at 60% blending.

Figure 4.10, shows the strength of the mortars at 90 days against the porosity calculated by GEMS for 4.9 a) scenario. Densities of anhydrous and hydrated phases used in the calculation were directly taken from the CEMDATA database, included in GEMS [95]. Note in addition that the calculated porosity corresponds to the left over water, without considering additional porosity that can arise from self-desiccation of pores or any capillarity volume increase due to the restrained prisms dimensions.

Although there is a general trend of decreasing strength with increasing porosity, the correlation for this small number of points is not strong and up to 45% level of blending there is almost no decrease in strength despite a significant increase in porosity.

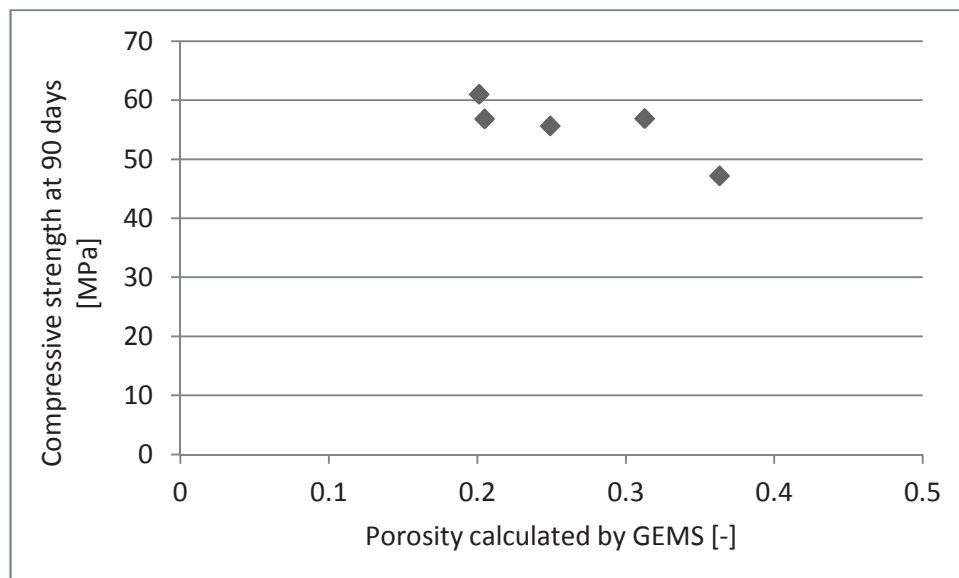


Figure 4.10: Compressive strength at 90 days represented as a function of its corresponding porosity calculated by GEMS.

It must be noted, that the density used for the C-S-H in the GEMS calculations does not include gel porosity, which is consequently included in the overall porosity, whereas such gel porosity is not usually considered detrimental to strength.

4.3.6. POROSITY

The results of Mercury Intrusion Porosimetry at 28 days are shown in Figure 4.11. The total porosity is higher for all the blended systems with the exception of B15. However, there is a refinement of the pore microstructure for all the blended systems compared to the pure PC, except for B60. These changes in pore size distribution probably also contribute to the lack of good correlation between strength and porosity calculated by GEMS discussed above.

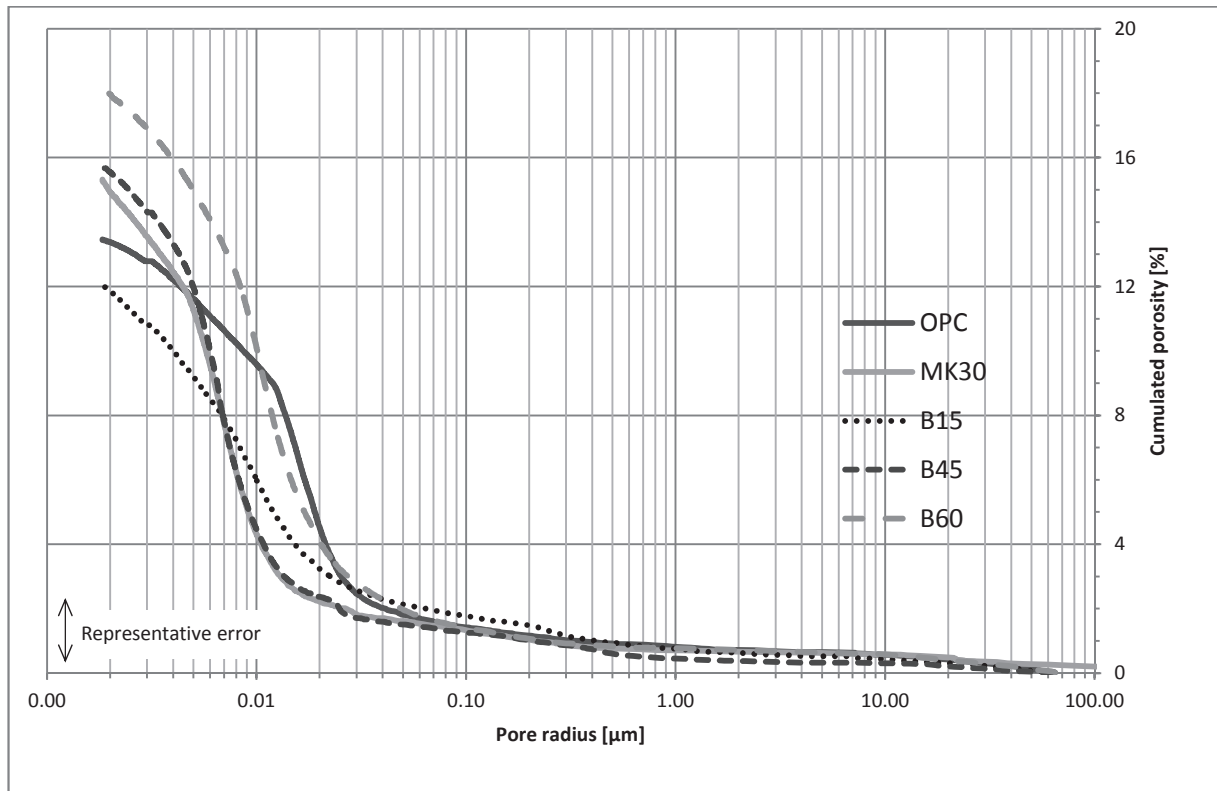


Figure 4.11 : Cumulated porosity as a function of pore entry radius at 28 days obtained by Mercury Intrusion Porosimetry.

A small and broad shoulder peak is seen in the plain Portland cement with low C₃A content, corresponding to the second formation of ettringite [97, 98], with a later peak even lower and broader associated to conversion of ettringite into monosulfate. Nevertheless in presence of metakaolin the first aluminate peak increases in intensity, is narrower and occurs earlier.

The second “conversion” peak occurs much earlier in the B45 and is merged together with the first peak in the case of higher blending percentage. It is not yet clear how metakaolin contributes to this peak, it can be supposed that it provide a considerable amount of new surface for heterogeneous nucleation of hydrates. It was not possible to determine whether aluminates originating from the metakaolin also participate in the reaction at this stage.

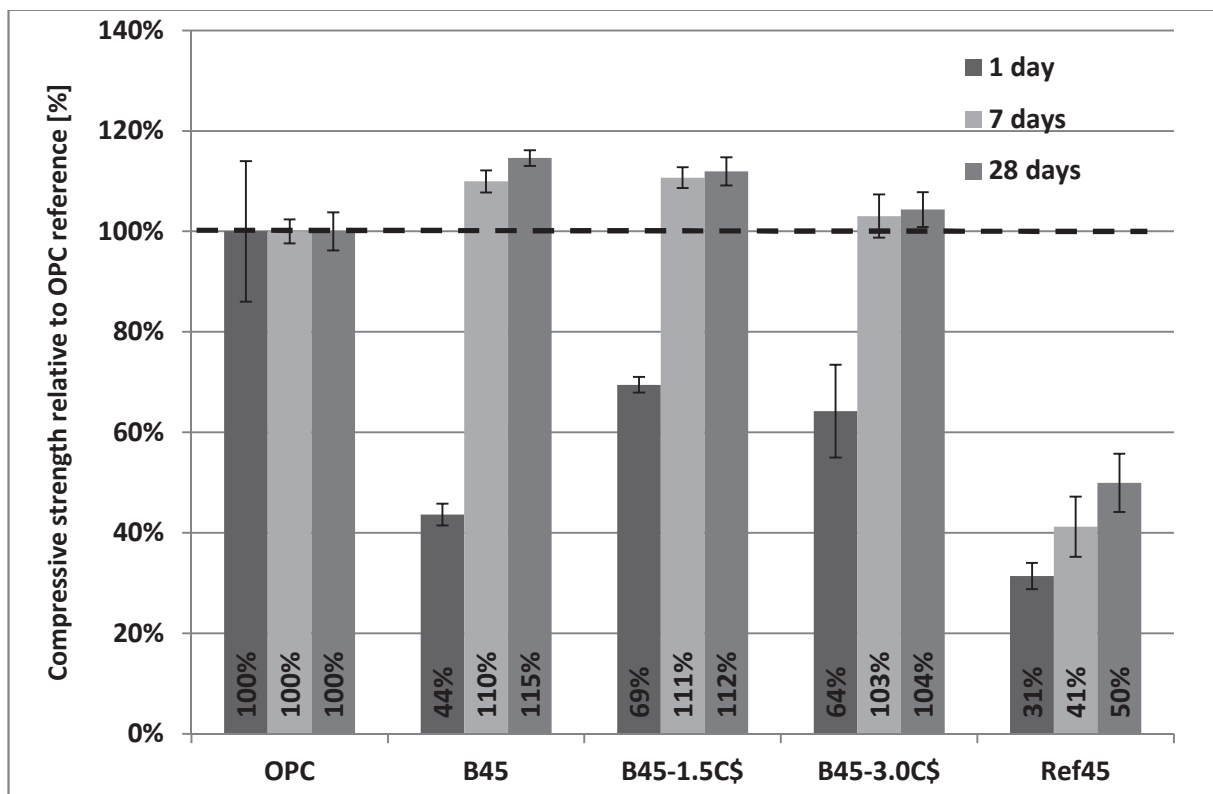


Figure 4.13: Evolution of the mechanical strength of Blends systems at 45% substitution as a function of the gypsum added at all ages.

For the highest levels of addition the systems appear under sulfated, with the sulfate depletion occurring before the maximum of the peak of the main silicate reaction.

Therefore the impact of adding extra gypsum to the blends was investigated. The results of gypsum additions of 1.5 and 3% on the compressive strengths of the B45 blends are shown in Figure 4.13 and calorimetry in Figure 4.14.

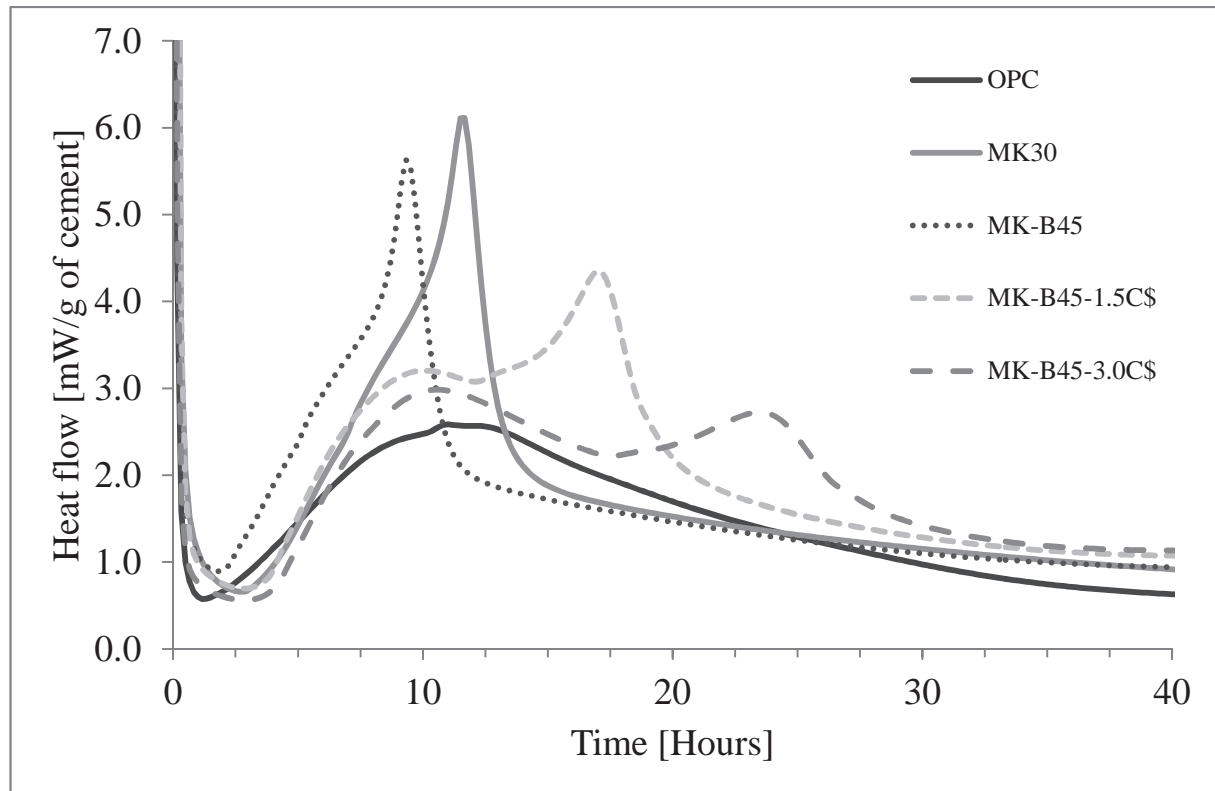
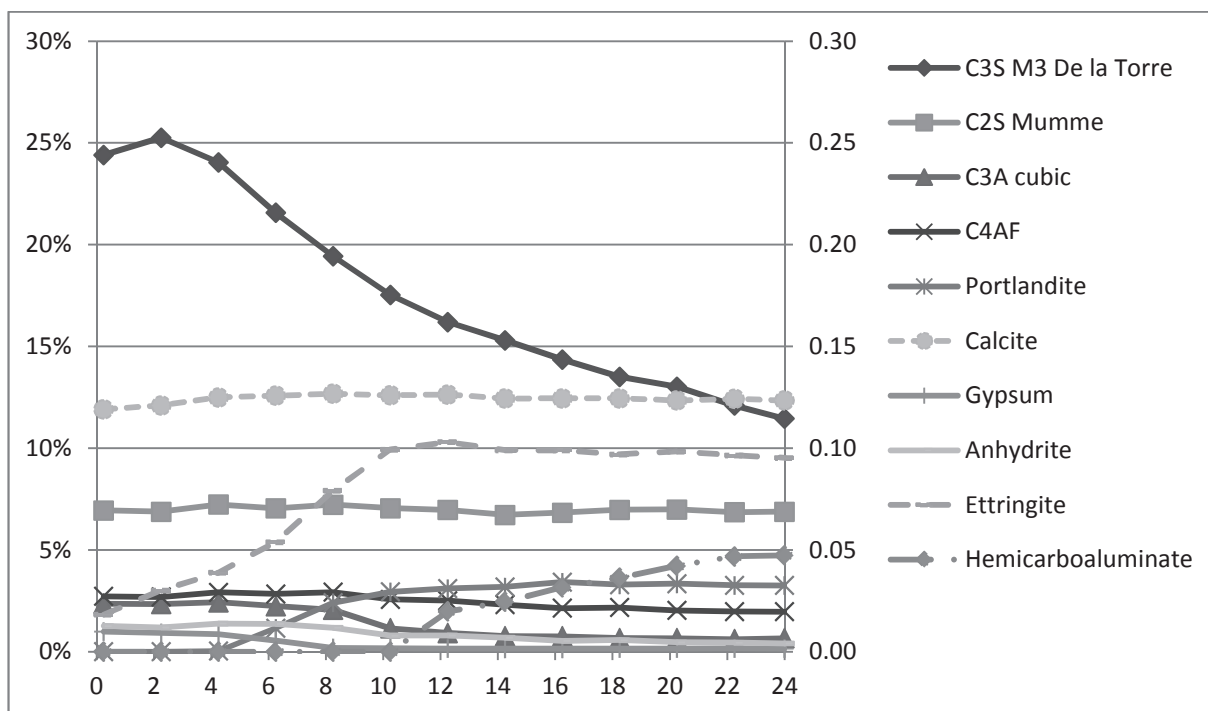
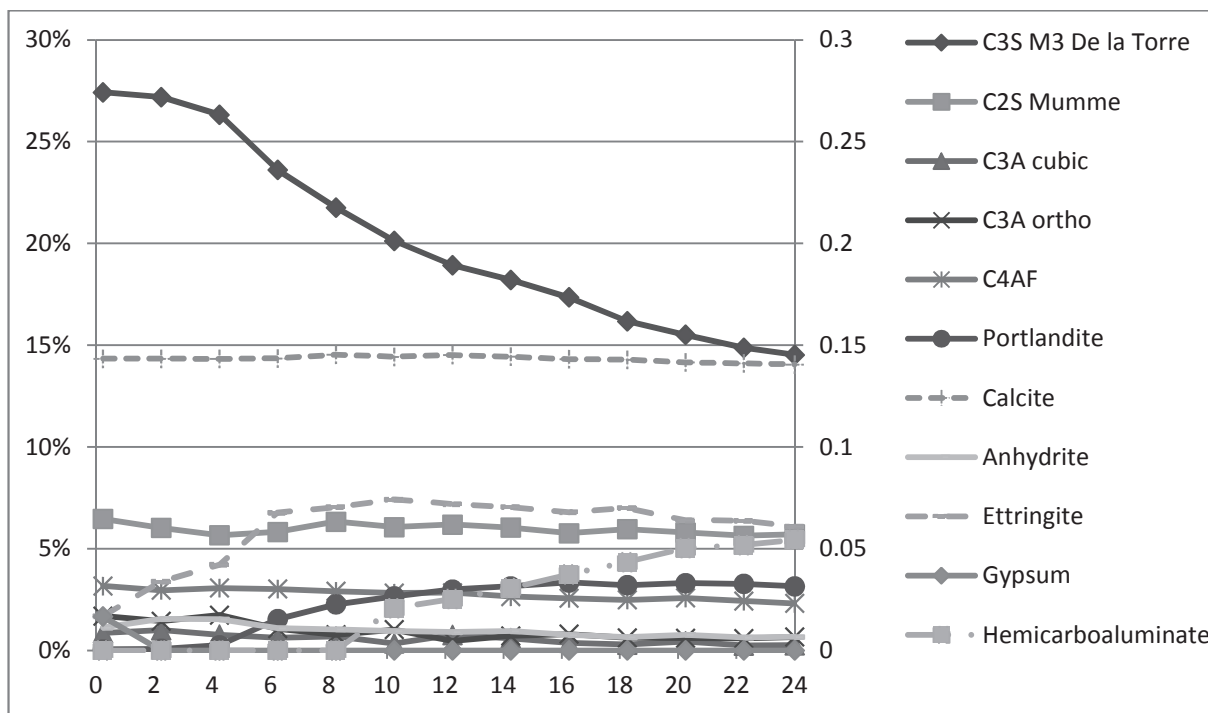


Figure 4.14: Isothermal calorimetric curves plotted for Blends systems at 45% substitution with different gypsum contents

With increasing sulfate content the strength at 1 day is considerably improved with 1.5% addition (69% of the reference pure PC compared to 44% without addition) and then slightly decreased to 64% with 3% addition. In the latter case the aluminate peak is not completed by 24 hours. At 7 and 28 days, compressive strengths are very similar across the range of gypsum additions.

In-situ XRD measurements with Rietveld refinement confirm the beneficial effect of 1.5wt% gypsum addition on the degree of reaction of C_3S at one day, which is increased from 47 without addition to 53%. The amount of ettringite also increases (from 5.9% with no addition to 10.5% with gypsum addition), Figures 4.15). For hemicarboaluminate, as there are no structural data available; a model phase derived from the unit cell parameters commonly accepted in the literature [99] has been used to estimate semi quantitatively its variation, which is plotted on a second axis.



Figures 4.15 : Evolution of phases obtained by Rietveld refinement of in-situ XRD during the first 24h of hydration for B45 (top) and B45 + 1.5wt% gypsum (bottom).

Gypsum addition enhances C_3S hydration as well as ettringite formation. The additions of gypsum will not lead to expansion as the total SO_3 content is still well below the threshold of 5 to 6% SO_3 , commonly accepted in the literature for expansion [100]

4.4. CONCLUSIONS

This study shows coupled substitutions of metakaolin and limestone for Portland cement can give excellent performance at relatively early ages. Up to 45% of substitution a 2:1 blend of metakaolin and limestone yields better mechanical properties at 7 and 28 days than the 100% Portland cement reference. Even 60% substitution has 93% of the pure Portland reference strength at 28 days. The XRD results show that calcium carbonate reacts with the aluminates in the metakaolin, forming significant amounts of hemicarboaluminate and to a lesser extent monocarboaluminate from as early as 1 day. Thermodynamic simulations coupled with simplified mass balance generally supported the experimental observations of the phase assemblages formed.

TGA shows that the reactions of metakaolin and limestone consume calcium hydroxide, which may be completely absent in blends with high levels of substitution at late ages. The metakaolin appears to react faster in the system with limestone than in the binary metakaolin / Portland cement blend. Also, the limestone reacts faster in the system with metakaolin than in the binary limestone / Portland cement blend. These results point to strong synergistic effects with coupled substitutions of this type. Of course the consumption of calcium hydroxide could mean that the high substitution level blends may carbonate more rapidly. This and other aspects of durability are currently being studied.

It was also shown that the level of sulfate addition has an important effect on the early strengths of the blends. In systems containing high volumes of fine calcined clays, the sulfate content should be adjusted in order to prevent undersulfation.

Acknowledgements

The Fonds National Suisse is acknowledged for funding this work, part of the FNS Project “Production of activated clays for low cost building materials in developing countries”. Barbara Lothenbach, EMPA helped with advice on the thermodynamic calculations, Ruben Snellings is thanked for his useful contribution to the in-situ XRD and the Rietveld refinement results. Burgess Pigment company is thanked for the donation of the Optipozz® Burgess metakaolin.

Chapter 5 : STRENGTH OF BLENDS WITH NATURAL CALCINED CLAYS

5.1. INTRODUCTION

In the previous chapter, the feasibility of blending cement with combined addition of metakaolin and limestone has been demonstrated. In order to generalize the use of such a blend, the blending should be tried with different natural clays. Unlike clays with high kaolinite content that are in high demand for the ceramic or the paper industry, the price of clays with average kaolinite content (30-70%) is accessible for the construction industry. It is therefore highly relevant to study various natural clays, with different kaolinite content.

The different results obtained during the thesis with natural clays are presented in this chapter. Due to the particularities of this collaborative project and the delay generated with the design and the fabrication of the Clay Activation Unit, the different results obtained during the thesis are presented according to chronological order. The importance of key cement parameters such as alkali, sulfate and limestone content has been underlined. The summary of the samples studied is given in Table 5.1.

- As an introduction, results of Fernandez's thesis [8] are reinvestigated considering the knowledge established in the previous chapter.
- A brief review of the different crucial parameters that need to be considered is given in the second section.
- Ternary blends made in Cuba and in Switzerland are then presented.
- The results of the investigation of the effect of the different calcination processes are presented in the last section.

Table 5.1: Summary table of all samples reported in this chapter.

	Cement	Na ₂ O _{eq} [wt%]	SO ₃ adjustment	Cement CaCO ₃ content [wt%]	Clays studied	Substitution rate	Temperature [°C]
Fernandez-series 1	PC6	0.87	-	0	K, I, M, Mani	30%	30
Fernandez-series 2	PC7	0.93	-	4.1	K, I, M, Mani	30%	30
Series 3	PC5	0.71	-	5	MK, Ar, Mani	30%, B15, B45	30
Series 4	PC1	0.82	-	0.6	MK, Ar, Cu	30%, B15, B45	23
Series 5	PC1	0.82	-	0.6	MK, Pont	30%, B45	23
Series 6	PC3	0.55; 0.8	Yes	1	MK, Pont	30%, B45	23
Series 7	PC4	0.55	Yes	6.5	K, M, KQ, MQ, KMQ, Mani	30%	30

-“K”, “I”, “M”, “Mani”, “Cu”, “Ar” & “MK” stand for Kaolinite, Illite, Montmorillonite, Cuban clay deflocculated, raw Cuban clay, Argeco and Metakaolin respectively.

KQ, MQ & KMQ used in Series 7 are model clays, made by mixing 45% kaolinite and 55% quartz, 45% montmorillonite and 55% quartz; 45% kaolinite, 45% montmorillonite and 10% quartz respectively

XRF compositions and key characteristics of the Materials are presented in Section (3.1.1)

5.2. REINVESTIGATION OF FERNANDEZ’S RESULTS

In his PhD thesis [8], Rodrigo Fernandez studied blended cements with 30% substitution with different calcined clays. He cast mortars with 0.5 water/binder ratio. His most interesting results were obtained with a Cuban calcined clay containing only 40% kaolinite content.

In the best series, this showed the same strength as reference Portland cement mortar at 7 and 28 days. One of the objectives of the current thesis was therefore to confirm Fernandez’s results with other natural clays.

His main results are given in Figure 5.1.

-600, 800 or 925 indicate calcination temperature.

-Finally 1 or 2 distinguish the different series, made with 2 different cements.

From this figure it is clear that the best results are obtained with the purest kaolinite sample, K600. The Cuban clay delivers the next best strength performance, with both cements. Illite and montmorillonite calcined at 600°C show almost no pozzolanic contribution, with strengths similar or lower than filler.

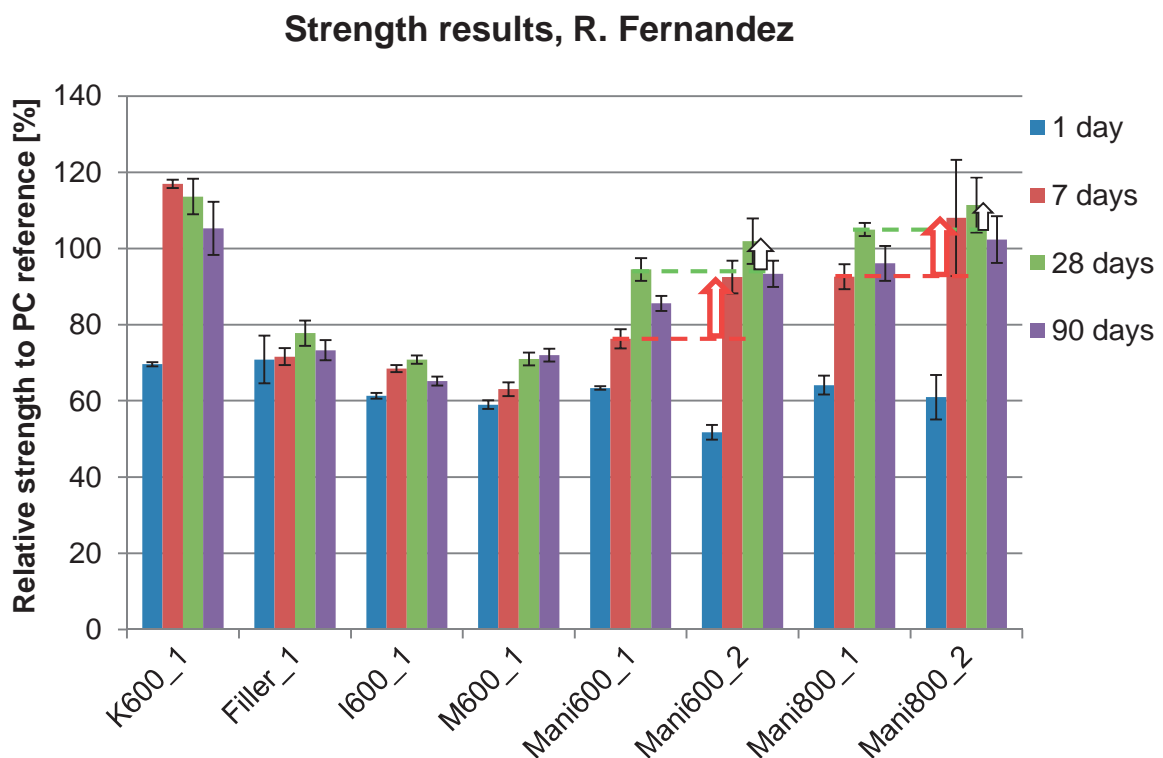


Figure 5.1: Compressive strengths obtained during Rodrigo Fernandez PhD work [8]

Fernandez's results were obtained at 30°C to match Cuban conditions. Most of the current work has been carried out at lab temperature, around 23°C. This is likely to give a small comparative advantage to Fernandez's results, since pozzolanic materials usually have higher activation energy than cement.

But it is fundamental to reconsider his results taking into account the knowledge of the synergetic effect due to the carboaluminates phases formation before any further natural clay investigation. Two different cements have been used by Fernandez; they had very similar alkali levels, but cement

used in series 2 contained almost 4.5% limestone while series 1 did not have any limestone. The Cuban clays are plotted next to each other (Figure 5.1) to better observe the differences. Indeed there is a clear improvement of the relative strengths with series 2, especially at 7 and 28 days, still visible at 90 days. There is no visible effect at 1 day.

The XRD diffractograms carried out on pastes made with same cement at 28 days confirm the formation of both important amount of hemicarboaluminate and monocarboaluminate for these materials (see Figure 5.2). The synergetic formation of carboaluminates can most likely explain the differences observed by Fernandez.

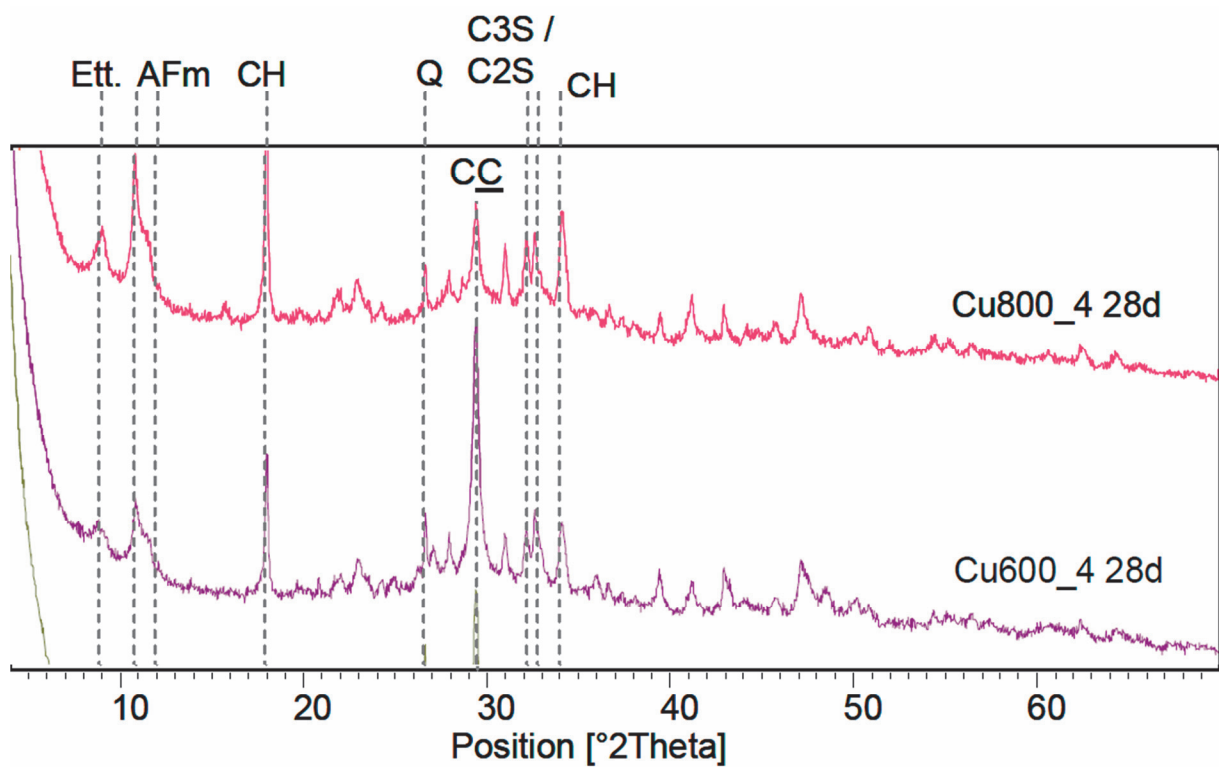


Figure 5.2: XRD Diffractograms for the Cuban clay calcined at 600 and 800°C with cement from series 2. Both carboaluminates peak are present in considerable amount after 28 days curing at 30°C[8].

5.3. INVESTIGATION OF SOME KEY PARAMETERS

5.3.1. ALKALI CONTENT

The compressive strengths of MK30 blends relative to their respective Portland cement reference as a function of the Portland cement equivalent alkali content [$\text{Na}_2\text{O}_{\text{eq}}$] at 1, 7 and 28 days are reported in Figure 5.3. Different Cem I cements have been used; only the metakaolin content, the added gypsum content and the superplasticizer were kept constant. Results are plotted together to show the determining influence of alkali content at 1 day. This effect is only pronounced at 1 day, and at 7 days the compressive strength gain is only visible for an increase from 0.55 to 0.66 % $\text{Na}_2\text{O}_{\text{eq}}$ and at 28 days there is almost no effect anymore. On the contrary from 7 days on it is possible that strength reaches its maximum for $\text{Na}_2\text{O}_{\text{eq}}$ content between 0.66 and 0.8 but more data would be required to fully confirm this trend.

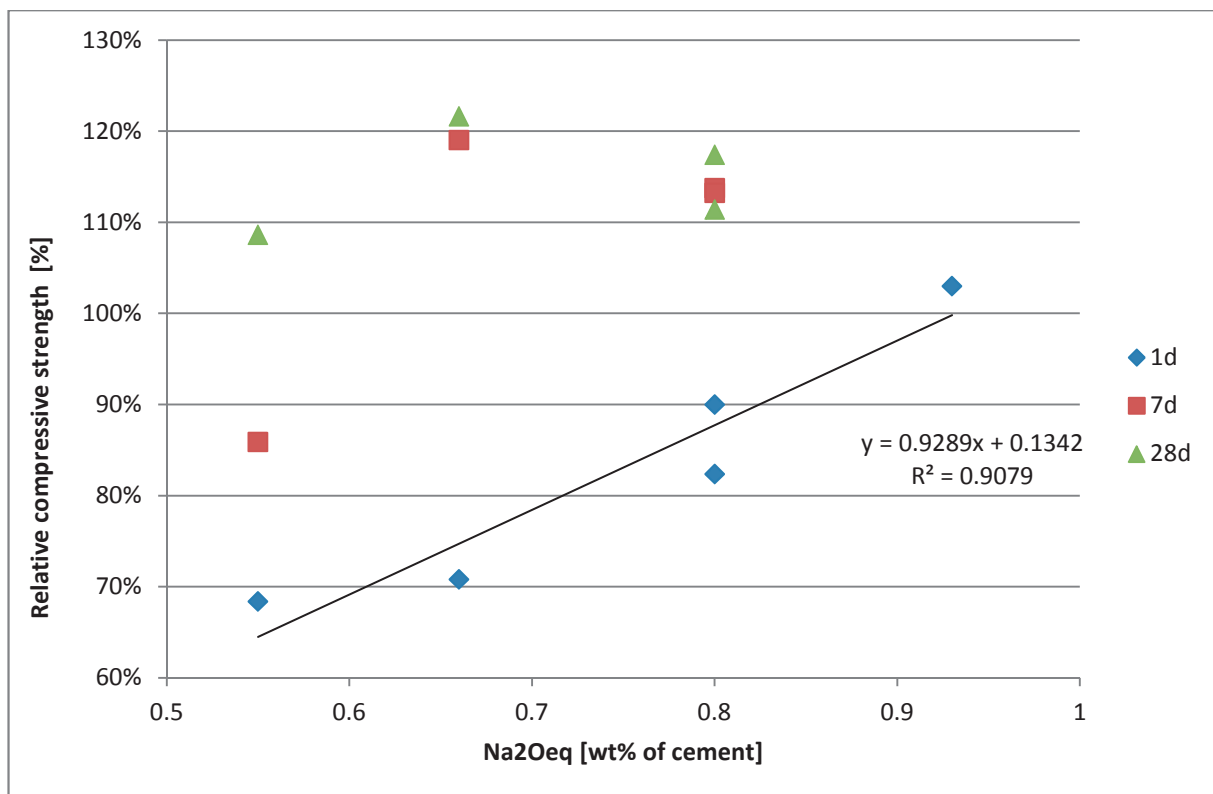


Figure 5.3: Plot of the relative compressive strength obtained at 1, 7 and 28 days as a function of the equivalent alkali content of cement in blends containing 30% pure metakaolin.

In order to investigate the influence of the alkalinity on a single system, the alkali content of the PC3 cement has been varied at 2 different levels; 0.58% and 0.8% Na₂O_{eq}. The results are presented in Figure 5.4. It confirms that increasing alkali to 0.8% benefits considerably to blended cement containing calcined clays, for both pure metakaolin (MK30) and the calcined Pontezuela clay (FC850-30) used here, at all ages. The positive effect is still present at 1 and 3 days but reduced for the MKB45 blend containing simultaneous addition of calcined clays and limestone.

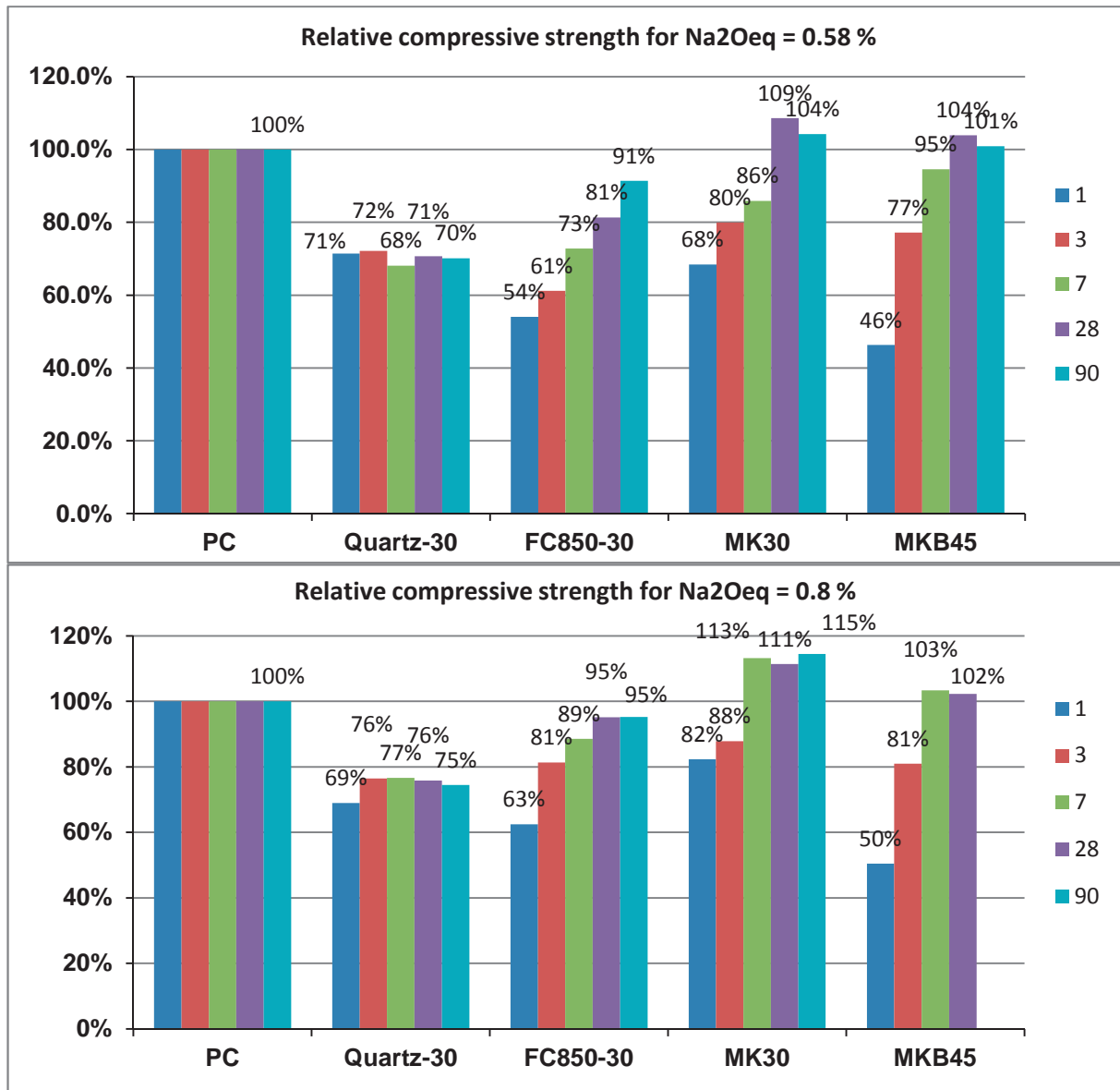


Figure 5.4: Strengths relative to PC3 at 2 different alkali contents for various blends (series 6).

Note that looking only at relative values compared with PC reference could be misleading, since not only the absolute compressive strength values of blends containing calcined clays increase, but also compressive strength of the reference PC slightly decreases. Absolute values are given in Table 5-2

Table 5.2: Compressive strength absolute values, for 0.55 and 0.8% Na₂O_{eq}

* Compressive strength [Mpa]					
Na ₂ O _{eq} 0.55%					
Age [days]	PC3	Quartz30	FC850-30	MK30	MKB45
1	33.5 (0.2)	23.9 (1.6)	18.1 (0.5)	22.9 (0.7)	15.5 (0.2)
3	52.4 (1.1)	37.8 (1.2)	32.0 (0.7)	41.8 (4.7)	40.4 (0.8)
7	60.1 (3-1)	40.9 (1.2)	43.8 (0.8)	51.6 (6.3)	56.9 (3.2)
28	68.0 (3.0)	48.1 (1.7)	55.3 (2.8)	73.8 (2.2)	63.2 (2.0)
90	70.0 (0.9)	49.1 (2.1)	64.0 (1.1)	73.0 (1.3)	70.7 (3.2)
Na ₂ O _{eq} 0.8%					
Age [days]	PC3	Quartz30	FC850-30	MK30	MKB45
1	32.1 (0.8)	23.1 (0.7)	20.0 (1.0)	26.4 (1.1)	16.2 (0.5)
3	50.2 (1.6)	38.4 (2.1)	40.8 (2.1)	44.1 (0.6)	40.7 (3.6)
7	55.5 (0.2)	42.5 (0.9)	49.1 (1.5)	62.8 (2.4)	57.3 (3.7)
28	63.2 (1.0)	47.9 (0.7)	60.1 (1.7)	70.4 (3.2)	64.6 (2.7)
90	66.6 (1.0)	49.6 (1.2)	63.4 (1.7)	76.3 (1.1)	/

*(standard deviation in brackets)

In order to understand the influence of the alkalinity, isothermal calorimetry, XRD and TGA were carried out on equivalent pastes systems. NaOH was added to the mixing water so that the equivalent alkali content was increasing by steps of 0.25wt%. The heat release normalized by weight of anhydrous cement is plotted in Figure 5.5 and the cumulated heat over 6 days in Figure 5.6. During the first 24 hours, a slight acceleration of the hydration is observed with increasing alkali content. But over 6 days there is almost no effect and all curves converge together. TGA and XRD on pastes of 7d were also carried out and no significant differences for the portlandite content were found.

Calorimetry, TGA or XRD did not provide any arguments to explain the influence of alkalinity on strength. This effect of alkali content on PC strength development is still poorly understood, contradictory results have been reported in the literature. But it seems that alkali, by modifying pore solution ionic strength and adsorption processes can modify hydrates morphology and growth; and mostly tend to increase C-A-S-H gel density and consequently affect strength development. Further

investigations should be carried out to understand the positive effect of alkalinity for blended cements containing calcined clays or any SCMs.

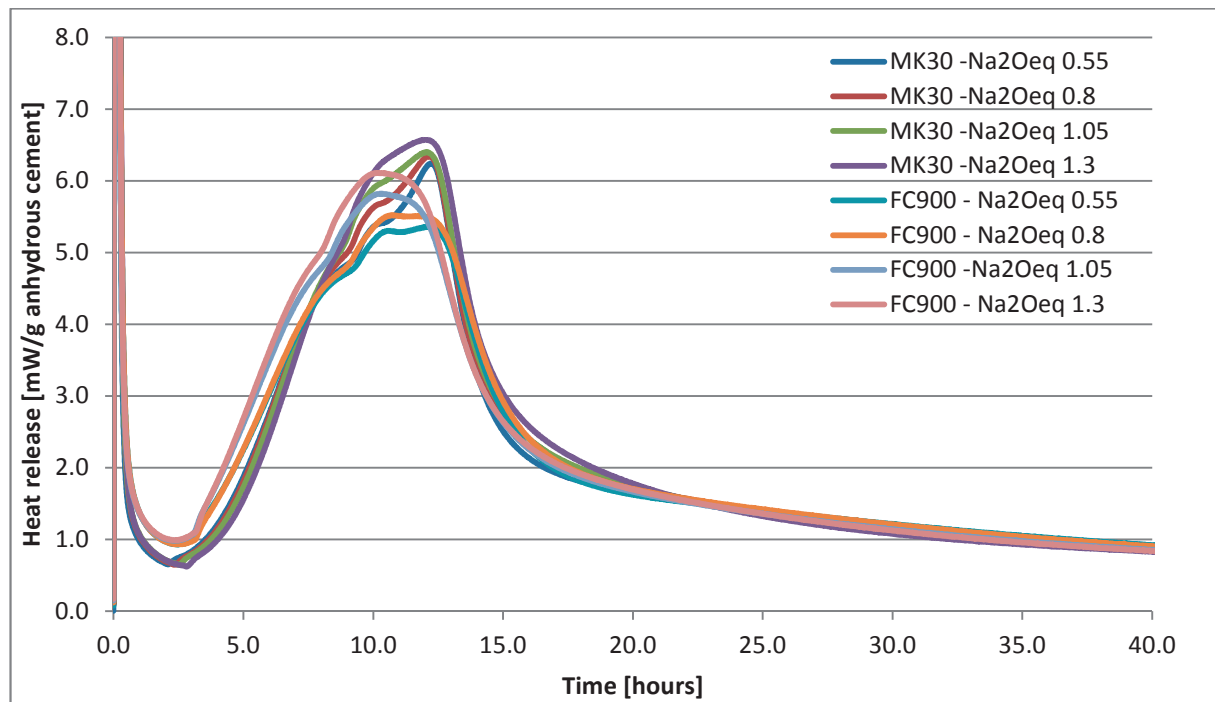


Figure 5.5: Heat released normalized by mass of cement for pastes with 30% calcined clays and different alkali addition at 20°C.

Another possible strategy to adjust alkalinity is also to take advantage of the need to adjust sulfate and add alkali sulfate. Figure 5.7 shows an example of addition of sodium sulfate Na_2SO_4 to the MK-B45 blend with PC1. The use of 1 and 2% Na_2SO_4 significantly enhances strength at 1 day, to respectively 90 and 130% of the PC value, but notably decreases the strength at later ages with strength values lower than PC reference.

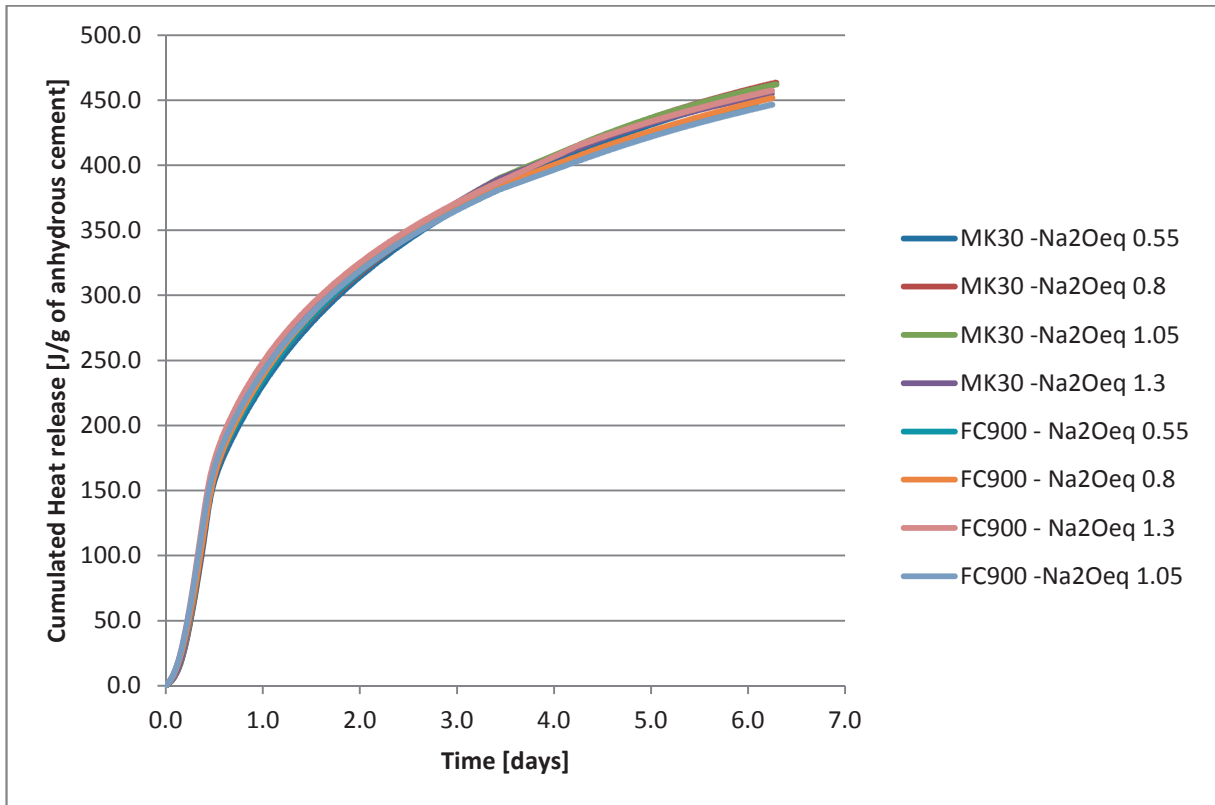


Figure 5.6 Cumulated heat released over 6 days normalized by weight of anhydrous cement for pastes at 20°C.

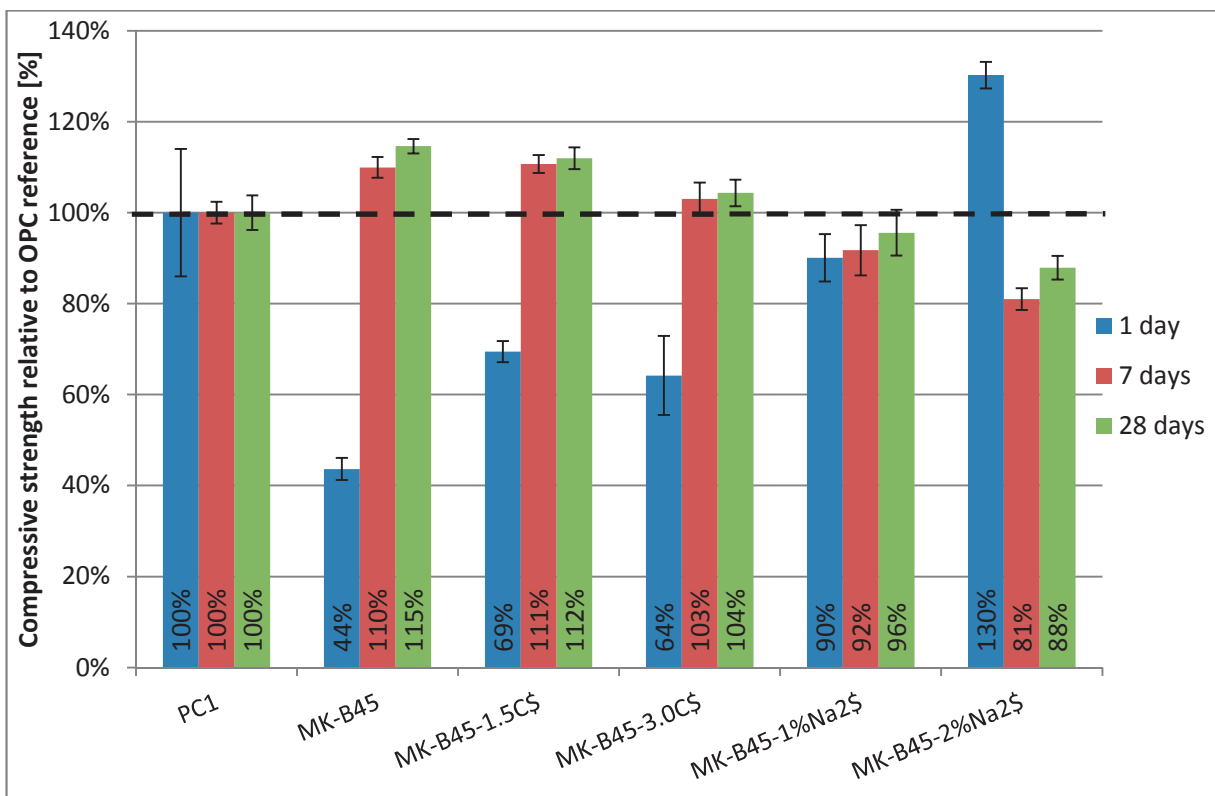


Figure 5.7: Relative compressive strengths obtained for MK-B45 blends with different amounts of gypsum (from previous chapter) and sodium sulfate, pointing out the crucial role of sulfate and alkali adjustment to optimize early age strength.

Figure 5.8 shows the heat evolution for pastes of the same systems during the first 80 hours at 20°C. The addition of Na₂SO₄ clearly provokes an earlier occurrence of the aluminate peak that becomes considerably more sudden and enhanced: the system appears undersulphated. Later on the strength development with addition of Na₂SO₄ is not as good as in cement or blended systems sulfated with CaSO₄, for we don't have a clear understanding either.

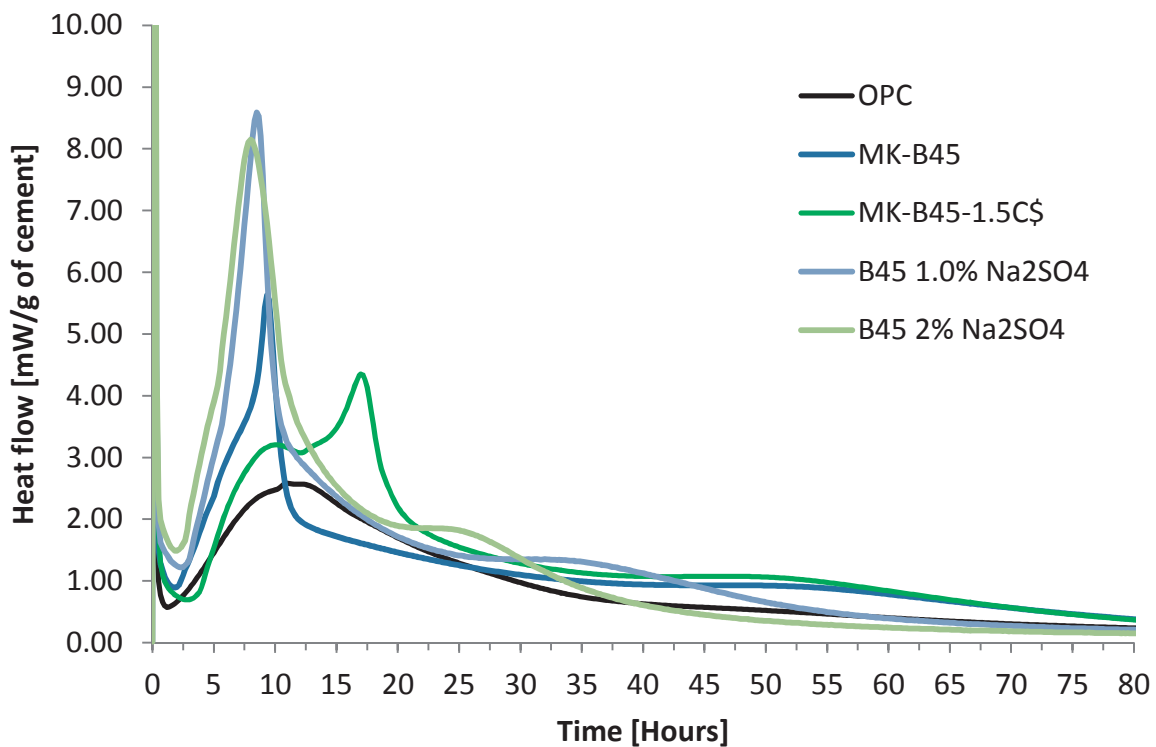


Figure 5.8: Heat flow monitored by isothermal calorimetry at 20°C to observe the effect of Na₂SO₄ addition.

5.3.2. FINENESS EFFECT

Fineness directly influences reactivity and consequently strength of cementitious materials. In the case of ternary blends of cement, calcined clays and limestone, the only phase for which fineness is really interesting to vary is limestone, since increasing cement fineness might have negative

consequences on self-heating and shrinkage or cracking complications. The increased fineness of calcined clays is likely to have a negative to impact on rheology in the fresh state.

Figure 5.9 shows the important strength gain obtained at 1 day for B45 blends made with pure metakaolin and PC1. There was little impact of fineness at later ages. Relative strength compared with PC could be increased from 44 to 58% by reducing the average diameter $D_{v,50}$ from 15 to 5 microns.

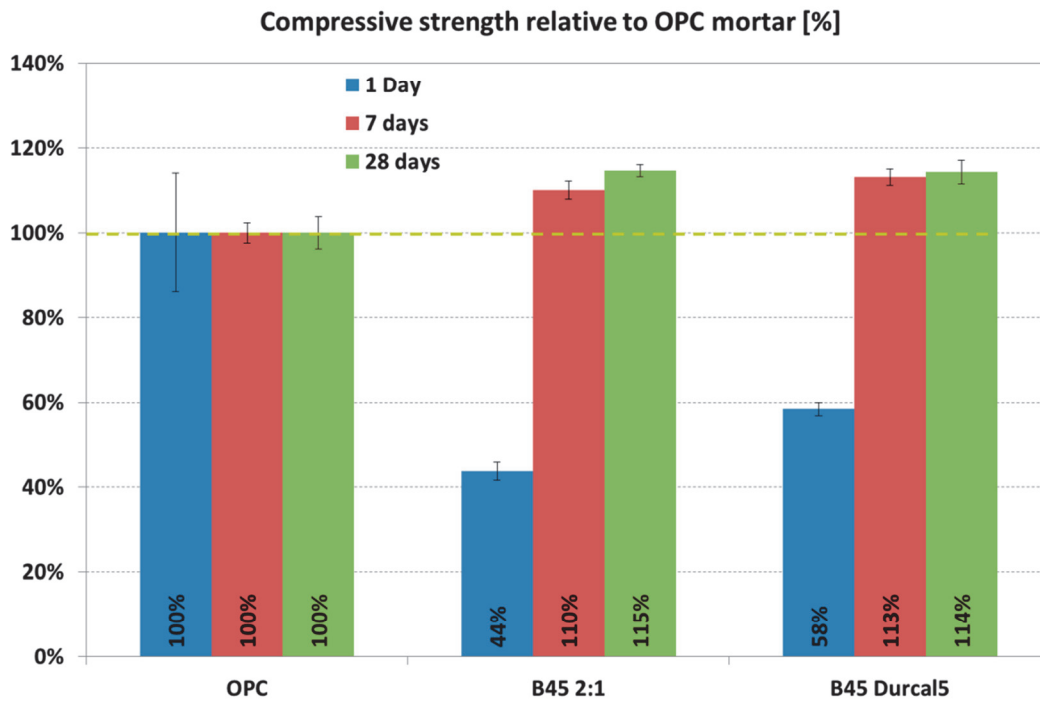


Figure 5.9: Relative compressive strength at 1, 7 and 28 days for different limestone sizes.

These results are in good agreement with Herfort [101] and Vance [102] who have shown that Portland cement substituted by 10 to 23% limestone show linear dependency of strength a 1day with limestone size. At 1 day this is most likely related to the enhanced C_3S hydration brought by the limestone providing extra surfaces available for nucleation. Note also that these results demonstrate that results obtained in the article (Chapter 4) with relatively coarse limestone are not fully optimized, and might explain some features observed such as persisting hemicarboaluminate presence at later ages. Packing density, and fresh state rheology, is also likely to be improved with better limestone fineness.

5.3.3. VARYING LIMESTONE / CALCINED CLAYS RATIO

The strength relative to PC1 obtained for B45 blends with varying metakaolin: limestone weight ratios are shown in Figure 5.10. This figure demonstrates the robustness of simultaneous addition of metakaolin and limestone. Ratios can be varied from 3:1 (75%:25%) down to 1:1 (50%:50%) and the relative compressive strengths remained equal or superior to PC reference. For 33%:67% metakaolin: limestone ratio, compressive strengths decrease to 83 and 92% at 7 and 28 days respectively. Note that these are still respectable results considering that such a blend contains 30% limestone and only 55% cement.

XRD Results for the same compositions are given in Figure 5.11. The following behaviour is observed:

- At 1 day, there is no massive difference that can be noticed among the different ratios: Al_2O_3/CO_2 ratio is not critical at this age .
- At 28 days: hemicarboaluminate forms in large amount and , hemicarboaluminate/ettringite ratio seems marginally related to Al_2O_3/CO_2 ratio, strätlingite forms at high Al_2O_3/CO_2 ratio , monocarboaluminate begins to form at low Al_2O_3/CO_2 ratio.
- At 90 days, the lower the Al_2O_3/CO_2 ratio the more hemicarboaluminate tends to convert to monocarboaluminate. Strätlingite has formed for every ratio.

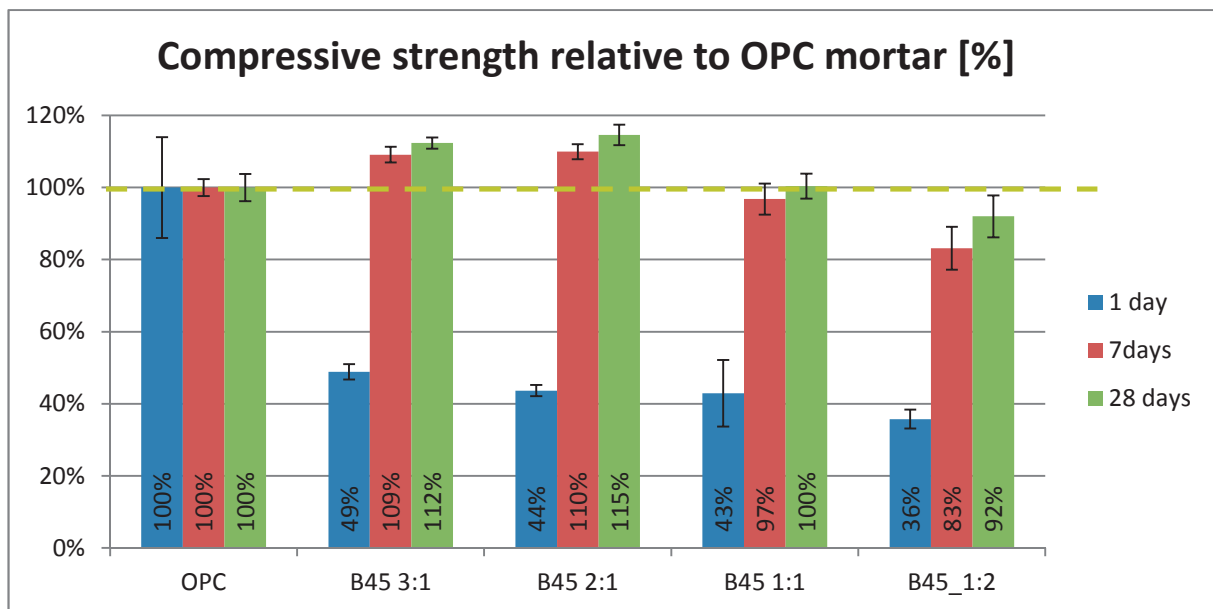


Figure 5.10: Relative compressive strength to PC for varying metakaolin: limestone ratios.

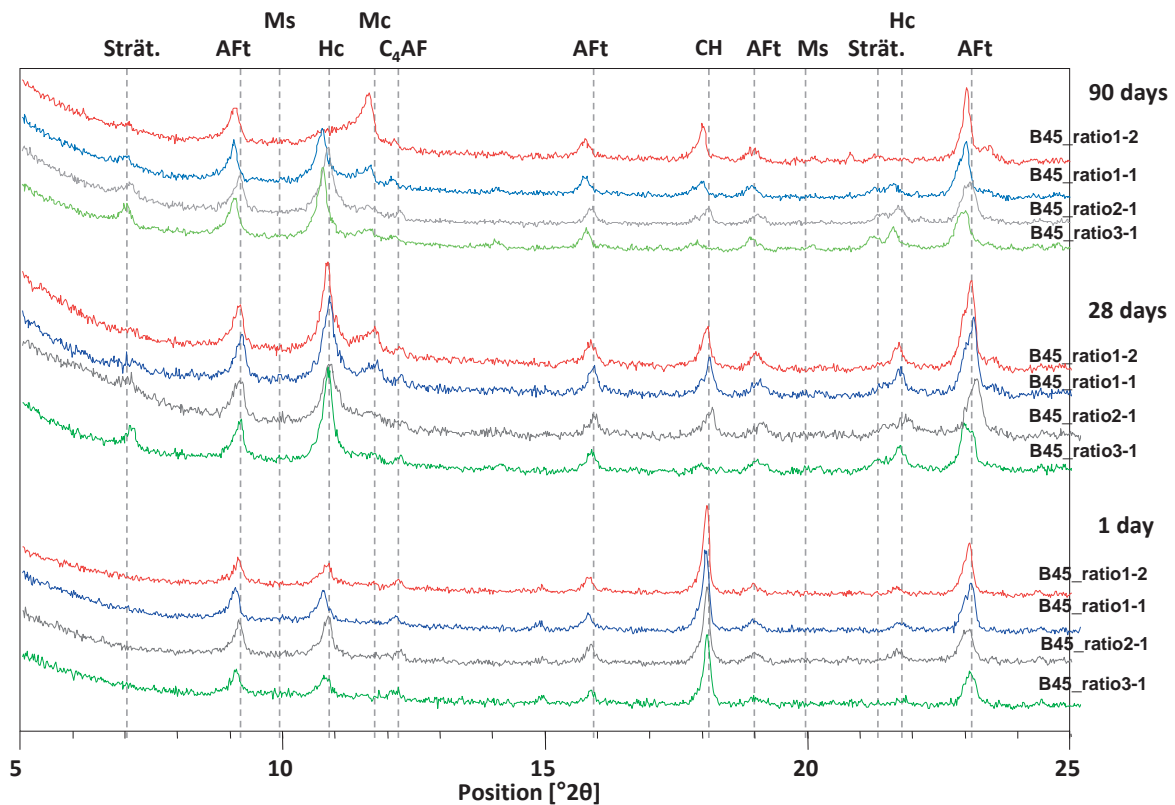


Figure 5.11: XRD Diffractograms for B45 blends made with varying metakaolin to limestone ratio.

5.3.4. INFLUENCE OF MIXED CLAYS

In order to investigate the effect the different clay components, series 7 was designed to replicate Fernandez results in conditions as similar as possible, using PC4, containing 6.5wt% limestone. Curing temperature was maintained at 30°C.

It should be noted that PC4 cement had a low alkali content, about 0.55% Na₂O_{eq}, and the sulfate was adjusted by adding 2.5% gypsum to the initial binder.

The Manicaragua clay (Mani) is a mixture of approximately 45% kaolinite, 45% montmorillonite and 10% quartz. Model clays have been created by mixing pure materials prior to calcination. Calcination has been carried out at 800°C to optimize reactivity of the different clays, according to their TGA results (Section 3.1.2, Figure 3.1). Except PC4 reference, all blends have been made with 30% substitution of cement by the following compositions:

- For reference, mortars with 30% fine quartz powder (K50, see only (named “quartz”) and 30% kaolinite only (“K800”) have been produced.
- Three model clays were prepared:
 - KQ800 with 45% kaolinite and 55% quartz powder K50,
 - MQ800 with 45% montmorillonite and 55% quartz powder K50
 - KMQ800, with 45% kaolinite, 45% montmorillonite and 10% quartz powder K50
- Two natural clays, “Mani” and “Pont” (Ponzezuela clay, approximately 45% kaolinite too) were also tested.

The relative strength relative to PC obtained for the different compositions is given here in Figure 5.12:

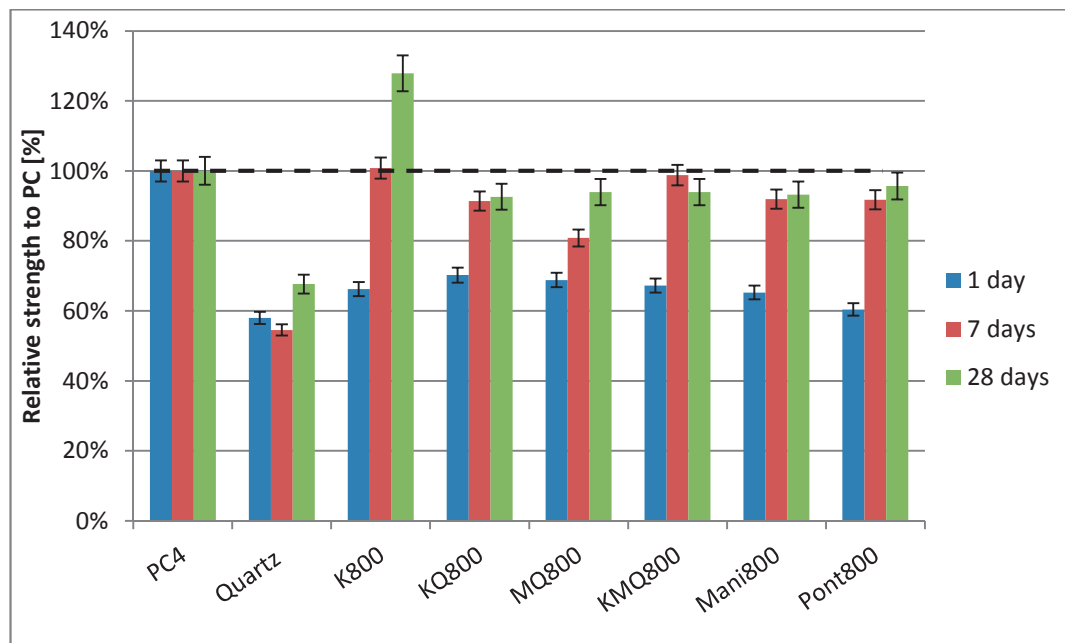


Figure 5.12: The relative compressive strengths in comparison with PC4 reference are plot for different mixed clays (30% cement substitution, mortars cured at 30°C).

Quartz behaves as filler at all ages. K800 demonstrates the best compressive strength and surpasses the PC4 reference at 7 and 28 days. All other mixed clays show very similar results, with about 70, 90 and 95% of PC4 strength at 1, 7 and 28 days respectively.

The exception to this trend is MQ800 at 7 days that reaches only 81% of PC strength. Montmorillonite is reactive but its contribution to strength development seems to have slightly slower kinetics.

Based on these results, the following interpretations can be made:

- Montmorillonite clays can deliver decent strength development at long ages, almost as good as kaolinitic clays.
- Model clays from mixed pure constituents reproduce closely the behaviour of natural mixed clays.
- Mixed clays do not seem to take advantage of the contributions of its different constituents. Clay with 45% kaolinite, 45% montmorillonite and 10% quartz such as KMQ800 and Mani800 do not show better strength results than KQ800 or Pont800, with 45% kaolinite as only reactive constituent. There is no obvious explanation for this result and this should be investigated.

5.4. SERIES 3: BLENDS PRODUCED IN CUBA

5.4.1. MECHANICAL PERFORMANCE

A series of samples was produced in Cuba during the master thesis of John Rossen. 16x4x4 cm bars of microconcrete were cast at water/binder ratio 0.5 and graded limestone aggregate and sand were used. Curing temperature was under ambient conditions, at 29 +/-3°C.

Two clays with about 40% kaolinite were used, the same Cuban clay as Fernandez (Mani) and the Argeco clay (Ar). In addition, blended cement (SIGB45) was produced by intergrinding 47.8% of PC5 clinker, 30% of Pontezuela kaolinitic clay, 15% Cuban limestone, and 7.2% gypsum. Characteristics of the clays are given in Table 5.3:

Table 5.3: Description of the clays used in Series 3,

Name	Origin	Activation	Kaolinite	SiO ₂	Al ₂ O ₃	Fe ₂ O ₃	BET [m ² /g]
Ar Argicem	Argeco	Flash calcination at 750°C	40%	67%	21%	11%	11.37
Mani	Manicaragua (Cuba)	1h at 800°C	40%	44%	25%	2.5%	11.75
SIG-B45	Pontezuela (Cuba), lab-made by intergrinding	1h at 800°C	~50%	45%	28%	21%	8.49

As the limestone content of the cements was not known during sample preparation, limestone addition was therefore not adjusted to take it in account: B15 blends contain 10% clay, 9.25% limestone and 80.75% clinker and B45 blends contain 30% calcined clay, 17.75% limestone and 52.25% clinker. Sulfate was not adjusted either.

The mechanical strength of Cuban mortars is shown in Figure 5.14. Blends containing only 15% substitution show about the same strength as PC at 7 and 28 days, for both Mani and Ar clays. The low strength of the Mani B15 at 1 day is not explained and might result from high dose of superplasticizer. Both ArB45 and CuB45 clays show similar strengths, around 60% at 1 day and 80% at 7 and 28 days. These results are not as good as the results obtained in Switzerland for the same clays, maybe because of the limestone content of the cement that modified the composition.

Outstanding results are obtained with the SIG-B45 lab-made cement. Although similar to other blends showing low values at 1 day, it surpasses all mortars including OPC at 7 and 28 days. This very interesting result is the area of investigation of Leng Vizcaino and the topic of an article about to be submitted for publication [103]. Figure 5.13 shows one of the main results of her article, where the different contributions of the metakaolin reactivity, metakaolin fineness and synergetic formation of carboaluminates are put in evidence.

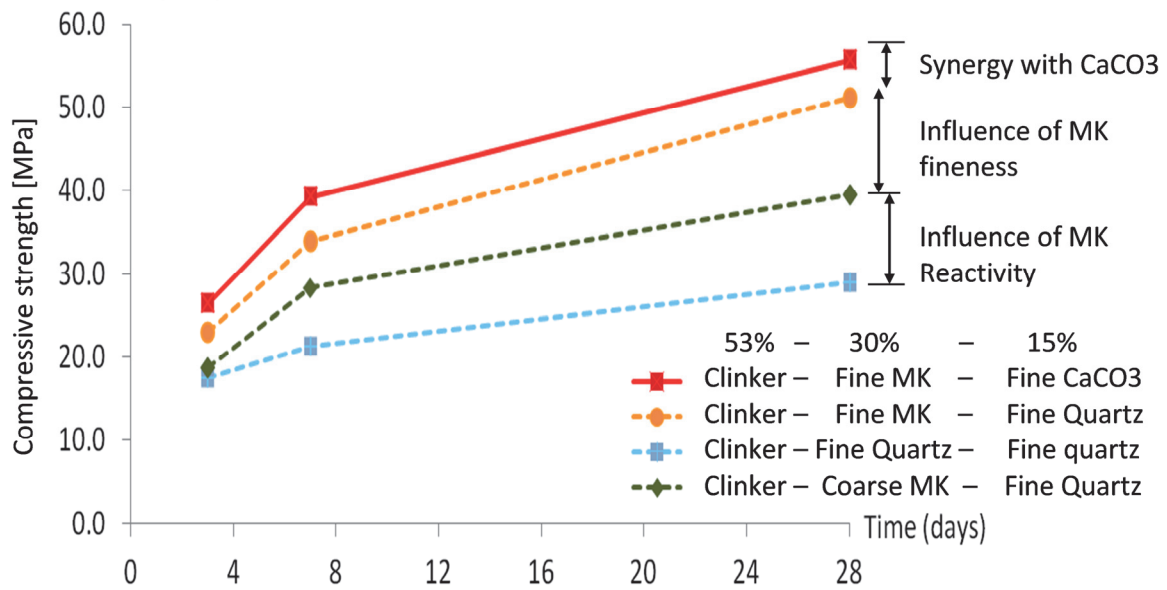


Figure 5.13: Compressive strengths obtained with B45 blends at 3, 7 and 28 days. Quartz filler and different fineness of Metakaolin have been used in order to decompose the contribution to strength development of the different fraction.

The intergrinding of all materials together has consequences for the preferential grinding of the softer particles, (clays, gypsum and limestone) by the harder ones (a result about the effect of limestone fineness is also given in Section 5.3.2). Similarly, quartz impurities comprised in Pontezuela clay have also helped to grind the clinker.

It is believed that the overall fineness and high specific surface of the blended cement, combined with an adequate sulfatation, explain these excellent results. It must be outlined that cement has a different particle size distribution in this blend; the comparison with PC5 is therefore not exactly correct. But still such effect is very likely to happen in an industrial production so it is worth mentioning.

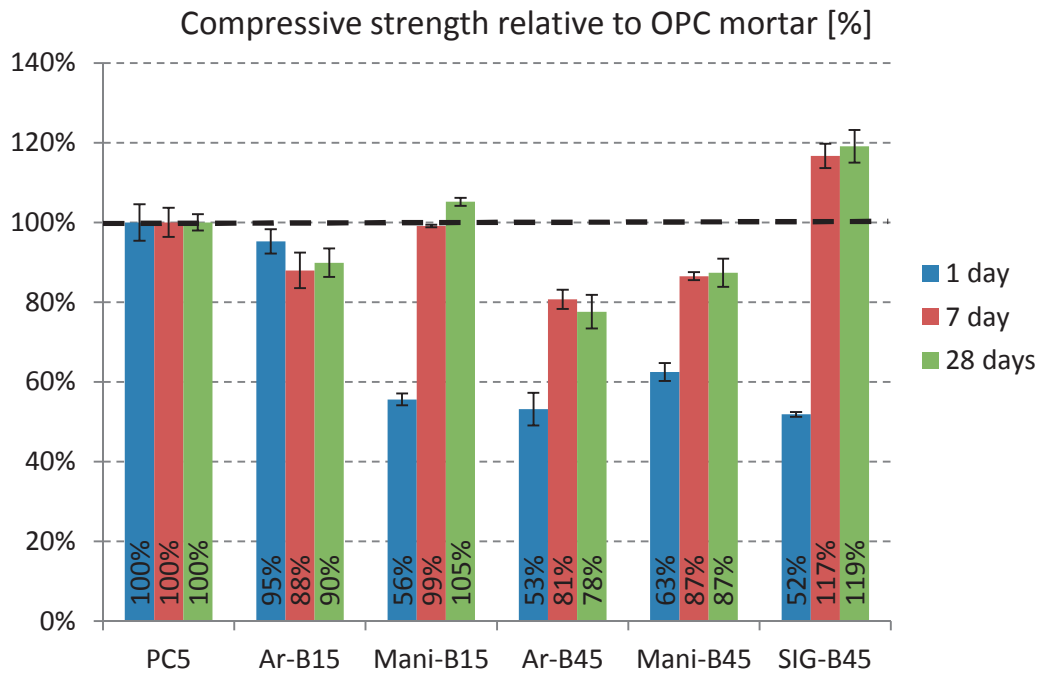


Figure 5.14: Compressive strength for Cuban formulations normalized to pure OPC

5.4.2. EVOLUTION OF PASTE SAMPLES

Pastes samples for the same composition were also cast (according to standard procedure, see section 3.2). Selected XRD patterns of blends at 7 and 28 days are given in

Figure 5.15. Knowing that Cuban OPC contains 5% of LS, XRD shows that ettringite is stabilized in all samples, while monosulfoaluminate is only barely detected in OPC at 7 and 28 days. Also, hemicarboaluminate is present in all blends including SIG-B45 at 7 days and detected slightly in OPC at 28 days. Finally monocarboaluminate is found in simple blends from 7 days and in trace amounts in OPC at 28 days.

Both blends (Mani and Ar) show a reversal in relative peak intensities of monocarboaluminate and hemicarboaluminate when increasing blend substitution. The 15% blends show a monocarboaluminate peak higher than hemicarboaluminate, while the 45% blends show a higher hemicarboaluminate peak compared to the monocarboaluminate. Strätlingite peak is not observed.

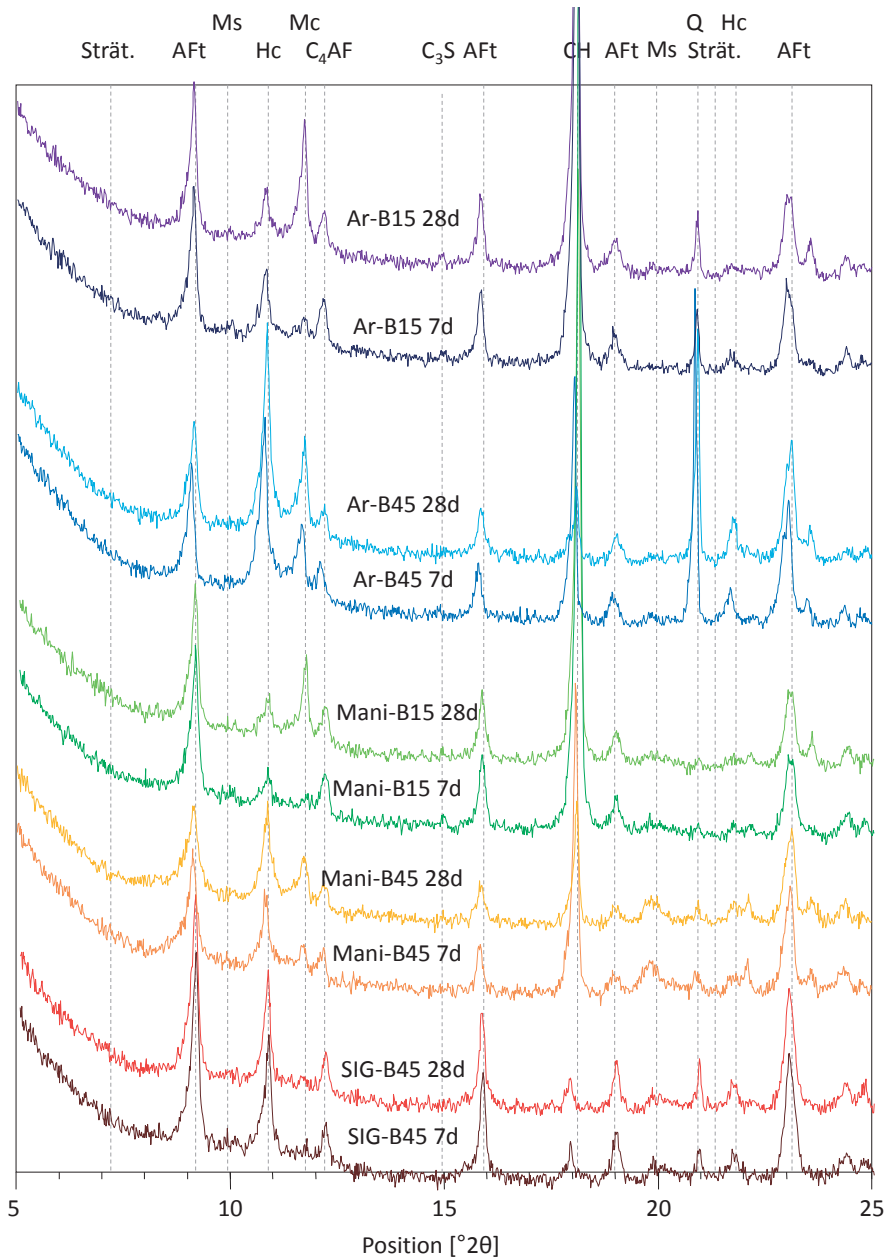


Figure 5.15: XRD patterns for all Cuban blends at 7 and 28 days

The portlandite (CH) contents normalized by weight of anhydrous cement at 1, 7 and 28 days for all blends are given in Figure 5.16. The 15% blends show similar trends with constant CH content from 7 to 28 days, indicating some pozzolanic activity. The 45% blends show a significant decrease in CH content. The Ar-B45 and SIG-B45 both seem to decrease even between 1 and 7 days, while the CH for Mani clay decreases massively from 7 days on. There is a slight disagreement between the CH content observed by TGA, showing Ar clay consuming more CH than Mani and the compressive

strengths measured, with Mani systematically above Ar clay, at both substitution levels, but it is within the margin of error of the measurements.

The SIG-B45 showed no measurable mass loss for CH from 7 days on, thus giving an apparent absence of CH. However, the XRD showed small but detectable amounts of CH (see

Figure 5.15).

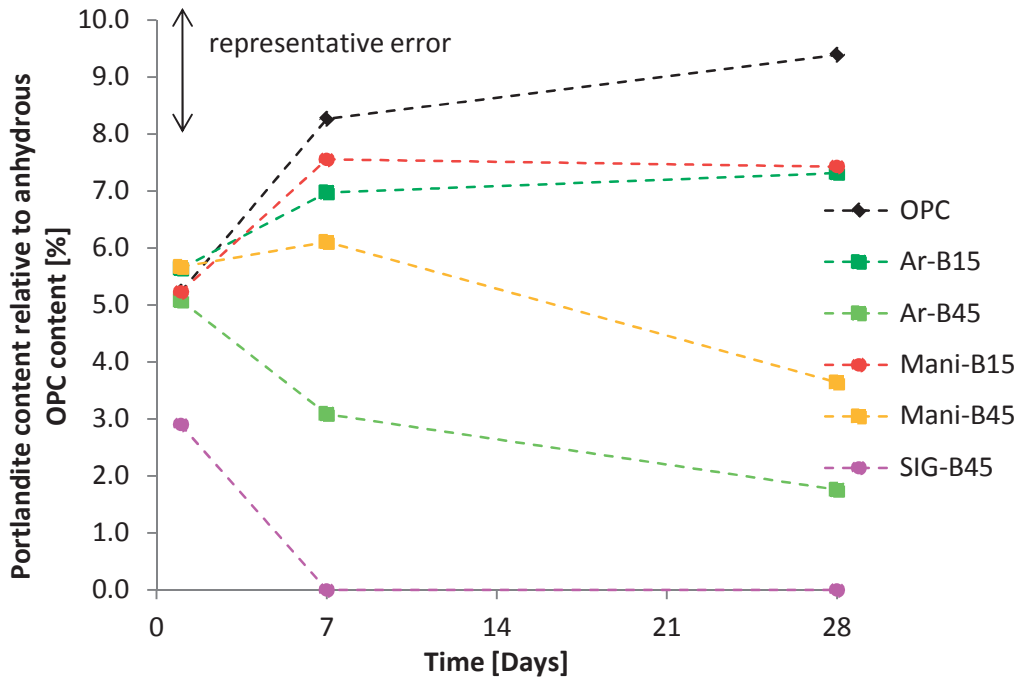


Figure 5.16: Evolution of the CH content of Cuban pastes (determined from TGA mass loss) normalized to the OPC content in the paste.

5.5. SERIES 4: BLENDS WITH NATURAL CALCINED CLAYS PRODUCED IN LAUSANNE

This series has been cast with PC1 cement and cured at 23 +/- 1°C and can therefore be compared with results from Chapter 4 obtained with pure Metakaolin. The description of the clays used in this series is given in Table 5.4: Three different substitutions were made: 30% calcined clays only; B15% and B45 with cosubstitution by calcined clays and limestone (2:1 clay:limestone).

Note that B45 mortars from this series have also been used to investigation chloride ponding (see Section 7.4).

Table 5.4: Description of the clays used in serie 4

Name	Origin	Activation	Kaolinite	SiO ₂	Al ₂ O ₃	Fe ₂ O ₃	BET [m ² /g]
MK	Burgess	Flash calcination	~100%	51%	47%	~0%	7.64
Ar Argicem	Argeco	Flash calcination at 750°C	40%	67%	21%	11%	11.37
Cu	Manicaragua (Cuba)	1h at 800°C	28%	44%	25%	2.5%	11.75

The compressive strengths relative to PC1 are given in Figure 5.17.

At all ages and for all substitution level, the strengths obtained show a strong dependency with kaolinite content of the clay. The higher the kaolinite content, the higher the strengths measured. Only MK B15 gives the same strength as PC1 at one day. At later ages, all clays perform as well as PC1 in B15 configuration.

For 30% replacement by calcined clays, only pure metakaolin can compete with PC1 at 7 and 28 days; Ar clay with 40% kaolin gives almost the same strength at 28 days.

Finally for the B45 blend, strengths higher than PC reference are obtained only with pure metakaolin, while ArB45 reaches about 85% and CuB45 about 70% at 28 days of PC1 compressive strength respectively.

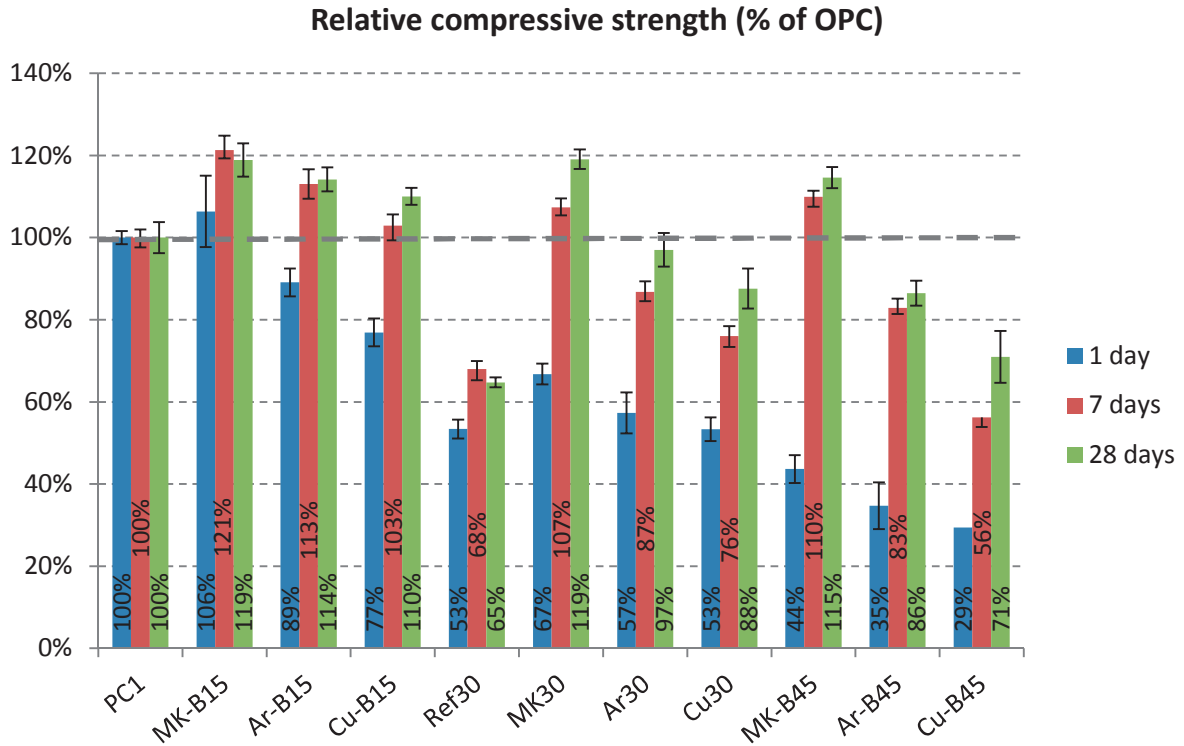
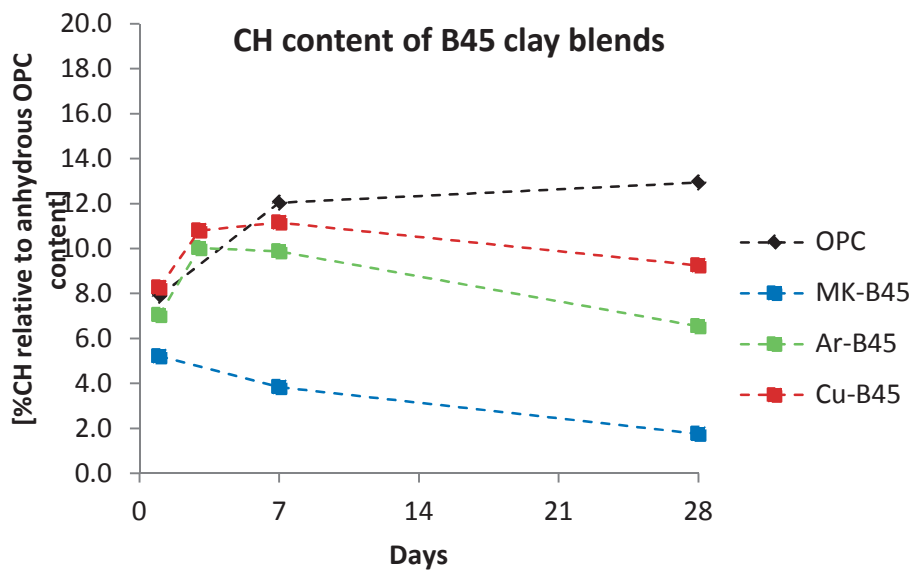
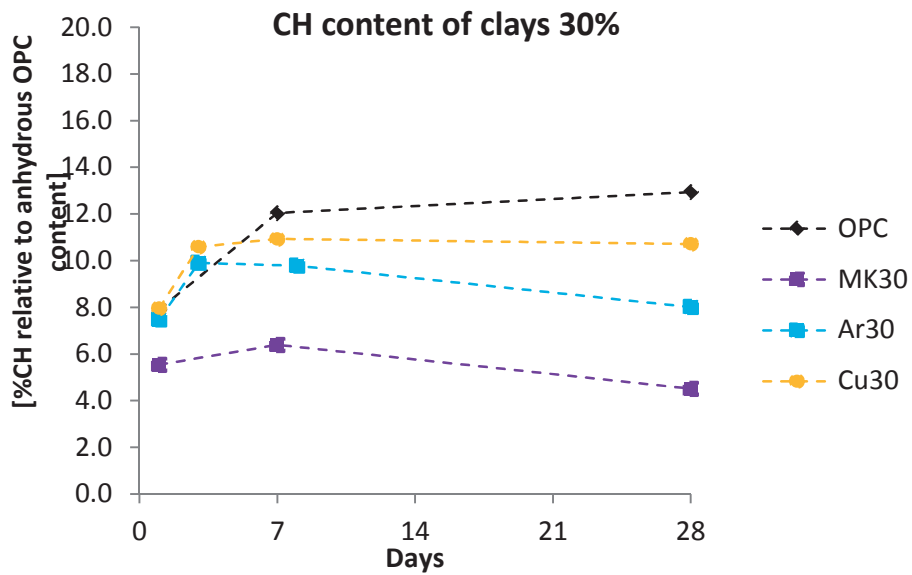
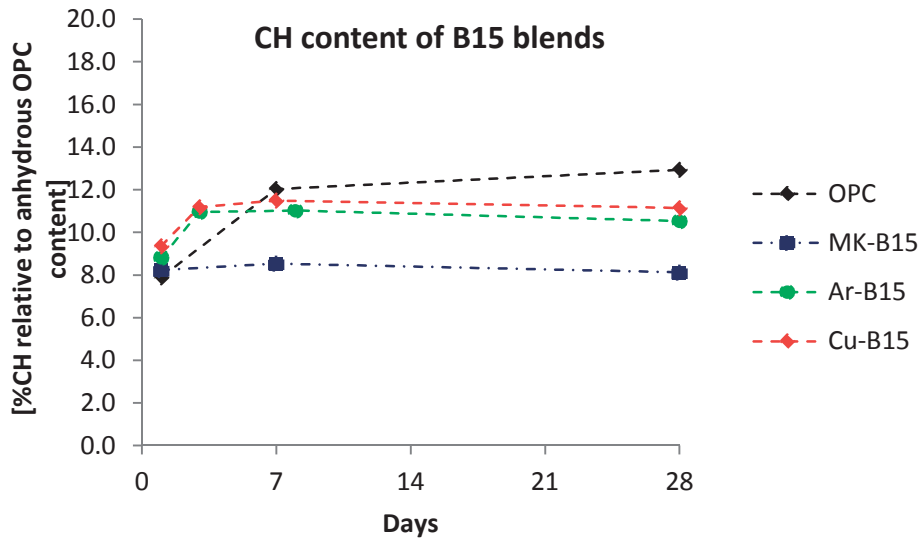


Figure 5.17: Relative strength to reference PC obtained with 3 different clays: metakaolin of Burgess (MK), Argicem from Argeco (Ar) with 40% kaolinite and

The portlandite contents normalized by weight of anhydrous cement on equivalent pastes are given in Figures 5.18. They fit very well with the compressive strengths observed in mortars.

For each substitution level, at each age, the higher the kaolinite content the lower the portlandite content (in other words the higher the consumption by pozzolanic reaction).



Figures 5.18: Portlandite content obtained at 1, 7 and 28 days for the 3 different blends made in series 4 with 3 clays containing varying kaolinite content.

5.6. EFFECT OF THE CALCINATION PROCESS

Kaolinite dehydroxylation upon heating has been extensively investigated in the literature. Brindley was the first to report a detail study of the transformations undergone by kaolinite upon heating [104-106]. The exact phenomena and structural transformations are not totally understood and still under investigation [30]. It is interesting to compare the influence of the chosen heating process on the final reactivity of the metakaolin product.

In this thesis static calcination and flash calcination processes have been used. Static calcination consists of calcination in a laboratory furnace with moderate heating rate and calcination at constant temperature for a duration in the order of one hour. Flash calcination is very different because the heating rate is considerably higher and the high temperature “seen” by the clay decreases rapidly because of the thermal losses. An example of these differences is observable in the schematic Figure 5.19, where temperature is plotted as a function of log (time) in seconds. Note that temperature experienced by a particle in flash calcination is never constant throughout the calcination tube. Flash calcination temperatures reported in this section are therefore only indicative of a local temperature measured by a thermocouple placed at the end of the main calcination tube. No direct comparison is possible between this temperature and the constant temperature in static calcination.

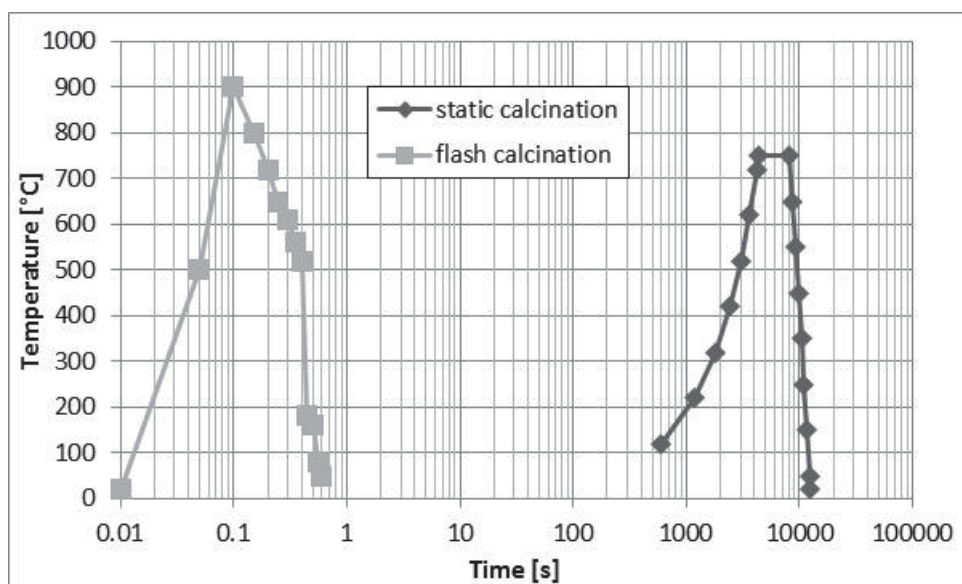


Figure 5.19: Example description of the temperature profiles in static and flash calcination processes.

5.6.1. STATIC CALCINATION

Static calcination can be carried out in a batch furnace and also approximates the situation in an industrial rotary kiln. Here all results presented come from clays calcined in a LH 30/14 Nabertherm furnace. Powder materials were placed in half-filled alumina mortars, if necessary covered with a magnesia lid to prevent eruptive dehydroxylation of goehite $\text{FeO}(\text{OH})$ upon heating above 200°C . A standard heating protocol was used, with $10^\circ\text{C}/\text{min}$ heating rate up to the chosen calcination temperature. The temperature was maintained for 1 hour, finally samples were removed and air cooled on a metal tray. The temperature was monitored throughout the calcination with the internal temperature sensor of the furnace and a K type sensor placed at the clay surface. The temperature variation during calcination was $\pm 5^\circ\text{C}$.

5.6.2. FLASH CALCINATION

In this thesis, two flash calcination systems were used. Temperature control in a simple flash calcination device, with a single burner such as the ones we have used is complex because temperature is never constant (see Figure 5.19) as clay particles flow within the calcination tube. In flash calcination the most important parameters are temperature profile, which can be decomposed into heating rate, maximum temperature “seen” by the clay particles and residence time that estimates the time spent by the particle over the dehydroxylation threshold.

Both flash calcination systems had intrinsic limitations such that the heating rate and residence time were neither controllable nor measurable; only a certain control was possible on the maximum temperature. In the first set of experiments Pontezuela clay was subjected to flash calcination in a flash calcination prototype from Argeco in Fumel, France, with an output of about 100kg/hour. The maximum temperature was limited because of the design of the prototype. There was no cyclone or heat exchange facility before the bag filter device used to recover powder after calcination. Because the efficiency of bag filters decreases very rapidly for temperatures higher than 200°C, calcination was stopped to prevent filter damage, preventing any calcination above 750°C.

In the second case, the same problem occurred with the CAU prototype built by our partners in Havana, even with the presence of a cyclone. This case had also much lower output, about 1 kg/hour, because of its small size. Temperatures recorded in the Havana prototype were higher than in Argeco, but cannot be directly compared because each installation is different.

The very short and non-controlled residence time, intrinsic to flash calcination in prototypes also means that calcination is likely to be imperfect, and it is possible to have a both non dehydroxylated material and overburnt or sintered material at the same time. The material undergoes a progressive phase transformation from metakaolin to mullite by surface and bulk ionic diffusion. Mullitization begins above 900°C and is usually completed above 1200°C. The optimal calcination conditions for dehydroxylation are clay specific, depending on clay mineralogy, presence of impurities and companion minerals, but also on clay particle size and humidity content.

Non dehydroxylated fraction corresponds to the ratio between the mass loss measured by the tangent method by TGA for the dehydroxylation peak around 600°C after and before calcination (see Figure 5.20).

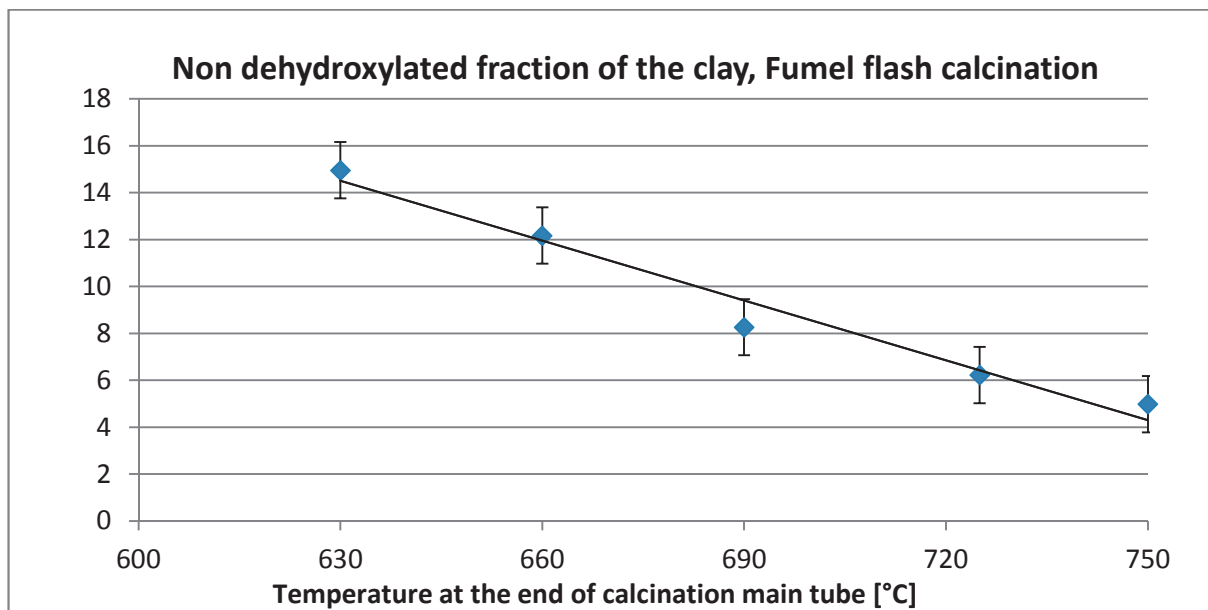


Figure 5.20: Graphical representation of the remaining non dehydroxylated fraction of the clay after flash calcination at the Fumel flash calcination prototype as a function of the temperature measured at the end of the main calcination tube. Dehydroxylation is linearly improved with increasing temperature.

However the quantification of overburnt and/or sintering is complex and could not be estimated; neither by TGA (no associated weight loss) nor by XRD, where mullite was absent (see Figure 5.21).

This measured dehydroxylation degree, considering no transformation of kaolinite into mullite, gives the following metakaolin content for the different calcining conditions (Table 5.5 below):

Table 5.5: Metakaolin content calculated from TGA measurement, 1st batch of Pontezuela clay, Series 5.

	For 100% dehydroxylation	Flash_630	Flash_660	Flash_690	Flash_725	Flash_750
Metakaolin content [%]	45	35	37	39	40	41

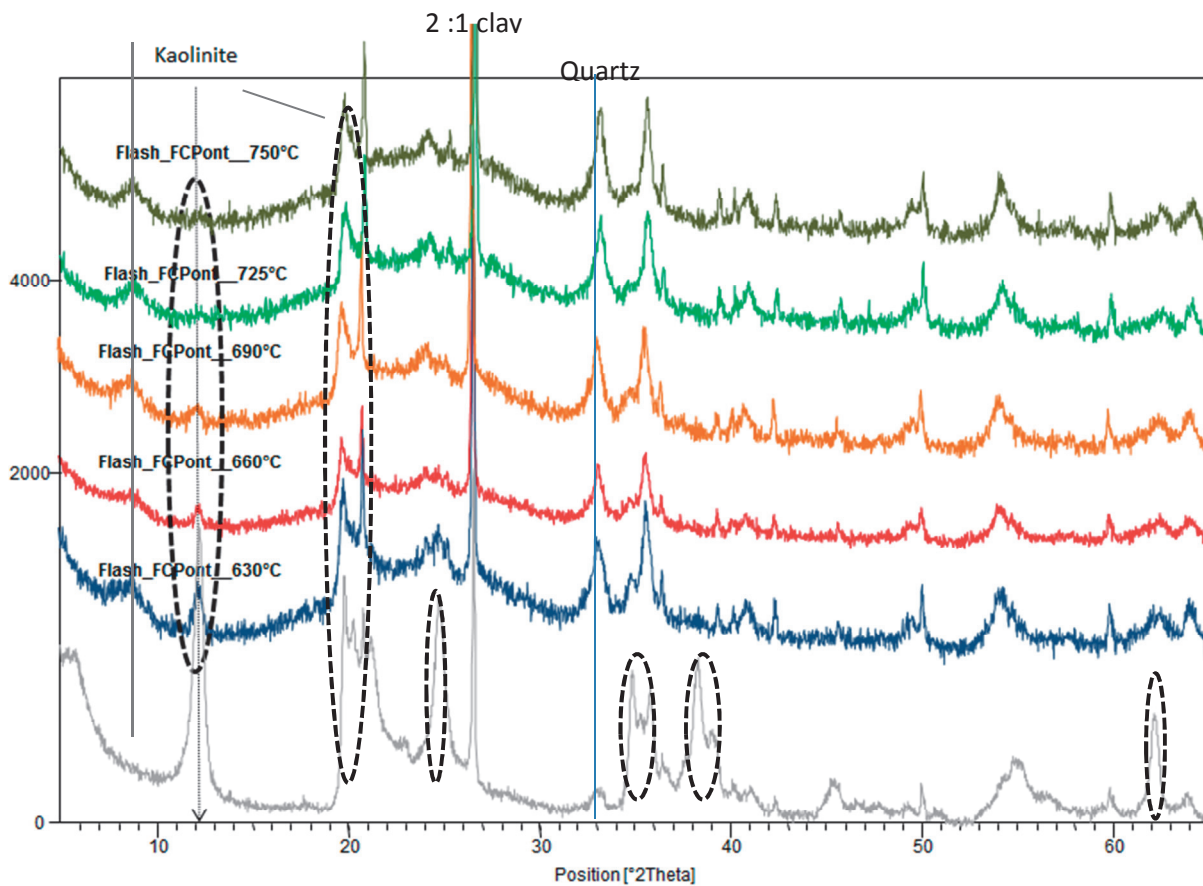


Figure 5.21: X-Ray diffractograms of Pontezuela clay as a function of flash calcination conditions. At the bottom in grey is represented the raw material, increasing temperatures given towards the top.

With differential scanning calorimetry the endothermic peak above 900°C of the metakaolin-mullite transformation seems to decrease in intensity but the complex background prevents quantification of this difference (Figure 5.22). It could indicate the onset of partial mullitization or atomic rearrangement and sintering. The investigation of the grain size distribution by laser granulometry (Figure 5.23) shows a clear coarsening with calcination but no major difference between static and flash calcination conditions to confirm this hypothesis.

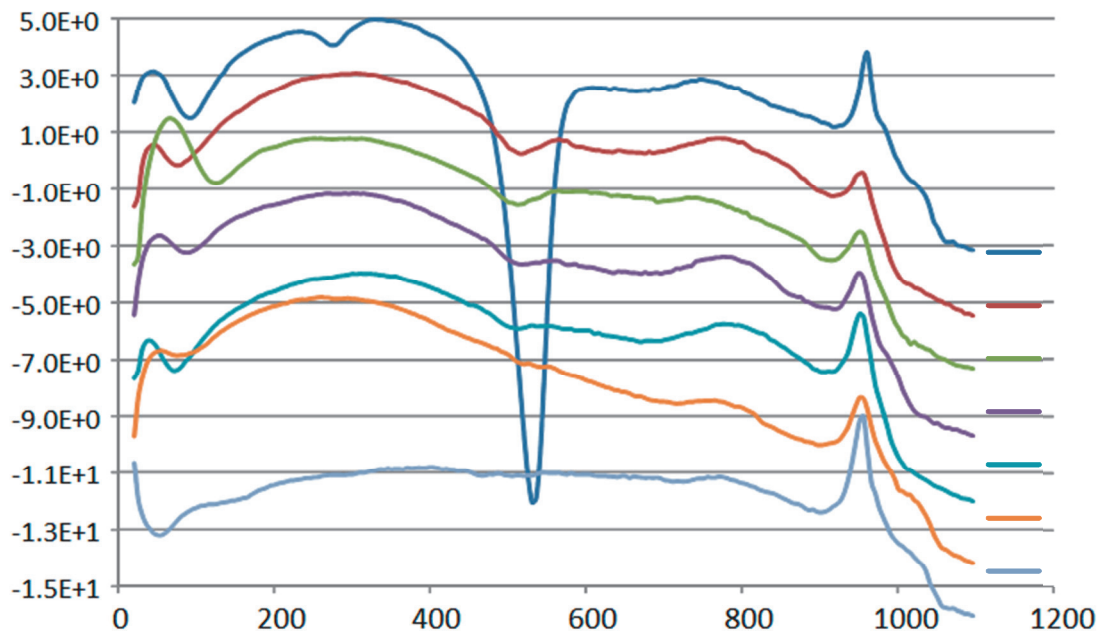


Figure 5.22: Differential Scanning calorimetry of the raw and flash calcined materials in different conditions given as a function of temperature, Fumel calcination.

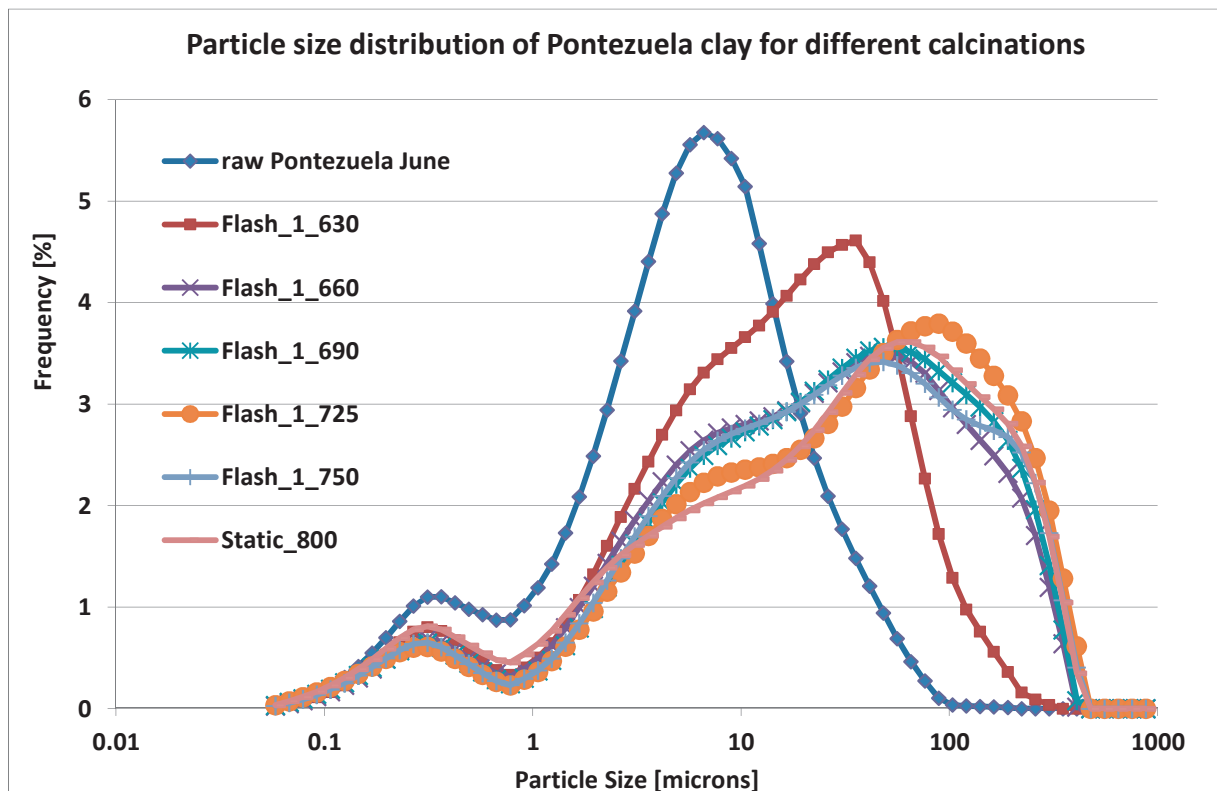


Figure 5.23: Particle size distribution of the clays measured by laser granulometry.

Figure 5.24 shows the compressive strength values obtained at the Fumel flash calcination site. Compressive strengths at 1 day are, between 32 and 52% of PC at same age and increase with increasing temperature of flash calcination.

At later ages the same trend is observed, with relative strength values varying between 64 and 78% at 7 days and 72 and 90% at 28 days respectively. The 660°C sample shows the highest strength at 7 and 28 days. This particular sample was the biggest sample calcined (few hundreds of kg compared to 20 kg for the other batches); some inhomogeneity in particle size distribution as well as in non-dehydroxylated content have been observed, this odd result is likely to be due to poor sampling.

In summary, the different flash calcinations carried out in this batch were not optimal. The trend is for higher strengths at higher temperatures. In addition, this calcined clay show modest pozzolanic properties, with strength superior to filler only at 28 days.

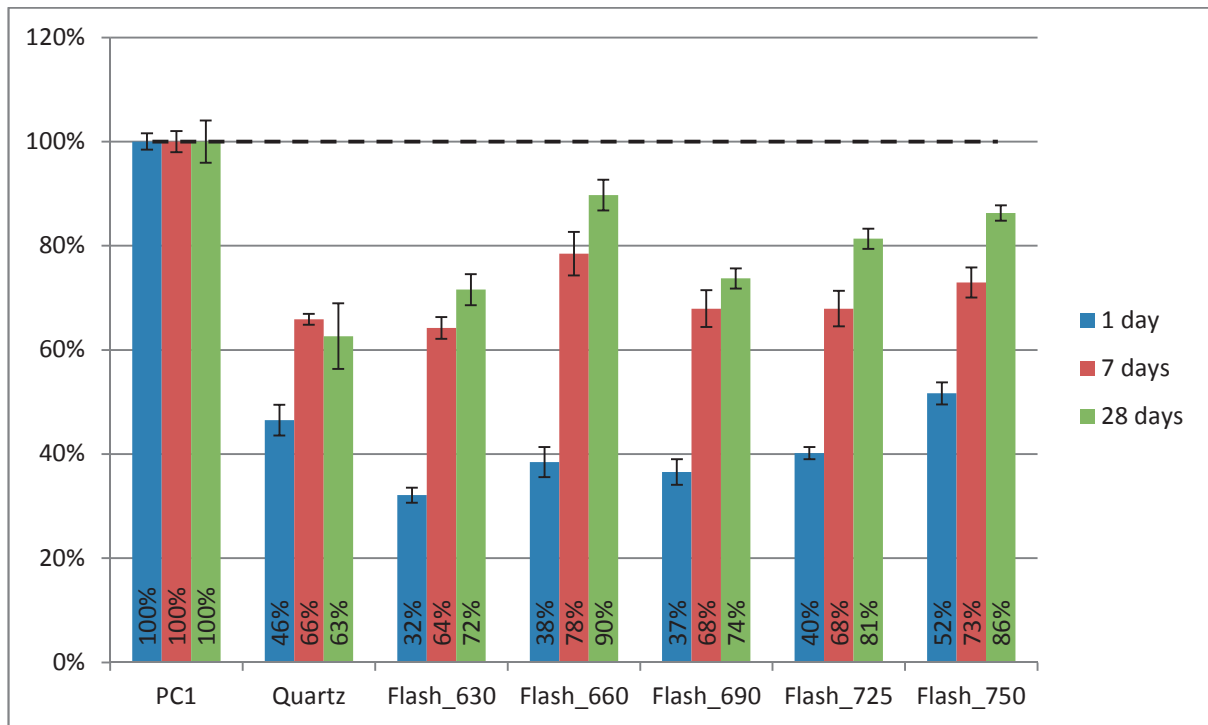


Figure 5.24: Relative compressive strengths compared with PC1 obtained for different flash calcination conditions carried out in Fumel for the first flash calcination trial (30% cement substitution). Series 5

5.6.3. COMPARISON FLASH AND STATIC CALCINATION

The second flash calcination was carried out in the Havana flash clay activation unit with a different clay batch with higher kaolinite content of 55% against 45% for the first batch. After correction for the non-dehydroxylated fraction by TGA, metakaolin content could be approximated as in Table 5.6:

Table 5.6: Metakaolin content calculated from TGA measurement, 2nd batch of clay, series 6.

	Flash_2_750	Flash_2_850	Flash_2_900	Static_2
metakaolin content [%]	38	50	52	55

The compressive strengths obtained for 30% substitution of PC3 are shown in Figure 5.25. Samples were cured at 23°C and PC3 has only 0.5% alkali (collaboration with Yanisleidy Oquendo Machado). The sulfate content was adjusted by adding and intergrinding with 2wt% gypsum.

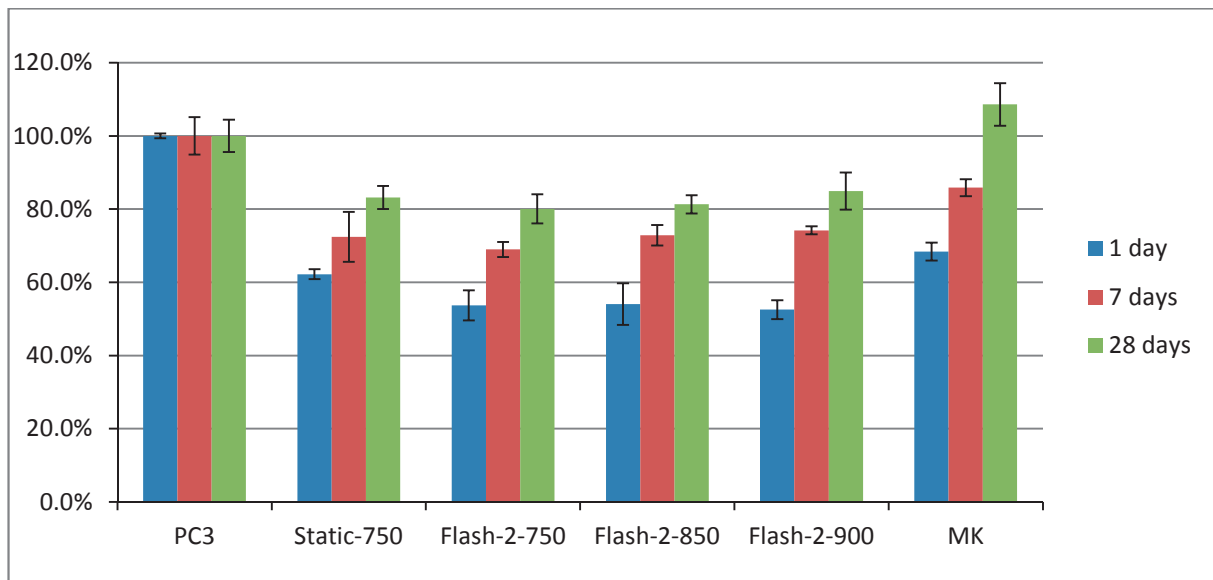


Figure 5.25: Relative compressive strengths obtained with the second batch of Pontezuela clay calcined in Havana, series 6.

Compressive strengths at 1 day range between 53 and 62% of PC of same age, the static calcined sample being the best. At later ages, there isn't any significant difference among the calcination conditions, with about 72% of PC strength at 7 days and above 80% at 28 days. Note that 1 day strength is considerably higher than strength obtained with the first flash calcination (Figure 5.24).

Although the slightly higher kaolinite may play a minor role in the strength difference, it is very likely to be due to the sulfate adjustment, absent in the former series 5.

These results show that, within the range of the flash calcination conditions investigated during this series 6, there is no major difference with static calcination. Since the flash calcination prototype were of simplified design with reduced possibilities of optimization, it isn't possible to speculate and extend such conclusion to the flash calcination of any clay deposit. A systematic "Time-Temperature-Transition (TTT) heating diagram would be required to fully resolve the optimum conditions of calcination for each clay type. More generally, it demonstrates that a modestly optimized flash calcination process doesn't impact significantly the reactivity of the product. The low alkalinity of this cement seems to adversely affect the strength development of the blends with calcined clays. This has been discussed in section 5.3.1.

5.7. SUMMARY AND OUTLOOK

This chapter presents some results on the different factors affecting the reactivity of calcined natural kaolinitic clays for cement substitution.

-Ternary blends with natural kaolinitic calcined clays and limestone can extend the cement substitution threshold. At constant calcined clay content, the further replacement of cement by limestone leads to the synergetic reaction between aluminates and carbonate.

-Sulfate should also be adjusted. Results obtained in Chapter 4 are confirmed for mixed clays. Proper sulfatation brings a significant strength gain after 1 day, and doesn't impair strength development at later ages when using calcium sulfate.

-The cement alkali content, $\text{Na}_2\text{O}_{\text{eq}}$ of the Portland cement is critical to good performance of calcined clays, especially at early age. It should be maintained above 0.7 / 0.8 wt%. Alkali levels below this threshold results dramatically decrease strength contribution from the clay, especially at 1 day and with decreasing importance as curing time increases. The explanation underlying these effects could not be clearly identified and require further investigations.

-Both last points underline that it is critical to use a single cement to benchmark different calcined clays and carry out systematic comparison of their reactivity.

-The kaolinite content of the clay plays a very important role. The results presented in this chapter tend to demonstrate that a kaolinite content of 40 to 50% is the lower limit to deliver compressive strengths at 7 or 28 days comparable (>90%) to PC reference for 30% substitution or B45 cosubstitution. The decrease is however not linear with kaolinite content. Since it has been established in the last chapter that the degree of reaction of pure metakaolin was below 50%, it is likely that degree of reaction increases when the clay is diluted with inert materials. This is a subject which needs to be looked at in more detail.

-At constant kaolinite content, mixed clays with kaolinite and montmorillonite content have similar compressive strengths to clays with kaolinite only. It has been observed both for model clays and natural clays. It confirms the crucial role of kaolinite content of mixed clays. This should be further investigated and could be related to the kinetics of dissolution or to a solution-controlled dependency.

-Use of alkali sulfate can boost 1 day strength but the later strength development is deteriorated in comparison with blends without alkali sulfate.

-Considering the elements listed above, for the design of ternary blends one should always first consider to properly choose or adjust if necessary the alkali and the sulfate content of the cement. In order to maintain compressive strength and depending on the kaolinite content of the natural clay:

- The calcined clays: limestone ratio can be increased
- The fineness can be increased
- The last possibility is to decrease the total substitution level

The optimum case will always correspond to the best balance between reactive alumina, portlandite amount, carbonate and sulfate content available giving the most voluminous hydrate assemblage. It could be precisely determined by thermodynamic modelling if these values were known.

Chapter 6 : CARBONATION OF TERNARY BLENDS OF CEMENT, CALCINED CLAYS AND LIMESTONE

Carbonation of concrete is a concern for reinforced concrete structures. It provokes a decrease of pore solution pH that can be detrimental for reinforced concrete structures where the high pH maintains steel rebar soundness due to the stability of a stable oxide passivation layer in this basic pH conditions. It is however very important to point out that optimal relative humidity conditions for carbonation is different than the optimal humidity for steel corrosion, as plotted in Figure 6.1.

In practice, it means that even if carbonation must be considered, there are relatively few situations in which it is a threat to concrete integrity. Dry concretes (indoor) or concrete exposed to rain are very unlikely to suffer from corrosion induced by carbonation.

Han & Park [1] have analysed the cause of rebar corrosion of 369 different elements in 69 places of coastal area in South Korea, they could identify that less than 10% were carbonation induced, the rest was due to either chloride induced corrosion and/or poor placing.

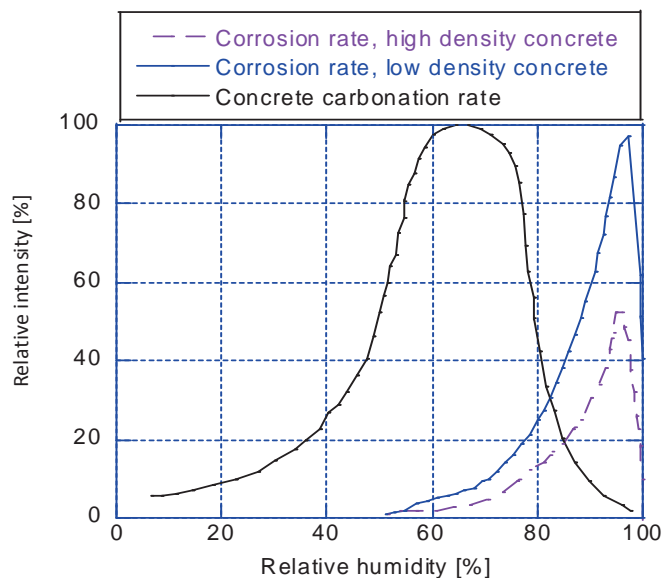


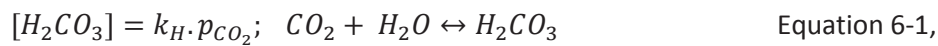
Figure 6.1: Comparison of corrosion rate and carbonation as a function of relative humidity (derived from [107, 108]) and for different concrete.

6.1. MECHANISMS OF CARBONATION

CO₂ is naturally present in air, ranging from about 0.04% in the earth atmosphere [109] and can go up to 0.1% in special urban areas such as tunnels.

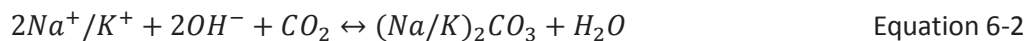
Verbeck in 1958 [110] proposed first that the mechanisms of carbonation can be divided into the following steps:

-CO₂ diffuses through empty pores and gets first solvated as aqueous CO_{2(aq)} and later on react with water to be dissolved into pore solution as carbonic acid, following Henry's law and according to the following Equation 6-1:



Where k_H is Henry's law constant for the dissolution of CO₂ in water in this case and p_{CO_2} the atmospheric partial pressure of CO₂.

It is important to note that in alkaline solution such as cement pore solution, soluble Na₂CO₃ and K₂CO₃ readily form. Alkali metal ions can therefore have significant influence on the kinetics of dissolution of aqueous CO_{2(aq)} into carbonic acid in the cement pore solution and Equation 6.1 can be written as Equation 6-2:



In addition, the reaction of carbonate ions with the alkali hydroxyls provokes a decrease in pH as hydroxyls ions are replaced by carbonates in the pore solution to maintain charge balance.

Carbonic acid is a weak acid that can dissociate further into two salts, the carbonate and the bicarbonate ion, following Equation 6-3 & Equation 6-4 respectively:



In conventional Portland cements portlandite is buffering the pH around 12.4. If portlandite is destabilized, calcium and hydroxide ions are released and carbonates ions are available for reaction to precipitate calcite. The reaction releases hydroxyl ions, buffering the pH (see Equation 6-5) and the reaction can goes on.



The reaction proceeds as long as calcium hydroxide is available. The behaviour of portlandite during carbonation is well understood. Further to its buffering role of pH during carbonation, Portlandite initially carbonates very fast and rapidly slows down. Groves [111] showed by TEM observation that this is because it forms a calcium carbonate rim around the original portlandite crystal that hinders the progress of the carbonation reaction. This is even more pronounced in accelerated carbonation conditions[112].

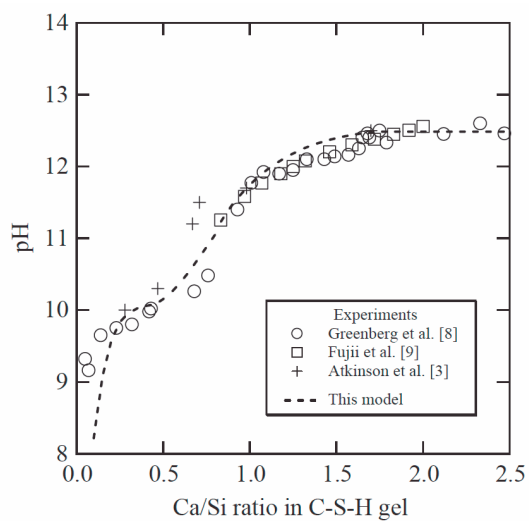


Figure 6.2: Variation of pH pore solution as a function of imposed Ca/Si ratio of synthetic C-S-H gel, from Sugiyama[113].

When portlandite is absent or has all been consumed the carbonation reaction proceeds further. pH is defined at that point by the composition of C-S-H (see Figure 6.2) and more generally from any calcium bearing hydrate present in the system and in equilibrium with the pore solution. C-A-S-H gel gets progressively decalcified and transformed into an intimate mixture of calcium carbonate and amorphous silica (and alumina) gel. Ettringite decomposes below a pH of around 10.4, and below pH 10 gypsum precipitates [114].

Considering the carbonation mechanisms, it can be said that carbonation of concrete can be limited by two rate determining processes.

1. As carbonation starts in a partially saturated microstructure, CO_2 freely diffuses and the initial rate of reaction is inversely proportional to the CaO content, since the more carbonatable content available the more CO_2 will be fixed and the slower this first step will proceed.
2. As soon as the carbonation of this first outer layer has occurred, the carbonation rate becomes limited by the CO_2 diffusion through the carbonated layer. The carbonation rate in this case is limited by the intrinsic permeability of concrete [115]. It will also be affected by the degree of saturation of the porosity. There is therefore a clear relationship between carbonation depth and air permeability, illustrated in Figure 6.3.

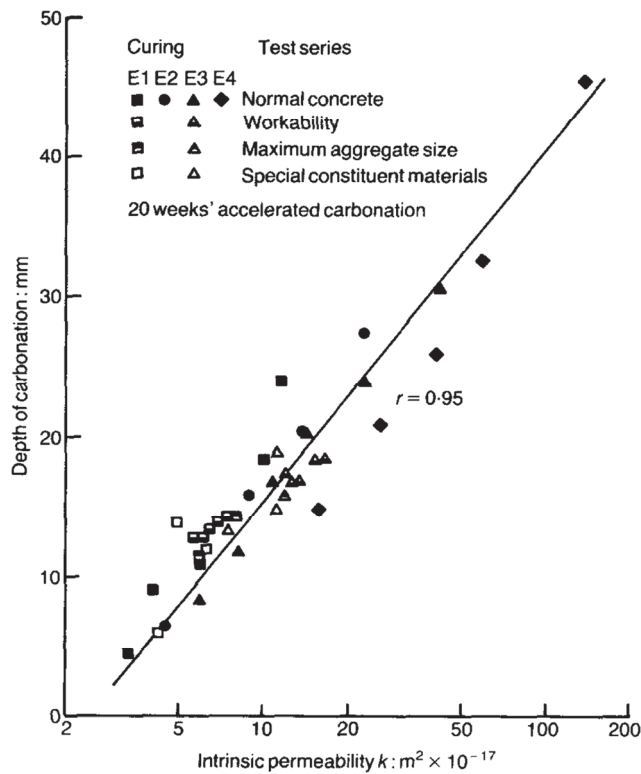


Figure 6.3 Linear relationship between carbonation depth and air permeability (from Dhir [116])

The carbonation depth is usually assumed to evolve accordingly to Fick's diffusion law, considering the CO₂ concentration gradient as the driving force of the diffusion (Equation 6-6):

$$x = C\sqrt{t} \text{ or } x = Ct^n \tag{Equation 6-6}$$

x being the carbonation depth [m] at time t [s], C a constant and n = constant, typically a value of m = 0.5 is used or sometimes lower.

However the differences between the two limiting rate reactions often results in the overestimation of carbonation of blended cements even after 1 or 2 year of natural carbonation compared with longer term carbonation over 10 or 15 years (see in Figure 6.4 the discrepancy found for fly ash).

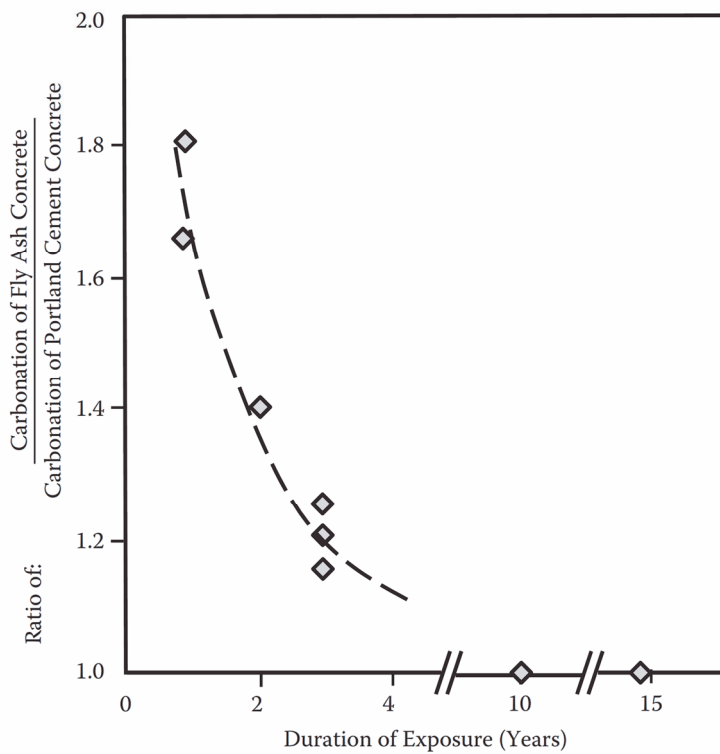


Figure 6.4: The ratio of the carbonation of fly ash concrete over the carbonation of Portland cement concrete is plotted as a function of exposure time. [117], [118]

Another result from Thomas shows that the carbonation depth after 10 years is almost independent of the fly ash content of the binder, as long as the strength is above 45 MPa. For lower strength materials, the extension of the cure to 7 days considerably improves the resistance to carbonation, see Figure 6.5. It shows that compressive strength can be a reliable indicator for long term carbonation resistance and has been pointed out by several other authors [119-121].

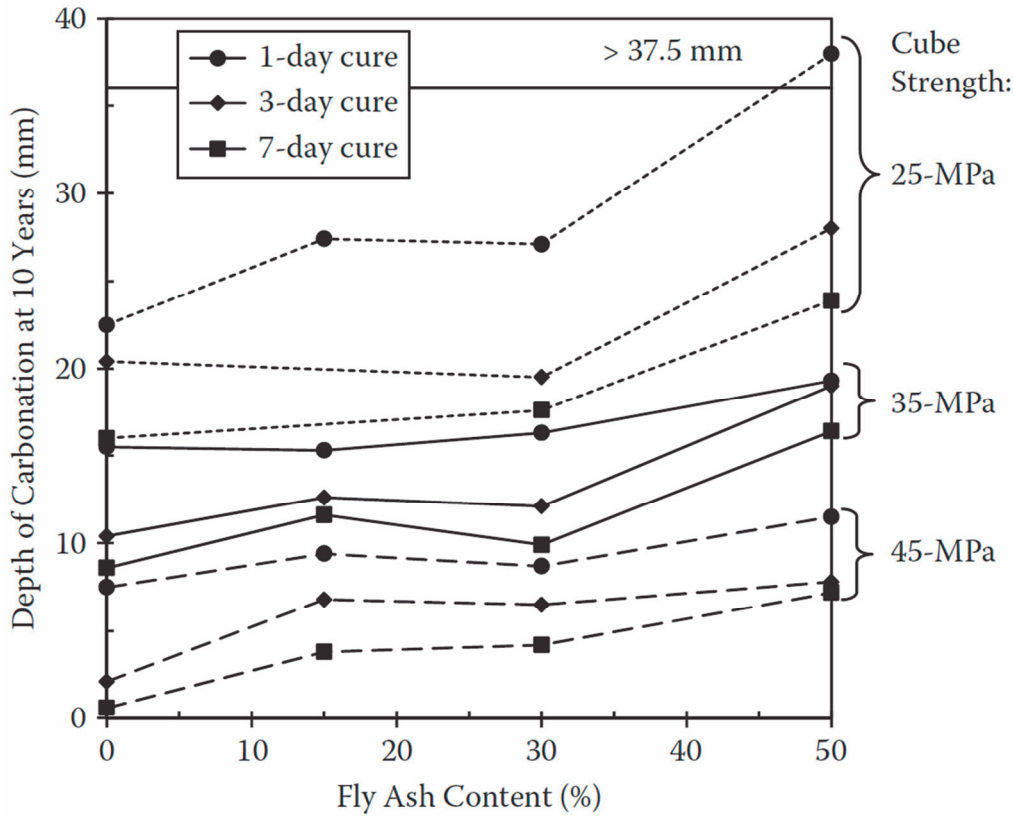


Figure 6.5: Carbonation depth at 10 years, for varying fly ash content and curing time[118].

6.2. ACCELERATED CARBONATION TEST AND CO₂ LEVEL

Most of the literature dealing with carbonation reports on accelerated carbonation tests. Such tests seem attractive because of their short duration. But there is no consensus among researchers or civil engineers on the procedure that should be followed to carry out accelerated carbonation tests. Harrison published recently some interesting articles of the differences among the procedures in Europe [122-124]. A selection of accelerated carbonation procedures used in Europe is given in Figure 6.6. The CO₂ vol. content varies from 1 to 50%, the time from 3 days to 20 weeks, preconditioning varies also significantly.

Country	Curing/preconditioning regime	Specimen type/size	Accelerated carbonation exposure conditions		Carbonation depth measurement method	Time of carbonation depth measurements	
			Carbon dioxide: % vol	Temp: °C RH: %			
Belgium	Water cured for 8 weeks then transferred to 60°C room for 14 days or until constant mass	Concrete prism 150 × 150 × 600 mm	1	20	55	RILEM CPC-18 (RILEM, 1988)	3, 7, 14, 28, 35, 42, 56 days
Germany	7 days water then 21 days lab conditions (20 ± 2°C, 65 ± 5%)	Concrete prism 100 × 100 × 500 mm	2	20	65		28 days
UK ^a	28 days water then 14 days lab conditions (20 ± 2°C, 65 ± 5%)	Concrete prism 100 × 100 × 500 mm	4.0 ± 0.5	20 ± 2	55 ± 5		Various ages up to 20 weeks.
France ^b	28 days or 90 days (water or RH > 95%) vacuum saturation for 24 h followed by oven drying for (48 ± 2) hours at 40 ± 5°C)	Concrete prism: 70 × 70 × 140 mm Concrete cylinder: 1100 × 70 mm	50 ± 5	20 ± 2	65 ± 5	AFPC-AFREM (similar to RILEM CPC-18)	At least 7, 14 and 28 days
Italy	3 days water, 25 days in air (20°C, 50% RH)	Concrete cylinder Ø = 80 mm × h = 200 mm	50	20	55	UNI 9944	3, 6, 9, 12, 15 days
Nordic	Minimum of 4 weeks in atmosphere of 23 ± 2°C and 50 ± 5% RH	Mortar prism 40 × 40 × 160 mm	20 ± 3	23 ± 3	65 ± 10	Phenolphthalein spray	Exposed for 8 days, tested every 48 h

RH, relative humidity
^a Active control on carbon dioxide, RH and temperature. Further details of this test method attached to this paper.
^b Active control on carbon dioxide
^c Other drying options: 1 month at T = 60 ± 5°C and at RH = 63 ± 5%, 1 month at T = 45 ± 5°C in ventilated oven (+ 1 month sealing at T = 45 ± 5°C)

Table 1. Summary of selected European accelerated carbonation tests

Figure 6.6: Diversity of the accelerated carbonation procedures depending on each country[124].

Besides the large variety in testing conditions for accelerated carbonation, there are doubts on the reliability of accelerated tests with very high CO₂ levels [125]. For example Castellote & co-workers have monitored the evolution of Si coordination by ²⁹Si MAS NMR as a function of CO₂ content of the carbonation atmosphere[126].

They could demonstrate that while 3% CO₂ seems to only accelerate the carbonation mechanisms of silicon in C-S-H, CO₂ levels of 10 and 100% lead to formation of pure silica gel, with only Q³ and Q⁴ coordination remaining after carbonation and even anhydrous Si Q⁰ disappearing. Results are reproduced below in Figure 6.7.

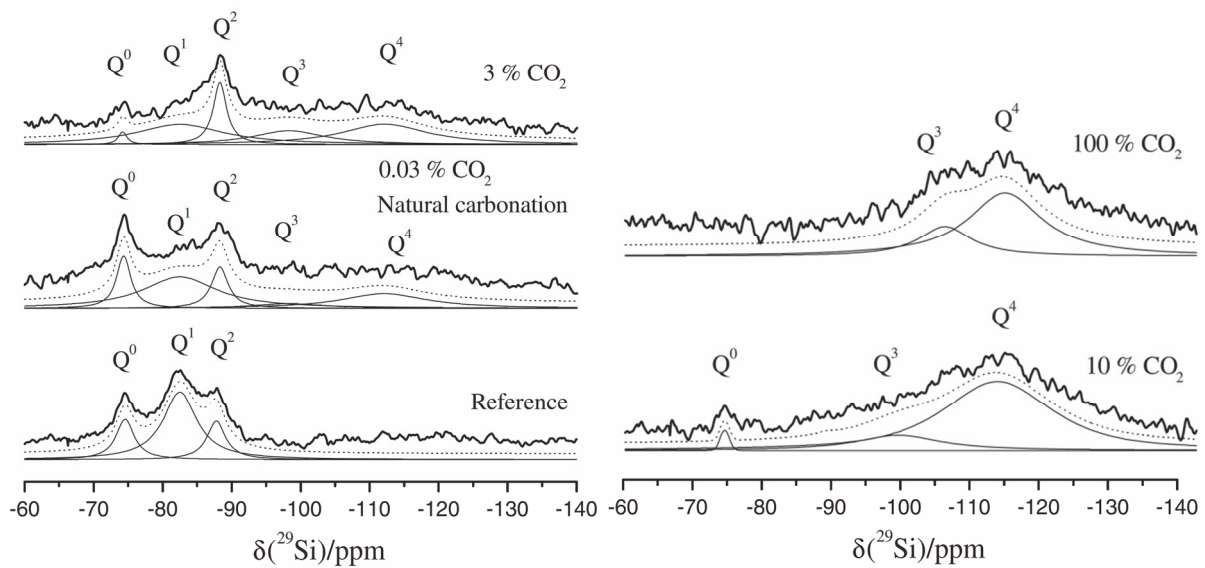


Figure 6.7: Effect of the CO₂ content of the carbonation atmosphere on Si coordination analysed by ²⁹Si MAS NMR [126]

In addition, accelerated carbonation also modifies the pore structure. Thiery found that porosity reduction (“clogging”) contribution by C-S-H was reduced for increasing CO₂ content, see Figure 6.8.

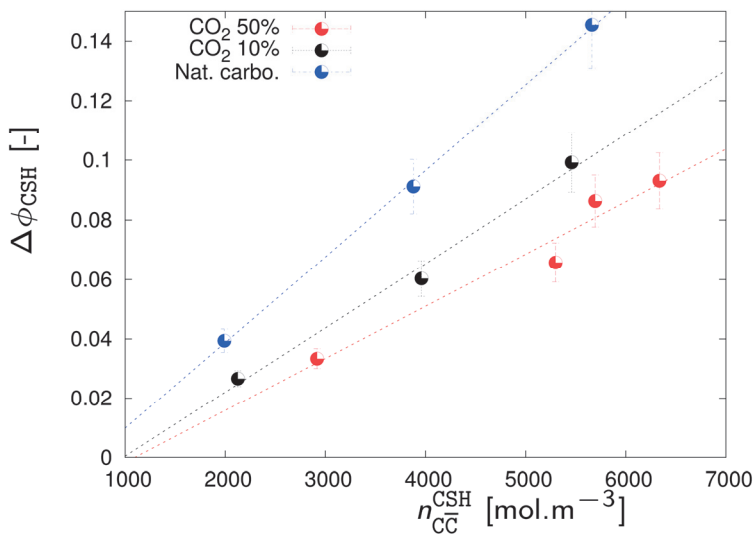
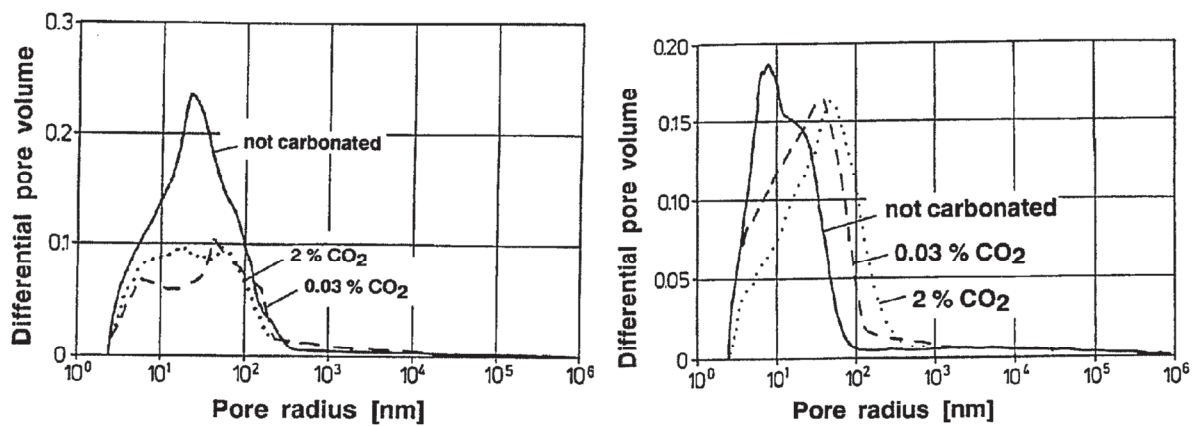


Figure 6.8: Reduction of porosity accounted for C-S-H carbonation, normalized by mole of C-S-H for Portland cement as a function of CO₂ atmospheric level, by Thiery [127]

Earlier Bier & Kropp [128] presented other results demonstrating the influence of CO₂ content on porosity evolution. In their case they were comparing Portland cement and Slag cement and pore size distributions were showing different behaviour upon carbonation (Figures 6.9). The authors related this result to the formation of different calcium carbonate polymorphs.



Figures 6.9. Pore size distribution by Mercury Intrusion Porosimetry as a function of CO₂ content during carbonation for Portland cement (left) and Slag cement (50% slags) (right) [128]

6.3. CALCIUM CARBONATE POLYMORPHS

The three polymorphs of calcium carbonate are calcite, vaterite and aragonite. Calcite is the most stable calcium carbonate polymorph with the lowest solubility in ambient conditions of pressure humidity and temperature. Aragonite is mostly known as a calcium carbonate forming in relation with biological processes, while vaterite is the least encountered species. But the three polymorphs have been reported to form during carbonation of cementitious phases.

The calcium carbonate polymorphs have different molar volume (34, 35 et 38 cm³.mol⁻¹ for aragonite, calcite and vaterite respectively, [129]).

Note that molar volume of all calcium carbonate polymorphs is higher than molar volume of portlandite ($33 \text{ cm}^3 \cdot \text{mol}^{-1}$). This difference is the main explanation for the so called “clogging” effect observed in carbonated PC.

The review of literature concerning the formation of the different polymorphs gives some trends:

- Overall, there is agreement that the first calcium carbonate forming during carbonation is amorphous [130, 131]. Ogino et al. have studied the mechanisms of formation of calcium carbonate in pure water, they confirmed that after the first rapid precipitation of amorphous calcium carbonate, it transformed to vaterite within minutes at ambient temperature. The vaterite in turn transforms to calcite via a dissolution-reprecipitation mechanism. Garbev confirmed this results for synthetic C-SH, they found that amorphous calcium carbonate, $\text{CaCO}_3 \cdot \text{H}_2\text{O}$ formed within minutes by contact with air [132].
- First reports of CSH carbonation were made by Sauman [133]. He proposed that vaterite was the first polymorph precipitating, later on converting into aragonite and finally calcite or directly to calcite; Ikeda confirmed this experimentally with 11\AA Tobermorite [134]. Sauman stated that the vaterite stability domain was extended at low CO_2 partial pressure, while calcite dominated at higher CO_2 content. Goodbrake [135] found aragonite to form in small amounts during carbonation of C-S-H when it is allowed to dry out, in contrast to the formation of calcite when kept C-S-H is kept wet. Black reported that vaterite seems to form preferentially on portlandite crystals, probably because of the similarities in their symmetries and their positive surface charge [131].
- As for the carbonation of Portland cement, calcite and vaterite are also the usual polymorphs forming during carbonation of portlandite and C-S-H. Spanos related favoured formation of vaterite for conditions of high pH [136]. In any case vaterite will tend to transform into calcite, but the transformation can be kinetically slowed down in low humidity conditions [130, 137].
- For blended cements, the picture seems even more complex and the three polymorphs are forming. Aragonite formation seems to be favoured by decreased Ca/Si ratio of C-A-S-H gels and therefore associated with C-A-S-H compositions influenced by pozzolanic reactions [128, 138, 139]. Black et al [131] have proposed that aragonite forms after full carbonation of C-A-S-H and forms preferentially on silica gel.

The review of the literature demonstrates that there is relatively little knowledge on the mechanisms of carbonation of blended cements with high replacement levels. There is also evidence that short term carbonation test tend to overestimate carbonation resistance of blended cements [118].

Short term carbonation tests should therefore be critically assessed taking in account the influence of the CO₂ level and the evolution of the phase assemblage to improve the understanding of carbonation mechanisms.

6.4. OVERVIEW OF CURRENT WORK

It has been demonstrated in chapter 4 that blending with 30% metakaolin consumes almost all the portlandite. This makes such blends unusual since the conventional view on carbonation is that this concerns mainly the reaction of portlandite. It is therefore crucial to investigate how materials devoid of portlandite are affected by natural and accelerated carbonation. The purpose of this chapter is to characterize the carbonation resistance of Portland cement and blends with high quantities of calcined clays, with and without limestone and look at their carbonation mechanisms both in natural and in accelerated carbonation.

Based on the review of the literature, it is crucial to look at the evolution of the phase assemblage in order to better understand the similarities and/or differences of the carbonation processes in accelerated and natural carbonation and with and without calcined clays.

A comparison with thermodynamic prediction by GEMS is also carried out to identify the relative importance of thermodynamics and of kinetics in the different processes taking part in carbonation.

Finally, it is also important to investigate how the pore size distribution evolves with carbonation and the possible consequences on strength and durability are briefly discussed.

6.4.1. THERMODYNAMIC MODELLING OF CARBONATION

Thermodynamic calculation is a tool that can be used to evaluate the phase assemblage and the pH reduction due to carbonation and discuss the differences between modelling and real observations.

The GEMS modelling tool (GEM-Selektor 3, [95]) is used, where C-S-H is described by the model proposed by Kulik [96, 140], two solid solutions, between the Jennite end member (Ca/Si ratio 1.67) and Tobermorite end-member (Ca/Si ratio 0.83) and between Tobermorite and pure amorphous silica gel are used in GEMS to capture decalcification of C-S-H upon carbonation. However this model has some known limitations, the main one is the absence of structural and solubility data of for C-A-S-H with incorporated alumina and their interactions with other ions such as alkali. Proper input data would also require having the exact evolution of CO₂ partial pressure since it can also modify phase solubility.

Having these limitations in mind, we can still discuss what GEMS predicts by considering the carbonation reaction as the incorporation of increasing amounts of carbon dioxide into a cementitious matrix. This gives a plot with the sound phase assemblage on the left and the fully carbonated phase assemblage on the right. The initial sound phase assemblage consists of C-S-H, portlandite, monocarboaluminate, ettringite and hydrotalcite. Figure 6.10 shows the plot based on the composition of the PC used for the 3% accelerated test.

With increasing additions of CO₂, portlandite is the first phase to react to give calcite as the thermodynamically stable phase. In reality, it appears that dissolution kinetics of calcium hydroxide are slowed down because of the diffusion of CO₂ through the calcium carbonate crystals formed and other phases such as C-S-H always begin to carbonate before full carbonation of portlandite.

When portlandite disappears, the Jennite fraction of C-S-H begins to disappear. As a direct consequence of the C-S-H Jennite-Tobermorite-Silica gel solid solution model, instead of a progressive decalcification, Jennite decomposes and ions are congruently released in solution. Later on, monocarboaluminate is the next phase reacting with CO₂.

This implies that silicon and aluminium concentrations in solution also increase because of Jennite and carboaluminate destabilization respectively and strätlingite is forming in return. This has never been reported in real system to our knowledge, and can be seen as inherent to the C-S-H GEMS model.

With introduction of increasing CO₂ amount, thermodynamic modelling predicts then the formation of thaumasite after ettringite destabilizes. In real cementitious systems, thaumasite has been reported to form at ambient temperature; however it seems that its kinetics of reaction is very slow

and it is rarely observed in real structures, probably because of the reduced solubility of the carbonate ions at ambient temperature.

It can be dealt with such phase appearance upon carbonation in GEMS that do not fit to reality by turning off precipitation of these phases. That doesn't modify significantly the picture of carbonation.

Finally when C-S-H is totally transformed into silica gel, pH is below 10 and gypsum precipitates.

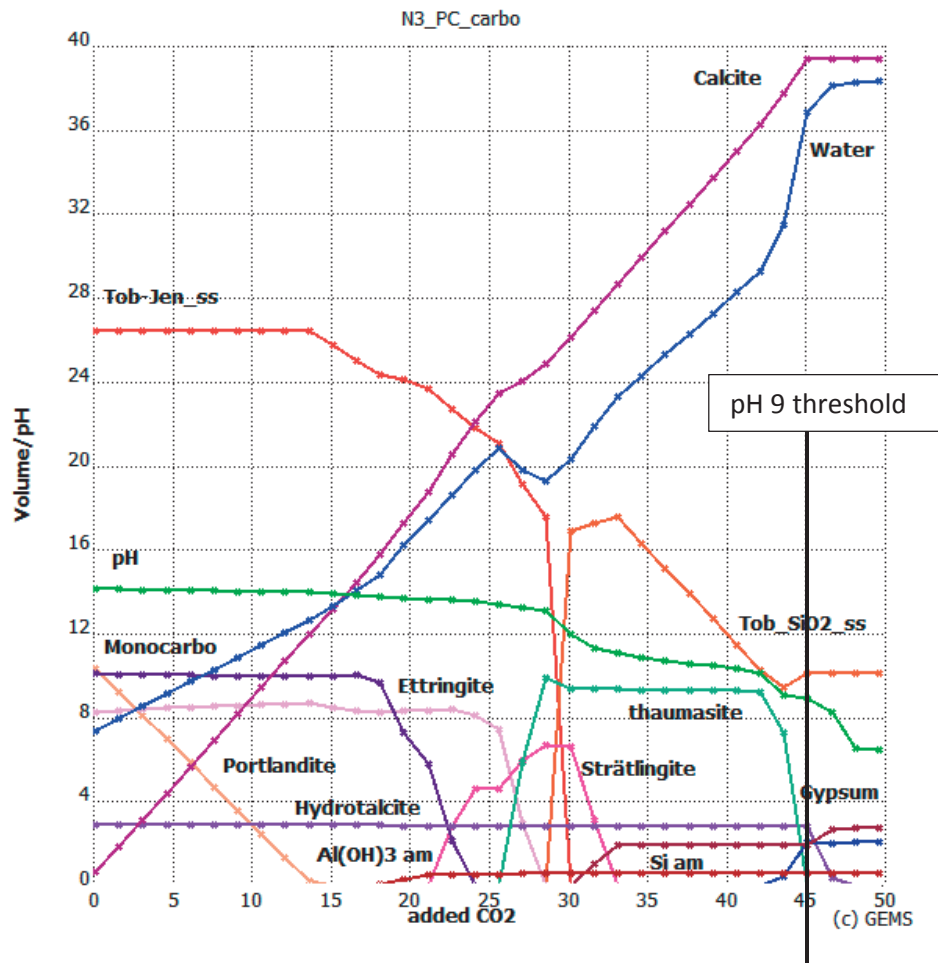


Figure 6.10: Plot of the volume variation of the cementitious phases as well as pH as a function of increasing CO₂, both normalized for 100g of initial anhydrous cement. Anhydrous phases are considered inert and neglected.

In Figure 6.11, the carbonated phase assemblage of B45 is shown. Based on the results obtained in the previous chapter, we defined that the PC reacted at 90%, metakaolin at 50% and limestone at 33% to produce the initial phase assemblage. It consists of C-S-H, strätlingite, monocarboaluminate, ettringite and hydrotalcite.

Monocarboaluminate and C-S-H are almost directly destabilized. When Jennite is all consumed pH drops at a level slightly above 10 and strätlingite as well as ettringite disappear. Gypsum becomes stable and the pH decreases below pH 9 with about half the CO₂ amount that was necessary in PC. This corresponds to the reduction of the buffering capacity and fits with the reduction of the total carbonatable content available, approximated to PC content since neither limestone or calcined clays are strictly speaking carbonatable.

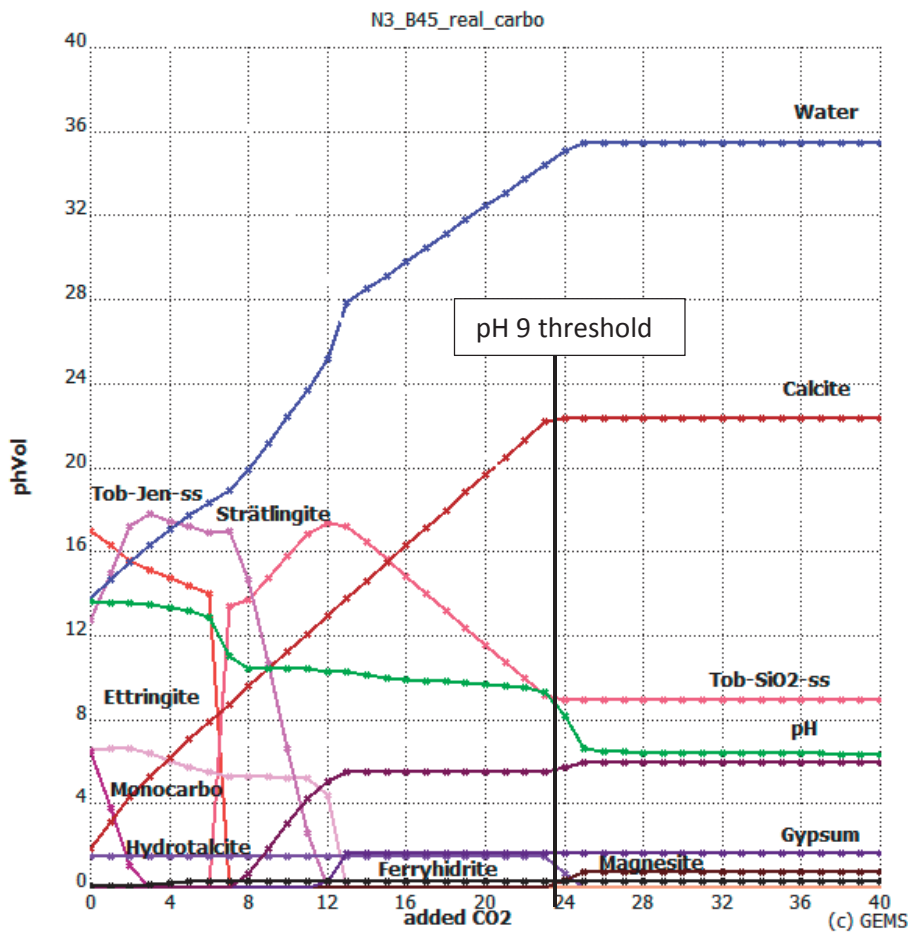


Figure 6.11: Plot of the volume variation of the cementitious phases as well as pH as a function of increasing CO₂, both normalized for 100g of B45.

6.5. EXPERIMENTAL DETAILS

6.6. PASTE RESULTS

6.6.1. NATURAL CARBONATION

6.6.1.1. PHENOLPHTHALEIN PROFILES

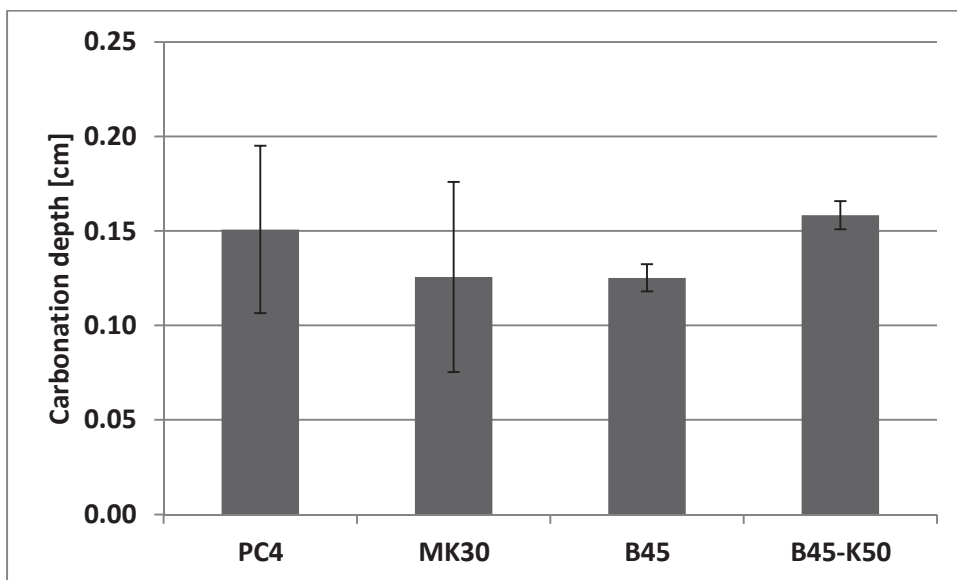
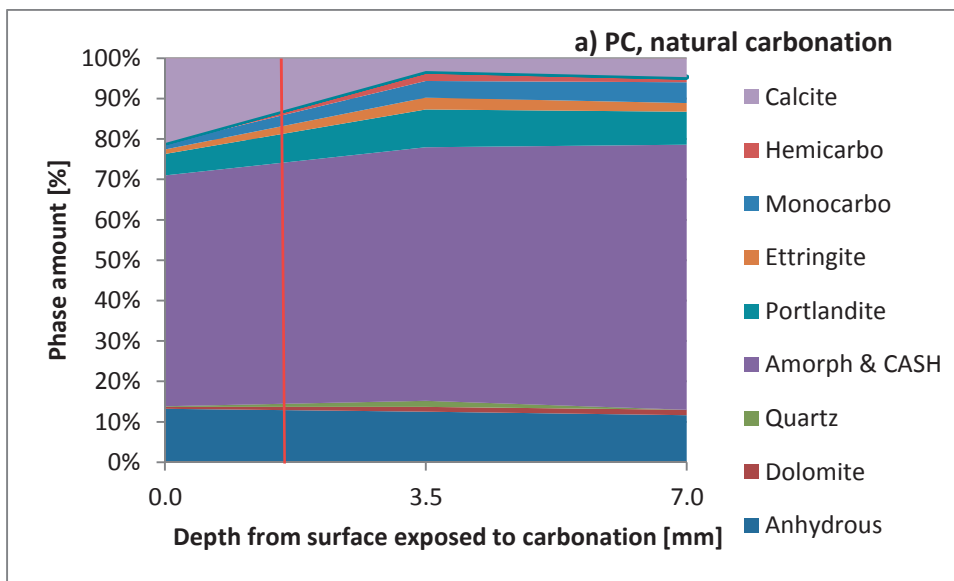


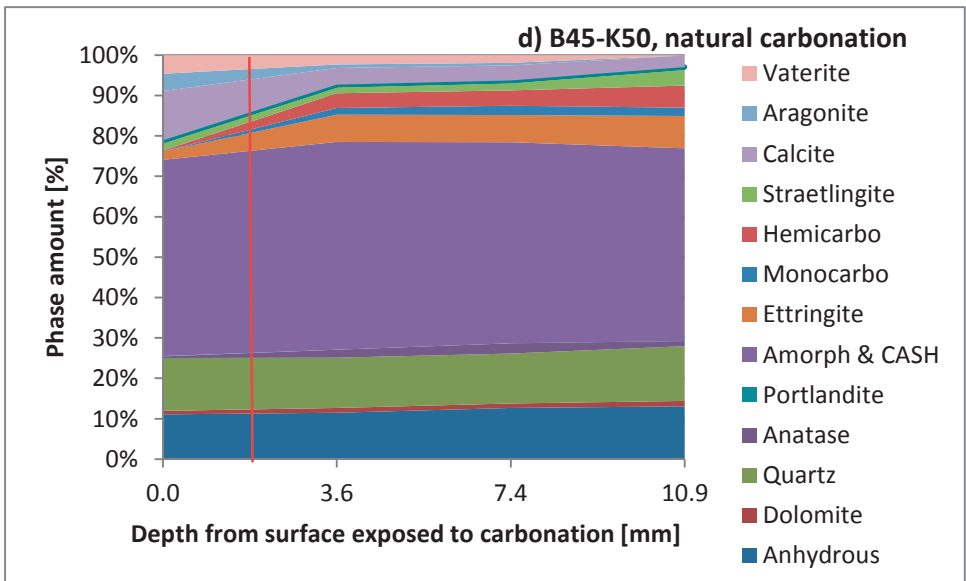
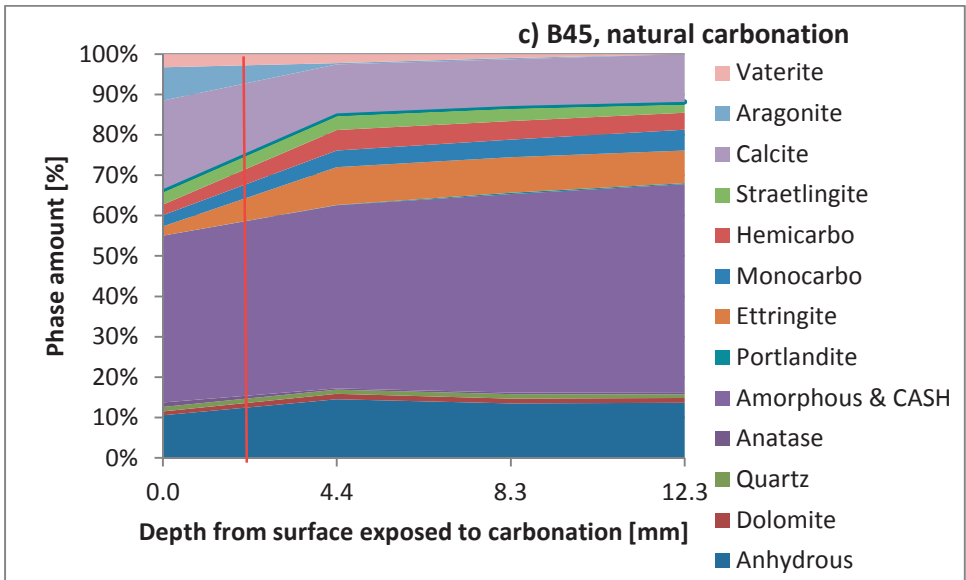
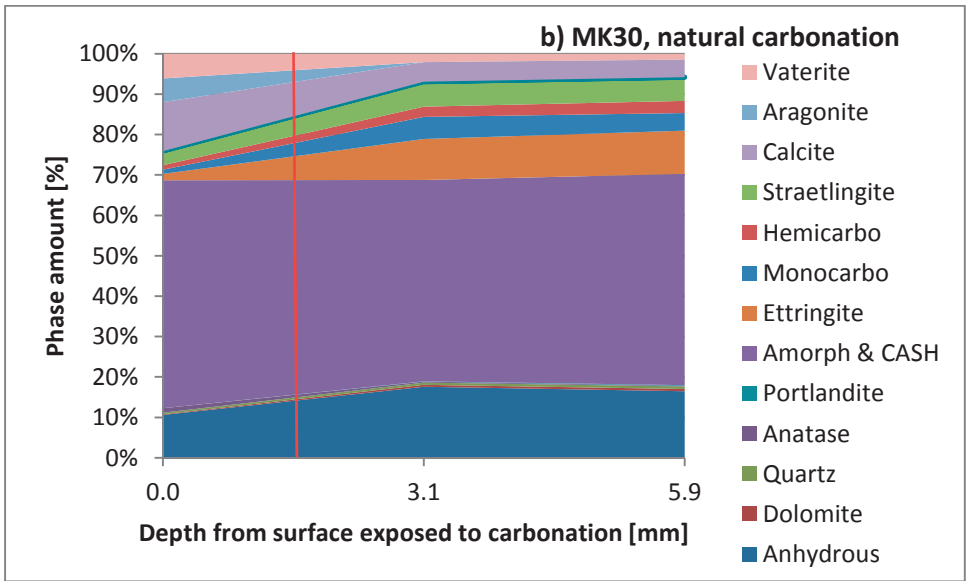
Figure 6.12: Carbonation penetration depth obtained by phenolphthalein test after 8 months of natural carbonation test on paste samples.

The measured carbonation depths obtained in natural carbonation at constant 53% relative humidity (Figure 6.12) were very small, between 1 and 2 millimetres after 8 months and the measurement error comparatively high so that it is not possible to identify any significant differences between the samples at this point.

6.6.1.2. XRD CHARACTERISATION

In Figures 6.13 the phase assemblages are given. Quantitative phase percentages are plotted as a function of the depth from the surface exposed to carbonation. At bottom the anhydrous phase fraction is the sum of the remaining C_3S , C_2S and C_4AF . Traces of quartz, anatase and dolomite present in the original anhydrous cement or calcined clay are also given. Then the different hydrated phases are plotted, the sum of all amorphous phases, including C-S-H, silica gel and non-reacted metakaolin, which cannot be identified nor quantified by XRD. Finally on the top are shown the different calcium carbonate polymorphs as well as gypsum (when present) that can form upon carbonation. A disadvantage of the XRD method is that it hardly allows the discrimination between amorphous phases of different composition. C-S-H is therefore diluted among the total amorphous content. It should also be noted, that the evolution has been linearly plotted between each layer studied, which is not necessarily the case.





Figures 6.13 a) b) c) & d): These graphs represent the semi-quantitative variation of crystalline phases as a function of the depth from the exposed surface to carbonation, for respectively PC, MK30, B45 and B45-K50. Red lines correspond to the phenolphthalein front experimentally observed.

These results confirm the observations made with the phenolphthalein indicator since the major changes of phase's assemblage are observed between the outer and the first layer immediately adjacent to the front. However it is interesting to see that calcium carbonate polymorphs are also present in small amount in the deeper layers. Carbonation is not strictly taking place at the front but seems to slowly progress deeper in the material.

In PC, calcite predominantly forms at the outer layer, aragonite and vaterite are negligible. Portlandite, ettringite and carboaluminates are reduced. In the second layer, calcite significantly decreases, while ettringite, carboaluminates, amorphous fraction and portlandite already remain. It does not appear that one phase, e.g. portlandite, is carbonating preferentially to the others.

For MK30, there is a considerable presence of calcite, vaterite and aragonite in the surface layer only. All calcium carbonate polymorphs decrease such that only calcite remains in much lower amounts at almost constant level from 3mm and deeper. A small amount of portlandite is present throughout the depth analysed. Ettringite is considerably reacted at the outer layer and then the intensity is stable in all deeper layers. Carboaluminates and strätlingite show similar behaviour to ettringite, but the decrease is less intense at the outer layer.

In B45 and B45-K50, the overall trend is the same as in MK30. The similarity between the phase assemblages obtained in MK30 and B45 can be explained by the fact that PC5 used in these blends contained significant amounts of calcite. In B45-K50, calcite is still continuously decreasing, indicating carbonation processes taking place. There is also a minor decrease of anhydrous phases intensity noticeable in the first layer for all blends, among which C_2S seems to be the phase decreasing the most, this effect was not observed for PC. Considering the very high amorphous content and the accuracy of the semi quantitative analysis carried out these changes are in the margin of error and should be taken with care.

Finally the amorphous content remains globally constant for all compositions. While the main component of amorphous, namely C-S-H should be reduced during carbonation, it is partly replaced by crystalline calcium carbonate and amorphous silica gel. There are also crystalline hydrates such as AFm and ettringite that carbonate and form new amorphous content such as $\text{Al}(\text{OH})_3$. Furthermore different authors have reported that transient metastable amorphous calcium carbonates can form and later reprecipitate into crystalline polymorphs, as Black demonstrated for the carbonation of C-S-H [131].

In summary, this study confirms that all the phases seem to carbonate simultaneously. According to the literature, carbonation processes are occurring over a much larger depth than given by the simple phenolphthalein front. Finally, the balances between calcium carbonate polymorphs seem to shift from almost only calcite and small amount of vaterite in PC to increasing amounts of aragonite and vaterite for the blends.

6.6.2. ACCELERATED CARBONATION WITH 3% CO_2 ON PASTES

6.6.2.1. CARBONATION PROFILES BY PHENOLPHTHALEIN

The depths of the carbonation phenolphthalein front for this accelerated test are given in Figure 6.14. First it can be observed that the carbonation depths are much higher. The depth of carbonation is lowest for PC, with less than 10mm penetration, followed by MK30, with similar behaviour but slightly higher carbonation, about 11.5 mm. B45 and B45-K50 show the greatest depth of carbonation, with almost 15 mm carbonation depth. Blending metakaolin, with either calcite or quartz seems to give the same behaviour during carbonation. The blends carbonate significantly more at the beginning, later on the rate of carbonation seems however only slightly higher for the B45's but is almost the same for MK30 than for PC. Carbonation rates calculated from these 3 points confirm this visual impression; MK30 and PC have very similar carbonation rate and B45's about 50% higher (see Table 6.1).

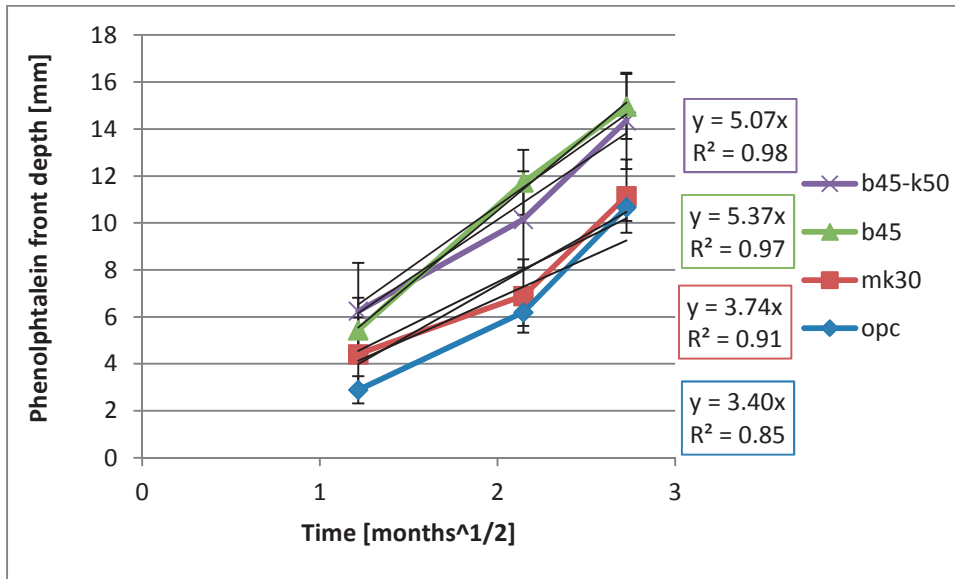


Figure 6.14: Carbonation profiles obtained by phenolphthalein test in accelerated carbonation test using 3% CO₂ on paste samples.

Table 6.1: Carbonation rates obtained in accelerated carbonation using 3% CO₂.

	PC4	MK30	MKB45	MKB45-K50
Carbonation rate [mm/square root(years)]	13.6	14.2	19.0	18.2
standard deviation	1.5	1.2	1.2	1.0

The depths are plotted in Figure 6.15 as a function of their PC content since the Portland cement content is roughly proportional to the content of carbonatable material. The higher the PC content the lower the carbonation during the initial phase.

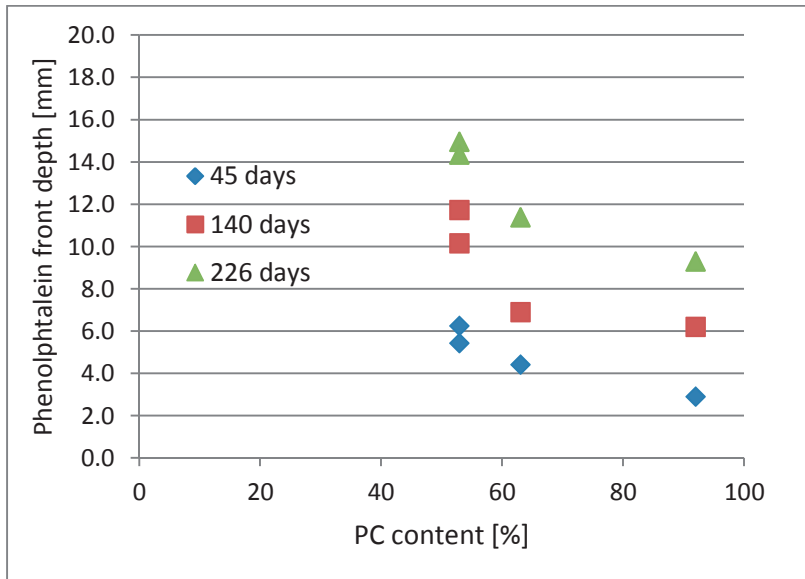
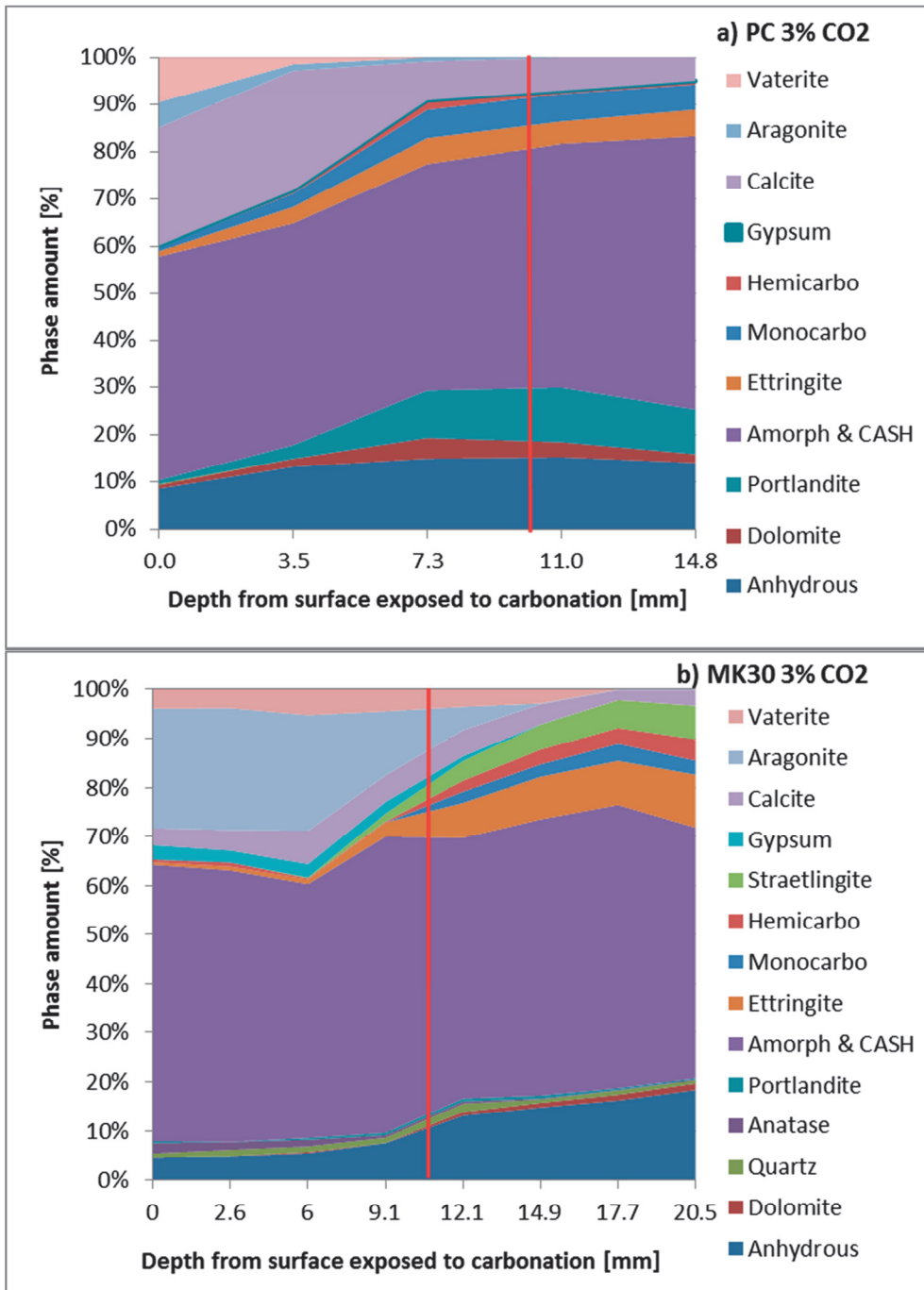


Figure 6.15: Carbonation depth measured by phenolphthalein as a function of PC content

6.6.2.2. XRD CHARACTERIZATION

Figure 6.16 show the phase assemblages obtained by semi-quantitative Rietveld analysis of the 4 different paste compositions after 226 days of accelerated carbonation:



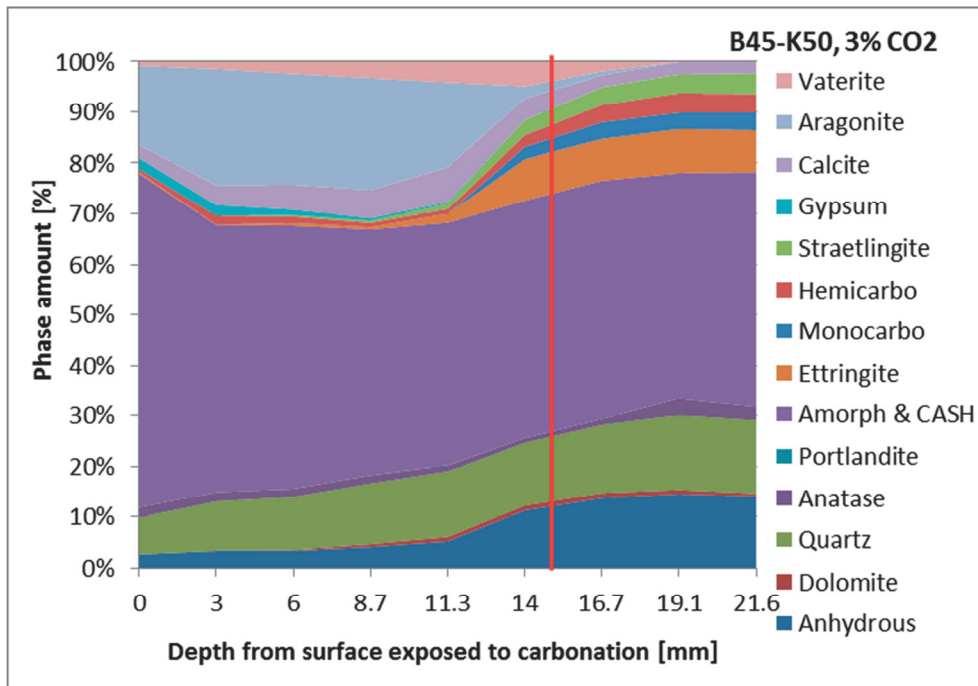
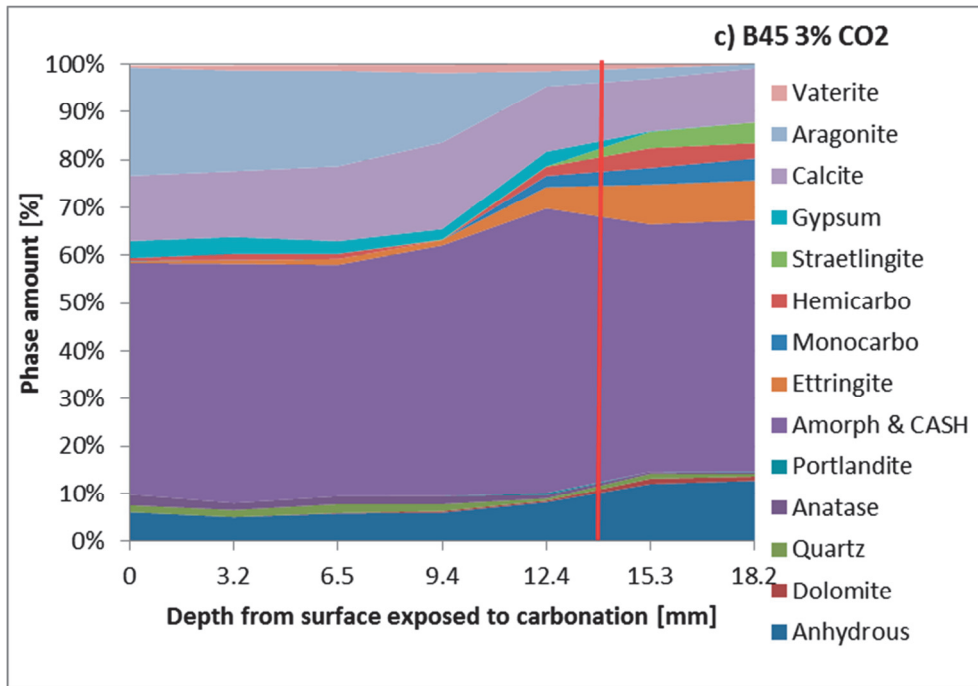


Figure 6.16 a) b) c) & d): Semi-quantitative quantification of crystalline phases of respectively PC, MK30, B45 and B45-K50 after accelerated carbonation as a function of the depth from the exposed surface to carbonation. Red lines correspond to the phenolphthalein front experimentally observed.

PC paste shows a phase assemblage with accelerated conditions similar to natural carbonation. The main difference lies in a slightly higher amount of vaterite and aragonite forming in the 2 upper layers compared to calcite. Almost 90% of portlandite had reacted at the surface.

All the cementitious phases carbonate simultaneously, both in natural carbonation conditions and in accelerated carbonation, independently of the presence of portlandite.

In the blends, at greater depth a phase assemblage similar to the sound material remains where more carboaluminates, ettringite, strätlingite, C-A-S-H all are present. At the surface however the accelerated carbonation changes dramatically the balance between the calcium carbonate polymorphs. Aragonite is systematically predominant in the carbonated zone compared to calcite and vaterite. Also gypsum precipitated in all blends while ettringite vanishes.

A main feature of the blended systems is also that the phenolphthalein front is no longer a good marker of the change of the phase assemblage. The carbonation profile is extending over 10 mm from the totally carbonated zone up to the non-carbonated zone. This has been demonstrated already in standard PC [112, 141, 142] but seems to be exacerbated with cements blended with high amount of metakaolin. This confirms that care should be taken in the interpretation of carbonation fronts obtained by phenolphthalein colorimetric indicator. Complementary investigation methods or pH measurement should be done for a more precise knowledge of pH of the pore solution.

Another important result is that anhydrous phases are considerably decreased by the accelerated carbonation process in all systems. The effect seems however more pronounced in blends than in PC. The C_3S and C_2S are considerably reduced, while C_4AF seems unaffected.

6.6.2.3. MERCURY INTRUSION POROSIMETRY

MIP measurements were made on samples subjected to accelerated carbonation, in the carbonated zones (first 3 mm) and in the sound zone away from the phenolphthalein front. The results are given in Figure 6.17. In the PC sample the total porosity is reduced and significantly refined. In the blends which contain metakaolin the total porosity is also lowered, but there is a coarsening of the porosity, nevertheless the breakthrough diameter in the blends is still less than in the plain PC sample.

Table 6.2 shows the values of the total porosity and of the threshold diameter found by intersecting linear approximation of the linear portion of the curve before and after the threshold.

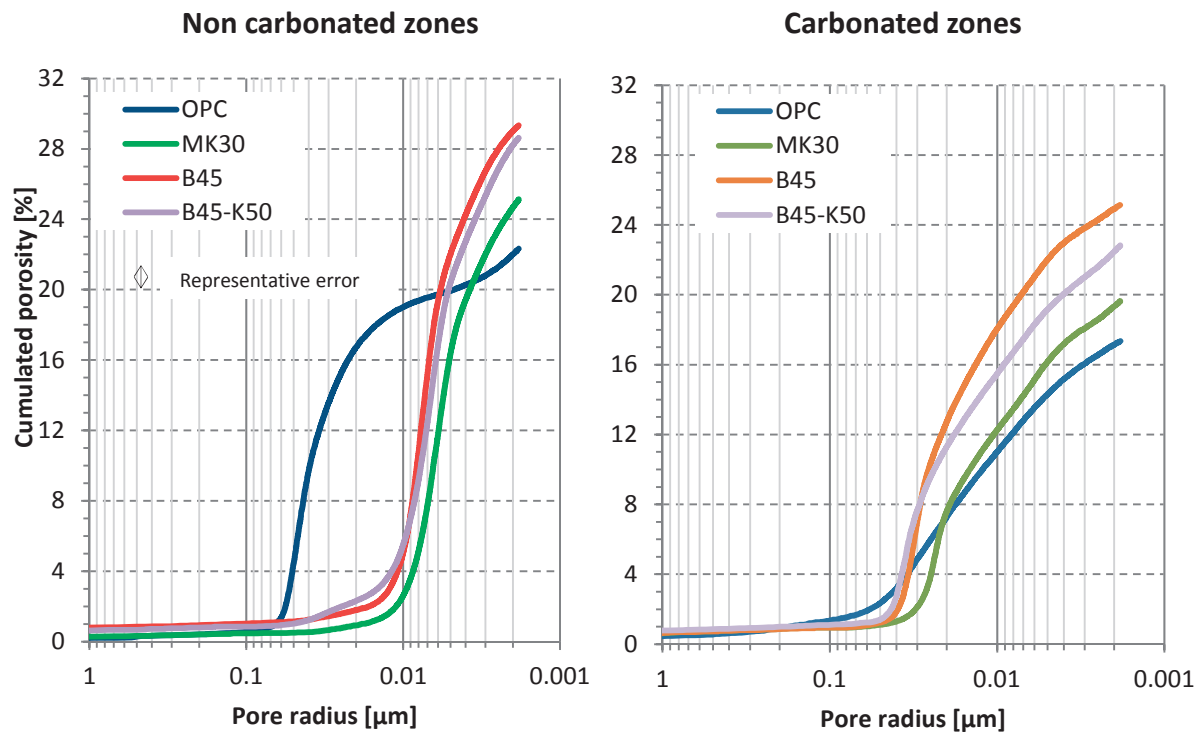


Figure 6.17: Cumulated MIP curves obtained in non-carbonated zones (left) and carbonated zones (right) after accelerated carbonation with 3% CO₂.

A coarsening of the microstructure for the blends containing calcined clays is observed and corresponds in term of mean threshold diameter to an increase by a factor 2 to 4, in the meantime the cumulated porosity was also significantly reduced. This is likely to be affected by the preferential formation of aragonite in blends compared to calcite for PC, since aragonite has a density 8% higher than calcite (2.927 vs 2.711 g/cm³ respectively)

Though Portland cement breakthrough diameter doesn't vary significantly the increase in porosity is steeper in the non-carbonated zone compared with the carbonated one, revealing also a refinement.

Table 6.2: Summarizing table for MIP results in non-carbonated and carbonated zones.

	Non-carbonated zone		Carbonated zone	
	Total cumulated porosity	Threshold diameter	Total cumulated porosity	Threshold diameter
	[%]	[microns]	[%]	[microns]
PC	22.3	0.060	17.3	0.055
MK30	25.1	0.010	19.6	0.027
B45	29.3	0.012	25.1	0.038
B45-K50	27.1	0.011	22.8	0.040

6.6.3. SUMMARY AND COMPARISON BETWEEN NORMAL AND ACCELERATED CARBONATION IN PASTES

- Normal carbonation during 8 months was not long enough to discriminate between the samples; at this point all samples had similar very low carbonation level.
- With accelerated carbonation PC shows the smallest carbonation depth, followed by MK30. Both B45 have the deepest carbonation. The ranking was unchanged between 1½, 4 and 8 months. This indicates that the PC content, directly proportional to the carbonatable content seems to be the critical parameter governing initial accelerated carbonation. After this initial phase, carbonation rate observed are however similar for PC and MK30, and about 50% higher for both B45 samples.
- The comparison of the different paste compositions in accelerated and normal carbonation conditions shows very significant differences. In PC the phase assemblage remains globally similar in both accelerated and normal carbonation conditions, with portlandite, as well as the other hydrates getting simultaneously and progressively consumed. The only minor difference is the relative increase of the vaterite and aragonite polymorphs in accelerated carbonation compared to normal conditions. The explanation relies most probably on the fact that portlandite is not fully carbonated in PC case, buffering the pore solution pH and

maintaining therefore similar conditions of carbonation. In this case accelerated carbonation can really be seen as an acceleration of the carbonation processes.

- In the case of the blends, no major differences were found between MK30, B45 and B45-K50. It is however not surprising since the phase assemblage of the initial pastes were similar, since the PC contained calcite. Normal and accelerated carbonation give very different phase assemblage. Looking at the XRD semi quantitative analysis, three critical differences have to be pointed out. In blended compositions, accelerated carbonation seems to promote predominant precipitation of aragonite in contrast to normal carbonation which gives calcite as the principal calcium carbonate precipitating. This is a critical point since their calcite molar volume is approximately 8% higher than aragonite. It could account for a significant increase of porosity that might not exist in slower natural carbonation, which is likely to leave time for aragonite to transform to calcite.
- The study of the porosity by MIP has shown a decrease of total porosity of all samples after accelerated carbonation. There was a refinement of the threshold pore size in PC against a coarsening in blends with calcined clays, but pore size entry still remain slightly smaller in blends. This behaviour is fully consistent for PC with the increase of solid volume observed upon carbonation of portlandite into calcite. For the blends, the changes occurring are more complex, since the total porosity evolution and the fineness give opposite trends. But this might be overestimated due to aragonite formation instead of calcite discussed above.
- In blends, ettringite disappeared in accelerated carbonation and gypsum precipitated. Accelerated carbonation obviously provoked such a brutal decrease of pH pore solution that ettringite becomes soluble and sulfate groups are released in solution and recombined into gypsum. Gypsum formation corresponds to a decrease of pH below 10, since ettringite is stable for pH above 10.7 [114]. We postulate that both these differences could be well linked in a more global picture of accelerated carbonation where decalcification of C-S-H is more intense, silica gel forming more rapidly [111]. The exact relationship between silica gel and aragonite formation isn't understood, but various authors have shown evidence that both are likely to preferentially cohabit [143-145].

- Additionally, C-A-S-H decalcification requires charge compensation that can be made by uptake of alkalis from the pore solution and incorporation into the C-A-S-H. There is therefore no progressive realkalisation as it is the case in normal carbonation and it can eventually lead to this pH drop low enough to explain ettringite dissolution and gypsum precipitation. Such a scenario would demonstrate that accelerated carbonation might be unfavourable for blends where portlandite is depleted and it will require more work in the future to prove whether results obtained by accelerated carbonation can be directly used to estimate normal carbonation and predict service life of reinforced structures.
- Finally, anhydrous phases did also considerably carbonate in accelerated carbonation up to almost total consumption of the C_3S and C_2S phases in the outer layers. C_4AF remains almost non-affected. In natural carbonation they seemed to have reacted to small extent. This is another possible source of carbonatable content that can explain aragonite formation. Several authors have indeed studied anhydrous phases carbonation, and reported calcite, vaterite, aragonite and silica gel formation by carbonation of C_3S and C_2S , [146] [147] [148, 149]. These authors have studied carbonation of C_3S and C_2S . There is a wide agreement between them that C_2S carbonate the fastest compared with C_3S , while C_4AF does almost not react and that C_2S reaction with CO_2 preferentially form aragonite and silica gel [148, 149].

6.7. MORTAR RESULTS

6.7.1. MORTARS NATURAL CARBONATION

These samples were exposed to laboratory atmosphere in a cupboard during 24 months ($22^\circ C \pm 1$; 50 to 70 %RH). Carbonation depths were measured with phenolphthalein test after 18 and 24 months and are plotted in Figure 6.18:

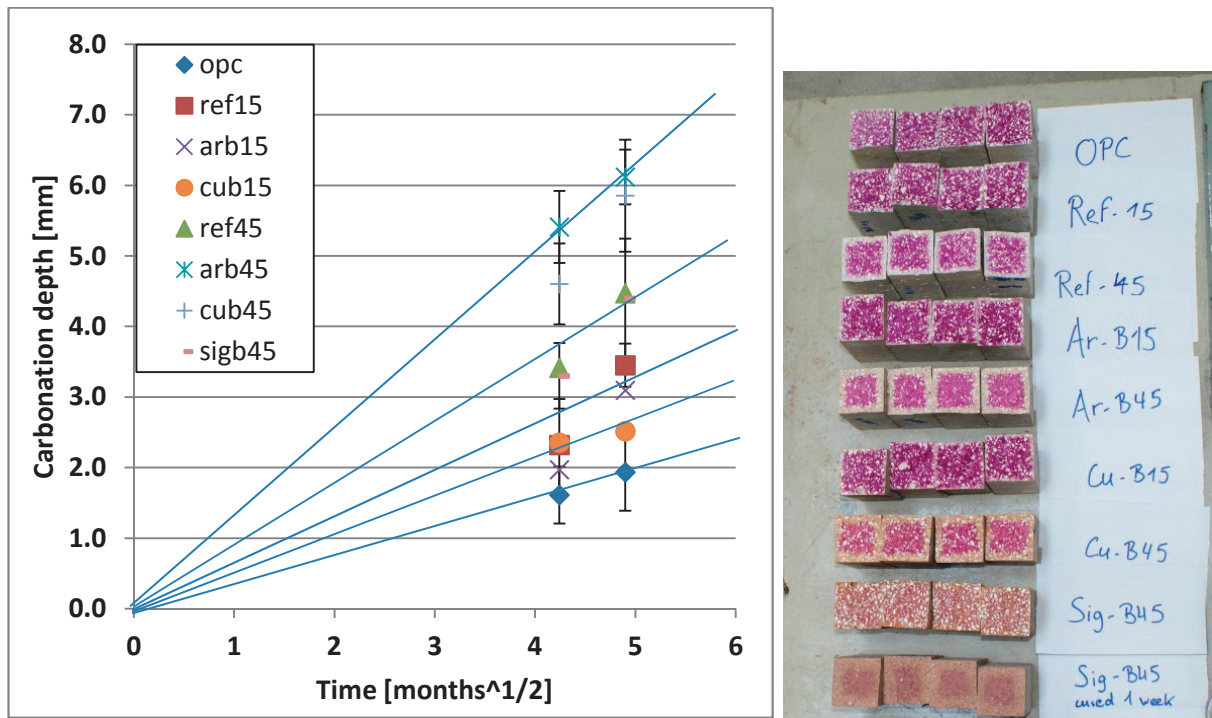


Figure 6.18: Carbonation penetration depth as a function of square root of time obtained by phenolphthalein test after 18 and 24 months of natural carbonation test on mortar samples (left) and picture of the carbonation depth by phenolphthalein spray after 24 months (right).

The carbonation depths are generally low, less than 6 mm after 2 years. PC shows the smallest carbonation depth, 2mm at 24 months, followed by all the blends substituted by 15%, grouped all between 2.5 and 3.5 mm. For 15% blending, the different kaolinite contents of the clay do not significantly affect the carbonation level. Then (with 4 mm) follow the samples containing 45% quartz together with the self-made SigB45 at same age. This blend had higher kaolinite content and showed higher strength, which can probably explain the better behaviour compared to the other B45 blends, showing around 6 mm carbonation depth. When reporting carbonation depths at 24 months as a function of the carbonatable content, carbonation depth again correlates with the carbonatable content. The scatter is very large between the clay with the highest kaolinite content around 60% and kaolinite content below 40%(ArB45 and CuB45, red circles), see Figure 6.19.

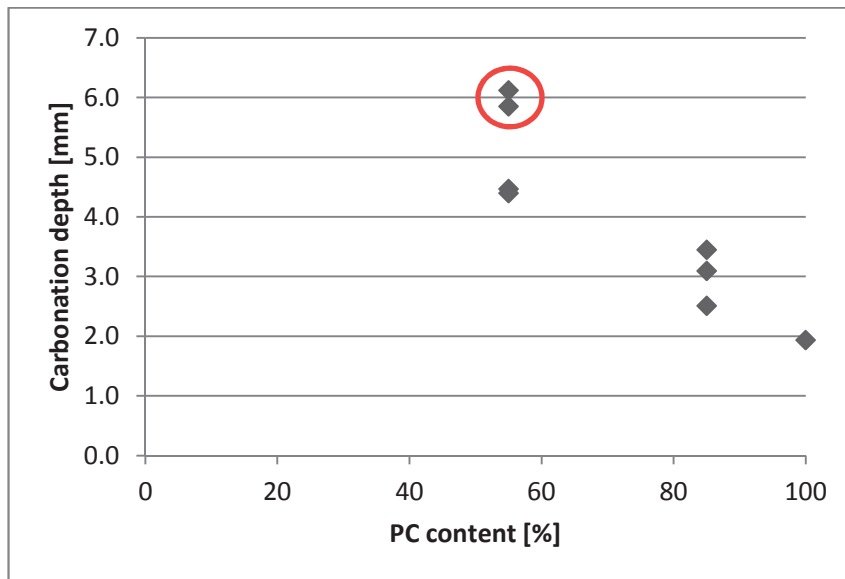


Figure 6.19: Carbonation depths represented as a function of PC content of the blend for natural carbonation.

6.7.2. ACCELERATED CARBONATION 10% CO₂ ON MORTARS

These mortar samples were exposed to air during several months and dried at 50°C for 1 month, (see Experimental details in Section 2.b.3.1.3.2.2 Mortars).

It explains why carbonation depth by phenolphthalein at instant $t=0$ of accelerated carbonation is already significant. In Figure 6.20 the carbonation depth obtained at 0, 2, 4 and 6 weeks by phenolphthalein test are given. The ranking among the samples remains globally the same at the different observation times.

The lowest carbonation depths were obtained for PC, then the blends containing 30% calcined clays and finally the ternary blends with 30% calcined clays and 15% limestone showed the highest carbonation.

In Figure 6.21 where carbonation depth is plotted as a function of Portland cement content the trend of increasing depth of carbonation with increasing substitution level can be better seen.

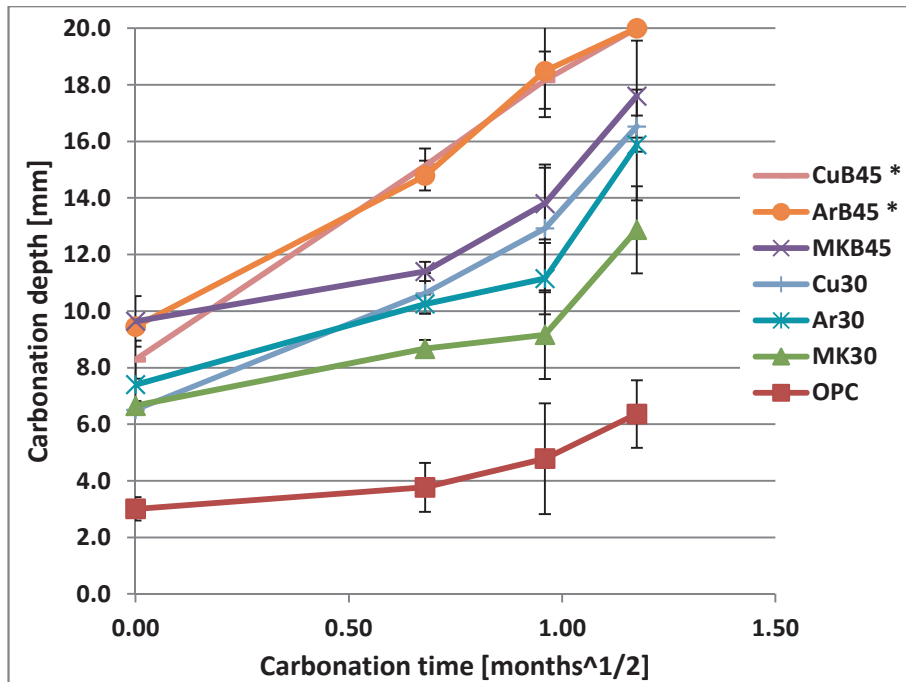


Figure 6.20: Carbonation depths obtained by phenolphthalein test after 6 weeks of accelerated carbonation test with 10% CO₂.

* These samples were fully carbonated after 6 weeks, 20 mm is the maximum.

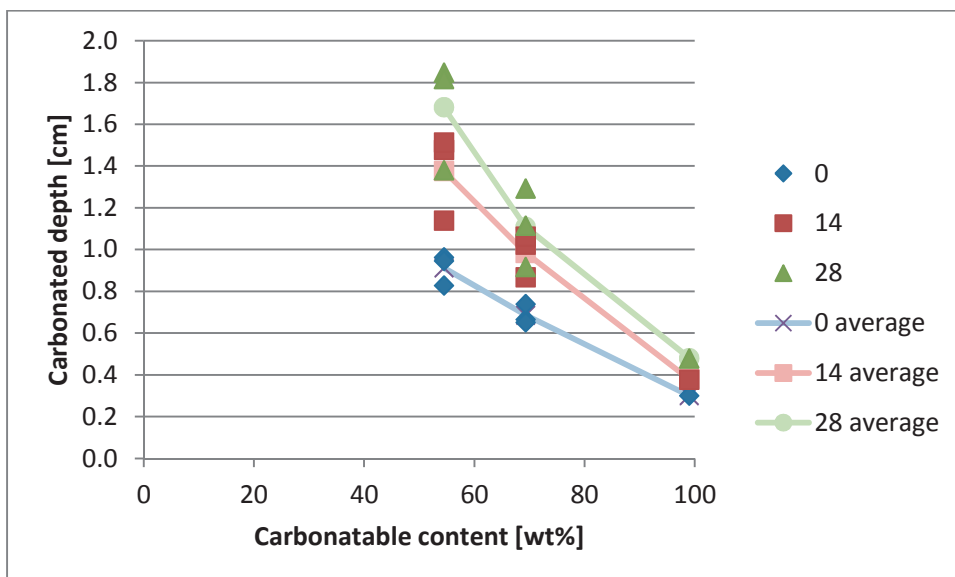


Figure 6.21: Carbonation depths represented as a function of PC content. The linear variation, independently from the composition of the rest of the cementitious binder is observable, at any age.

The kaolin content of the clay plays a minor role, as it can be seen on

Figure 6.22. It seems that carbonation depth is lowest for calcined clays with the highest kaolinite content, both in composition with and without combined addition of limestone.

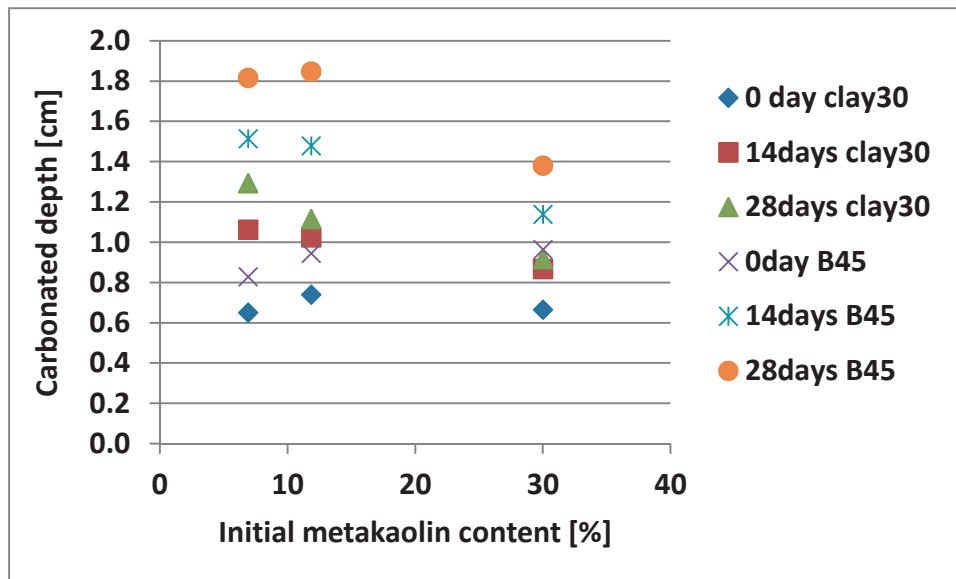


Figure 6.22: Carbonation depths represented as a function of initial metakaolin content of the blend, approximating carbonatable content equal to the PC content.

Considering only natural carbonation, at time 0, the metakaolin content doesn't seem to play a major role. With accelerated carbonation, only the highest metakaolin content in the blend lowers the carbonation depth.

6.7.3. CARBONATION AND STRENGTH

With this experiment it was intended to verify if compressive strength of ternary blends are maintained after carbonation. While it is not a problem at all in Portland cement concrete due to the clogging effect on porosity with the positive balance of solid volume of the carbonation reaction of

calcium hydroxide, our study did not achieve to establish a clear answer for the B45 blends. MIP results have indeed shown that the porosity coarsens but get simultaneously reduced with carbonation.

In another series of experiments made by Rances Castillo in our lab with the same materials used for the accelerated carbonation at 10% CO₂ but for blending up to 30% only, compressive strength of mortar bars were measured after full carbonation, every carbonated strength was higher than the non-carbonated reference. Results are shown in Figure 6.23 (complete description of this series is given in Section 3.1.3.3):

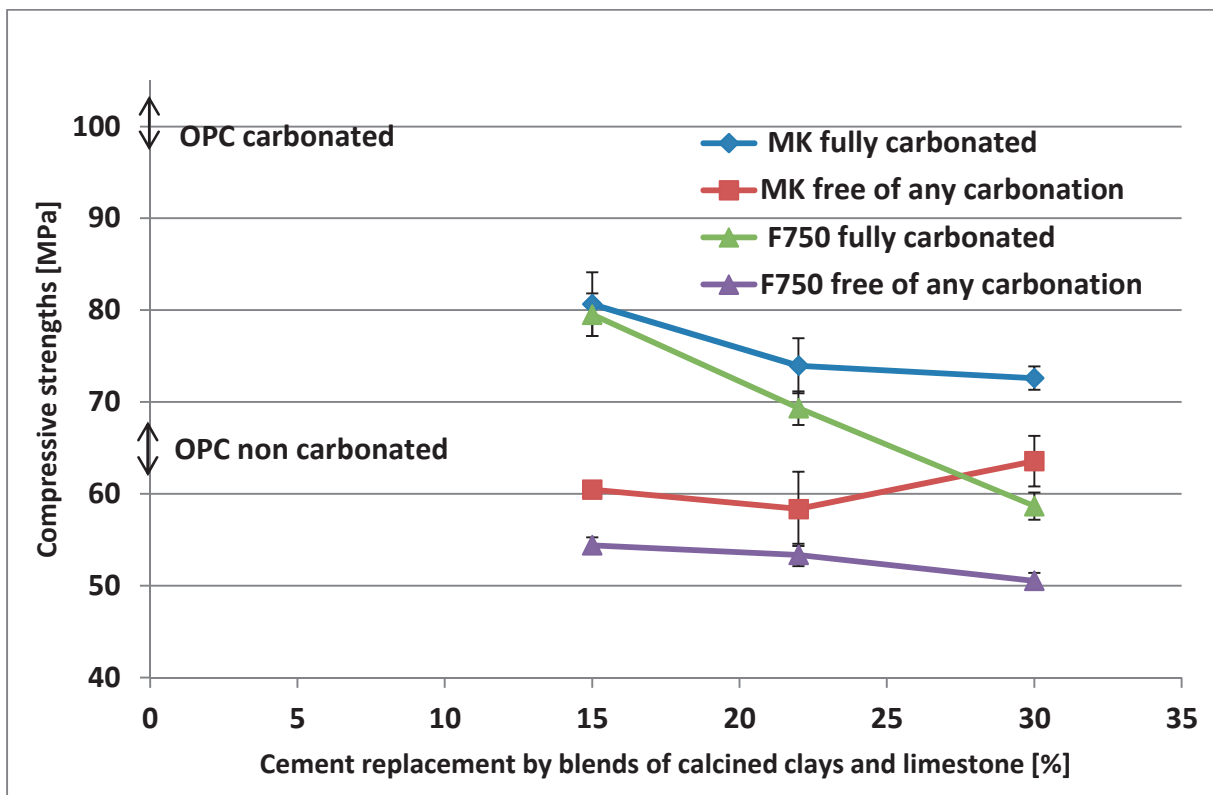


Figure 6.23: Compressive strengths obtained for full carbonation and without any carbonation for the serie of accelerated carbonation carried out with 10% CO₂. Samples fully carbonated had systematically higher strength after carbonation; however the strength gain upon carbonation is decreasing with increasing blending.

6.7.4. COMPARISON OF THE STUDIES ON MORTARS

In Figure 6.24, all the carbonation depths of the mortars subjected to normal and accelerated carbonation are represented as a function of their PC content. The carbonation rates for B45 blends are 2 to 4 times higher than PC carbonation rate in all carbonation conditions. It is not possible to conclude based on this figure if accelerated carbonation alters the picture for blends in comparison with natural carbonation.

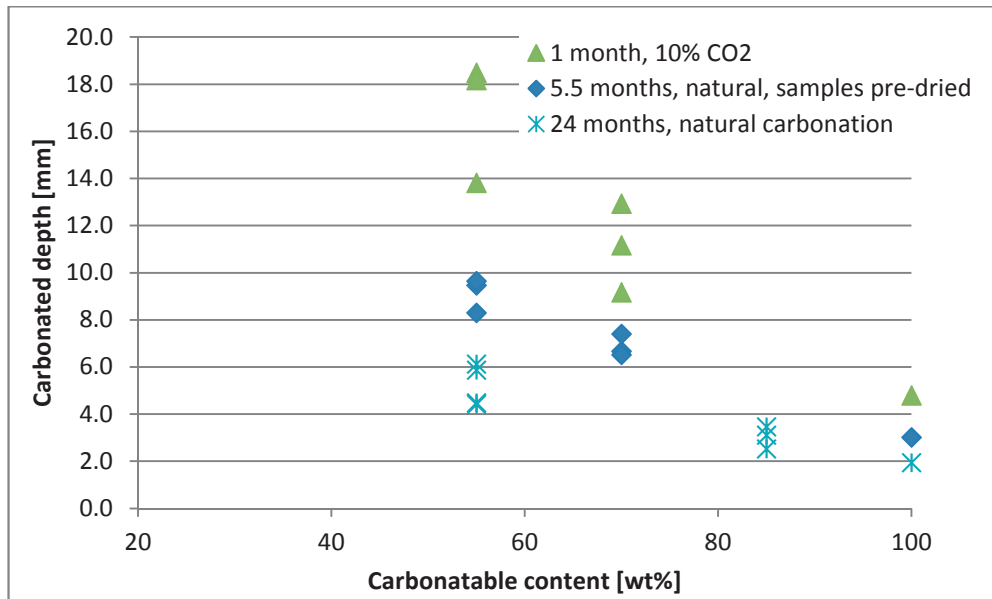


Figure 6.24: Carbonated depth as a function of carbonatable content plotted all together.

Carbonation rates obtained for mortars are summarized all together in Table 6.3.

Table 6.3: Carbonation rates calculated for the different mortars samples and conditions in mm/square root(year)

Carbonation rate [mm/square root(years)], mortars													
	PC	MK 30	MK B45	Ar 30	Ar B45	Cu 30	Cu B45	Sig b45	Sigb45 7d curing	Ref 15	Ref 45	Ar B15	Cu B15
10% CO2	9.9	18.3	23.5	25.0	31.1	29.5	34.5						
Pre-dried	4.4	9.8	14.1	10.9	13.9	9.6	12.2						
Natural	1.3				4.1		3.9	2.9	7.6	2.3	3.0	2.1	1.7

It underlines that not only the CO₂ acceleration level plays a major role but also the exposition and preconditioning procedure since those were exposed to constant relative humidity of 70% in a ventilated room and later one predried 1 month at 50°C. This effect is well documented in the literature[107, 108] but often neglected when comparing carbonation results from the lab and from real structures. With these changes in preconditioning the carbonation rate is almost multiplied by 3 in comparison with natural drying.

It is a similar increase in carbonation rate than the increase observed when comparing 1 year and 1 week curing time (for SigB45).

Accelerated carbonation test with 10% CO₂ also gave results indicating a significant decrease of carbonation resistance in blends containing 30% of calcined clays and smallest carbonation resistance of blends with combined addition of 30% calcined clays and 15% limestone powder. These results have also shown to be directly related to the dilution of the carbonatable content associated with the substitution. Here, the role of kaolinite content of the clay was getting more important as accelerated carbonation was proceeding: a trend of increasing carbonation was perceptible when lowering the kaolinite content of the clay but no samples with purely quartz substitution were available in this series to compare with natural carbonation.

6.8. SUMMARY AND DISCUSSION

The results obtained have shown that there are some major differences in term of phase assemblage obtained in normal and accelerated carbonation.

It is interesting to observe that accelerated carbonation of the blends have directly led to a phase assemblage very similar to the final thermodynamic equilibrium in Figure 6.11, while for PC the

phase assemblage obtained was significantly different from what could be predicted. It definitively put in evidence two important points. First the higher total carbonatable content of PC leads to higher buffering capacity compared with blends and higher carbonation resistance. In addition, the presence of portlandite, which reaction rate decreases with proceeding carbonation, prevents the establishment of fully carbonated phase assemblage that would correspond to thermodynamic predictions.

Thermodynamic simulation does not help for the prediction of porosity evolution. Water content of silica gel is indeed largely unknown. However the assumption can be taken that most of the water from the C-S-H should be conserved in the silica - alumina gel. One recent study on carbonation of Cem I and fly ash cement tends to confirm this assumption [150].

It would be interesting to look more precisely if there are differences in the porous structure of the silica gel formed in PC and blends with high quantities of calcined clays. Morales-Florez and co-workers have recently established by Small Angle X-Ray Scattering in a recent paper that silica gel porosity, both from synthetic C-S-H and hydrated PC is based on two hierarchical levels with a primary particle size of 4.2 nm and building clusters that agglomerated and formed pores of 13 nm [151].

CO₂ availability in already carbonated samples is the factor limiting the rate of carbonation; the investigation of the porosity before and after carbonation delivers important results. At the onset of carbonation, the finest pore size distribution in blends can comparatively improve the carbonation resistance because of their higher fraction of saturated pores reducing permeation and consequent delayed drying. However when carbonation is already advanced and the microstructure already carbonated, it has been observed that that the breakthrough diameter in PC and in the blends were similar. It can therefore be estimated that CO₂ diffusion through the unsaturated porosity in already carbonated samples is approximately the same in PC and blends. This also correlates with the carbonation rates measured for pastes.

6.9. CONCLUSIONS

The different carbonation experiments provided a first insight of the characterization of the carbonation resistance of blends with combined addition of metakaolin and limestone.

All results have shown a general tendency towards increased depth of carbonation with increasing substitution level. Carbonation rates in mortars of B45 blends were 2 to 4 times higher than PC, but this is very much amplified by accelerated conditions. Carbonation levels were too low in natural carbonation on pastes to discriminate.

The main characteristic of a blend such as B45 is definitively its intrinsic reduced carbonatable content and the associated absence or significantly reduced presence of portlandite. These makes the blends with high quantity of calcined clays, with or without combined addition of limestone behave differently during carbonation and especially during accelerated carbonation.

Accelerated carbonation is usually believed in the literature to deliver results that can be linearly linked to natural carbonation and serve to predict natural carbonation at longer term. While it might be true for concrete that are globally similar in term of portlandite content and pore size distribution, it has been demonstrated with the development of this investigation methodology of the phase assemblage by semi quantitative Rietveld analysis that there are significant differences for our blends between normal carbonation and accelerated carbonation, even at only 3% CO₂.

Accelerated carbonation of blends induces stabilization of predominant aragonite instead of calcite during the short term normal carbonation exposure in this experiment. No such effect has been found with PC. This is supposed to adversely affect carbonation resistance of blends and increase the rate of carbonation by coarsening the pore size volume due to the difference in molar volume between calcite and aragonite. In addition, anhydrous phases were found to significantly react, which is also not representative of the reality and is a further argument that distinguish normal and accelerated carbonation mechanisms.

However, when looking strictly to carbonation rates and carbonation depths, both in mortars and pastes, there was no dramatic increase of the carbonation rate observed in accelerated carbonation for the blends in comparison with natural carbonation.

Considering the significant differences observed between natural and accelerated carbonation, this result is hard to explain and might be due to the contrary influences of the finer pore size distribution of the blends, lower pH that reduce carbonate ion activity in solution, acting positively against carbonation while aragonite stable formation tends to increase carbonation.

Thermodynamic simulation has proved to be a valuable but limited tool in the investigation of carbonation resistance. With the improvement of the C-S-H model and database it can help in the future to predict the phase assemblage after full carbonation.

More systematic investigation of the differences between natural carbonation over long term and accelerated carbonation are required to confirm the differences discerned in this work. The effect of drying should be more precisely taken in account. The use of Thiery's approach [152], derived from Bakker's approach [153], or of the drying module of Stadium should be considered, since it obviously plays a major role as carbonation is established and rate limited by the diffusion of CO₂ through the carbonated porous network.

The influence of curing time requires as well a detailed investigation in order to have a more complete picture of the behaviour of blends of combined addition of metakaolin and limestone in real conditions, both in terms of evolution of compressive strength or with carbonation resistance; and benchmark them against other SCMs. It is likely that for a given cement substitution level, calcined clays with their fast kinetics of reaction behaves comparatively better than SCMs such as slags or fly ashes; this remains to be demonstrated. Such studies are indispensable in order to define adequate rules and practices as for curing, cover thickness, etc... for in field applications.

Finally for our colleagues in Cuba it is worth to note that in a tropical climate, with higher average temperature but relative humidity between 70 and 90% all year, carbonation is likely to be considerably reduced compared to the tempered climate found in Europe, and testing conditions should be tailored to reproduce these conditions.

Chapter 7 : CHLORIDE RESISTANCE AND TRANSPORT PROPERTIES

7.1. STATE OF THE ART

7.1.1. CHLORIDE INDUCED CORROSION

The corrosion of rebars is the main durability concern of reinforced structures. Carbonation can induce corrosion; it has been studied in the previous chapter. But chloride ions can also lead to depassivation of rebars that can result in steel corrosion even when the pH is still high. Under normal circumstances chloride levels in raw materials; cement, aggregates and mixing water are negligible, and chloride-induced corrosion is a result of the penetration of chloride ions from the environment through the porous structure of the concrete cover.

The two main mechanisms reducing chloride ion penetration (which may be combined) consist of reducing water ingress by refinement and reduction of porosity on one hand and enhancing chloride binding capacity of the cementitious matrix on the other hand. With the use of calcined clays, both of the mechanisms of reduction of chloride penetration are likely to be affected.

7.1.2. CHLORIDE BEARING PHASES

In order to improve the understanding of the interactions of any cementitious binder with chloride, it is necessary to know the different phases forming. Considerable advances have been recently made considering the different chloride bearing phases forming. They are summarized here:

It is first well established that AFm phases such as monosulfoaluminate $3\text{CaO}\cdot\text{Al}_2\text{O}_3\cdot\text{CaSO}_4\cdot 12\text{H}_2\text{O}$ ($\text{C}_4\text{A}\overline{\text{S}}\text{H}_{12}$) and hydroxyl-AFm ($\text{C}_4\text{A}\text{-FH}_x$) may react with chloride ions to form

Friedel's salt, $3\text{CaO}\cdot\text{Al}_2\text{O}_3\cdot\text{CaCl}_2\cdot 10\text{H}_2\text{O}$ ($\text{C}_4\text{A}\overline{\text{C}}_2\text{H}_{10}$) and to a lesser extent at low chloride concentration

Kuzel's salt, $3\text{CaO}\cdot\text{Al}_2\text{O}_3\cdot 1/2\text{CaSO}_4\cdot 1/2\text{CaCl}_2\cdot 11\text{H}_2\text{O}$; ($\text{C}_3\text{A}(\text{C}\overline{\text{S}})_{0.5}(\text{Ca}\overline{\text{C}}_2)_{0.5}\text{H}_{11}$).

Polymorphisms of Friedel's salt have been identified with pure synthetic phases. One monoclinic (disordered) and one rhombohedral (more ordered) polymorph of Friedel's salt exist. Both polymorph structures have been refined [154].

In the presence of carboaluminates AFm, Mesbah and co-workers have demonstrated that two different polymorphs exist for the chloro-carboaluminate phase $[\text{Ca}_2\text{Al}(\text{OH})_6]\cdot[\text{Cl}_{1-x}\cdot(\text{CO}_3)_{x/2}\cdot(2+x/2)\text{H}_2\text{O}]$ both with an extended solid solution with $0.25 < x < 0.95$ [155] (note that this phase is called here hydrocalumite, by extension from the natural occurrence of the mineral reported by Sacerdoti & Passaglia [156]).

Furthermore, they reported with Raman micro-spectroscopy the equivalent anionic arrangement in both chloro-carboaluminate polymorphs with a carbonate stretching band at 1086 cm^{-1} characteristic of interlayer carbonate. Hemicarboaluminate structure has also been recently resolved by Runcevski [157], they could identify that the carbonate is positioned exactly identically, showing the same characteristic stretching band at 1086 cm^{-1} . Both structures are therefore compatible for a complete solid solution involving OH^- , CO_3^{2-} and Cl^- ions.

Mesbah and colleagues also report the refinement of the structure of Kuzel's salt [158, 159] and of the uptake of Cl^- and CO_3^{2-} ions by monosulfoaluminate [159].

Balonis et al have described the thermodynamic equilibrium found in AFm phases containing sulfate, carbonate and chloride [160]. They postulate from thermodynamic data that limestone containing cement should have less chloride binding capacity than classical Portland cement systems containing only sulfate and hydroxyls AFm. It is in accordance with the description of hydrocalumite solid solution by Mesbah.

Balonis and co-workers also considered the volume balance due to chloride interaction. In carbonate free systems chloride binding is associated with ettringite precipitation by displacement of sulfate groups into solution. This is confirmed by thermodynamic calculation [160, 161]. Some authors

proposed that this could even lead to expansion, but deterioration due to such reaction has not been demonstrated.

With calcite, the presence of carbonate already destabilizes monosulfoaluminate at the expense of ettringite, so that reaction of carboaluminates with chloride will lead to calcite precipitation, without much change in total solid volume.

In order to link these data based on pure synthesized phases or thermodynamic data to real cementitious systems, chloride interaction with cementitious matrix needs to be characterized.

In a real cementitious system, conditions of pH and alkalinity are indeed considerably different and the chloride binding is usually reduced because of the higher solubility of Friedel salt at high pH [162].

Chloride binding experiment is usually used for this purpose. It consists in the indirect measurement of chloride uptake by a known quantity of a cementitious material in a defined volume of solution at different NaCl concentrations. The experiment duration is fixed so that thermodynamic equilibrium can be reached (several months usually). Different isotherm models exist in order to fit the obtained data, Langmuir and Freundlich isotherms are the most common ones and their equations are presented here:

$$C_b = \alpha \cdot C_f^\beta \quad \text{Equation 7-1, Freundlich isotherm}$$

$$C_b = \frac{\alpha \cdot C_f}{(1 + \beta \cdot C_f)} \quad \text{Equation 7-2, Langmuir isotherm}$$

Tang & Nilsson [163] have shown that while Langmuir provides the best fit for very low concentration (<0.05M), Freundlich isotherm becomes more accurate for higher concentrations. The Figure 7.1 gives a good example of improved fitting with Freundlich compared to Langmuir.

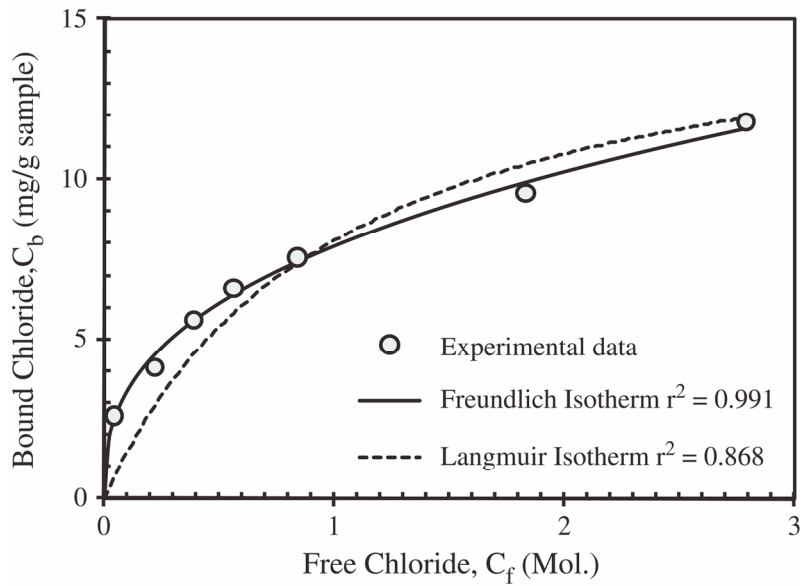


Figure 7.1: Example of best-fit possible with Freundlich & Langmuir isotherms for a cement paste at water/cement ratio 0.5. Freundlich isotherm gives the best fit (from[164]).

7.1.3. EFFECT OF SCMS

It is well established that SCMs tend to refine pore size distribution and therefore tend to reduce ion diffusion into the cover concrete. It is the main effect of SCMs on chloride resistance.

SCMs also modify the possible interaction mechanisms of chloride with the cementitious matrix. With aluminium containing SCMs, there are two main reasons that can explain the increased chloride binding with SCMs:

- Chemical binding is enhanced because of the formation of chloro-AFm.

Thomas et al [164] have investigated the influence of SCMs with different alumina content on chloride binding isotherm experiments. Their most important findings are presented below. Figure 7.2 confirms that in this case the Friedel salt peak intensity by XRD could be almost linearly related to the bound chloride measured by chloride binding isotherm.

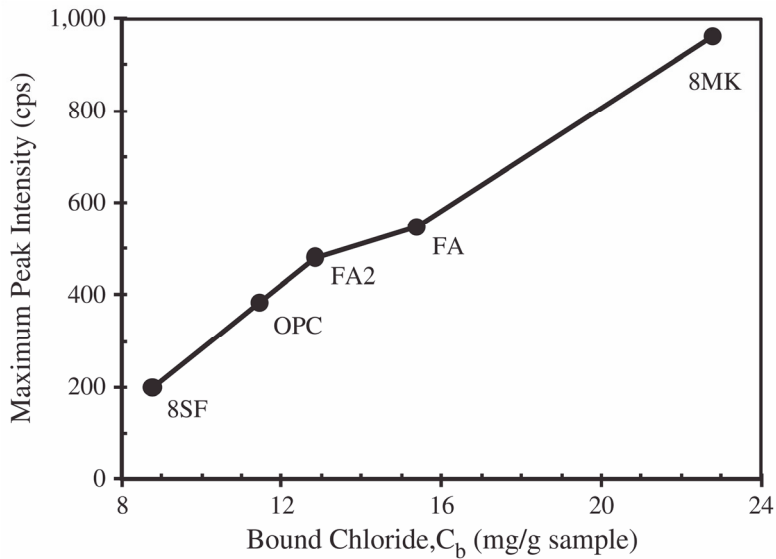


Figure 7.2: Maximum Friedel peak intensity by XRD plot as a function of the bound chloride measured by chloride binding isotherm [164].

Figure 7.3 shows that for the samples studied, the bound chloride measured by chloride binding isotherm demonstrates a dependency with the alumina content of the binder. Note that with fly ash, the trend is less evident and deviates.

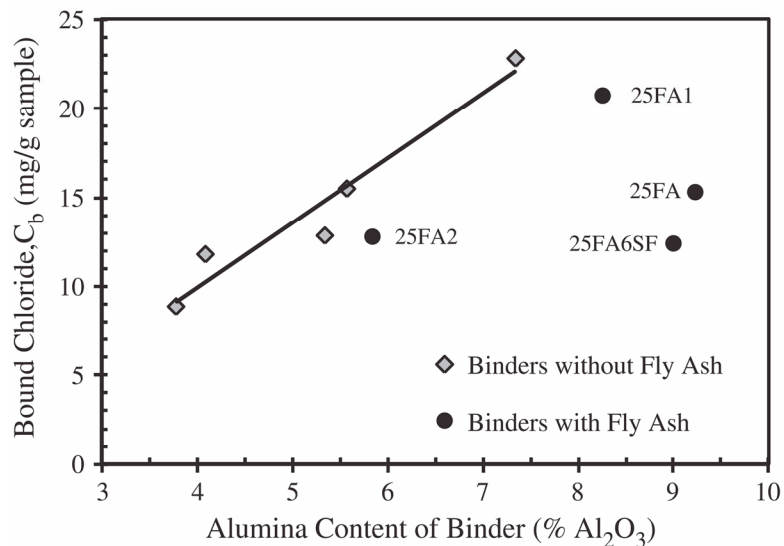


Figure 7.3: Bound chloride (for 3M NaCl) obtained by chloride binding isotherm measurement plot as a function of the alumina content of the binder, water/binder ratio 0.5, Temperature 23°C [164]

- The physical binding by C-A-S-H is adversely affected by SCMs. It tends to be increased by physical adsorption due to the increased C-A-S-H formation but at the same time cement content is diluted. In addition, physical binding is reported to decrease when average Ca/Si ratio of C-A-S-H decreases [165].

In the ternary blends with combined addition of calcined clay and limestone, strätlingite can be found. There are very few studies in the literature about its behaviour in presence of chloride. Zibara and co-workers have studied different metakaolin-lime ratio in pastes [165]. Results are given in Figure 7.4, where bound chloride is plotted as function of free chloride concentration for 3 different ratios (Mk indices in the plot stand for the MK/Lime weight ratios: MK₁₂ means that MK/Lime weight ratios is equal to 1/2). The results are surprising, while binding linearly increases for 2/1 and 1/1 weight ratio, for MK12 the binding is extremely important from 0.1 M NaCl. Unfortunately this sample was obviously severely carbonated, attested to by the monocarboaluminate peak observable in Figure 7.5. The formation of Friedel salt at increasing NaCl concentrations seems therefore to be predominantly due to carboaluminates conversion, although strätlingite totally disappears at 1M NaCl.

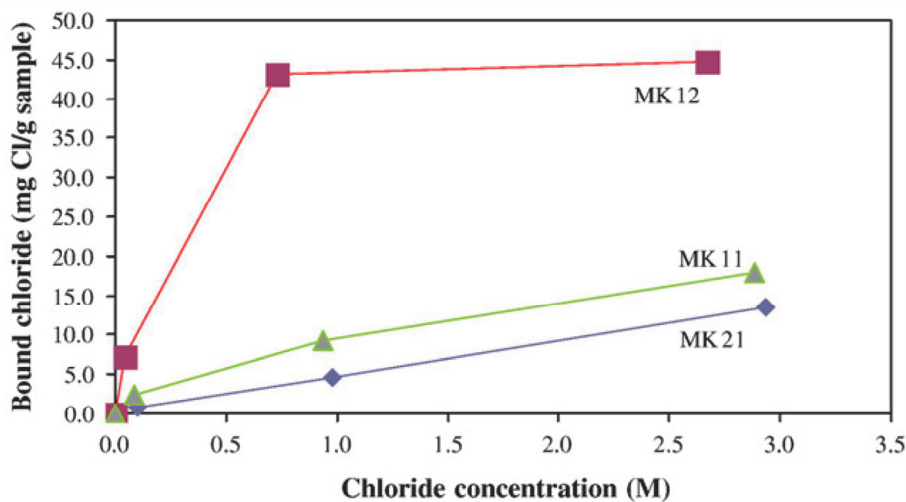


Figure 7.4: Bound chloride plotted as function of free chloride concentration for 3 different ratios MK/Lime ratios [165].

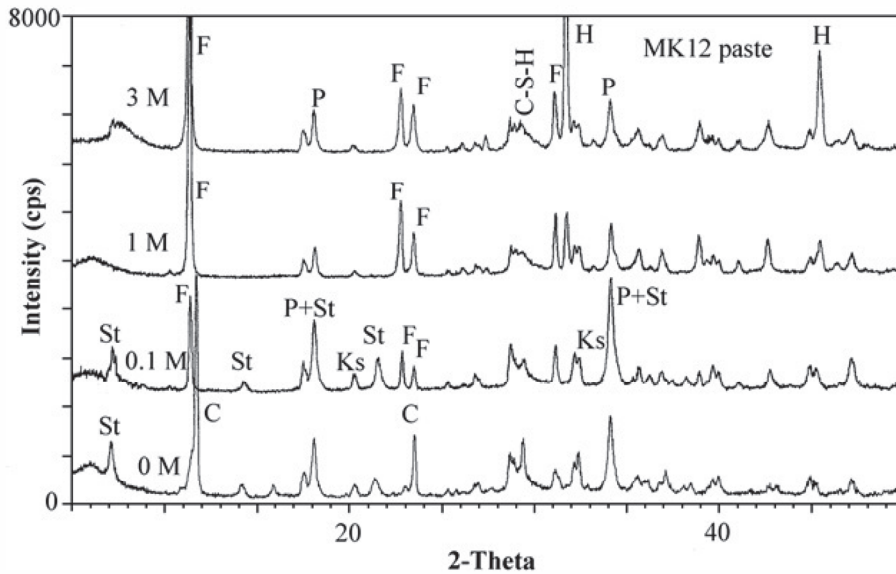


Figure 7.5: XRD Diffractograms obtained for MK12 sample after chloride binding experiment for various NaCl concentrations [165].

Saikia and colleagues [166] have also postulated that chloride can be incorporated into strätlingite structure by ionic exchange because they are both AFm phases with the same basic building unit $[\text{Ca}_4\text{Al}_2(\text{OH})_{12}]^{2+}$. Their case was however different since they were adding Cl salt at mixing time. There is in addition no experimental evidence supporting this point

Concerning the effect of limestone, Ipavec et al recently published on the effect of limestone addition and alkalinity on chloride binding for fly ash cements [167]. pH was controlled at 12.8 and 13.5 by using a simulated pore solution with mixture of NaOH and KOH.

At pH 13.5, chloride binding was considerably decreased in presence of limestone, especially for free chloride concentrations below 0.5M). They also found that chloride binding was proportional to the binder alumina content when using SCMs (see Figure 7.6). In addition, the reduction of chloride binding in presence of limestone can be observed in this figure. For the same NaCl concentration, empty symbols for systems containing limestone are systematically below filled symbols (without limestone). The linear dependency with Al_2O_3 content at pH 13.5 seems also to be slightly reduced in presence of limestone. However at pH 12 the effect of limestone on chloride binding was becoming almost negligible.

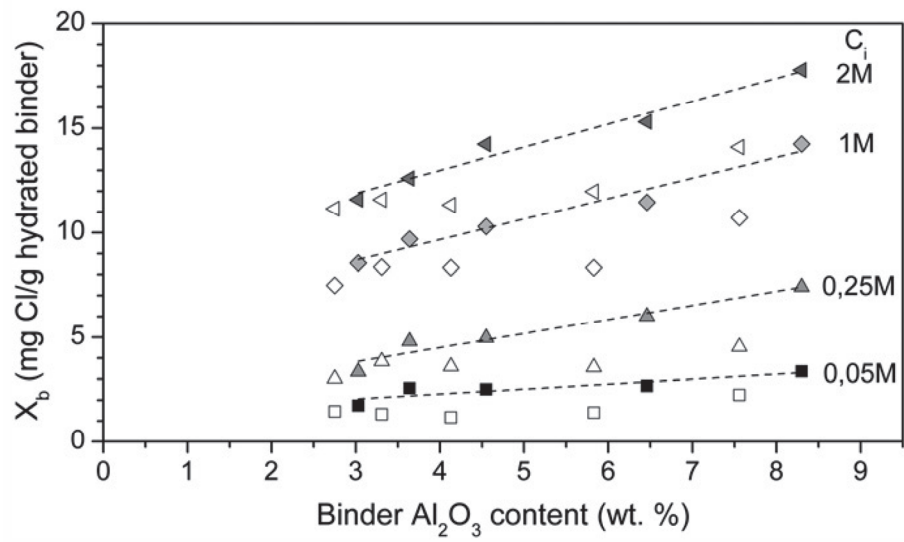


Figure 7.6: Chloride binding values at pH 13.5 by chloride binding isotherm as a function of Al_2O_3 binder content. Empty and filled symbols stands for systems with and without limestone, respectively (from [167]).

7.2. OUTLINE OF EXPERIMENTAL WORK

Based on the state-of-the-art section, there is agreement that using SCMs containing alumina is likely to improve chloride binding of the cementitious matrix. Therefore considering the high alumina content of our blended cement, it is expected that it will also have a high chloride binding potential. However it is not well known how the overall phase assemblage obtained with the ternary blends, containing strätlingite and hemicarboaluminate interact with chloride ions.

To investigate the chloride resistance of our blends, it was decided to look at three different inter related aspects.

1. The first procedure was the ponding test, where mortar samples are immersed in a NaCl 0.5 M ponding solution with only one surface in contact with the solution so that the chloride penetration is unidirectional. It follows the ASTM ponding method [78] the duration was extended to 2 years.
2. The second aspect was to characterise the chloride binding isotherm. It gives the amount of chloride ions bound by a cementitious system at equilibrium for a certain concentration of free chloride ions. The bound chloride is the sum of the physically adsorbed chloride ions and the chemically bound chloride.
3. Finally the third test is the SIMCO[®] migration test, which is a modified version of the Rapid Chloride Permeability test (RCPT)[168]. The RCPT procedure as given in the ASTM standard suffers from various drawbacks that this modified procedure avoids. RCPT and even modified versions such as the NT Build 492 are more indicative tests of the sample resistivity [169] and their analysis based on a pure diffusion (it is not a permeability test per se) using Fick's law does not take into account any of the physical and chemical binding of chloride ions with the cementitious matrix. Besides, the voltage applied is too high and has been shown to produce a self-heating and temperature increase that impairs the validity of the test. The SIMCO test, through the comparison with a model, gives the estimation of the transport properties of the material and can give an overview of the chloride resistance of the materials.

7.3. MATERIALS

Different series of materials were studied; they are listed in Table 7.1. The compositions of Series 1a (described in Table 3.7) aimed to study calcined clays with different kaolinite contents.

Table 7.1: Compositions studied in chloride chapter

Preliminary Series	PC2	MK30			PontB45				
Series 1a	PC1	MK30/ Pont30 Ar30	MKB45	/	Pont-B45	/	ArB45		
Series 1b	PC1	/	MKB45	MKB15	Pont-B45	PontB15		PontB22 /B30	MKB22 /MKB30
Series 2	PC3	MK30	MKB45	MKB15	PontB45	PontB15			

7.4. PONDING EXPERIMENTS

7.4.1. EXPERIMENTAL PROCEDURES

Experimental procedures is given in Section 3.4

7.4.1.1. CHLORIDE QUANTIFICATION

To assess the various errors in the process (grinding process, drying, acidic extraction, dilution step and the manual determination of the peak) several samples were analysed at different times. Two examples are given in the Figure 7.7. This indicates generally good reproducibility, apart from the odd points that fall off the trend line.

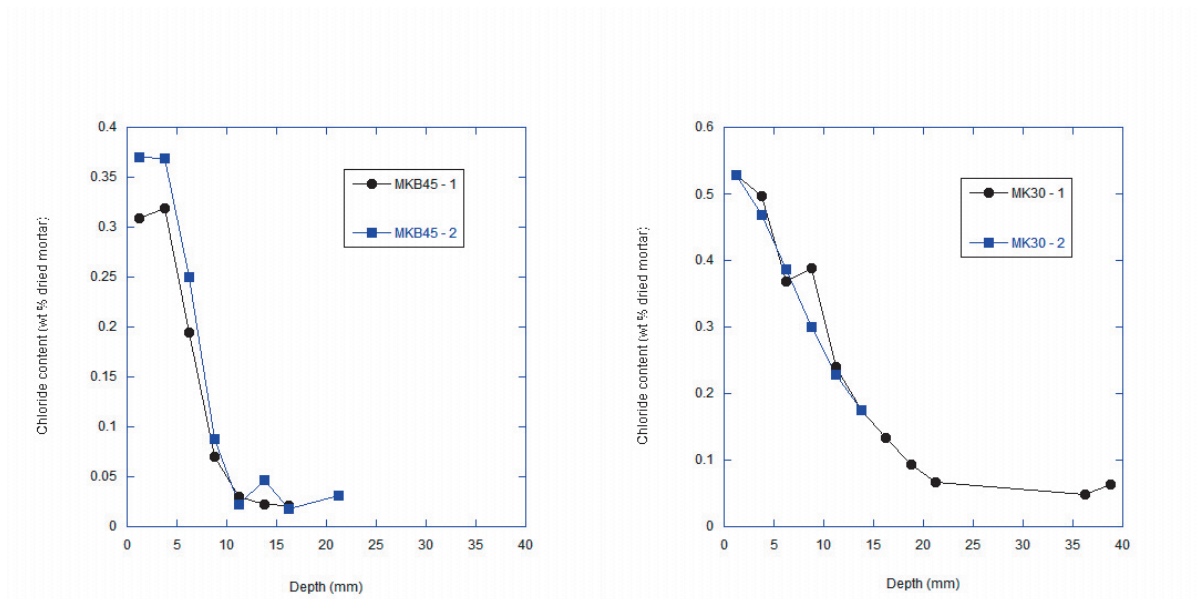


Figure 7.7: Examples of reproducibility trials of chloride quantification for ponding experiments with composition B45 (top) and MK30 (bottom). The biggest standard deviation ± 0.06 wt% was found in the layer exposed to the solution that is more subject to local heterogeneity.

Different authors have shown that acidic dissolution [170, 171] only partially dissolves the total chloride, usually between 80 to 90% of the real total chloride content that can be measured by XRF (the most precise method). Therefore it was decided to work at very high acid concentration and leave always the acid for minimum of 12 hours.

7.4.1.2. XRD

Before the drying and chloride extraction steps, X-Ray Diffraction was carried out on selected powder samples to obtain a picture of the evolution of the phases. Samples were scanned between 6 and 35 $[\theta]$. Semi-quantitative analysis based on the deconvolution of the peak refined with Rietveld analysis was carried out on the 6-20 $[\theta]$ range that excludes any quartz peak. Anhydrous cement phases and calcite were ignored. With such an approach, the evolution of the phase assemblage of one samples exposed to different conditions can be followed. But quantitative comparison between different compositions is not possible.

It was not possible to distinguish the rhombohedral from the monoclinic polymorph of either Friedel salt or hydrocalumite. Both have very close peak positions, and XRD on mortars has a poor signal/noise ratio. Considering that both polymorphs coexist at ambient temperature, that the transition temperature between both is about 35°C and 45°C for Friedel salt and hydrocalumite respectively [154, 172], the phases are anyway likely to be converted with the heating due to the frictional forces during grinding. It was decided to use lattice structures for hemicarboaluminate, hydrocalumite, Friedel salt and monocarboaluminate which were kept constant and imposed from their position at the outer layer (for Friedel salt) and in the deepest layer (for hemi and monocarboaluminate) in order to improve the peak deconvolution. Only the phase intensity and the broadening factor were allowed to change.

7.4.1.3. SEM & EDS POINT COUNTING

At the end of the ponding experiment a slice was cut in the middle of each mortar bar perpendicular to the exposed surface. Hydration was stopped by immersion in isopropanol for 7 days, and then the sample was vacuum-dried in a desiccator for 7 more days. These slices were carefully polished, epoxy resin impregnated under vacuum and polished with the automatic disc polishing procedure described elsewhere. Samples were investigated in the SEM with back-scattered electrons imaging and EDS point counting analysis was carried out following the procedure described in [173]. But as we were interested in chloride penetration we plotted Cl/Al ratio as function of Si/Al to investigate intermixing and phase assemblage.

7.4.2. RESULTS

7.4.2.1. TOTAL CHLORIDE LEVELS

All the total chloride contents are summarized in section 10.1, normalized by gram of mortar and g. of cement respectively. In the next paragraphs comparisons are carried out in order to look more

detail at the effect of the cosubstitution with limestone, the kaolinite content of the clay and the level of blending.

Comparison of effect of clay grade

The chloride profiles for all the samples with 30% substitution of calcined clay and PC for comparison are plotted in Figure 7.8. In the PC mortar a constant concentration of chloride is observed and chloride penetrated completely through the sample. In the blended cement mortars with calcined clays, the chloride concentration decreases with depth., The higher the kaolinite content, the less the penetration. Also, the highest total concentration close to the surface was found with lower kaolinite content of the clay. Samples with lower kaolinite content have indeed higher porosity and are more subject to leaching because they still have large amount of portlandite.

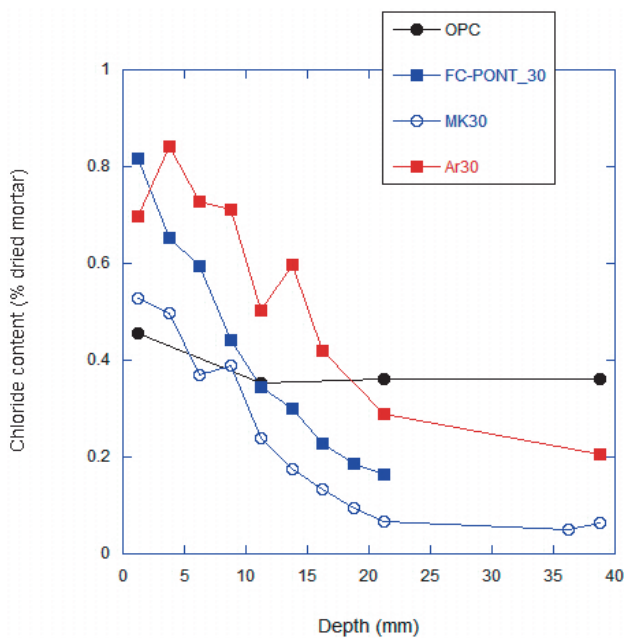


Figure 7.8: Total chloride content measured by acidic dissolution for 30% of cement substitution by calcined clays with varying kaolinite content.

Figure 7.9 shows profiles of all total chloride contents for the samples with 30% substitution of calcined clays and 15% limestone. The trend here is similar to that seen without calcite, the lower the kaolinite content, the deeper the penetration. Also, the highest total concentration close to the surface also increased with lower kaolinite content of the clay.

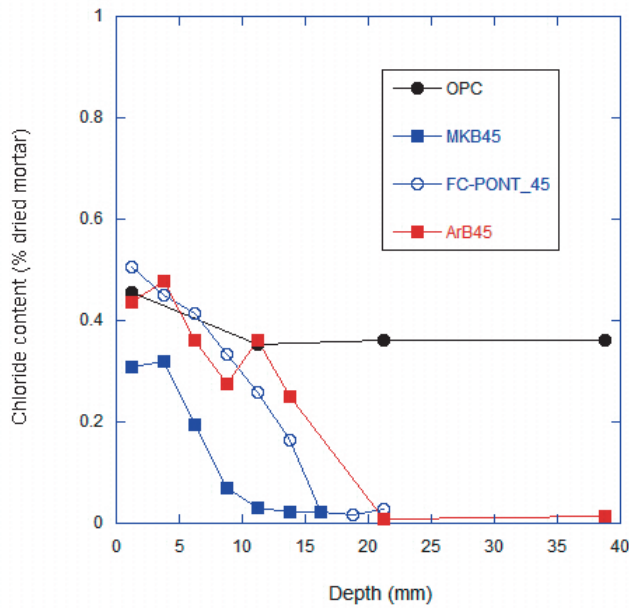


Figure 7.9: Total chloride content measured by acidic dissolution for 45% of cement substitution blends by combined addition of 30% calcined clays with varying kaolinite content and 15% limestone.

Effect of blend content

In Figure 7.10 the chloride profile over the depth are given for all the different blending levels. The two calcined clays are separated for clarity.

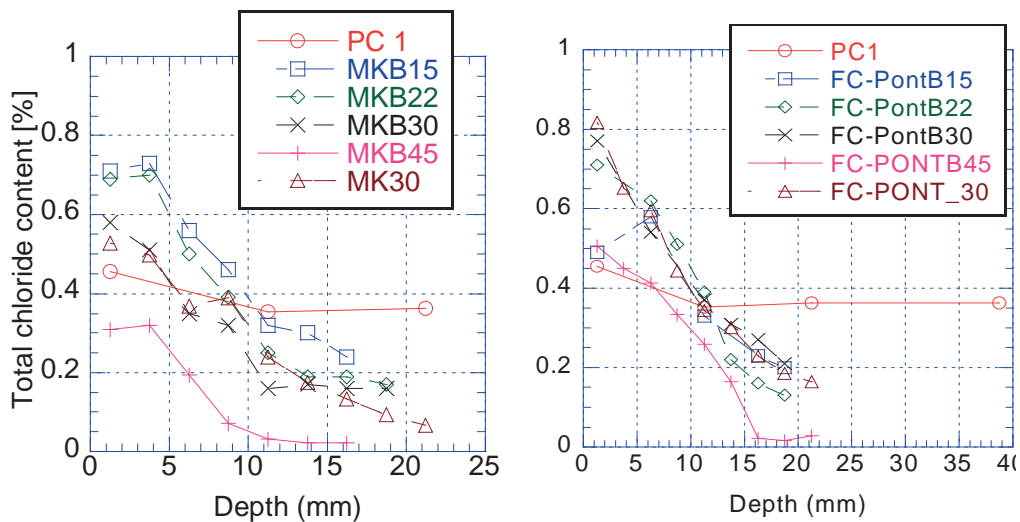


Figure 7.10: Total chloride contents as a function of the depth from the outer layer exposed to the ponding solution. On the left all the samples containing pure metakaolin are given while samples with the Pontezuela calcined clay are given on the right.

Blending improves chloride resistance compared with the PC1. With increasing blending rate chloride penetration decreases. The chloride content in the outer layer shows a maximum for 15 to 22wt% blending, in pure metakaolin and 22 to 30wt%, for Pontezuela case. A blending level of 45% produces a considerable decrease of chloride penetration with both clays. It is interesting to note that substitution by simultaneous addition of 20% calcined clays and 10% limestone give almost identical chloride penetration than 30% calcined clays for both calcined clays.

In Figure 7.11 the total chloride content in the outer layer directly in contact with the ponding solution is normalized by Al_2O_3 content (by XRF) in the blend. The total chloride content increases until a maximum around 10% Al_2O_3 above which it decreases. It seems to indicate that the extra alumina brought from calcined clays increases chloride binding up to a certain level of addition, beyond which the clays seem to only play a filler role and the extra aluminium does not take part in chloride binding. Note also that Al_2O_3 maximum content, around 10 to 12% for the first increasing part is in agreement with Thomas or Ipavec values [164, 167] (but they did not report binding values for higher Al_2O_3 content). The figure has to be taken with care, since in outer layer of a small finite thickness the gradient can also be important. Much care has been taken in order to keep the samples sealed between the removal from the ponding solution and grinding, but evaporation and water advection might also have modified this figure.

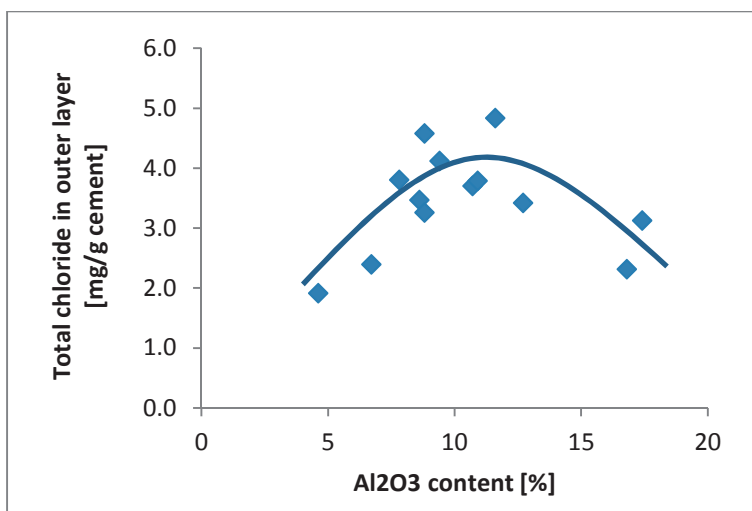


Figure 7.11: Representation of the total chloride content as a function of Al_2O_3 content in the outer layer in contact with the ponding solution.

7.4.2.2. XRD

X-ray diffractograms are shown only in the range between 6° 2θ and 14° 2θ where main diffraction peak of AFm and AFt phases are present. Around 9° 2θ is the main peak for Ettringite (Ettr.), 11.2° 2θ for Friedel salt (Fr.), 10.9° 2θ Hydrocalumite (Hydr.), 10.7° 2θ Hemicarboaluminate (Hc.), 11.7° 2θ Monocarboaluminate (Mc.) and below 7° 2θ Strätlingite (Str.). C-A-S-H gel, the main hydrate precipitating in our blends is not detectable by XRD because of its low crystallinity. It tends to form an amorphous hump located around 30° 2θ , but it was not possible to quantify it.

OPC

For the OPC mortar, the diffractograms all look very similar with increasing depth. Only ettringite and Friedel's salt are evident (Figure 7.12).

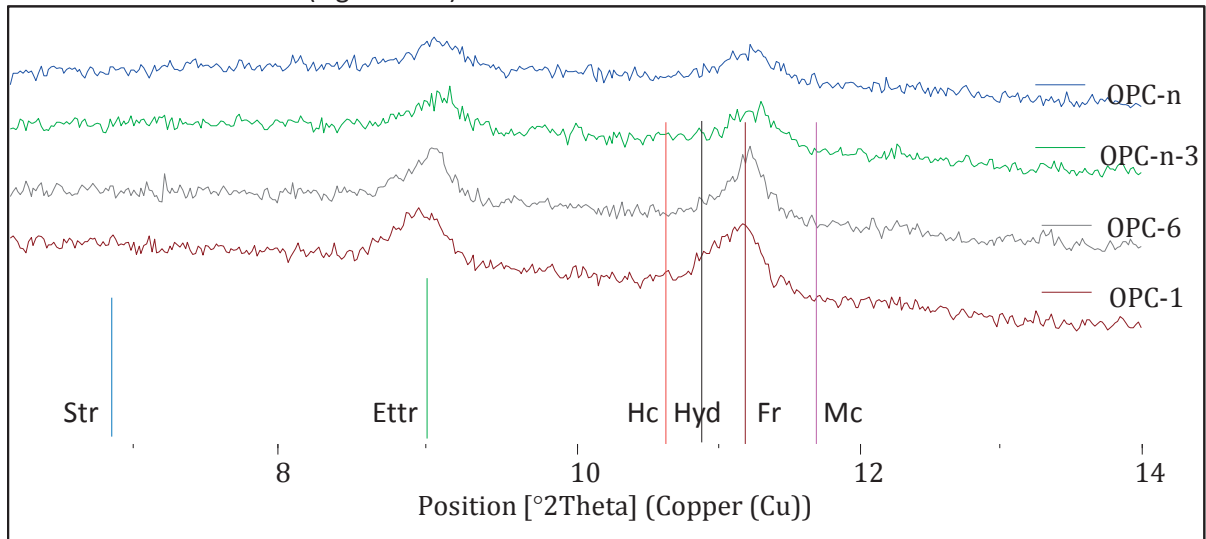


Figure 7.12: X-Ray Diffractograms obtained after 2 years Ponding for OPC. The number corresponds to the layer number, starting from surface in contact with ponding solution.

By semi-quantitative Rietveld analysis, the same features are confirmed (see Figure 7.13) and occurrence at the outer layer of hydrocalumite as well as Friedel salt is determined (it can be indeed also observed by the broader left shoulder of the peak in Figure 7.12 at 2θ angle 11.2°). Also, Portlandite content is lower at the surface; it has probably been slightly dissolved in the outer layer. Friedel salt is present throughout the depth and there are no traces of sulfo or carbo-AFm, confirming the complete penetration of chloride.

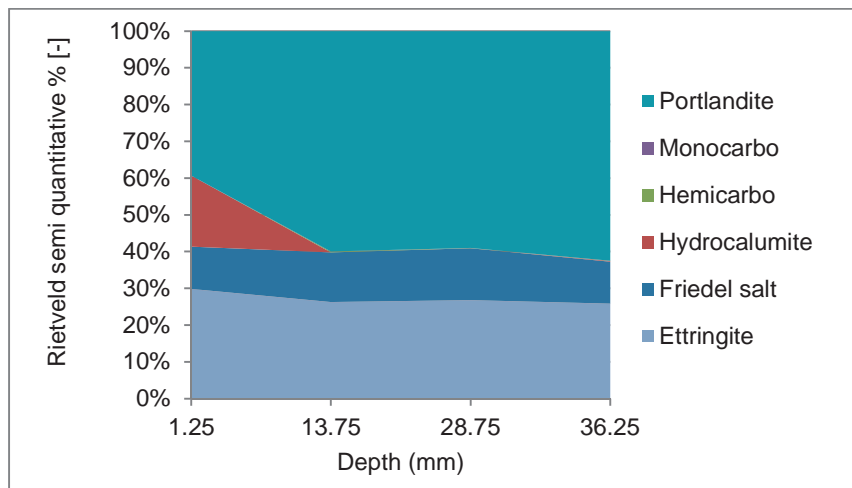


Figure 7.13: Hydrates phase assemblage evolution observed by semi-quantitative Rietveld analysis for PC1 after 2 years ponding.

MK30

X-Ray diffractograms for MK30 are given in Figure 7.14. The surface layer contains Friedel salt, strätlingite and ettringite. Already in next layer Friedel's salt is vanishing and completely disappears in layer 3. The Strätlingite intensity seems smaller on the surface than in deeper layers. No monosulfate was identified except traces at the very bottom. The changes in relative intensity of strätlingite and Friedel's salt coincide well so that we can postulate that strätlingite has been partially converted into Friedel's salt, as previously claimed[165]. Ettringite is present in every layer, in decreasing amount as the depth increases.

Close to ettringite around $9.8\ 2\theta$ there seems to be a growing peak with increasing depth that could not be definitely identified. It could correspond to the U-phase. This Na or K bearing phase, belongs to the group of hexagonal or pseudo-hexagonal layered structures like AFm, but differing from the

latter in the fact that it contains sodium between the layers and possessed a higher interlayer distance. The U-phase is known to precipitate in presence of Al, Ca, and high concentration of sulfate, alkali and hydroxyl ions concentrations [174-176]. However, as the pH in blends was originally lower than 13, presence of U-phase is not expected. At this stage it is not possible to conclude on the nature of this phase.

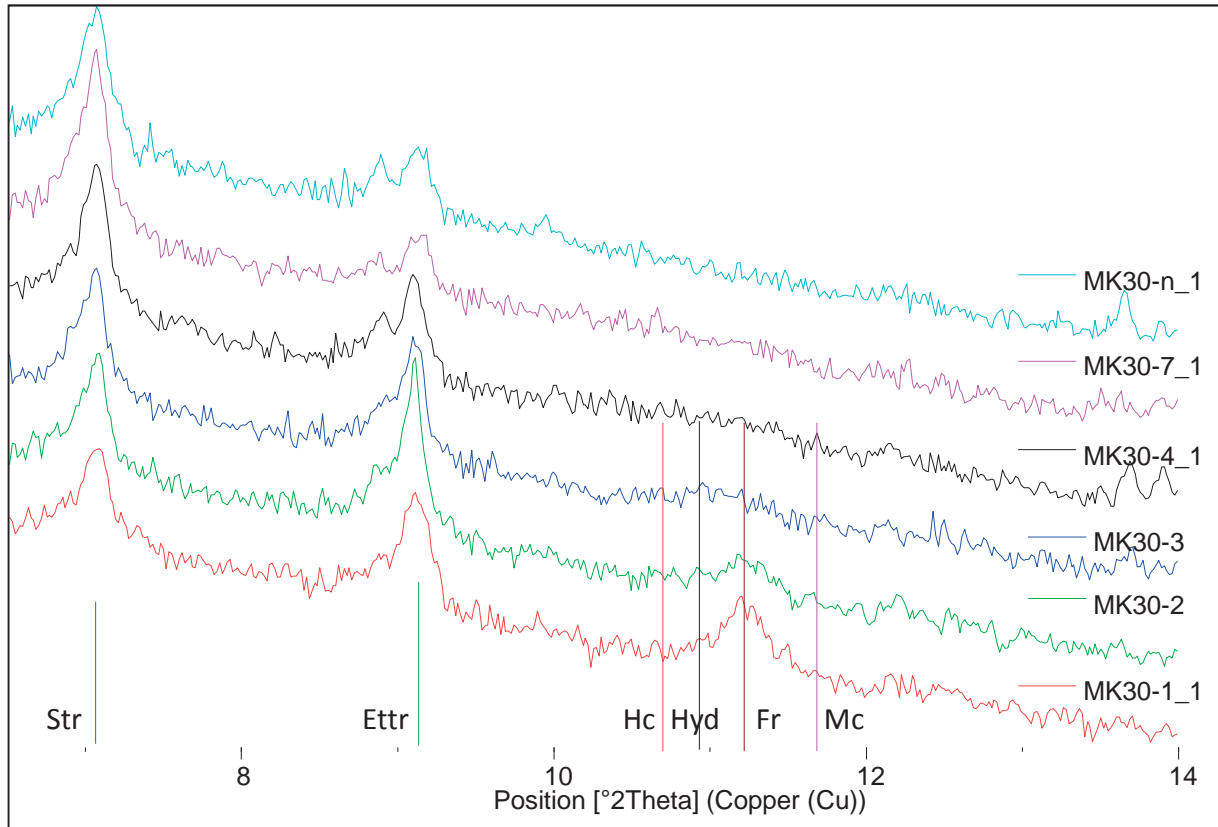


Figure 7.14: X-Ray Diffractograms obtained after 2 years Ponding for MK30

Figure 7.15 confirms the different behaviour of mortars containing only metakaolin, with low content of Friedel salt forming only close to the exposed surface by apparent consumption of strätlingite. Ettringite level seems higher close to the surface than deep in the sample. No traces of monosulfaluminate or of Kuzel salt were found.

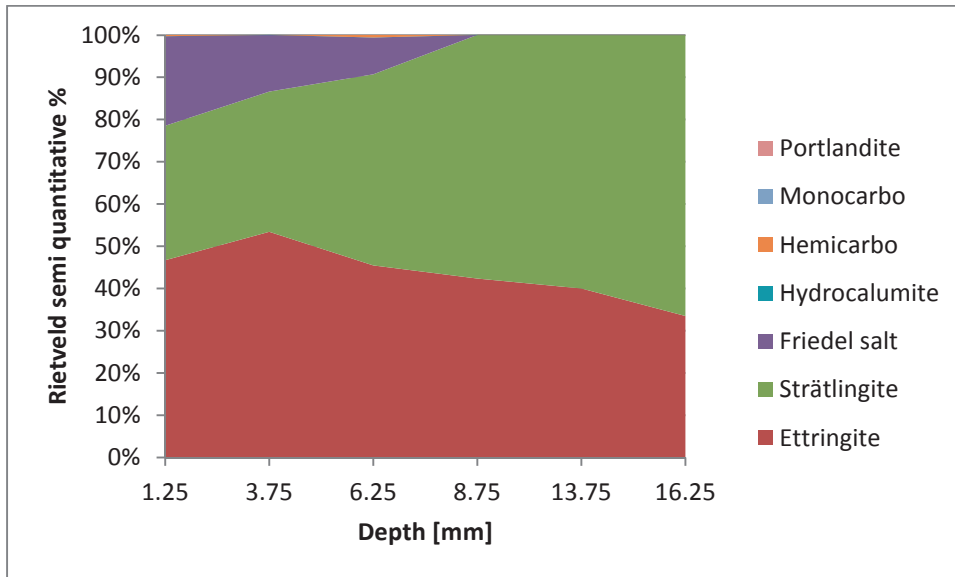


Figure 7.15: Hydrates phase assemblage evolution observed by semi-quantitative Rietveld analysis for MK30 after 2 years ponding.

MKB45

B45 shows a high peak of Friedel's salt at the surface, with ettringite and traces of strätlingite. Looking at deeper layers, the Friedel's salt peak progressively shifts to lower angle until in layer 5 appears peak of monocarboaluminate (Figure 7.16). This shift to lower angle is related to the progressive change from a mixture of Friedel's salt and hydrocalumite to hemicarboaluminate, as reported by Mesbah, Renaudin et al [155, 177], who showed that depending on carbonate and chloride concentration, hydrocalumite solid solution with coexisting anion CO_3^{2-} and Cl^- can form. In layer number 7, hydrocalumite is still present in small amounts and hemicarboaluminate dominates; however its position seems to be stable from layer 5. The semi-quantitative peak deconvolution based on Rietveld refinement supports these observations (Figure 7.17), and finally in layer 9 (at 21.25mm) there are only carboaluminates remaining and no more traces of chloride bearing phases.

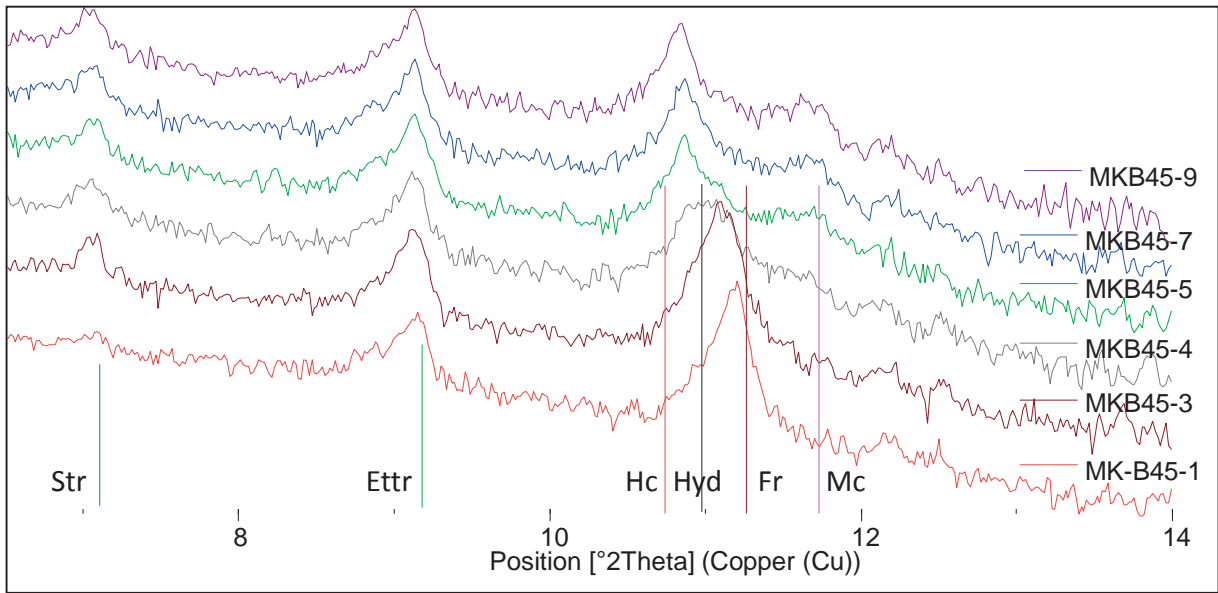


Figure 7.16: X-Ray Diffractograms obtained after 2 years Ponding for MKB45

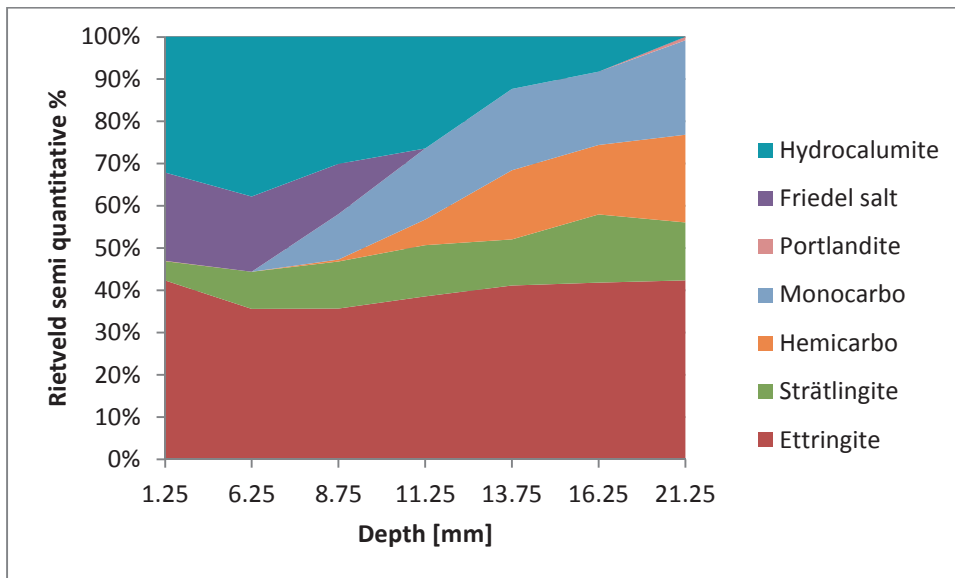
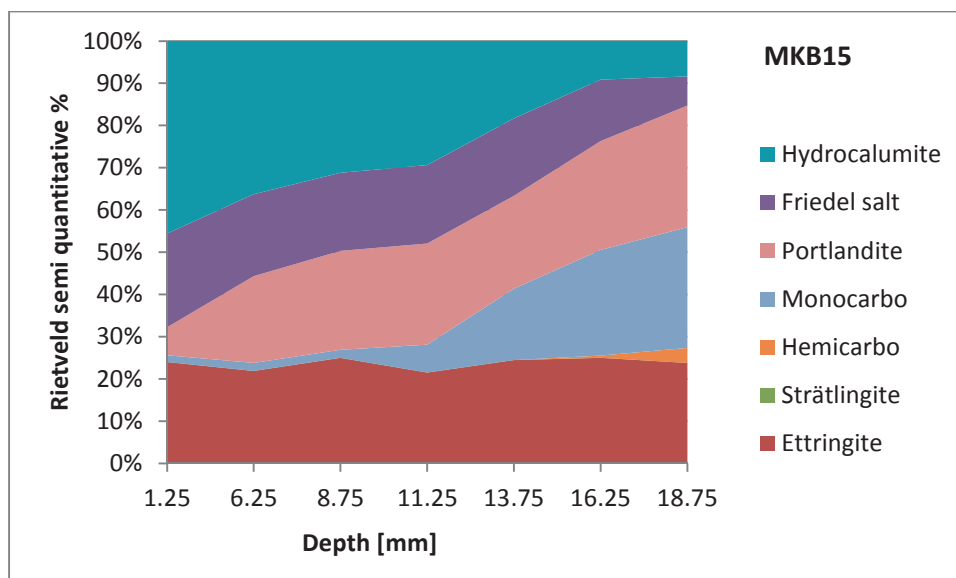


Figure 7.17: Hydrates phase assemblage evolution observed by semi-quantitative Rietveld analysis for MKB45 after 2 years ponding.

MKB15, MKB22 & MKB30

The X-Ray Diffractograms of layers after 2 years of chloride ponding for MKB15, MKB22 and MKB30 are given in annex (Figures 10.1). Evolution of the Phase assemblage for these materials is given in Figure 7.18. As the addition of metakaolin and limestone decreases, the penetration of chloride increases. Hydrocalumite seems to be the main AFm phase forming for all blends. Close to the surface, Friedel's salt forms in all blends, but the depth to which this phase is found decreases with increasing level of blending. Carboaluminates are absent close to the surface where they have presumably all been converted to chloride bearing phases. Strätlingite however is still present and reduced only in the very outer layer.



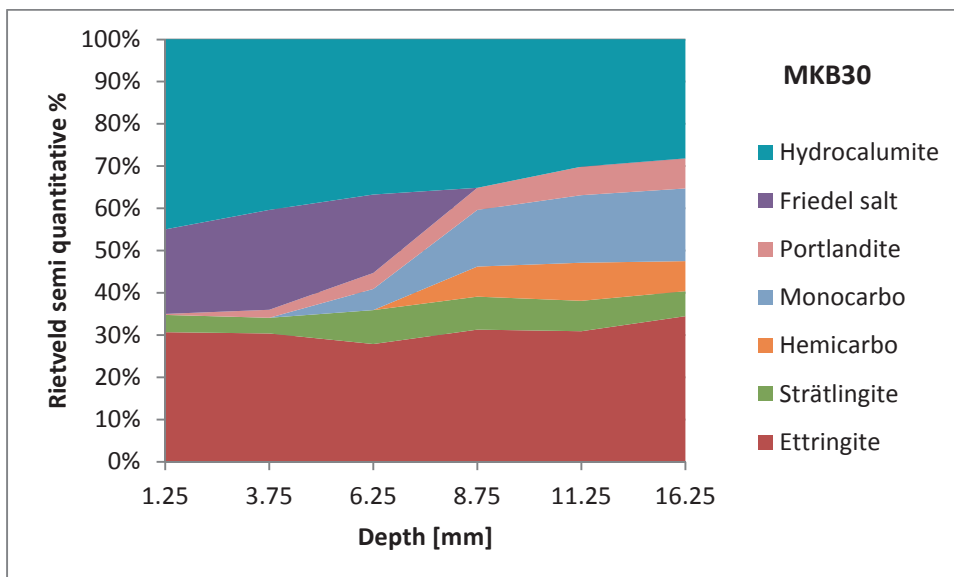
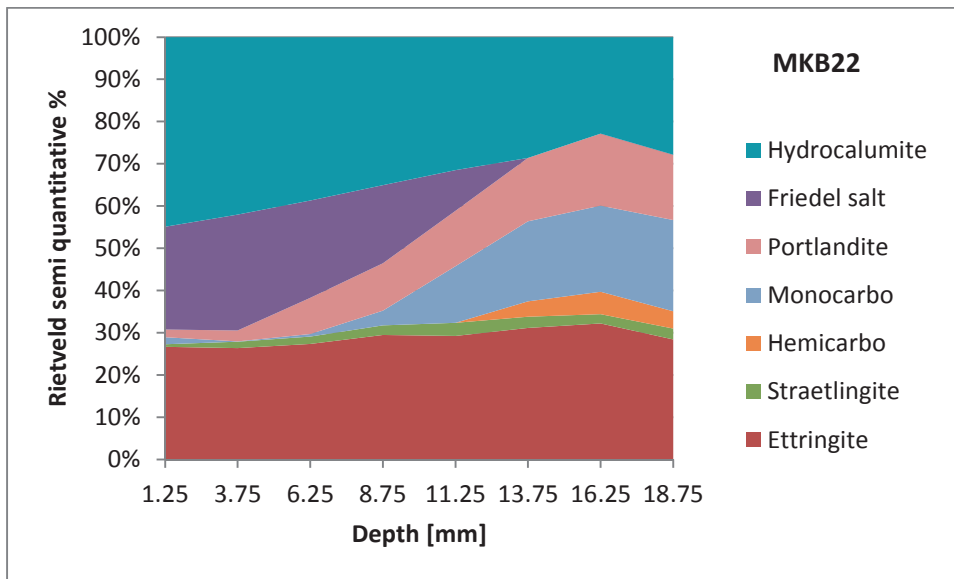


Figure 7.18: Hydrates phase assemblage evolution observed by semi-quantitative Rietveld analysis for MKB15, MKB22 and MKB30 after 2 years ponding.

With Pontezuela and Argeco clay

X-Ray Diffractograms for Pont30 show very high formation of Friedel's salt in the top layers, with decreasing intensity as we proceed to deeper layers (in Annex, Figures 10.2). Strätlingite on the contrary is absent at the surface but its peak is growing with increasing depth. Ettringite seems

stable throughout. It shows similar phase assemblage than MK30 but with increasing chloride binding in deeper layers.

PontB45 (Figure 10.3, Annex) shows also similar phase assemblage with MKB45, but the relative intensity of the chloride bearing AFm phases compared with ettringite is considerably higher. Ettringite stays constant over the depth. In the deepest layers, monocarboaluminate is clearly present as well as strätlingite, and it coincides with a decrease in intensity of the hydrocalumite peak. The same progressive shift observed in B45 from Friedel's salt on the surface to hydrocalumite and or hemicarboaluminate with increasing depth is seen in this sample.

As the addition of calcined clay (Pontezuela) and limestone decreases, the penetration of chloride increase, with deeper formation of Friedel salt, together with less intermixing with hydrocalumite. There are 2 main differences with metakaolin sample at equivalent blending that can be pointed out:

- Chloride penetrated systematically slightly deeper.
- In the sound phase assemblage, monocarboaluminate is systematically present and hemicarboaluminate absent.

The same conclusions of even deeper penetration of chloride were found for the Argeco clay that contains only 40% kaolinite (Figure 10.5 & Figure 10.6, section 10.1).

7.4.2.3. SEM-EDS POINT ANALYSIS

Comparison of the first layer in PC, MK30 and B45.

Figure 7.19 shows the Cl/Ca atomic ratios as a function of Si/Ca atomic ratios for PC, MK30 and MKB45 within the first 2.5 mm thickness, corresponding to layer 1. With such a plot it is possible to observe the intermixing of the C-A-S-H gel with other Cl bearing phases as well as the level of incorporation of Cl into the C-A-S-H. All the mortars show intermixing with Friedel's Salt, and probably also with hydrocalumite in the case of B45, consistent with the phase assemblage observed by XRD.

The level of Cl incorporation within the C-A-S-H zone seems constant for all compositions around 0.06 Cl/Ca atomic ratio. All points with Si/Ca ratio above 0.85 were discarded since they correspond to high intermixing with metakaolin and not representative of C-A-S-H (see Figure 7.21 for illustration). Finally for clarity EDS points are not given in deeper layers since they did not show any change for PC.

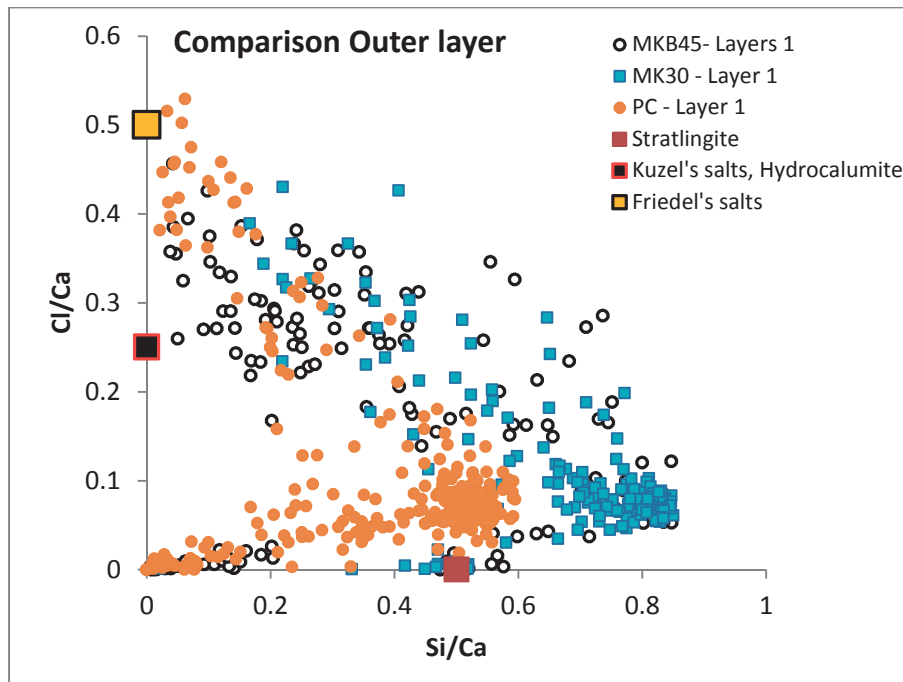


Figure 7.19: Cl/Ca atomic ratio as a function of Si/Ca atomic ratio for PC, MK30 and MKB45 within the first 2.5 mm thickness, corresponding to layer 1.

MK30

For blended cements containing pure metakaolin, Figure 7.20 clearly shows how C-A-S-H is intermixed with Friedel' salt in the outermost layer, then in the next layers Friedel's salt vanishes until in layer 4 there is intermixing with only a compound having Cl/Ca=0.25, that can either be hydrocalumite or Kuzel's salt that both share this stoichiometric ratio. In the next layer there are only few traces of chloride presence.

Average Cl/Ca levels in C-A-S-H progressively change from 0.06 in Layer 1, 0.05 in Layer 4 and finally around 0.02.

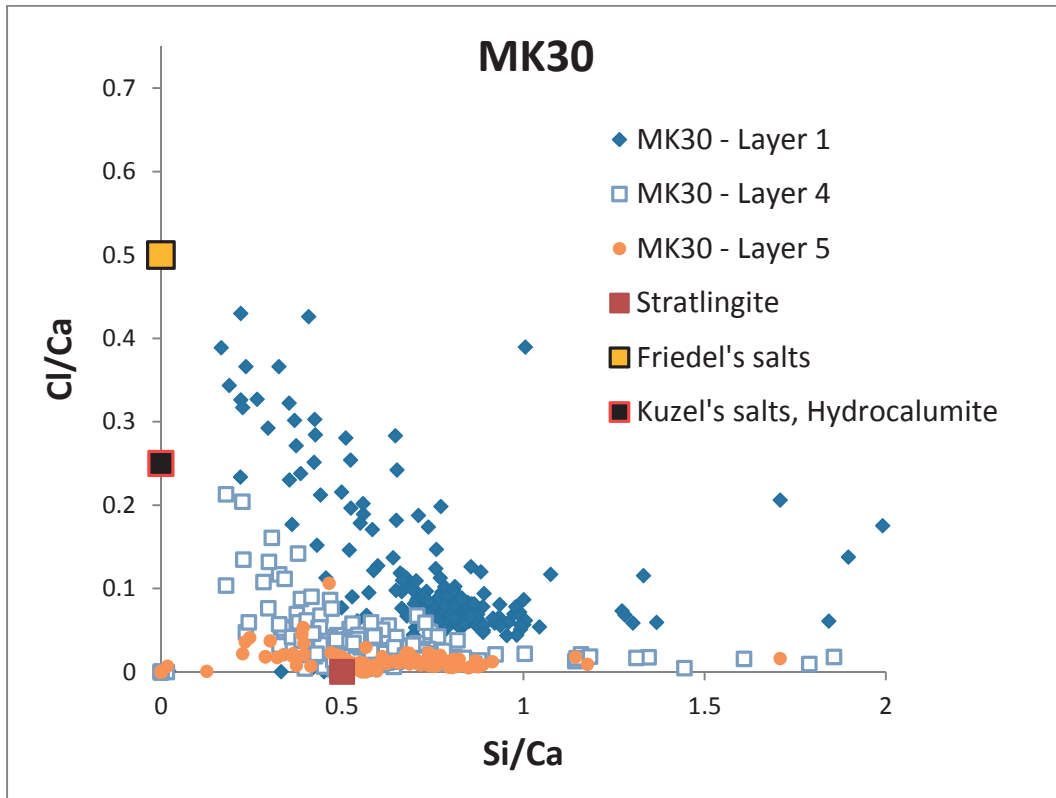


Figure 7.20: Cl/Ca atomic ratio as a function of depth for MK30. Layer 1 has been taken in the first 2.5 mm, layer 4 around 9.25mm and 5 at 11.25mm.

Al/Ca ratio as a function of Si/Ca ratio is shown in Figure 7.21. The intermixing of C-A-S-H with strätlingite and metakaolin is evident for all compositions. The C-A-S-H composition seems to be stable over the different layers.

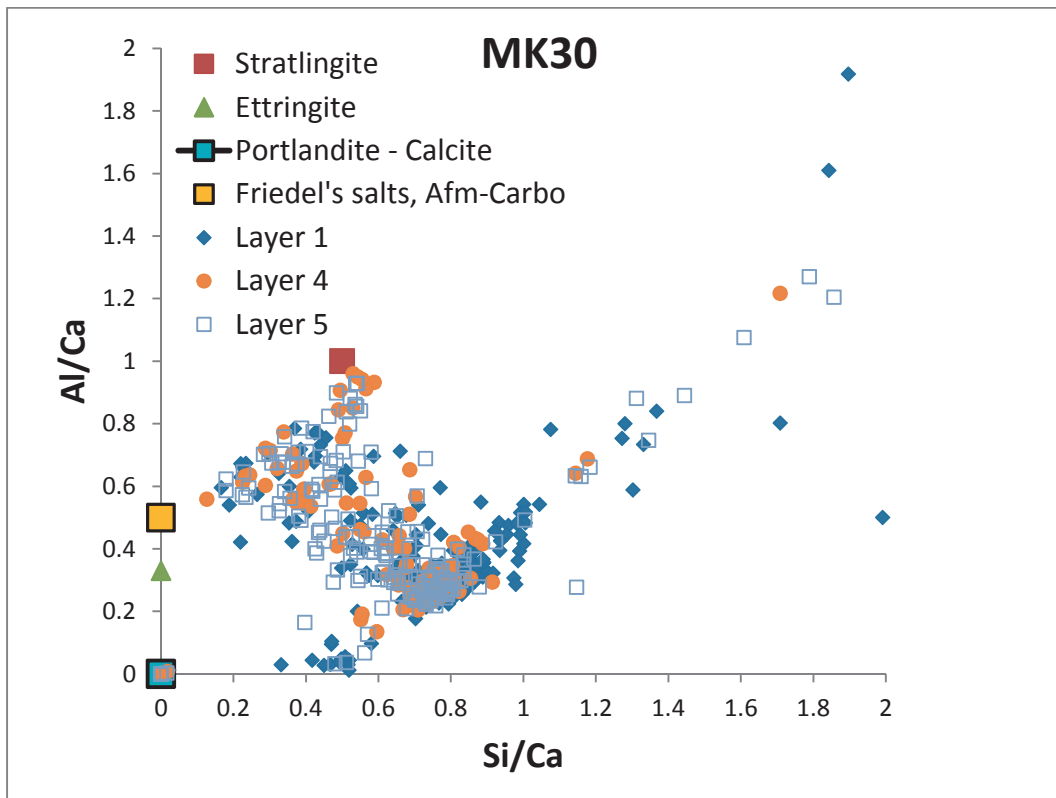


Figure 7.21: Al/Ca atomic ratio as a function of depth for MK30. Layer 1 has been taken in the first 2.5 mm, layer 4 around 8.75mm and 5 at 11.25mm.

B45

The Cl/Ca ratio as a function of Si/Ca ratio is plotted in Figure 7.22. This is very similar to MK30 (Figure 7.20) but for equivalent intermixing the depth is lower. Layer 2 already shows intermixing of C-A-S-H with hydrocalumite and layer 4 shows negligible amount of Cl incorporation into C-A-S-H and almost no intermixing.

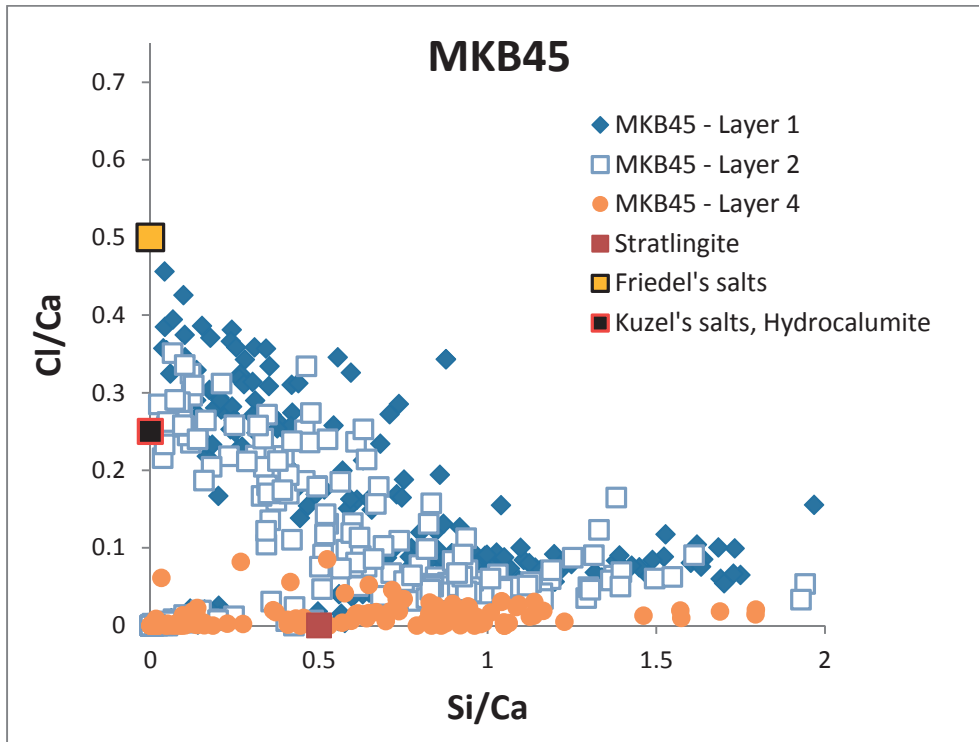


Figure 7.22: Cl/Ca atomic ration as a function of depth for MK30. Layer 1 has been take in the first 2.5 mm, layer 2 around 3.75mm and 4 at 8.75mm.

Figure 7.23 shows the EDS points analysis obtained in MKB45 sample in layers 1, 2 and 4. There seems to be a higher density of points closer to Friedel's salt in layer 1, intermixed with C-A-S-H, strätlingite and metakaolin in comparison with MK30. In the next layers, the intermixing becomes more centred on C-A-S-H with some intermixing toward AFm phases, strätlingite and metakaolin. The C-A-S-H composition is maybe slightly enriched in Al and Si compared to MK30 as seen more clearly in Figure 7.23.

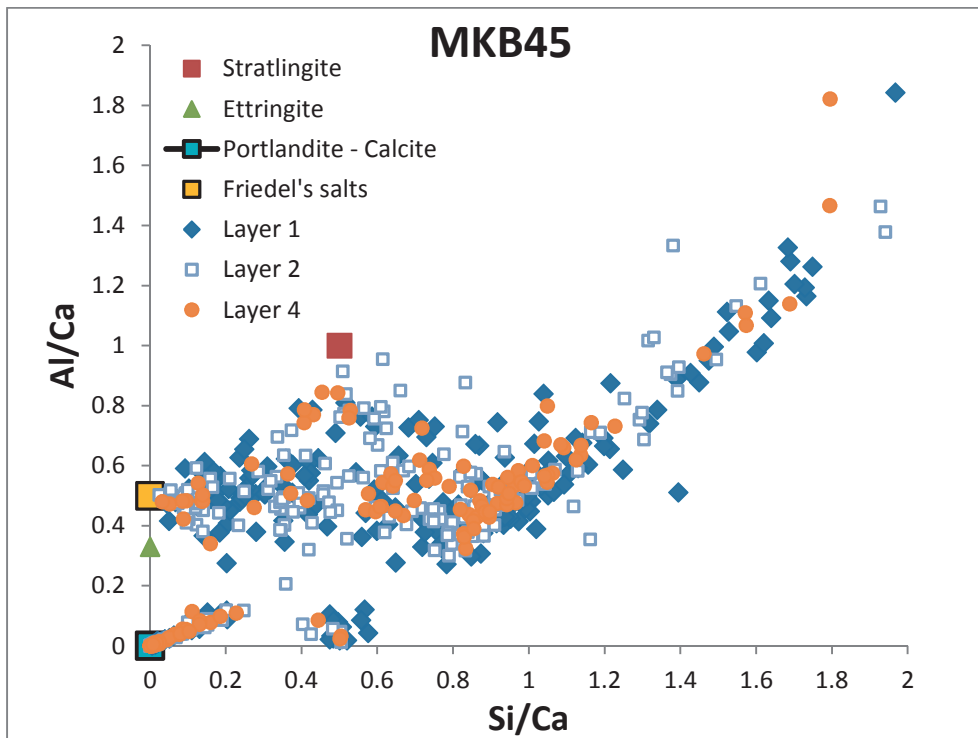


Figure 7.23: Al/Ca atomic ratio as a function of depth for MKB45. Layer 1 has been take around 1.25 mm deep, layer 2 around 3.75mm and 4 at 8.75mm.

With Pontezuela clay

The same behaviour was observed with Pontezuela calcined clay. There is Friedel's salt intermixed in the surface layer, then hydrocalumite and finally no more Cl intermixed or incorporated with C-A-S-H. This progressive shift to deeper layers is correlated with the slightly deeper chloride penetration observed. In the sound layer, the same intermixing with AFm and Strätlingite is observed. Aluminium incorporation in the C-A-S-H is however considerably less in comparison with system made with pure Metakaolin. The average level of Al incorporation into C-A-S-H is much lower, around $Al/Ca = 0.13$.

Summary ponding experiment

Blending with a combined addition of calcined clays and limestone improves considerably the resistance to chloride penetration compared to OPC, and also compared to calcined clays added alone.

With calcined clay containing only 50% kaolinite, chloride penetration is slightly increased but the same trends are found. With 40% kaolinite content, chloride penetration increases further but these blends still show improved resistance to chloride penetration compared to PC.

In the layers where chloride penetrated, considerable amounts of Friedel's salt are found. Hydrocalumite is also systematically present if the initial composition contains carboaluminates phases. No Kuzel's salt was found in these ponding experiments.

By EDS point analysis, the same features could be identified. It could be observed that the maximum level of chloride in C-A-S-H is the same for every blend, independently of Al content or its Si/Ca ratio.

Chloride bearing phases in Friedel's salt and hydrocalumite only partially explain the total chloride measured by extraction, especially in the case of the blends with calcined clays alone. These blends show higher level of total chloride but lower formation of Friedel salt. Physical binding in C-A-S-H needs to be taken into account. Considering that every other parameters are equal or similar (maximum chloride amount adsorbed in C-A-S-H gel, C-A-S-H composition, pH, porosity), the most plausible explanation for this difference is to be found in the total amount of C-A-S-H. Blends with 30% calcined clays are believed to have the highest amount of C-A-S-H compared to PC, because of the pozzolanic reaction and the total consumption of portlandite, and compared with B45 where the low cement content and the synergetic formation of carboaluminates limits C-A-S-H.

C-A-S-H content can be estimated by thermodynamic modelling or deduced by Rietveld refinement from the amorphous content calculation. It has been done in Section 7.8.1 for another cement. The C-A-S-H content obtained by Rietveld refinement are very similar for PC, MK30 and MKB15 and about 20% lower for MKB45.

7.5. CHLORIDE BINDING ISOTHERMS

7.5.1. EXPERIMENTAL PROCEDURE

Pastes were cast at a constant water/binder ratio of 0.5. At the end of the curing period the pastes were de-moulded and cut into 3-mm thick discs. The sliced samples were then vacuum-dried for three days in a desiccator containing silica gel and soda lime. The dried samples were transferred to a glove box containing soda lime to remove carbon dioxide from the air, and kept at 11% RH for a month. After storage, the 3-mm thick discs were broken into small fragments and samples weighing approximately 5 g were placed in 25-mL plastic bottles under vacuum for 2 h. The bottles were then filled with approximately 100 mL of NaCl solution using 5 different concentrations (0.1, 0.3, 0.5, 0.7, 1.0 M), sealed and stored at 23 ± 1 °C. The samples were stored for 21 weeks but solution concentrations were monitored after 6 and 13 weeks. It was considered that 21 weeks were adequate to ensure that equilibrium was reached between the pore solution of the samples and the host solution. The samples were then dried at 110°C until constant weight and then dissolved in acid⁴ to analyse their total chloride content by chromatography.

7.5.2. RESULTS

i. Total chloride by acidic dissolution

The total chloride contents obtained were corrected by subtracting the free chloride content contained in the water accessible porosity (assumed to be the same as the overall solution concentration) and bound chloride values are given here in Figure 7.24. The best fit with Freundlich isotherm is also given for each composition.

⁴ Samples were finely crushed and contain significant powder material, a gel-like formed in most of the samples that prevented us to follow the conventional method by analysis of the chloride content of the host solution. The analysis of this gel by XRD did not allow us to identify its nature.

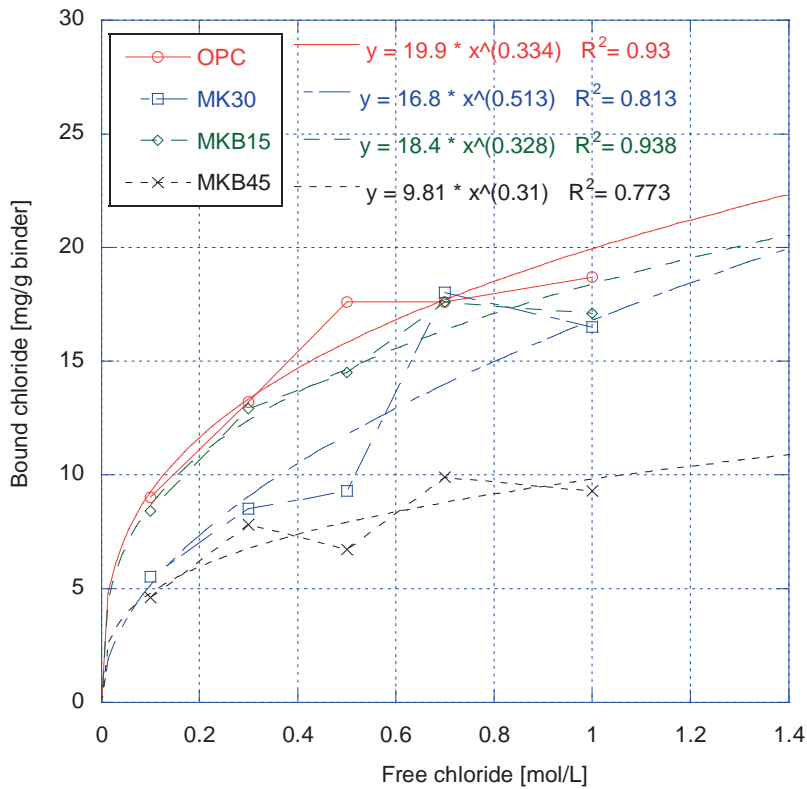


Figure 7.24: Chloride binding isotherm with Freundlich isotherm best fit for PC2, MK30, MKB15 and MKB45. The total chloride content normalized by dried weight of binder is given as a function of free chloride concentration.

This figure shows that chloride binding normalized by weight of binder are in the same order of range for PC2 and MKB15. The binding capacity of MK30 and MKB45 are significantly lower for concentrations up to 0.5 M NaCl. At 0.7 and 1M NaCl, they seem to diverge; MK30 reaches chloride binding level similar with PC and MKB15 while MKB45 remains considerably lower, at approximately half the binding capacity of the other compositions.

It can be noted that correlation factor R^2 is acceptable but not as precise as values obtained in studies using the quantification method by AgNO_3 titration of host solution [164, 167]. Various errors may have indeed been introduced through the manipulation of the powders, the acidic dissolution, the dilution required prior to chromatography, the error associated to the manual peak deconvolution obtained from chromatography and the estimation of the free chloride content in the open porosity of the cement paste.

But the sudden jump observed for MK30 between 0.5 and 0.7 M NaCl suggests also the formation of a solid phase that could invalidate the isotherm approach, strätlingite dissolution and reprecipitation into Friedel salt is a possible option.

It is also important to remark that α coefficient values of Freundlich isotherm are remarkably higher than what has been reported in the literature. For example, Thomas et al have reported α values for Freundlich isotherm of 7.6 for similar PC composition [164], Ipavec reported more recently between 9.4 up to 10.1 depending on pH value [167]. We do not have the initial Cl content of the cement, which might partly explain this high level. Also, total $\text{Al}_2\text{O}_3 + \text{Fe}_2\text{O}_3$ of PC2 (4.6 and 3.5% respectively) is higher than for Ipavec or Thomas (4.6 and 2.9%; 4.1 and 2.9%, respectively).

ii. XRD analysis

All the phase assemblages in the pastes after exposure were analysed by semi-quantitative Rietveld analysis (already described in Section 3-a. 7.4.1.2) (Figure 7.25).

The phases formed differ depending on the initial phase assemblage (Annex chapter 10.3.1).

PC contains portlandite, ettringite, monosulfoaluminate, hemicarboaluminate and monocarboaluminate. At 0.1M already only a small amount of monosulfoaluminate and both carboaluminates remain. Kuzel salt is present only at 0.1 M NaCl. Friedel salt and hydrocalumite are also present at 0.1M NaCl, and Friedel salt progressively becomes the only chloride bearing phase as NaCl concentration increases.

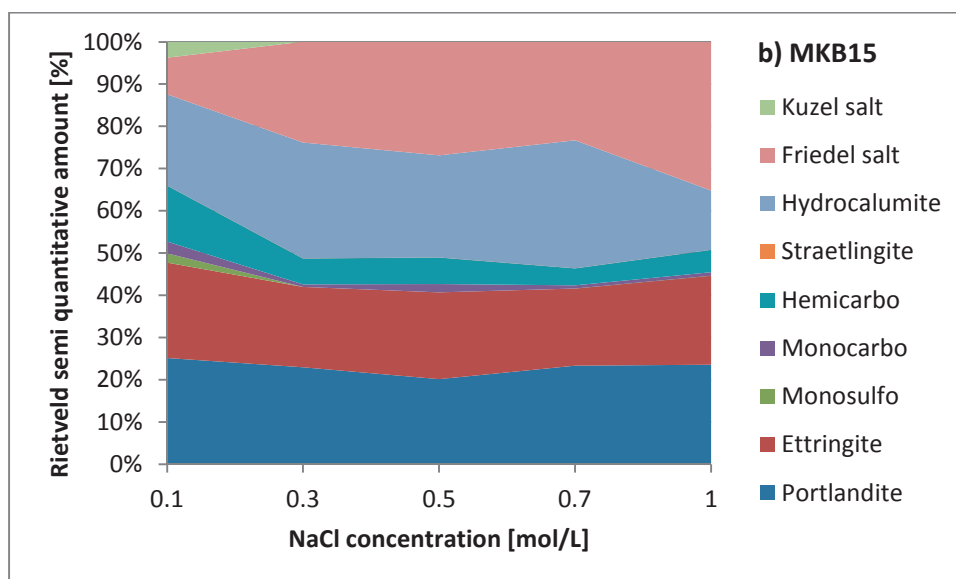
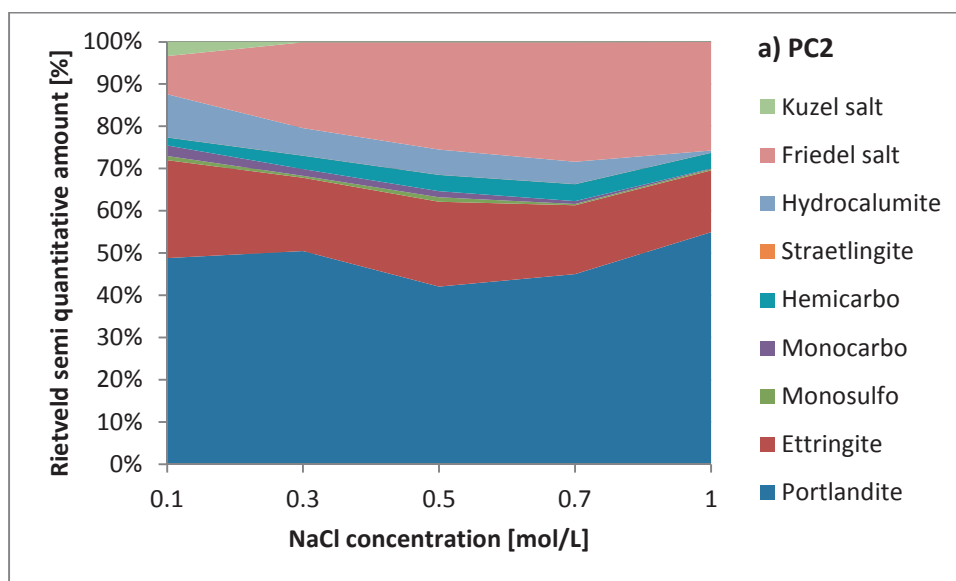
MKB15 has a composition relatively close to PC so similar phase assemblages are observed at the different chloride concentrations. However since MKB15 has considerably higher hemicarboaluminate content, considerably higher amounts of hydrocalumite form. This is the most important chloride containing phase up to 0.7M, above which Friedel salt has the highest content.

The similar total chloride bound is probably explained by the higher C-A-S-H content in PC compared to MKB15, balanced with the higher carboaluminates content for MKB15 compared with PC.

In MK30, the initial phase assemblage contains ettringite, strätlingite, monosulfoaluminate and traces of carboaluminates and portlandite. Since initially more monosulfate is present Kuzel's salt forms in higher amount at all NaCl concentration except 1M NaCl where only traces remain.

The low initial amount of carboaluminates correlates well with the very low amount of hydrocalumite formed at all NaCl concentrations. It is interesting to note that monosulfate totally disappears only at 0.7M NaCl, coinciding with the increase of Friedel's salt formation as well as the abrupt increase of total bound chloride observed (Figure 7.24). At 1M Ettringite content also increases. Strätlingite decreases slightly but remains mostly stable with increasing NaCl content.

In MKB45, hydrocalumite is the main phase formed at all NaCl concentrations. It increases with increasing NaCl. In addition, with increasing free NaCl concentration Strätlingite, Hemicarbo and Monocarboaluminate are decreasing and Friedel salt increasing.



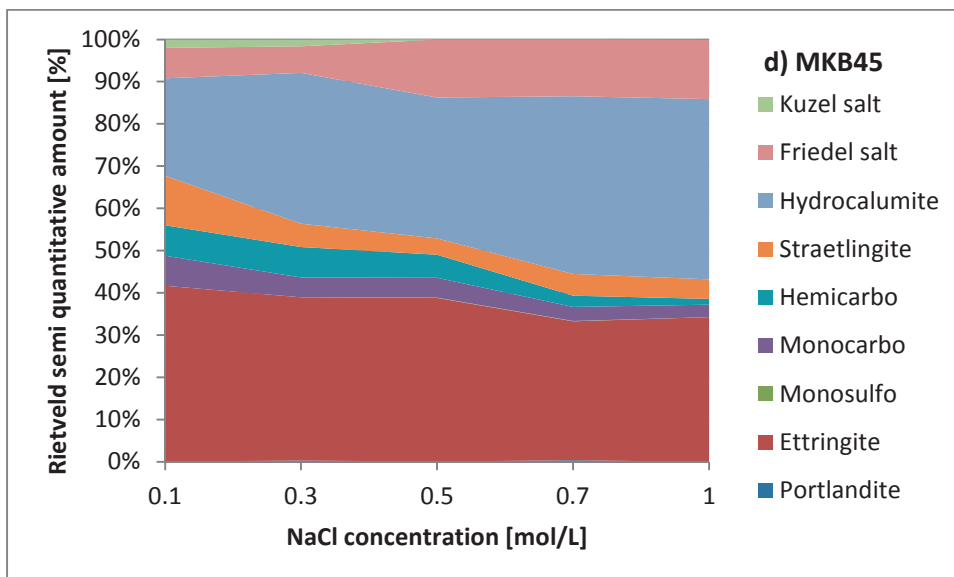
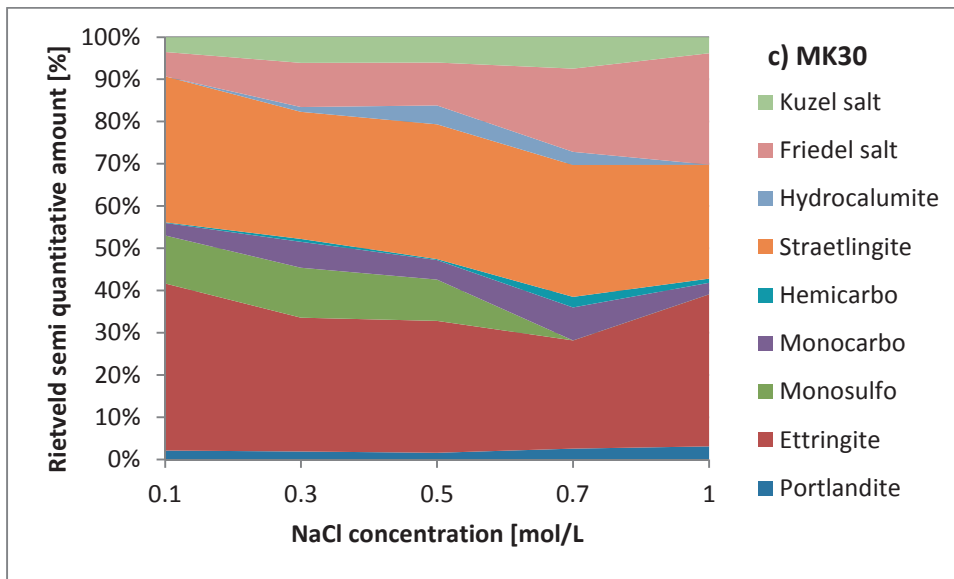


Figure 7.25: Semi quantitative phase assemblage obtained for PC2 (a), MKB15 (b), MK30 (c) and MKB45 (d) respectively after 13 weeks of chloride binding experiment with 0.1; 0.3; 0.5; 0.7 and 1 M NaCl solution.

In summary, the chloride binding isotherms show the following results:

- Normalized by g. of paste, PC, MK30 and B15 show relatively close binding isotherm, while B45 seems to bind less chloride.
- Friedel salt forms in all experimental conditions and its intensity growing with increasing NaCl concentrations
- When carboaluminates are present in the initial phase assemblage, hydrocalumite is systematically present at low NaCl concentration. With increasing NaCl concentration, it is progressively converted in Friedel salt.
- Kuzel salt was detected in small amount only for low NaCl concentration. Except for MK30 where it seems to persist. It is related to the higher monosulfoaluminate quantity in MK30
- Strätlingite seems to marginally convert to Friedel salt for NaCl concentrations above 0.7 M only

7.6. CHLORIDE MIGRATION TEST: THE SIMCO RCPT MODIFIED PROCEDURE

7.6.1. EXPERIMENTAL SET-UP

In this test, a fully saturated cylindrical sample (100 mm diameter and 35 mm thickness) is placed between an upstream cell containing both 0.5 M sodium chloride and 0.3 M sodium hydroxide and a downstream cell with only 0.3 M sodium hydroxide. A constant DC voltage is applied; the current as well as the voltage between the two sides of the tested sample are measured daily over 14 days (Figure 7.26). In addition, the chloride concentration is regularly measured in the downstream bath. The water accessible porosity value was measured according to norm ASTM C642 [178]. It consists in the measurement of the water saturated weight in air and water, and in air after drying until constant weight at 110°C. The pore solution was extracted by mechanical compression. Compositions (K, Na, Ca, Al, Si and Sulfate) were quantified by ICP, and OH considering equilibrium of

charges) were obtained on other paste replica samples to characterize the sample prior to the migration test.

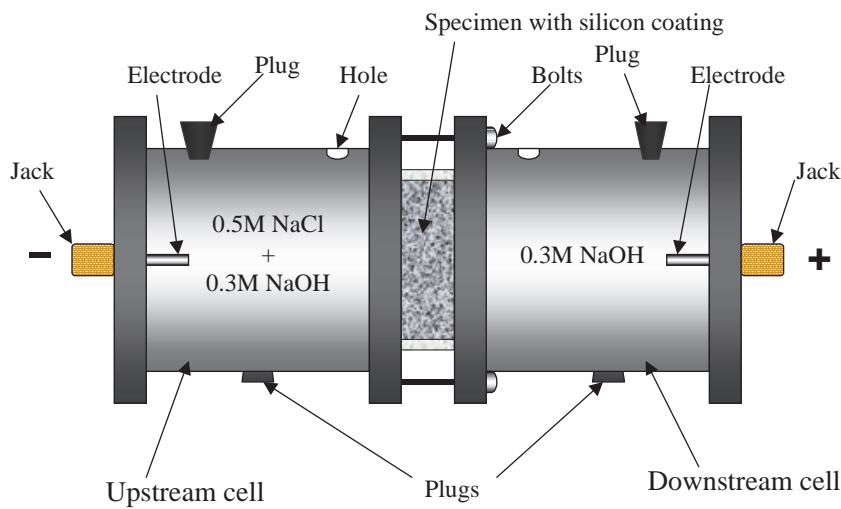


Figure 7.26. Schematic representation of the migration test (Stadium®)

7.6.2. MODELLING, THEORETICAL BACKGROUND

STADIUM allows the interpretation of the results of migration tests using the Nernst-Planck-Poisson set of equations (see the summarized approach with the equations in Annex section 10.3). It is a multiionic transport model considering electrical coupling among the ions. Advection term can also be included, but in the migration test samples are always water saturated and the advection term is not active.

The model allows step by step solution of the mass conservation equations for each ionic species as well as the chemical equilibrium relationships for the reactions between the pore solution and the hydrated cement paste.

The equations are first written at the microscopic scale. They are then integrated over a representative elementary volume using a homogenization (averaging) technique, to yield the equations at the macroscopic scale. It allows a single coefficient τ to be determined characterizing

the whole pore structure that applies to all ionic species. The coefficient is called “tortuosity” and is defined in Equation 7-3:

$$\tau = \frac{D_i}{D_i^0} \quad \text{[Equation 7-3]}$$

Where D_i & D_i^0 are the diffusion coefficients in the sample and in free water of the species i respectively (see D_i^0 values in Annex, section 10.3.1)

Note that the use of the tortuosity term by Stadium is counter intuitive, since in this approach tortuosity $0 < \tau < 1$ and decreases as porosity decreases and effective travel distance increases and is the inverse of the classical definition of tortuosity: the ratio of the effective travel distance through the pore channel to the shortest straight path through the medium and $\tau > 1$. In this work we use therefore the term “inverse tortuosity” to denominate τ .

Besides the current and the voltage evolution during the migration test, the model, based on a finite element approach requires the boundary conditions defined by the upstream and downstream bath composition, the porosity value, the cementitious phase assemblage and the pore solution composition.

The chemical reactions between chloride ions and monosulfoaluminate to form Friedel’s salt are taken into account according to both dissolution/precipitation and ionic exchange mechanism (Equation 7-5)

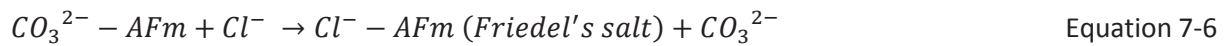
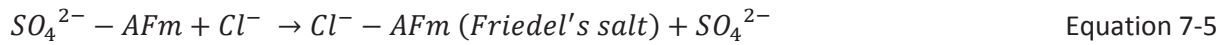
Up to now, the Stadium model did not including any carboaluminates hydrates.

As a first approach, It was decided to assume that carboaluminates have the same chloride binding capacity as monosulfoaluminate hydrates, and can form Friedel’s salt by ionic exchange [179], according to Equation 7-6. At this point hydrocalumite solid solution is not considered in the model.

Similarly it was also necessary to introduce an ionic exchange process in order to form Friedel’s salt from strätlingite (Equation 7-7). This was further simplified by considering that only aluminium hydroxide $[Al(OH)_3]^-$ was released in solution by the ionic exchange process instead of an aluminosilicate ion $[AlSi(OH)_8]^-$ as it is the case in reality .

In first approximation, all ionic exchange processes were initially defined with the same equilibrium constant, in Equation 7-4:

$$\log(K)=-3, \text{ with } K_{Cl/SO_4} = \frac{\{Cl\}^2 [AFmSO_4]}{\{SO_4\} [AFmCl]} \quad \text{Equation 7-4}$$



An analysis of parameter sensitivity is also presented in the annex (10.3.2).

7.6.3. CURRENT RESULTS

7.6.3.1. PRELIMINARY SERIES

With this very first series, preliminary results were obtained after 14 days of testing applying 10V DC.

The current values, monitored over 14 days of test, are given in the Figure 7.27. The initial current value is much higher for PC than for both other blended cements. While there is strong current decrease during 6 days and later on an increase for PC, the current regularly but slowly decreases in both MK30 and PontB45 mortars. Figure 7.27 shows significantly distinct behaviours between PC and the blended mixtures. The blended mixes were highly resistive which denotes a low ionic flow.

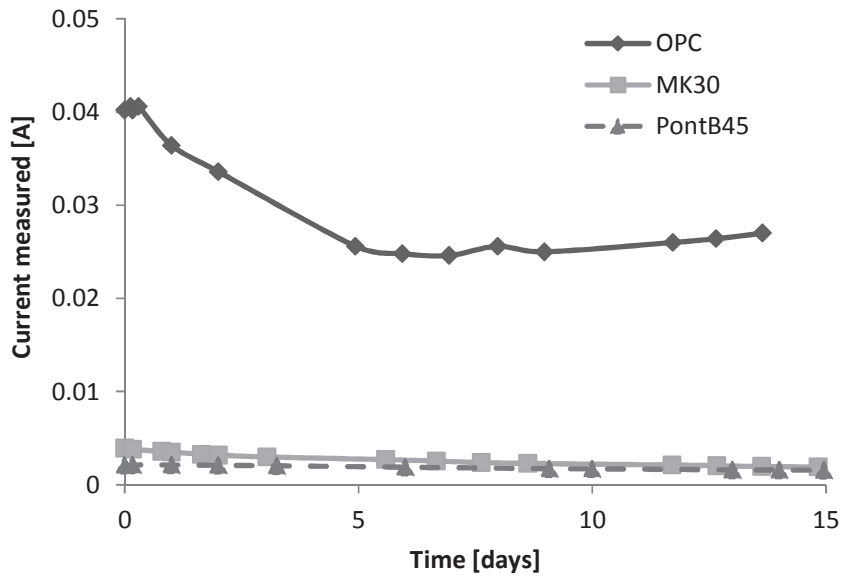


Figure 7.27. Current evolution during migration test for the three different samples

Figure 7.28 shows the evolution of the downstream chloride concentrations during the migration test for the different mixtures. The measurements of the chloride content in the downstream cell confirmed the previous results on the current evolution through the samples. An increase of the chloride concentration was observed for PC while no chloride ions were found in the downstream cell for the blended mixtures. The arrival of chloride ions in the downstream cell corresponds to the increase of the total current as seen in Figure 7.27. Indeed, in the case of the PC mix, after five days of testing, current and chloride concentration started to increase. This increase was therefore not observed for the blended mixtures.

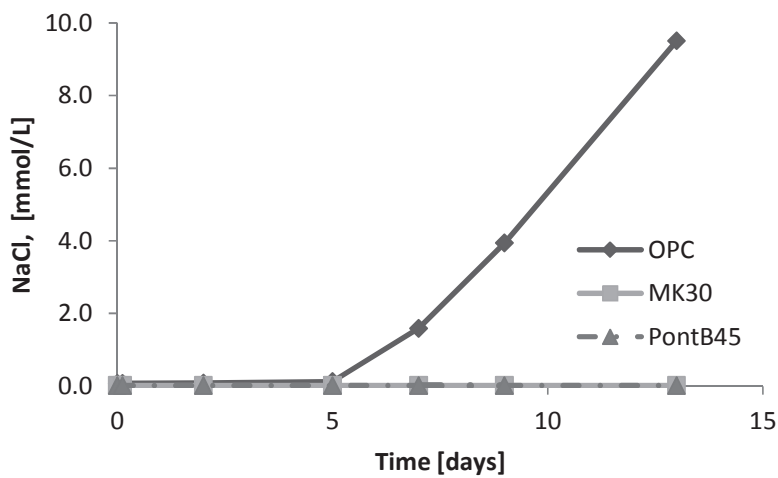


Figure 7.28: Chloride downstream concentrations monitored during the migration test and quantified by chromatography

Additionally, after the migration test, the samples were gradually ground and their total chloride content determined. Figure 7.29 presents the chloride profile for each mixture.

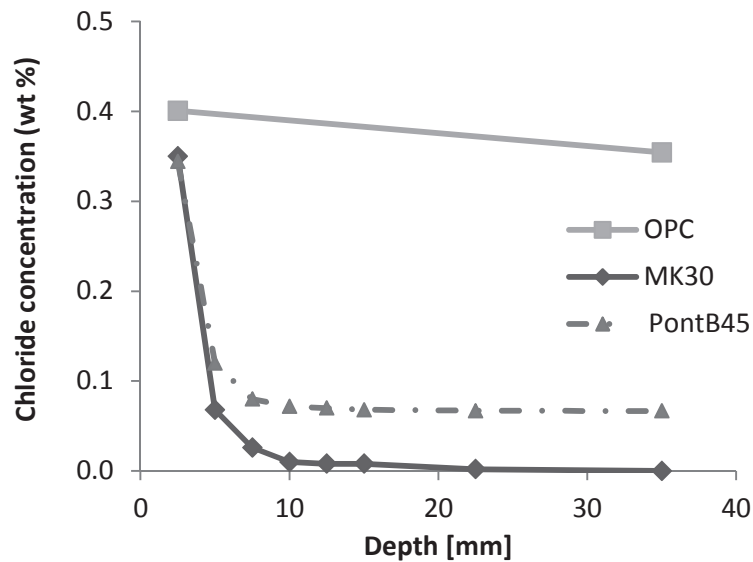


Figure 7.29. Chloride profiles of the PC, MK30, and PontB45 after applying 10V during 14 days

The chloride profiles measured after the migration test confirmed that chloride ions passed through the PC sample with a high amount at both sides, while the chloride content decreased rapidly after 5 mm from the exposed surface for both blended mixtures. These results are in agreement with the previous measurements presented in Figure 7.27 & Figure 7.28: Chloride ingress has clearly been slowed down in the case of the blended mixes in comparison with the PC mix.

7.6.3.2. SERIES 2

For this new series, it was decided to adapt the applied voltage for each mortar composition (PC remaining at 10V, 30V for blends with Burgess metakaolin PC and 20V for PontB15 and PontB45) and decrease the thickness in order to optimize and accelerate the passing of chloride ions through the blended samples using the first experience gained with the preliminary series and staying within a the range of correct experimental conditions. Current evolutions are given in Figure 7.30.

PC shows the highest initial current values (above 70mA) and the fastest establishment of chloride passing through the sample despite having the lowest applied voltage.

The 2 replicas of MK30 and MKB15 had different thicknesses, resulting in different current behaviour. MKB15 showed the highest initial current (around 40 mA), followed by MK30 (around 25 mA) and MKB45 (below 12 mA) with significantly lower current. Blends with Pontezuela clay Pont-B45 and Pont-B15 show behaviour close to the ones observed with Burgess MK, but the applied voltage at 20V was lower. Initial currents around 50 mA and 15 mA respectively were found for these compositions.

The initial current decrease is very marked for PC, much less for the blends. After 2 weeks, only the B45s samples did not show the current increase due to chloride passing through the sample. MK30 showed unusual behaviour with decreasing current after the increase associated with the passing of Cl ions and is discussed later (Annex, section 10.3.2)

Current values, 28days old samples

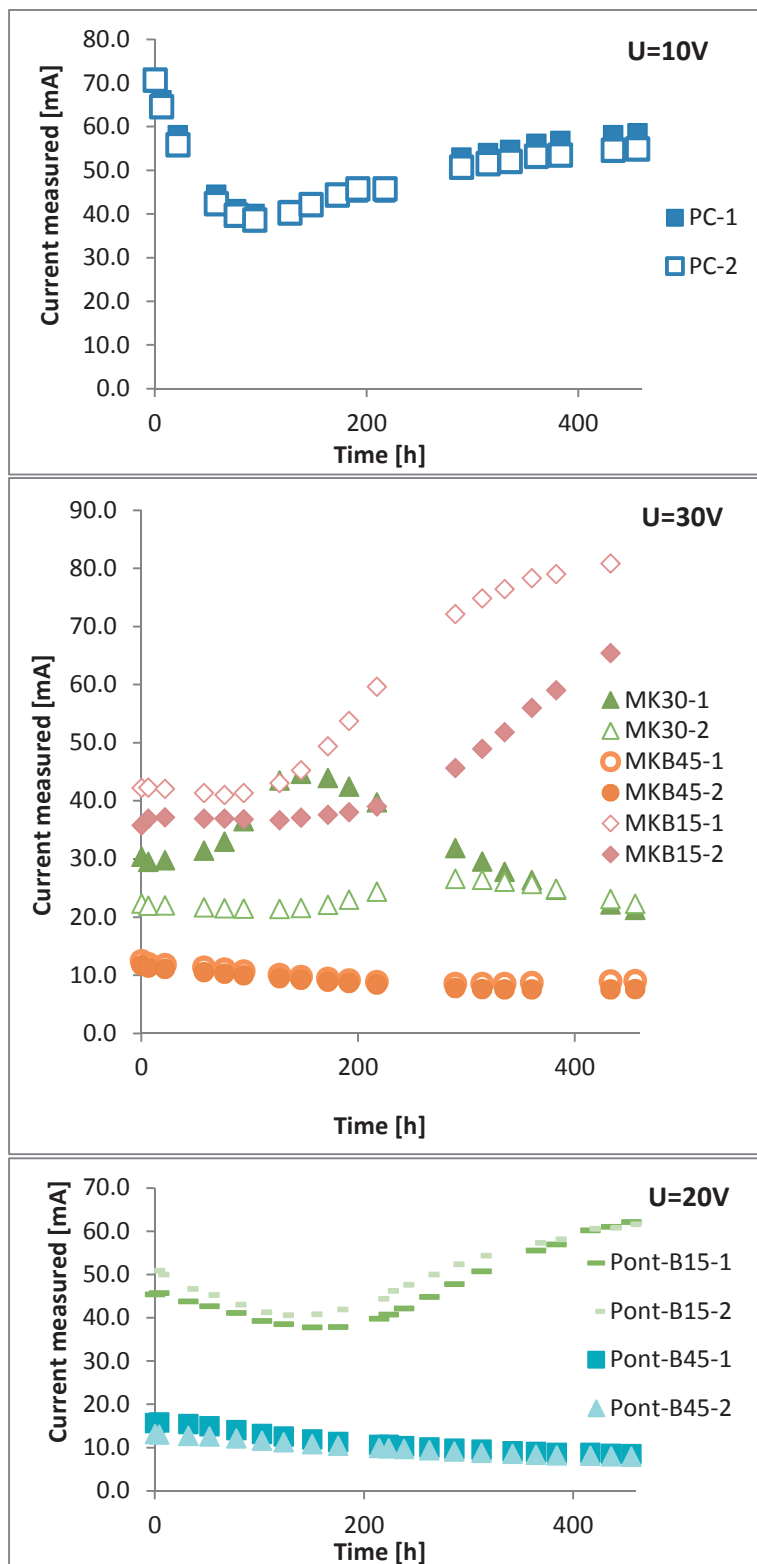


Figure 7.30: Current evolution for all samples during the migration test carried out for samples cured 28d. These current values have been obtained for an applied voltage of 30V for MK30, MKB45 and MKB15, 10V for PC and 20V for PontB15 and PontB45.

The chloride contents in the downstream bath were also monitored and the first chloride increase systematically correlated well with the onset of current increase.

110 days old samples

Results are given in the annex (Annex section, Figure 10.11) and globally present the same trends as the results at 28days. The discussion of the differences is given in the next section.

7.7. MODELLING CHLORIDE MIGRATION: INVERSE TORTUOSITY AND DIFFUSION COEFFICIENT CALCULATION

7.7.1. RESULTS OF PRELIMINARY SERIES

The various transport parameters are summarized in Table 7.2. The diffusion coefficient of all the species in the system is calculated from the inverse tortuosity obtained by the modelling; in particular, the diffusion coefficient of hydroxyls ions has been estimated with the other characteristics values regarding the transport properties of the cementitious mixtures. The simulations lead to hydroxyl diffusion coefficient (D_{OH}) values of 19.05 for PC, 1.51 for MK30, and $1.61 \cdot 10^{-11} \text{ m}^2/\text{s}$ for PontB45 respectively. τ values are then 36.10, 2.85, and 3.04 for PC, MK30, and PontB45 respectively. These results mean that the porous structure of the blended mixtures is much more refined than that of PC.

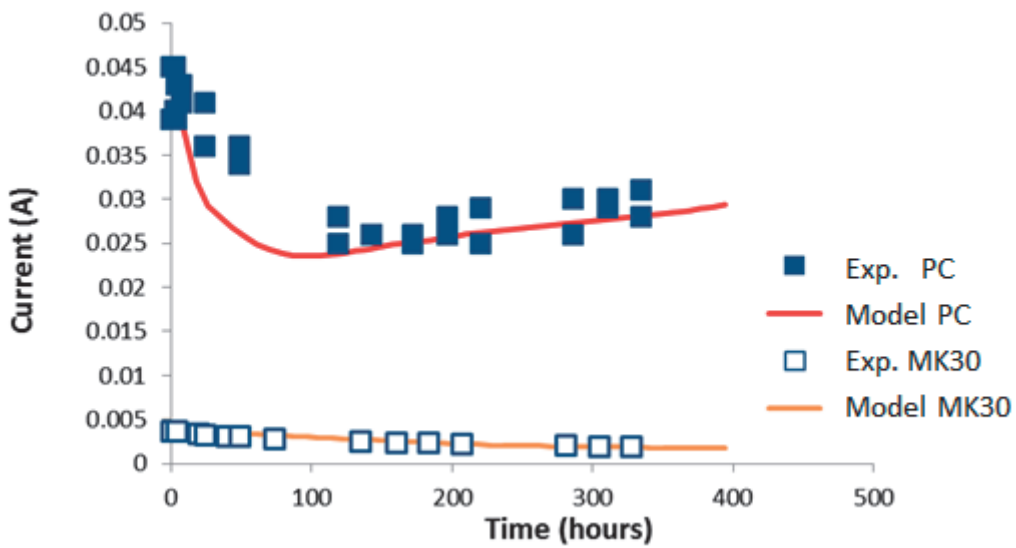


Figure 7.31. Simulations of the current evolution during the migration test for PC and MK30

Table 7.2 shows that the refinement of the microstructure is not dependent on the total pore volume. Indeed, the porosity of PC was lower than blended mixtures while the inverse tortuosity, related to the refinement of the porous network, was much higher for PC. That indicates the remarkable effect of the calcined clays as cement replacement in concrete. The use of calcined provided a significant enhancement of the transport properties of the blended materials.

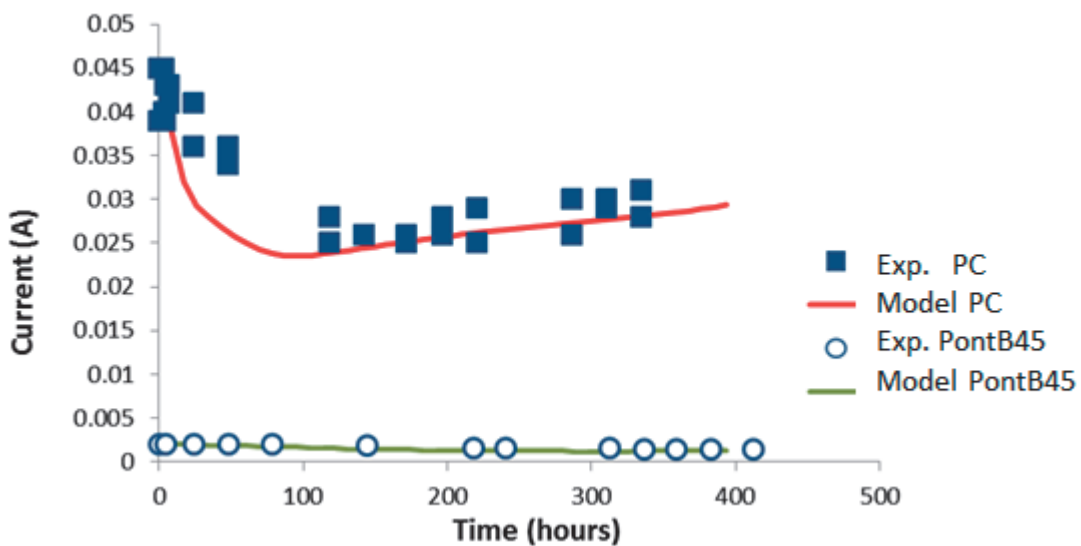


Figure 7.32. Simulations of the current evolution during the migration test for OPC and B45

Table 7.2: Summary of properties of the different mixtures, Preliminary series

	Porosity (%)	Initial pore solution composition [mmol/L]						Inverse tortuosity [10 ⁻³]	DOH ^{**} [10 ⁻¹¹ m ² /s]
		Na ⁺	K ⁺	Ca ²⁺	Al(OH) ₄ ⁻	SO ₄ ²⁻	OH ^{-*}		
PC	14.9	105.0	123.4	1.7	0.3	3.1	225.3	36.10	19.05
MK30	20.2	63.4	49.1	0.1	2.4	1.7	106.9	2.85	1.51
PontB45	19.4	67.9	47.5	0.1	3.2	3.8	104.8	3.04	1.61

(*): estimated from the electroneutrality law

(**): Chloride diffusion coefficient is smaller by a factor 2.60 (see also Section 10.3.1)

7.7.2. SERIES 2, 28D

The results of Series 2 at 28 days are summarized in Table 7.3. This series was made with a different Portland cement, but shows the same trends as previously, although it should be noted that this cement PC3 itself has a considerably lower diffusion coefficient than PC2, probably because PC3 is a higher strength class cement (42.5) than PC2 (32.5).

Table 7.3: Summary of properties of the different mixtures, Series 2 at 28days

Serie 2, 28days	Porosity (%)	Initial pore solution composition [mmol/L]						Inverse Tortuosity [10 ⁻³]	D _{OH⁻} [10 ⁻¹¹ m ² /s]
		Na ⁺	K ⁺	Ca ²⁺	Al(OH) ₄ ⁻	SO ₄ ²⁻	OH ^{-*}		
PC3	17%	108.9	485.4	1.4	0.2	1.9	535.0	38.4	7.80
MKB15	20%	156.4	375.0	1.0	2.3	2.3	473.9	18.9	3.85
MK30	19%	36.2	42.5	0.5	1.2	0.6	74.7	12.1	2.45
MKB45	23%	41.5	49.9	1.0	2.2	1.0	83.9	3.7	0.75
PontB15	20%	69.0	250.9	1.4	0.1	0.8	299.5	28.1	5.70
PontB45	21%	30.4	67.7	1.9	0.6	0.3	95.5	6.2	1.25

In order to find the best fit of the current curve, a first simulation of the phase assemblage was automatically given by StadiumLab (the detailed explanations can be found in reference [180] and phases amount were progressively modified in order to improve the fit.

Finally the best fits were obtained using the phase assemblage given on the right in Table 7.5. The phase assemblages obtained by Rietveld refinement are given in the same table on the left for comparison.

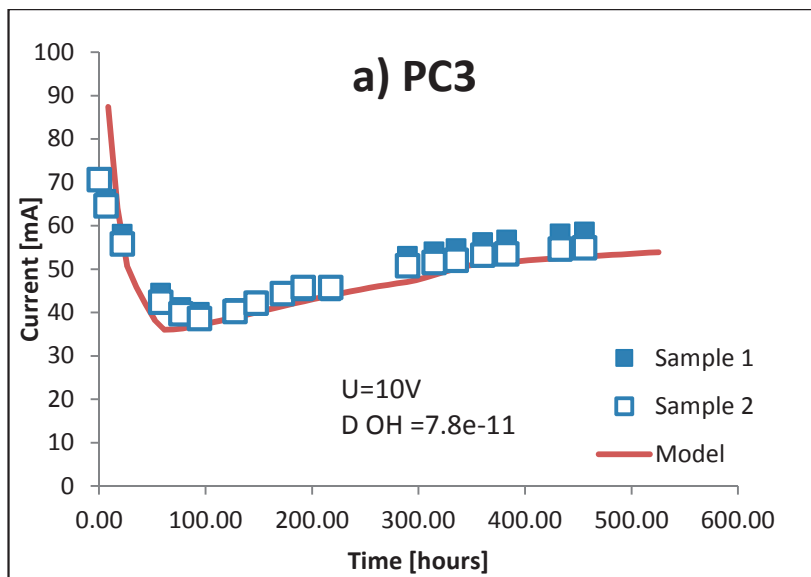
It is positive to see that despite the elementary description of the chloride interaction in the cementitious matrix that was postulated it was possible to obtain reasonable fits of the current during the migration test using a phase assemblage close to reality.

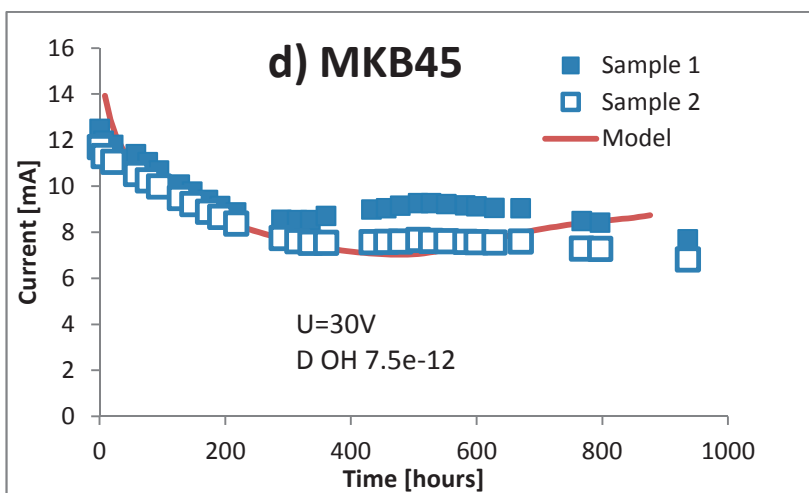
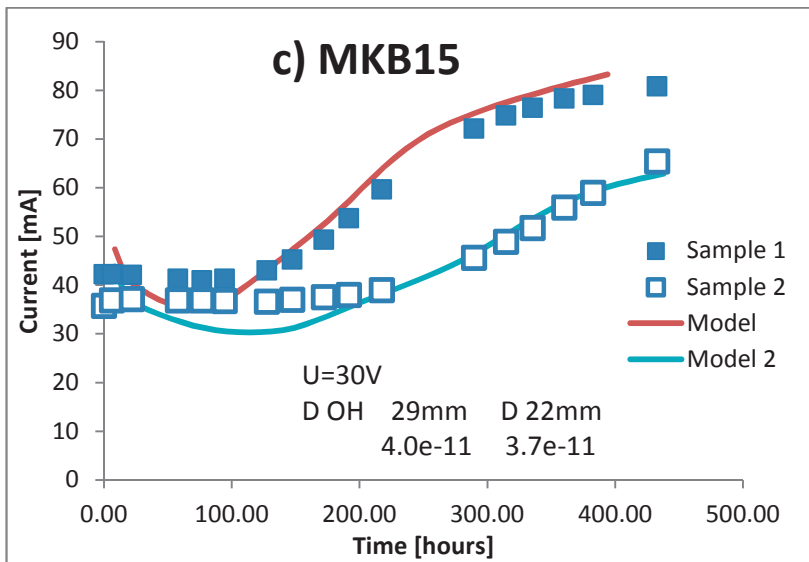
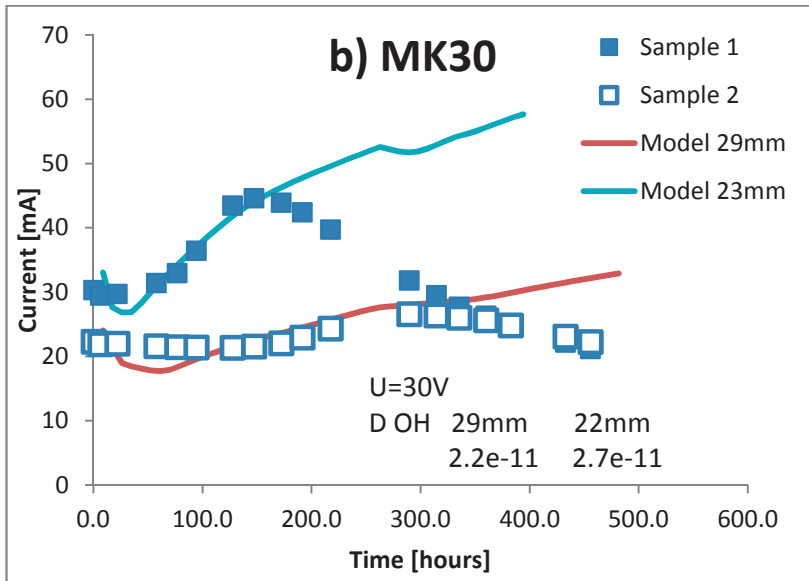
In Figures 7.33 the best fits obtained with Stadium modelling are given with the experimental current values measured during the migration test for all these samples.

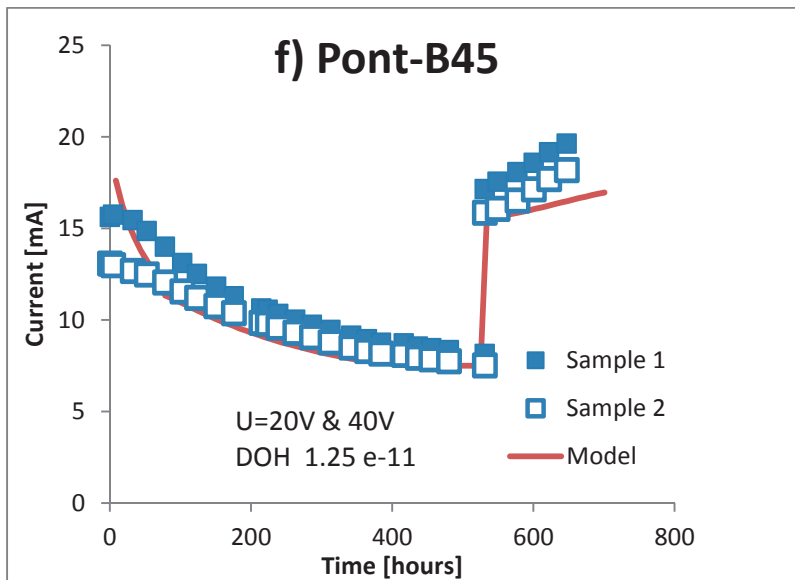
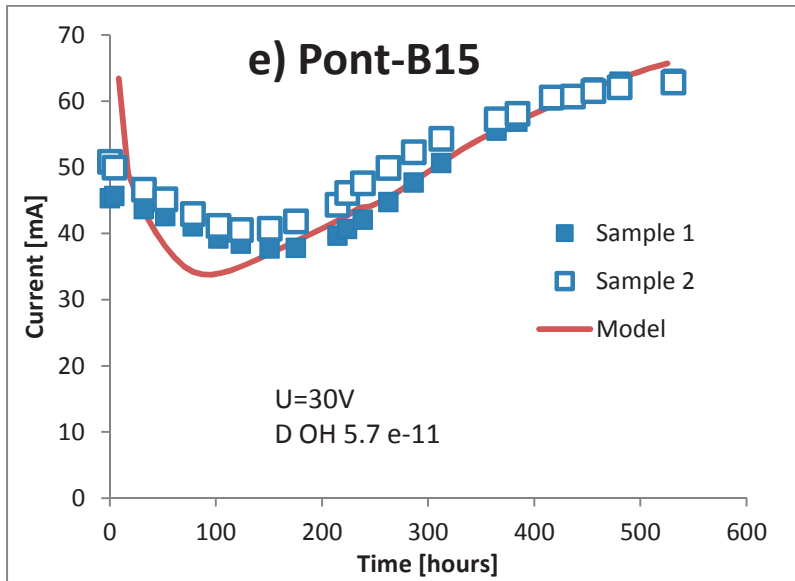
Blends with co-substitution and 45% replacement have the lowest diffusion coefficient, followed by MK30, about 3 times higher. Blends with only 15% substitution present a diffusion coefficient about 4 times higher than B45. PC3 has the highest diffusion coefficient, about 10 times higher than B45. Blends with Pontezuela clay shows diffusion coefficient less than 2 times higher than equivalent blends with pure metakaolin, and remain significantly better than PC2.

It can be observed that for samples with identical thickness the reproducibility and one single D_{OH} value allow to model the current values with good accuracy. But when the two thicknesses for a single sample were different, it was harder to model them with one identical D_{OH} and their values differ from about 10% (case of MKB15 and of MK30, the D_{OH} values are reported on the figure). For such low thicknesses it can be related to presence of bigger pores and inhomogeneity.

The first hours of current evolution are sometimes difficult to capture with the model, it is not necessarily very critical and can be related to partial drying and not totally saturated samples during the sample preparation.







Figures 7.33: Current values in mA obtained by migration test and given as a function of time in hours. Best fit obtained with the corresponding D_{OH^-} value calculated for each composition are also given for each composition studied in this serie

7.7.3. SERIES 2, 110D

Migration tests were also made with the same materials cured for 110days. The current and the best fit obtained are given in the Annex (Figure 10.12). The summary of the results obtained are given in Table 7.4

Table 7.4: Summary of properties of the different mixtures, Serie 2 at 110days

Serie 2, 110days	Porosity (%)	Initial pore solution composition [mmol/L]						τ [10 ⁻³]	D_{OH^-} [10 ⁻¹¹ m ² /s]
		Na ⁺	K ⁺	Ca ²⁺	Al(OH) ₄ ⁻	SO ₄ ²⁻	OH ⁻ *		
PC3	16%	138.1	291.6	1.1	0.2	5.5	318.5	15.2	8.0
MKB15	19%	60.9	219.9	1.0	0.5	2.2	263	6.3	3.3
MK30	20%	35.5	47.2	0.8	1.6	1.7	76.7	3.8	2.0
MKB45	20%	27.2	42.2	1.3	1.9	0.9	64.3	0.8	0.4
PontB15	18%	*						9.5	5.0
PontB45	21%	*						1.7	0.9

* Initial pore solution values at 28 days were used to estimate τ and D_{OH^-} values.

7.8. DISCUSSION

7.8.1. PHASE ASSEMBLAGE CALCULATIONS

As the materials and the initial phase assemblage were new and their law of interaction with chloride not defined in STADIUM, it was necessary for us to proceed by progressive improvement of the fit of current data.

Porosity values, hydroxyls concentration were allowed to vary by +/- 5% to improve the fit.

A first simulation of the phase assemblage was automatically given by StadiumLab (the detailed explanations can be found in reference [180] and phases amount were progressively modified in order to improve the fit.

Finally the best fits were obtained using the phase assemblage given on the right in Table 7.5. The phase assemblages obtained by Rietveld refinement are given in the same table on the left for comparison. It is very positive to see that despite the elementary description of the chloride interaction in the cementitious matrix that was postulated it was possible to obtain reasonable fit of the current during the migration test using a phase assemblage close to reality.

Table 7.5: Comparison of phase assemblage obtained by Rietveld and used as input for the best fit of current in migration test, 28 days

	Rietveld				Stadium input for best fit			
	OPC	B15	B45	MK 30	OPC	B15	B45	MK 30
Portlandite	43	20	1	2	70	50	30(*)	40(*)
CSH	148	145	120	151	108	108	100	100
Ettringite	7	9	11	4	10	15	15	15
Hemicarboaluminate	9	24	8	2	0	15	15	0
Monocarboaluminate	2	2	2	1	0	0	0	0
Monosulfate	5	0	0	6	10	0	0	0
Straetlingite	0	0	4	20	0	0	5	20
C4FH13	0	0	0	0	2	0	0	0

(*)Portlandite content derived from Stadium definition of C-S-H

Note that it wasn't possible to simultaneously use hemicarboaluminate and monocarboaluminate in Stadium, the modelling systematically crashed, it was therefore decided to systematically replace monocarboaluminate by hemicarboaluminate since it was the phase present in higher quantities in all cases. (*) Also, Stadium considers C-S-H as a mixture of a C-S-H with defined composition together with portlandite, according to a C-S-H model from Berner [180, 181]. This model considers that C-S-H with $1 < Ca/Si < 2.5$ is described by a mixture of $Ca(OH)_2$ and CaH_2SiO_4 are selected to describe the solubility behaviour of C-S-H-gel, with CaH_2SiO_4 having a fixed solubility product ($\log K = -8.16$). In Stadium C-S-H has a fix Ca/Si ratio at 1.65 and corresponding $Ca(OH)_2/CaH_2SiO_4$ ratio equals 0.26. This explains why Portlandite appears in so high amount in the input data for MK30 and MKB45.

The effect of the main parameter affecting the fit is briefly discussed in the annex (10.3.2)

7.8.2. EFFECT OF BLENDING AND CURING TIME

The coefficients of diffusion determined at 28 and 110 days are given in Table 7.6:

Table 7.6: Summary of D_{OH} coefficients estimated with Stadium after migration tests.

DOH [10 ⁻¹¹ m ² /s]	Curing time [days]	PC2	MK30	MKB15	MKB45	PONT-B15	PONT-B45
	28	7.8	2.5	3.9	0.8	5.7	1.3
	110	8.0	2.0	3.3	0.4	5.0	0.9

Diffusion coefficients all decrease with longer curing time. The ranking obtained at 28 days remains the same after 110d of curing.

The effect of curing is interestingly much more pronounced in the blends with high substitution than in PC or B15 blends. This may not have been expected considering the fast kinetics of reaction of calcined clays and the low content of portlandite remaining to feed the pozzolanic reaction.

7.8.3. COMPARISON WITH FORMATION FACTOR

Snyder et al. estimated the ionic diffusion by calculating the formation factor [182-184]. The formation factor is defined as the ratio of the pore solution electrical conductivity to the bulk (solid and pore solution) conductivity (the inverse of the τ coefficient calculated by Stadium).

They described a method to estimate pore solution conductivity from the concentration of alkali and hydroxyls ions in the pore solution while bulk conductivity is calculated from the initial resistivity measured in the migration test (described more in detail in annex in Section 0).

The formation factor and D_{OH} calculated by this alternative method are given in Figure 7.34 and Table 7.7. The results are globally in accordance with the results obtained by our modelling and confirm results obtained with Stadium.

The calculation of diffusion coefficients by the formation factor method tends to overestimate the D_{OH} in comparison with Stadium probably because it does not take into account chloride binding. However for blends with 15% substitution the opposite is the case.

Table 7.7: Summary of initial resistivity values, formation factor and D_{OH} calculated by formation factor method during migration tests:

	Curing time [days]	OPC	MK30	MKB15	MKB45	PONT-B15	PONT-B45
Initial Resistivity [$\Omega.m$]	28	38	327	222	752	102	350
	110	40	796	172	1628	130	886
Formation factor [-]	28	426	579	2221	1497	675	787
	110	345	1456	101	2529		
D_{OH} by formation factor [$10^{-11} m^2/s$]	28	7.2	4.5	1.2	1.6	3.9	3.2
	110	9.4	1.8	2.8	1.0		

It is worth mentioning that the formation factor decreased with longer curing in OPC and MKB15 while it considerably increased for MK30 and MKB45. It is explained by the reduction of the ionic concentrations in pore solution for OPC and MKB15 (see Table 7.3 & Table 7.4) at 110 days compared to 28 days, while current measured remains almost the same, in opposition to MK30 and MKB45 where current further decreased with curing. While the decrease for MKB15 can be explained by the on-going pozzolanic reaction, for PC it is likely to be an error since pore solution should not vary unless leaching takes place.

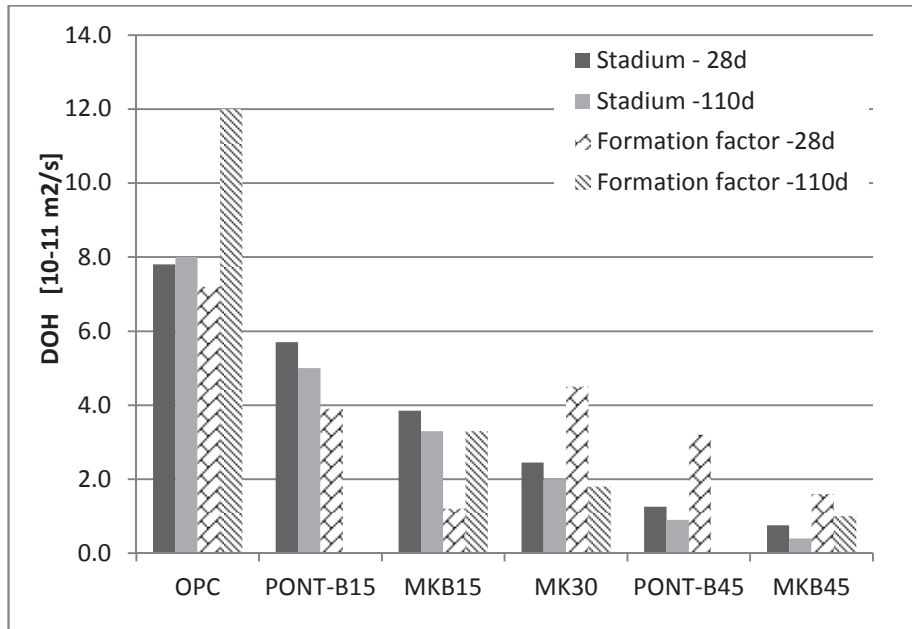


Figure 7.34: Comparison of Diffusion Coefficient obtained with Stadium and Formation factor calculations at 28 and 110 days.

7.9. CONCLUSIONS AND OUTLOOK

It has been established in this chapter that combined addition of calcined clays and limestone considerably reduce chloride ingress.

We have observed that chloride penetration after 2 years ponding was systematically and considerably decreased with increasing content of blends of calcined clays and limestone. This improvement has been observed with pure metakaolin but also with Pontezuela clay with around 50% kaolinite content. B45 blends had also the lowest chloride penetration compared with MK30, B15 or PC in two distinct conditions: a long term ponding experiment without renewal of solution and a 3 months ponding experiment with solution renewal.

These results were confirmed with two different cements and different clays with lower kaolinite content and show promising robustness of chloride resistance of blends with simultaneous addition of calcined clays and limestone.

This excellent resistance to chloride penetration cannot be explained by a reduction in total porosity, since total porosity estimated from drying is smaller for PC than for blends. It is however certainly related to its finer porosity, already observed by MIP (Figure 4.11).

The study of the phase assemblage by XRD for the different cementitious systems after 2 years ponding has been carried out. The total chloride content correlated very well with the presence of chloride bearing phases detected by XRD but also the EDS measurements obtained by SEM and confirms the measurements.

In Portland cement, Friedel's salt formed uniformly throughout the depth, confirming total chloride level measured. In blends containing simultaneous addition of calcined clays and limestone, hydrocalumite and Friedel salt were systematically present. The amount of Friedel's salt decreased systematically as the total chloride content decreased. The position of the hydrocalumite peak changed position due to the progressive change from Cl rich solid solution to CO_3^{2-} dominated solid solution.

The total chloride binding capacity was maintained with increasing substitution up to 30%, above which it was reduced. The level of chloride incorporation in the C-A-S-H, observed by SEM point counting appears to remain stable in the 2 years ponding samples, independently from the Ca/Si ratio. It is possible that the reduction of chloride physically adsorbed on the C-A-S-H (C-A-S-H amount is reduced by dilution of PC content, despite the extra C-A-S-H formed by pozzolanic reaction) is compensated by the chloride chemical binding into Friedel's salt and hydrocalumite. It should be further investigated. More generally quantification of the chloride physically bound in the C-A-S-H, also taking in account the effect of pH and counter-ions nature and the thermodynamics underlying these phenomena as well as associated adsorption processes need to be studied more in detail in the future. U-phase formation should also be reinvestigated.

The results of chloride binding isotherm have demonstrated that B15 has the best chemical binding capacity, above PC, MK30 and B45 had the lowest.

The migration test protocol from Stadium was applied to these materials. As the model did not include phases containing carbonate; carboaluminates were added and their conversion to Friedel's salt by ionic exchange included in the model. Coefficient of diffusion could be calculated by modelling and the ranking among the samples is in accordance with results obtained by ponding: B45 samples that have shown the best resistance to chloride penetration also have the lowest diffusion coefficient. MK30 also demonstrated excellent behaviour but with slightly higher diffusion coefficient. Calculation of the diffusion coefficient by an alternative method confirmed the results obtained with Stadium.

This confirms that replacement of high quantity of cement by calcined clays refines considerably the pore structure, resulting in decreased chloride diffusion coefficient. In addition, the further replacement of cement by limestone powder doesn't seem to change this fineness of pore structure, but seems to improve the tortuosity of the system, giving its outstanding chloride resistance to these blends.

These first results show promising chloride resistance of blends containing high amount of calcined clays and limestone that should be further investigated. It is not yet clear how the ternary blending shows improved tortuosity compared with blends with calcined clays alone. Also, the effect of alkalinity should be better studied, since it affects considerably thermodynamic equilibrium and phase's solubility.

The incorporation of carbonate and carboaluminates AFm into Stadium seems to deliver meaningful results. Yet it was a basic first step and should be further improved. Hydrocalumite could be included and the constant of equilibrium of ionic exchange for each pure phase should be determined by kinetic investigation. It should also be looked with more attention to chloride interaction of strätlingite which is still poorly understood. It seems to have different kinetics and probably strätlingite has lower solubility in high chloride concentration. The changes of porosity and total solid volume should also be better taken into account in order to improve the fit.

Chapter 8 : CONCLUSIONS AND OUTLOOK

8.1. CONCLUSIONS

- The thesis has demonstrated the viability of a new cementitious material with up to 60% of clinker replaced by a combination of calcined clay and limestone.
- One of the key advantages of this ternary blend is its significantly improved strength at 7d (and to a lesser extent at 28 days) compared to other blends with equivalent high volume pozzolanic addition. From the characterization of the phase assemblage, this improvement can be related to formation of high amount of carboaluminates phases. The experimentally determined phase assemblage is consistent with thermodynamic simulation.
- The key parameters that can affect the strength development have been investigated. An alkali content of around 0.8 wt% $\text{Na}_2\text{O}_{\text{eq}}$ is needed to optimize the strength development. In addition, sulfate adjustment is also critical and can considerably improve early age (1day) strength without any detrimental consequence on later age strength.
- The thesis also gives promising insights on the possibility of producing reactive materials with low or average grade clayey soil. Various natural and model clay systems have been investigated, the most crucial parameter affecting the final strength of the product is the kaolinite content. The synergetic formation of carboaluminates was not modified by the reduction of the kaolinite content in the calcined clays. It opens the possibility to use low cost calcined clays that can impact the availability and cost of manufacture of supplementary cementitious materials, especially in developing countries.

- The resistance to carbonation has been characterized. With the absence of portlandite and their lower carbonatable content, the early results tend to demonstrate that the ternary blends have to some extent lower carbonation resistance than Portland cement. But performance in natural carbonation condition is still good. The carbonated pore structures don't seem significantly different in blends or in PC, though there is evidence of pore structure coarsening of blended systems. Longer term carbonation measurements are required to validate these results.
- The Rietveld analyses carried out on pastes in accelerated and normal carbonation conditions underline that accelerated carbonation not only accelerates but also modifies the phases forming by carbonation. Aragonite precipitation seems to be favoured by the accelerated conditions in the blends, creating extra pore volume considering the 8% difference in density between the calcium carbonate polymorphs.
- The investigation of the chloride resistance has demonstrated outstanding resistance of ternary blends against chloride penetration. After two years ponding the B45 blends had the lowest chloride penetration depth, better than blends with only calcined clays and considerably better than PC. Chloride penetration depth clearly increased when substitution level was decreased. The Stadium® modelling tool was adapted to our blend with reasonable accuracy by implementing the formation of Friedel salt by ionic exchange with the hemicarboaluminate phase and strätlingite. It allowed the calculation of the tortuosity factor and the ionic diffusion coefficient. For 28 days samples, B45 calculated hydroxyls diffusion coefficient (D_{OH^-}) was about 3 times lower than D_{OH^-} of MK30 and more than 10 times lower than PC, that correlate well with ponding results. B45 blends with Pontezuela clay containing about 50% kaolinite demonstrated also high chloride resistance, only slightly lower than B45 with pure metakaolin. Chloride binding isotherm results indicate that binding is lower in B45 blends than in PC, B15 or MK30 and tend to demonstrate that the high chloride resistance of B45 blends is really related with an especially high tortuosity and/or low pore connectivity of its microstructure.

- The resulting ternary blend cement can be used for various purposes and can potentially represent an economically and environmentally attractive alternative to Ordinary Portland cement. Considering the high replacement rate achieved, the new blended cement can potentially significantly lower CO₂ emissions compared to PC currently in production. During the summer of 2013 the Cuban cement industry has already begun to implement the production of the new blend. An industrial trial has been carried out with positive perspectives to commercialize the products.

8.2. OUTLOOK:

This thesis has dealt with some critical aspects of the novel ternary blends of cement with calcined clays and limestone. It has been demonstrated that very interesting strengths can be obtained at early age, even with average kaolinite content. Also, improved chloride resistance has been observed and carbonation resistance comparable to other blended cements. This work also opened several questions that should be investigated more in detail in the future:

- With the aim to spread ternary blends of cement-calcined clays and limestone, natural calcined clays deposits with average kaolinite content will be the materials of choice. The kaolinite content required to obtain strength equivalent to Portland cement seems to be above about 50%. But each clay deposit is unique and the other companion clays can also bring their contribution. This highlights the need for some quick pozzolanic test that can be related to strength. Also, cement composition, and especially limestone, alkali and sulfate content can largely influence the compressive strengths. This should always be kept in mind in the purpose of establishing a benchmark among different clays. A standard Portland cement with adequate composition, exempt of limestone and with sufficient alkali should be chosen and carefully stocked.
- It was difficult to estimate the degree of reaction of metakaolin in blended cements. If such a measurement could be provided, by MAS NMR for example it would considerably help to differentiate the filler and the pozzolanic contribution and would serve as input for more precise thermodynamic simulation of phase assemblage and therefore of porosity evolution.

- The properties of concretes made with these blends in the fresh state were not included in the scope of the thesis. They are however of critical importance for these blends. Superplasticizers were required during this work to obtain satisfactory flowability for casting. First insights into the subject have shown that Polycarboxylate type water admixture give the best performance. This topic will have to be tackled in the future to find practical solutions at reasonable cost, although the several examples (currently in Brazil, France or previously India, dams)) of use of calcined clays have already demonstrated their feasibility.
- Also, and in direct connection to our work, a first industrial trial has been carried out during summer 2013 and 130 Tons of B45 blends with Pontezuela clay were produced. Particular care has been taken during intergrinding in order to keep Blaine surface below 4000 cm²/g and this was shown to be sufficient to produce mortars with similar rheology (tested with minicone) as conventional zeolite blended cement commercially produced in Cuba without any admixture (for a water/binder ratio of 0.5). It is a very important result, showing that optimization of grinding processes and control of particle size distribution of each mineral component is one of the key issues in order to industrially produce ternary blends with calcined clays and limestone. There is still important work to be done regarding the optimization of the calcination process, both in term of reactivity of the calcined clay and its energetic efficiency. Finally, the CO₂ emissions associated with the processing and the use of calcined clays should be investigated and coupled with a global life cycle assessment.
- Another important theoretical issue that has not been covered in this work is the packing density. It has been demonstrated that in B45 blends, both calcined clays and limestone mostly play a filler role and only partially react. Still they bring exceptional contribution both to the compressive strength and durability issues. It is very likely that fineness and particle size distribution of the different materials taking part to hydration can be optimized. Such a work should be carried out in order to optimize the mix design, further minimize the cement content and contribute to improve fresh state flowability.

- It has been demonstrated that the phase assemblage optimisation for blends of cement, calcined clays and limestone requires a precise sulfatation that help to maximise ettringite and carboaluminates content within the $\text{CaSO}_4\text{-CaCO}_3\text{-C}_3\text{A}$ as well as the early age strength. Additionally the effect of alkalinity on the development of compressive strength has been established. The possibility to carefully control sulfatation with alkali sulfate should be considered. Also, there is the possibility to introduce quaternary blends where fly ashes or slags could be added to PC with metakaolin and limestone. This could allow optimisation of the synergetic reaction between alumina and carbonates/sulfate, and the later age strength and improved flowability with fly ash.
- The investigation of carbonation has given some first insights of the carbonation mechanisms in accelerated and natural carbonation of our ternary blends. There are crucial differences between accelerated and natural carbonation on one hand and Portland cement and blended cement on the other hand that need to be confirmed.

The investigation of the carbonation of the ternary blends cement-calcined clays-limestone requires much longer term experience to assess with more substantial evidence how the significant changes of the cementitious matrix with a significantly finer porosity but a considerably lower carbonatable content. This will also help to validate new short term and accelerated carbonation experiments that are required.

- Ternary blends of cement with calcined clays and limestone have demonstrated excellent chloride resistance. A semi-quantitative approach has been used in order to characterize the chloride chemical chloride binding. Both polymorphs of Friedel salt and hydrocalumite could be implemented in order to refine this approach. It would also considerably improve the approach if physical binding with C-A-S-H could also be included.

In addition, strätlingite partial conversion to Friedel salt and simultaneous persistence at high sodium chloride concentration has been demonstrated. It would be helpful to synthesize pure strätlingite in order to characterize its chloride binding isotherm separately and study strätlingite-chloride interactions more carefully.

The interaction of C-A-S-H gel with chloride and sodium should also be investigated more in detail both on a more theoretical basis with C-A-S-H synthesized phases and in real paste conditions. Also, there was some doubt on the eventual formation of U-phase at the extent of ettringite during chloride penetration experiment that needs to be further investigated.

- The low diffusion coefficient observed for the blends could be related to the very low ionic diffusivity due to the porosity refinement and high tortuosity. Characterization of the pore structure and pore size distribution by other methods should be considered to confirm these results and improve their characterization and understanding. In addition, the low ionic diffusion observed gives us confidence that the resistance of our blend to other durability threats related to movement of water or ions should also be good. But it remains to be investigated.
- A first approach of the implementation of the carboaluminates phases and their interactions with chloride in Stadium has been done. This work should be extended in order to validate the first modelling and can be improved. The drying set of experiment could also be included and prediction of chloride penetration could be determined to validate on site the properties found in the lab.
- Chloride penetration is reduced, but the consequences of this on the onset of corrosion need to be further investigated. For example is the threshold chloride concentration for corrosion the same? Also, impact of carbonation on chloride resistance is a delicate subject that should be evaluated.

Chapter 9 BIBLIOGRAPHY

1. Habitat, U.; Available from: <http://www.unhabitat.org>.
2. Catalogtree, P.S. *World housing shortage*. Volume: The Block, 2010 **21**.
3. Gartner, E., *Industrially interesting approaches to "low-CO₂" cements*. Cement and Concrete Research, 2004. **34**(9): p. 1489-1498.
4. Purnell, P. and L. Black, *Embodied carbon dioxide in concrete: Variation with common mix design parameters*. Cement and Concrete Research, 2012. **42**(6): p. 874-877.
5. Damtoft, J.S., et al., *Sustainable development and climate change initiatives*. Cement and Concrete Research, 2008. **38**(2): p. 115-127.
6. Locher, F.W., *Cement: Principles of Production and Use* 2006: Bau+Technik GmbH.
7. Souza, P.S.L. and D.C.C. Dal Molin, *Viability of using calcined clays, from industrial by-products, as pozzolans of high reactivity*. Cement and Concrete Research, 2005. **35**(10): p. 1993-1998.
8. Fernandez Lopez, R., *Calcined clayey soils as a potential replacement for cement in developing countries*, 2009, EPFL.
9. Salvador, S., *Production de pouzzolanes de synthèse par calcination flash de sols argileux: étude des produits et conception d'une installation*, in *INSA Mecanique* 1992, INSA Toulouse: Toulouse.
10. Salvador, S. and O. Pons, *A semi-mobile flash dryer/calciner unit to manufacture pozzolana from raw clay soils -- application to soil stabilisation*. Construction and Building Materials, 2000. **14**(2): p. 109-117.
11. Argeco. Available from: <http://www.argeco.fr/>.
12. Matschei, T., B. Lothenbach, and F.P. Glasser, *The role of calcium carbonate in cement hydration*. Cement and Concrete Research, 2007. **37**(4): p. 551-558.
13. De Weerd, K., et al., *Hydration mechanisms of ternary Portland cements containing limestone powder and fly ash*. Cement and Concrete Research, 2011. **41**(3): p. 279-291.
14. Mielenz, R.W., L; and Glantz, O., . *Effect of Calcination on Natural Pozzolans*. in *Symposium on Use of Pozzolanic Materials in Mortars and Concretes*. 1950.
15. Mielenz, R.C., K.T. Greene, and N.C. Schieltz, *Natural pozzolans for concrete*. Economic Geology, 1951. **46**(3): p. 311-328.
16. Saad, M.N., W.P. De Andrade, and V.A. Paulon, *Properties of mass concrete containing an active pozzolan made from clay*. Concrete International, 1982. **4**(07): p. 59-65.
17. Ramachandran, V.S., *Concrete Admixtures Handbook, 2nd Ed.: Properties, Science and Technology* 1996: Elsevier Science.
18. Kennedy, B.A., M. Society for Mining, and Exploration, *Surface Mining* 1990: Society for Mining, Metallurgy, and Exploration.
19. Grim, R., *Applied clay mineralogy*, ed. i.s.i.t.e. science 1962: McGraw-Hill.
20. Bergaya, F., B.K. Theng, and G. Lagaly, *Handbook of clay science*. Vol. 1. 2011: Elsevier.
21. Grim, R.E. and R.E. Grim, *Applied clay mineralogy* 1962: McGraw-Hill New York.
22. J.K. Mitchell, *Fundamentals of soil behaviour, 3rd edition* 2005: John Wiley & Sons, Inc.
23. White, C.E., et al., *What Is the Structure of Kaolinite? Reconciling Theory and Experiment*. Journal of Physical Chemistry B, 2009. **113**(19): p. 6756-6765.
24. Bish, D.L., *Rietveld refinement of the kaolinite structure at 1.5 K*. Clays and Clay Minerals, 1993. **41**(6): p. 738-744.
25. He, H., et al., *The Influence of Random Defect Density on the Thermal Stability of Kaolinites*. Journal of the American Ceramic Society, 2005. **88**(4): p. 1017-1019.

26. Mielenz, R.C., N.C. Schieltz, and M.E. KING, *Thermogravimetric analysis of clay and clay-like minerals*. Clays and Clay Minerals, 1953. **2**: p. 285-314.
27. San Nicolas, R., *Approche performantielle des bétons avec métakaolins obtenus par calcination flash*, 2011, Université Paul Sabatier-Toulouse III.
28. Sanz, J., et al., *Aluminum-27 and Silicon-29 Magic-Angle Spinning Nuclear Magnetic Resonance Study of the Kaolinite-Mullite Transformation*. Journal of the American Ceramic Society, 1988. **71**(10): p. C418-C421.
29. Fernandez, R., F. Martirena, and K.L. Scrivener, *The origin of the pozzolanic activity of calcined clay minerals: A comparison between kaolinite, illite and montmorillonite*. Cement and Concrete Research, 2011. **41**(1): p. 113-122.
30. White, C.E., et al., *Density Functional Modeling of the Local Structure of Kaolinite Subjected to Thermal Dehydroxylation*. Journal of Physical Chemistry A, 2010. **114**(14): p. 4988-4996.
31. White, C.E., et al., *Structure of kaolinite and influence of stacking faults: Reconciling theory and experiment using inelastic neutron scattering analysis*. Journal of Chemical Physics, 2013. **138**(19).
32. He, C., E. Makovicky, and B. Osbaeck, *Thermal stability and pozzolanic activity of calcined illite*. Applied Clay Science, 1995. **9**(5): p. 337-354.
33. He, C., E. Makovicky, and B. Osbaeck, *Thermal stability and pozzolanic activity of raw and calcined mixed-layer mica/smectite*. Applied Clay Science, 2000. **17**(3-4): p. 141-161.
34. He, C., E. Makovicky, and B. Osbaeck, *Thermal treatment and pozzolanic activity of sepiolite*. Applied Clay Science, 1996. **10**(5): p. 337-349.
35. He, C., E. Makovicky, and B. Osbaeck, *Thermal treatment and pozzolanic activity of Na- and Ca-montmorillonite*. Applied Clay Science, 1996. **10**(5): p. 351-368.
36. He, C., E. Makovicky, and B. Osbaeck, *Thermal stability and pozzolanic activity of calcined kaolin*. Applied Clay Science, 1994. **9**(3): p. 165-187.
37. He, C., B. Osbaeck, and E. Makovicky, *Pozzolanic reactions of six principal clay minerals: Activation, reactivity assessments and technological effects*. Cement and Concrete Research, 1995. **25**(8): p. 1691-1702.
38. Sabir, B.B., S. Wild, and J. Bai, *Metakaolin and calcined clays as pozzolans for concrete: a review*. Cement and Concrete Composites, 2001. **23**(6): p. 441-454.
39. Siddique, R. and J. Klaus, *Influence of metakaolin on the properties of mortar and concrete: A review*. Applied Clay Science, 2009. **43**(3-4): p. 392-400.
40. Bich, C., J. Ambroise, and J. Péra, *Influence of degree of dehydroxylation on the pozzolanic activity of metakaolin*. Applied Clay Science, 2009. **44**(3-4): p. 194-200.
41. Murat, M., *Hydration reaction and hardening of calcined clays and related minerals.: II. Influence of mineralogical properties of the raw-kaolinite on the reactivity of metakaolinite*. Cement and Concrete Research, 1983. **13**(4): p. 511-518.
42. Chakchouk, A., B. Samet, and T. Mnif, *Study on the potential use of Tunisian clays as pozzolanic material*. Applied Clay Science, 2006. **33**(2): p. 79-88.
43. Tironi, A., et al., *Kaolinitic calcined clays: Factors affecting its performance as pozzolans*. Construction and Building Materials, 2012. **28**(1): p. 276-281.
44. Samet, B., T. Mnif, and M. Chaabouni, *Use of a kaolinitic clay as a pozzolanic material for cements: Formulation of blended cement*. Cement & Concrete Composites, 2007. **29**(10): p. 741-749.
45. Habert, G., et al., *Effects of the secondary minerals of the natural pozzolans on their pozzolanic activity*. Cement and Concrete Research, 2008. **38**(7): p. 963-975.
46. Salvador, S., *Pozzolanic properties of flash-calcined kaolinite: A comparative study with soak-calcined products*. Cement and Concrete Research, 1995. **25**(1): p. 102-112.

47. Cadoret, G.I., avenue de la Bourdonnais, Paris, G-75007, FR), *Method and installation for the dehydroxylation treatment of aluminium silicate*, 2004, Saint-gobain, Materiaux De Construction -SGMC S. A. S. S. A. S. (18, avenue d'Alsace, Courbevoie, F-92400, FR).
48. Taylor, H.F.W., *Cement Chemistry*1997: T. Telford.
49. Renaudin, G., et al., *Structural characterization of C-S-H and C-A-S-H samples--Part I: Long-range order investigated by Rietveld analyses*. Journal of Solid State Chemistry, 2009. **182**(12): p. 3312-3319.
50. de Silva, P.S. and F.P. Glasser, *Phase relations in the system CaO---Al₂O₃---SiO₂---H₂O relevant to metakaolin - calcium hydroxide hydration*. Cement and Concrete Research, 1993. **23**(3): p. 627-639.
51. Cabrera, J. and M.F. Rojas, *Mechanism of hydration of the metakaolin-lime-water system*. Cement and Concrete Research, 2001. **31**(2): p. 177-182.
52. Frías, M. and J. Cabrera, *Influence of MK on the reaction kinetics in MK/lime and MK-blended cement systems at 20°C*. Cement and Concrete Research, 2001. **31**(4): p. 519-527.
53. Serry, M.A., et al., *Metakaolin--lime hydration products*. Thermochemica Acta, 1984. **79**: p. 103-110.
54. García, R., et al., *Mineral phases formation on the pozzolan/lime/water system*. Applied Clay Science, 2009. **43**(3-4): p. 331-335.
55. Lothenbach, B., et al., *Influence of limestone on the hydration of Portland cements*. Cement and Concrete Research, 2008. **38**(6): p. 848-860.
56. Matschei, T. and F.P. Glasser, *The influence of limestone on cement hydration. Zum Einfluss von Kalkstein auf die Zementhydratation*, 2006. **59**(12): p. 78-86.
57. Matschei, T. and F.P. Glasser, *Temperature dependence, 0 to 40 °C, of the mineralogy of Portland cement paste in the presence of calcium carbonate*. Cement and Concrete Research, 2010. **40**(5): p. 763-777.
58. Damidot, D., et al., *Thermodynamics and cement science*. Cement and Concrete Research, 2011. **41**(7): p. 679-695.
59. Herfort, D.K., DK-9520, Skørping, DK), Damtoft, Jesper Sand (Skovtoften 10, DK-9000, Aalborg, DK),, *Portland limestone calcined clay cement*, 2010, Aalborg, Portland A/s (Rordalsvej 44, 9220 Aalborg Ost, DK).
60. Ramlochan, T. and M. Thomas, *Effect of metakaolin on external sulfate attack*. ACI Special Publication, 2000. **192**.
61. Al-Akhras, N.M., *Durability of metakaolin concrete to sulfate attack*. Cement and Concrete Research, 2006. **36**(9): p. 1727-1734.
62. Shi, C., D. Wang, and A. Behnood, *Review of Thaumaside Sulfate Attack on Cement Mortar and Concrete*. Journal of Materials in Civil Engineering, 2012. **24**(12): p. 1450-1460.
63. Skaropoulou, A., et al., *Use of mineral admixtures to improve the resistance of limestone cement concrete against thaumasite form of sulfate attack*. Cement and Concrete Composites, 2013.
64. Bellmann, F. and J. Stark, *Prevention of thaumasite formation in concrete exposed to sulphate attack*. Cement and Concrete Research, 2007. **37**(8): p. 1215-1222.
65. Bellmann, F. and J. Stark, *The role of calcium hydroxide in the formation of thaumasite*. Cement and Concrete Research, 2008. **38**(10): p. 1154-1161.
66. Chappex, T. and K.L. Scrivener, *The influence of aluminium on the dissolution of amorphous silica and its relation to alkali silica reaction*. Cement and Concrete Research, 2012. **42**(12): p. 1645-1649.
67. AFPC-AFREM. *Essai de carbonatation accélérée - methodes recommandées pour la mesure des grandeurs associées a la durabilité*. in journées techniques AFPC AFREM Durabilité des betons 1997. Toulouse.

68. Scrivener, K.L., A.K. Crumbie, and P. Laugesen, *The Interfacial Transition Zone (ITZ) Between Cement Paste and Aggregate in Concrete*. Interface Science, 2004. **12**(4): p. 411-421.
69. Jansen, D., et al., *A remastered external standard method applied to the quantification of early OPC hydration*. Cement and Concrete Research, 2011. **41**(6): p. 602-608.
70. Stutzman, P.E., *Guide for X-ray powder diffraction analysis of Portland cement and clinker* 1996: US Department of Commerce, Technology Administration, National Institute of Standards and Technology, Office of Applied Economics, Building and Fire Research Laboratory.
71. Gutteridge, W.A., *On the dissolution of the interstitial phases in Portland cement*. Cement and Concrete Research, 1979. **9**(3): p. 319-324.
72. Rinaldi, R., M. Sacerdoti, and E. Passaglia, *Straetlingite; crystal structure, chemistry, and a reexamination of its polytype vertumnite*. European Journal of Mineralogy, 1990. **2**(6): p. 841-849.
73. Renaudin, G., et al., *Structural characterization of C–S–H and C–A–S–H samples—Part I: Long-range order investigated by Rietveld analyses*. Journal of Solid State Chemistry, 2009. **182**(12): p. 3312-3319.
74. Bonaccorsi, E., S. Merlino, and A.R. Kampf, *The Crystal Structure of Tobermorite 14 Å (Plombierite), a C–S–H Phase*. Journal of the American Ceramic Society, 2005. **88**(3): p. 505-512.
75. Le Bail, A., S. Ouhenia, and D. Chateigner, *Microtwinning hypothesis for a more ordered vaterite model*. Powder Diffraction, 2011. **26**(1): p. 16-21.
76. Demichelis, R., et al., *A new structural model for disorder in vaterite from first-principles calculations*. CrystEngComm, 2012. **14**(1): p. 44-47.
77. Caspi, E., et al., *On the structure of aragonite*. Acta Crystallographica Section B: Structural Science, 2005. **61**(2): p. 129-132.
78. ASTM, *C1543 Standard Test Method for Determining the Penetration of Chloride Ion into Concrete by Ponding*. 2010.
79. Antoni, M., et al., *Cement substitution by a combination of metakaolin and limestone*. Cement and Concrete Research, 2012. **42**(12): p. 1579-1589.
80. Murat, M. and C. Comel, *Hydration reaction and hardening of calcined clays and related minerals III. Influence of calcination process of kaolinite on mechanical strengths of hardened metakaolinite*. Cement and Concrete Research, 1983. **13**(5): p. 631-637.
81. Love, C.A., I.G. Richardson, and A.R. Brough, *Composition and structure of C-S-H in white Portland cement-20% metakaolin pastes hydrated at 25 °C*. Cement and Concrete Research, 2007. **37**(2): p. 109-117.
82. Rocha, J. and J. Klinowski, *Festkörper-NMR-Untersuchungen zur Struktur und Reaktivität von Metakaolinit*. Angewandte Chemie, 1990. **102**(5): p. 539-541.
83. Coleman, N.J. and W.R. McWhinnie, *The solid state chemistry of metakaolin-blended ordinary Portland cement*. Journal of Materials Science, 2000. **35**(11): p. 2701-2710.
84. Menéndez, G., V. Bonavetti, and E.F. Irassar, *Strength development of ternary blended cement with limestone filler and blast-furnace slag*. Cement and Concrete Composites, 2003. **25**(1): p. 61-67.
85. Carrasco, M.F., et al., *Strength optimization of "tailor-made cement" with limestone filler and blast furnace slag*. Cement and Concrete Research, 2005. **35**(7): p. 1324-1331.
86. Güneyisi, E. and M. Gesoğlu, *Properties of self-compacting portland pozzolana and limestone blended cement concretes containing different replacement levels of slag*. Materials and Structures, 2011: p. 1-12.

87. Mounanga, P., et al., *Improvement of the early-age reactivity of fly ash and blast furnace slag cementitious systems using limestone filler*. Materials and Structures, 2011. **44**(2): p. 437-453.
88. Ghrici, M., S. Kenai, and M. Said-Mansour, *Mechanical properties and durability of mortar and concrete containing natural pozzolana and limestone blended cements*. Cement and Concrete Composites, 2007. **29**(7): p. 542-549.
89. De Weerd, K., et al., *Hydration mechanisms of ternary Portland cements containing limestone powder and fly ash*. Cement and Concrete Research. **2011**, **41**(3) P. **279-291**.
90. Moesgaard, M., et al., *Physical performances of blended cements containing calcium aluminosilicate glass powder and limestone*. Cement and Concrete Research. **2011**, **41**(3) P. **359-364**.
91. Marsh, B.K. and R.L. Day, *Pozzolanic and cementitious reactions of fly ash in blended cement pastes*. Cement and Concrete Research, 1988. **18**(2): p. 301-310.
92. Lothenbach, B., K. Scrivener, and R.D. Hooton, *Supplementary cementitious materials*. Cement and Concrete Research, 2011. **41**(3): p. 217-229.
93. Beaudoin, J.J., et al., *Solvent Replacement Studies of Hydrated Portland Cement Systems: The Role of Calcium Hydroxide*. Advanced Cement Based Materials, 1998. **8**(2): p. 56-65.
94. Berodier, E.S., K. L., *unpublished results*. 2012.
95. Kulik, D. *GEMS-PSI*, available at. 2009; Available from: <http://gems.web.psi.ch>.
96. Kulik, D.A. and M. Kersten, *Aqueous Solubility Diagrams for Cementitious Waste Stabilization Systems: II, End-Member Stoichiometries of Ideal Calcium Silicate Hydrate Solid Solutions*. Journal of the American Ceramic Society, 2001. **84**(3-12): p. 3017-3026.
97. Scrivener, K., *Development of the microstructure during the hydration of Portland cement*, 1984.
98. Quennoz, A.G., E.; Scrivener, K., *Calcium silicate – calcium aluminate interactions and their influence on cement early hydration*. CCR, 2012.
99. Fischer, R. and H.J. Kuzel, *Reinvestigation of the system C 4A.nH 2O C 4A.Co 2.nH 2O*. Cement and Concrete Research, 1982. **12**(4): p. 517-526.
100. H.F.W, T., *Cement Chemistry 2nd edition*1997: Thomas Telford. p. 220.
101. Herfort, D., *Portland limestone cements 2012*: ECRA Seminar on the Hydration of Blended Cements, Düsseldorf, November 8, 2012.
102. Vance, K., et al., *Hydration and Strength Development in Ternary Portland Cement Blends Containing Limestone and Fly Ash or Metakaolin*. Cement and Concrete Composites, 2013.
103. Vizcaino L. , A.M., Alujas A.,F. Martirena, Scrivener K, *Low clinker cements made with ternary blends of calcined clay and limestone. Influence of grinding procedures on mechanical properties*. Cement & Concrete Composites, 2013, to be submitted.
104. Brindley, G.W. and M. Nakahira, *The Kaolinite-Mullite Reaction Series: II, Metakaolin*. Journal of the american ceramics society, 1959. **42**(7): p. 314-318.
105. Brindley, G.W. and M. Nakahira, *The Kaolinite-Mullite Reaction Series: I, A Survey of Outstanding Problems*. Journal of the american ceramics society, 1959. **42**(7): p. 311-314.
106. Brindley, G.W. and M. Nakahira, *The Kaolinite-Mullite Reaction Series: III, The High-Temperature Phases*. Journal of the american ceramics society, 1959. **42**(7): p. 319-324.
107. Bertolini, L., et al., *Corrosion of Steel in Concrete: Prevention, Diagnosis, Repair*2013: Wiley.
108. Richardson, M.G., *Fundamentals of durable reinforced concrete*2004: Taylor & Francis.
109. US Earth System Research Laboratory, G.M.D. *Trends in Atmospheric Carbon Dioxide*. 2013; Available from: <http://www.esrl.noaa.gov/gmd/ccgg/trends/>.
110. Verbeck, G., *Carbonation of hydrated portland cement*. Cement and Concrete, 1958: p. 17-36.

111. Groves, G.W., et al., *Progressive Changes in the Structure of Hardened C3S Cement Pastes due to Carbonation*. Journal of the American Ceramic Society, 1991. **74**(11): p. 2891-2896.
112. Thiery, M., et al., *Investigation of the carbonation front shape on cementitious materials: Effects of the chemical kinetics*. Cement and Concrete Research, 2007. **37**(7): p. 1047-1058.
113. Sugiyama, D. and T. Fujita, *A thermodynamic model of dissolution and precipitation of calcium silicate hydrates*. Cement and Concrete Research, 2006. **36**(2): p. 227-237.
114. Gabrisová, A., J. Havlica, and S. Sahu, *Stability of calcium sulphoaluminate hydrates in water solutions with various pH values*. Cement and Concrete Research, 1991. **21**(6): p. 1023-1027.
115. Jones, M., et al., *Comparison of 2 year carbonation depths of common cement concretes using the modified draft CEN test*. Materials and Structures, 2001. **34**(7): p. 396-403.
116. Dhir, R., P. Hewlett, and Y. Chan, *Near-surface characteristics of concrete: prediction of carbonation resistance*. Magazine of Concrete Research, 1989. **41**(148): p. 137-143.
117. Hobbs, D.W. *Carbonation of concrete containing pfa*. Magazine of Concrete Research, 1988. **40**, 69-78.
118. Thomas, M., *Ch. 9 Durability of Concrete, Supplementary Cementing Materials in Concrete*2013: CRC Press.
119. Ye, Q., *Influence of early age wet curing time, clinker and CaO content on the carbonation resistance of C40 ordinary concrete*, 2011. p. 1894-1900.
120. Ho, D.W.S. and R.K. Lewis, *Carbonation of concrete and its prediction*. Cement and Concrete Research, 1987. **17**(3): p. 489-504.
121. Parrott, L.J., et al., *A Review of Carbonation in Reinforced Concrete*1987: Cement & Concrete Association of Great Britain.
122. Kandasami, S., et al., *Benchmarking UK concretes using an accelerated carbonation test*. Magazine of Concrete Research, 2012. **64**(Article): p. 697-706.
123. Harrison, T.A., et al., *Effectiveness of the traditional parameters for specifying carbonation resistance*. Magazine of Concrete Research, 2012. **64**(Article): p. 487-497.
124. Harrison, T.A., et al., *Experience of using the prTS 12390-12 accelerated carbonation test to assess the relative performance of concrete*. Magazine of Concrete Research, 2012. **64**(Article): p. 737-747.
125. Knöfel, D. and G. Eßer, *Einfluß unterschiedlicher Kohlendioxidkonzentrationen auf Zementmörtel*. Werkstoffwissenschaften und Bausanierung, Teil, 1993. **3**.
126. Castellote, M., et al., *Chemical changes and phase analysis of OPC pastes carbonated at different CO₂ concentrations*. Materials and Structures/Materiaux et Constructions, 2009. **42**(4): p. 515-525.
127. Thiery, M.e.a., *Influence of carbonation on the microstructure and moisture properties of cement-based materials Case of materials prepared with fly ash*, 2011.
128. Bier, T., J. Kropp, and H. Hilsdorf. *Formation of Silica Gel During Carbonation of Cementitious Systems Containing Slag Cements*. in *Third International Conference Proceedings. Fly Ash, Silica Fume, Slag, and Natural Pozzolans in Concrete*. 1989.
129. Houst, Y.F. and F.H. Wittmann, *Retrait de carbonatation*, in *IABSE Symposium: Durability of Structures*1989, IABSE: Lisbon. p. 255-260.
130. Ogino, T., T. Suzuki, and K. Sawada, *The formation and transformation mechanism of calcium carbonate in water*. Geochimica et Cosmochimica Acta, 1987. **51**(10): p. 2757-2767.
131. Black, L., et al., *Structural Features of C–S–H(I) and Its Carbonation in Air—A Raman Spectroscopic Study. Part II: Carbonated Phases*. Journal of the American Ceramic Society, 2007. **90**(3): p. 908-917.
132. Garbev, K., et al., *Structural Features of C–S–H(I) and Its Carbonation in Air—A Raman Spectroscopic Study. Part I: Fresh Phases*. Journal of the American Ceramic Society, 2007. **90**(3): p. 900-907.

133. Šauman, Z., *Carbonization of porous concrete and its main binding components*. Cement and Concrete Research, 1971. **1**(6): p. 645-662.
134. Ikeda, Y., et al., *²⁹Si MAS NMR Study on Structural Change of Silicate Anions with Carbonation of Synthetic Tobermorite*. Journal of the Ceramic Society of Japan, 1992. **100**(1165): p. 1098-1102.
135. Goodbrake, C.J., J.F. Young, and R.L. Berger, *Reaction of hydraulic calcium silicates with carbon dioxide and water* Journal of the American Ceramic Society, 1979. **62**(9-10): p. 488-491.
136. Spanos, N. and P.G. Koutsoukos, *Kinetics of precipitation of calcium carbonate in alkaline pH at constant supersaturation. Spontaneous and seeded growth*. The Journal of Physical Chemistry B, 1998. **102**(34): p. 6679-6684.
137. Ogino, T., T. Suzuki, and K. Sawada, *The rate and mechanism of polymorphic transformation of calcium carbonate in water*. Journal of crystal growth, 1990. **100**(1): p. 159-167.
138. Borges, P.H.R., et al., *Carbonation of CH and C-S-H in composite cement pastes containing high amounts of BFS*. Cement and Concrete Research, 2010. **40**(2): p. 284-292.
139. Kobayashi, K., K. Suzuki, and Y. Uno, *Carbonation of concrete structures and decomposition of C-S-H*. Cement and Concrete Research, 1994. **24**(1): p. 55-61.
140. Kulik, D.A., *Improving the structural consistency of C-S-H solid solution thermodynamic models*. Cement and Concrete Research, 2011. **41**(5): p. 477-495.
141. Parrott, L., *Carbonation, moisture and empty pores*. Advances in Cement Research, 1991. **4**(15): p. 111-118.
142. Houst, Y.F. and F.H. Wittmann, *Depth profiles of carbonates formed during natural carbonation*. Cement and Concrete Research, 2002. **32**(12): p. 1923-1930.
143. Imai, H., et al., *Self-organized formation of porous aragonite with silicate*. Journal of crystal growth, 2002. **244**(2): p. 200-205.
144. Kotachi, A., T. Miura, and H. Imai, *Formation of Planar Aragonite-Type Carbonate Crystals Consisting of Iso-Oriented Subunits*. Crystal Growth & Design, 2004. **4**(4): p. 725-729.
145. Kitano, Y., M. Okumura, and M. Idogaki, *Behavior of dissolved silica in parent solution at the formation of calcium carbonate*. GEOCHEMICAL JOURNAL, 1979. **13**(6): p. 253-260.
146. Goodbrake, C.J., J.F. Young, and R.L. Berger, *Reaction of beta-dicalcium silicate and tricalcium silicate with carbon dioxide and water vapor*. J Am Ceram Soc, 1979. **62**(3-4): p. 168-171.
147. Bukowski, J.M. and R.L. Berger, *Reactivity and strength development of CO₂ activated non-hydraulic calcium silicates*. Cement and Concrete Research, 1979. **9**(1): p. 57-68.
148. Goto, S., et al., *Calcium silicate carbonation products*. Journal of the American Ceramic Society, 1995. **78**(11): p. 2867-2872.
149. Shtepenکو, O., et al., *The effect of carbon dioxide on β-dicalcium silicate and Portland cement*. Chemical Engineering Journal, 2006. **118**(1-2): p. 107-118.
150. A, M., *Influence des cendres volantes sur la carbonatation de matrices cimentaires à base de CEM I* in 31èmes Rencontres de l'AUGC, 2013: E.N.S. Cachan, .
151. Morales-Florez, V., N. Findling, and F. Brunet, *Changes on the nanostructure of cementitious calcium silicate hydrates (C-S-H) induced by aqueous carbonation*. Journal of Materials Science, 2011. **47**(2): p. 764-771.
152. Thiery, M., C. Cremona, and V. Baroghel-Bouny, *Application of the reliability theory to the assessment of carbonation-induced corrosion risk of rebars*. European Journal of Environmental and Civil Engineering, 2012. **16**(3-4): p. 273-287.
153. Bakker, R., *Model to calculate the rate of carbonation in concrete under different climatic conditions*, 1993: Imuiden, The Netherlands: CMIJ bv Laboratorium.
154. Rapin, J.P., et al., *Structural transition of Friedel's salt 3CaO·Al₂O₃·CaCl₂·10H₂O studied by synchrotron powder diffraction*. Cement and Concrete Research, 2002. **32**(4): p. 513-519.

155. Mesbah, A., et al., *A New Investigation of the Cl—CO₃²⁻ Substitution in AFm Phases*. Journal of the American Ceramic Society, 2011. **94**(6): p. 1901-1910.
156. Sacerdoti, M. and E. Passaglia, *Hydrocalumite from Latium, Italy: its crystal structure and relationship with related synthetic phases*. Neues Jahrbuch für Mineralogie Monatshefte, 1988(10): p. 462-475.
157. Runcevski, T., et al., *Crystal structures of calcium hemicarboaluminate and carbonated calcium hemicarboaluminate from synchrotron powder diffraction data*. Acta Crystallographica Section B, 2012. **68**(5): p. 493-500.
158. Mesbah, A., et al., *Crystal structure of Kuzel's salt 3CaO·Al₂O₃·1/2CaSO₄·1/2CaCl₂·11H₂O determined by synchrotron powder diffraction*. Cement and Concrete Research, 2011. **41**(5): p. 504-509.
159. Mesbah, A., et al., *Uptake of chloride and carbonate ions by calcium monosulfoaluminate hydrate*. Cement and Concrete Research, 2012. **42**(8): p. 1157-1165.
160. Balonis, M., et al., *Impact of chloride on the mineralogy of hydrated Portland cement systems*. Cement and Concrete Research, 2010. **40**(7): p. 1009-1022.
161. Loser, R., et al., *Chloride resistance of concrete and its binding capacity—Comparison between experimental results and thermodynamic modeling*. Cement and Concrete Composites, 2010. **32**(1): p. 34-42.
162. Nielsen, E.P., D. Herfort, and M.R. Geiker, *Binding of chloride and alkalis in Portland cement systems*. Cement and Concrete Research, 2005. **35**(1): p. 117-123.
163. Luping, T. and L.-O. Nilsson, *Chloride binding capacity and binding isotherms of OPC pastes and mortars*. Cement and Concrete Research, 1993. **23**(2): p. 247-253.
164. Thomas, M.D.A., et al., *The effect of supplementary cementitious materials on chloride binding in hardened cement paste*. Cement and Concrete Research, 2012. **42**(1): p. 1-7.
165. Zibara, H., et al., *Influence of the C/S and C/A ratios of hydration products on the chloride ion binding capacity of lime-SF and lime-MK mixtures*. Cement and Concrete Research, 2008. **38**(3): p. 422-426.
166. Saikia, N., S. Kato, and T. Kojima, *Thermogravimetric investigation on the chloride binding behaviour of MK—lime paste*. Thermochemica acta, 2006. **444**(1): p. 16-25.
167. Ipavec, A., et al., *Chloride binding into hydrated blended cements: The influence of limestone and alkalinity*. Cement and Concrete Research, 2013. **48**(0): p. 74-85.
168. ASTM, *ASTM C1202 - 12 Standard Test Method for Electrical Indication of Concrete's Ability to Resist Chloride Ion Penetration*. 2012.
169. Nordtest, *NT BUILD 492 Chloride migration coefficient from non-steady-state migration experiments 1999*, Nordtest: Finland.
170. Castellote, M. and C. Andrade, *Round-Robin test on chloride analysis in concrete—Part I: Analysis of total chloride content*. Materials and Structures, 2001. **34**(9): p. 532-549.
171. Dhir, R.K., M.R. Jones, and H.E.H. Ahmed, *Determination of total and soluble chlorides in concrete*. Cement and Concrete Research, 1990. **20**(4): p. 579-590.
172. Mesbah, A., et al., *Crystal Structures and Phase Transition of Cementitious Bi-Anionic AFm-(Cl⁻, CO₃²⁻) Compounds*. Journal of the American Ceramic Society, 2011. **94**(1): p. 261-268.
173. Scrivener, K.L., *Backscattered electron imaging of cementitious microstructures: understanding and quantification*. Cement and Concrete Composites, 2004. **26**(8): p. 935-945.
174. Li, G., P. Le Bescop, and M. Moranville-Regourd, *Synthesis of the U phase (4CaO . 0.9Al₂O₃ . 1.15O₃ . 0.5Na₂O . 16H₂O)*. Cement and Concrete Research, 1997. **27**(1): p. 7-13.
175. Li, G., P. Le Bescop, and M. Moranville, *The U phase formation in cement-based systems containing high amounts of Na₂SO₄*. Cement and Concrete Research, 1996. **26**(1): p. 27-33.

176. Dosch, W. and H. Zur Strassen, *An alkali-containing calcium aluminate sulfate hydrate*. Zement-Kalk-Gips, 1967. **20**: p. 392-401.
177. Mesbah, A., et al., *Crystal Structures and Phase Transition of Cementitious Bi-Anionic AFm-(Cl⁻, CO₃²⁻) Compounds*. Journal of the American Ceramic Society, 2010: p. no-no.
178. C642, A. *Standard Test Method for Density, Absorption, and Voids in Hardened Concrete*. 2001. ASTM Philadelphia, PA.
179. Glasser, F.P., J. Marchand, and E. Samson, *Durability of concrete — Degradation phenomena involving detrimental chemical reactions*. Cement and Concrete Research, 2008. **38**(2): p. 226-246.
180. Samson, E. and J. Marchand, *Modeling the transport of ions in unsaturated cement-based materials*. Computers & Structures, 2007. **85**(23–24): p. 1740-1756.
181. Berner, U.R., *Evolution of pore water chemistry during degradation of cement in a radioactive waste repository environment*. Waste Management, 1992. **12**(2–3): p. 201-219.
182. Samson, E., et al., *Modeling ion and fluid transport in unsaturated cement systems in isothermal conditions*. Cement and Concrete Research, 2005. **35**(1): p. 141-153.
183. Snyder, K.A., et al., *Estimating the electrical conductivity of cement paste pore solutions from OH⁻, K⁺ and Na⁺ concentrations*. Cement and Concrete Research, 2003. **33**(6): p. 793-798.
184. Snyder, K., *The relationship between the formation factor and the diffusion coefficient of porous materials saturated with concentrated electrolytes: theoretical and experimental considerations*. Concrete Science and Engineering, 2001. **3**(12): p. 216-224.
185. Samson E., M.J., Henocq P., Beausejour P. *Recent advances in the determination of ionic diffusion coefficients using migration test results in RILEM Proceedings 58 - Conmod 2008*. 2008. Delft: Schlangen & De Schutter.
186. Samson, E., et al., *Modeling chemical activity effects in strong ionic solutions*. Computational Materials Science, 1999. **15**(3): p. 285-294.
187. Xu, T., et al., *TOUGHREACT—A simulation program for non-isothermal multiphase reactive geochemical transport in variably saturated geologic media: Applications to geothermal injectivity and CO₂ geological sequestration*. Computers & Geosciences, 2006. **32**(2): p. 145-165.

Chapter 10 : ANNEXES

10.1. CHLORIDE FIGURES

Table 10.1: Total chloride content, normalized by weight of mortar.

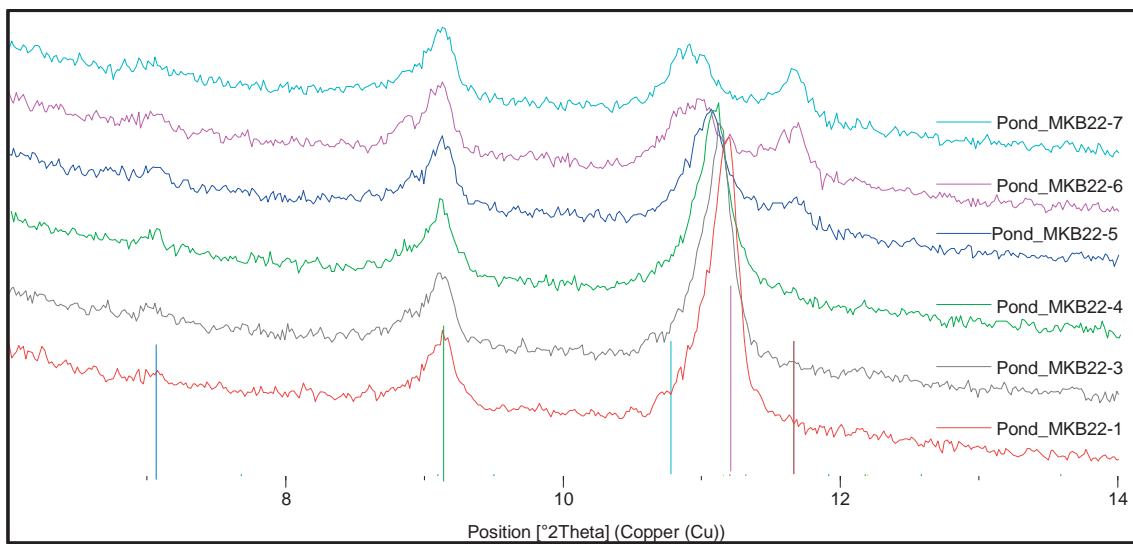
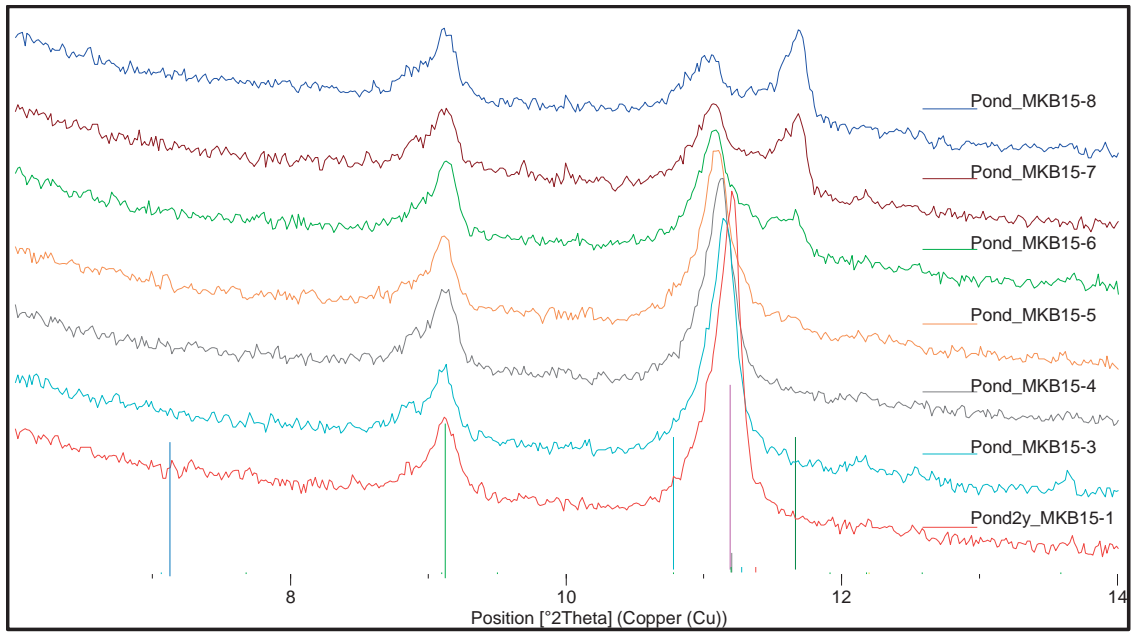
Depth [mm]	total Cl, mg/g mortar												
	OPC	MK 30	MK B15	MK B22	MK B30	MK B45	Pont 30	Pont B15	Pont B22	Pont B30	Pont B45	Ar 30	Ar B45
L1-1.25	0.46	0.53	0.71	0.69	0.58	0.31	0.82	0.49	0.71	0.77	0.51	0.70	0.44
L2-3.75	0.49	0.50	0.73	0.70	0.51	0.32	0.65				0.45	0.84	0.48
L3-6.25		0.37	0.56	0.50	0.35	0.19	0.59	0.58	0.62	0.54	0.41	0.73	0.36
L4-8.75		0.39	0.46	0.39	0.19	0.07	0.44		0.51		0.33	0.71	0.27
L5-11.25	0.35	0.24	0.32	0.25	0.16	0.03	0.34	0.33	0.39	0.37	0.26	0.50	
L6-13.75		0.17	0.30	0.19	0.17	0.02	0.30		0.22	0.31	0.16	0.60	
L7-16.25		0.13	0.24	0.17	0.16	0.02	0.23	0.23	0.16	0.27	0.02	0.42	
L8-18.75		0.09		0.17	0.16		0.19	0.20	0.13	0.21	0.02		
L9-21.25	0.36	0.07					0.16				0.03	0.29	0.01

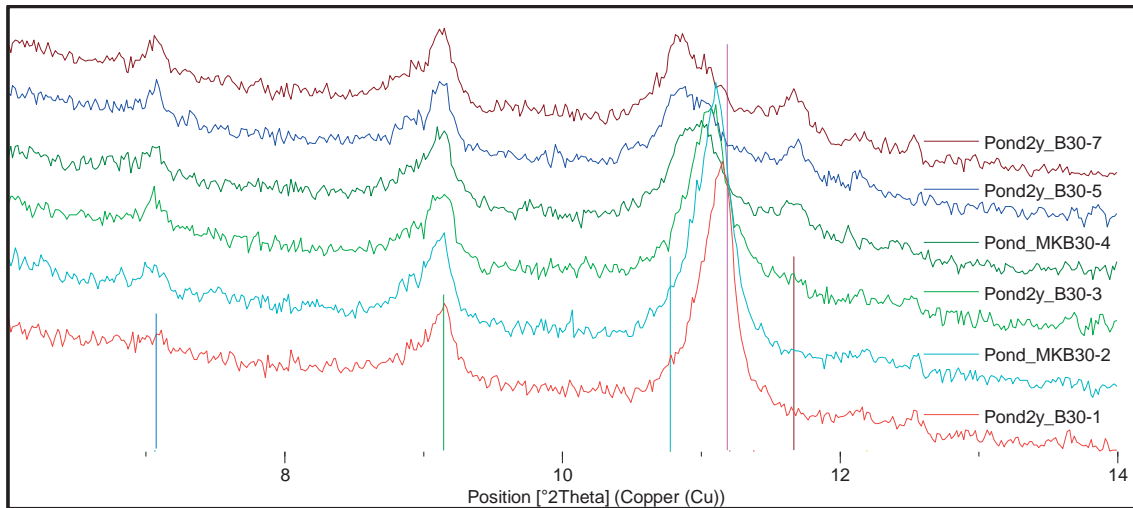
L14-33.75										0.14			
L15-36.25		0.05											
L16-38.75	0.36	0.06										0.20	0.02

Table 10.2: Total chloride content, normalized by weight of anhydrous cement present in the mortar.

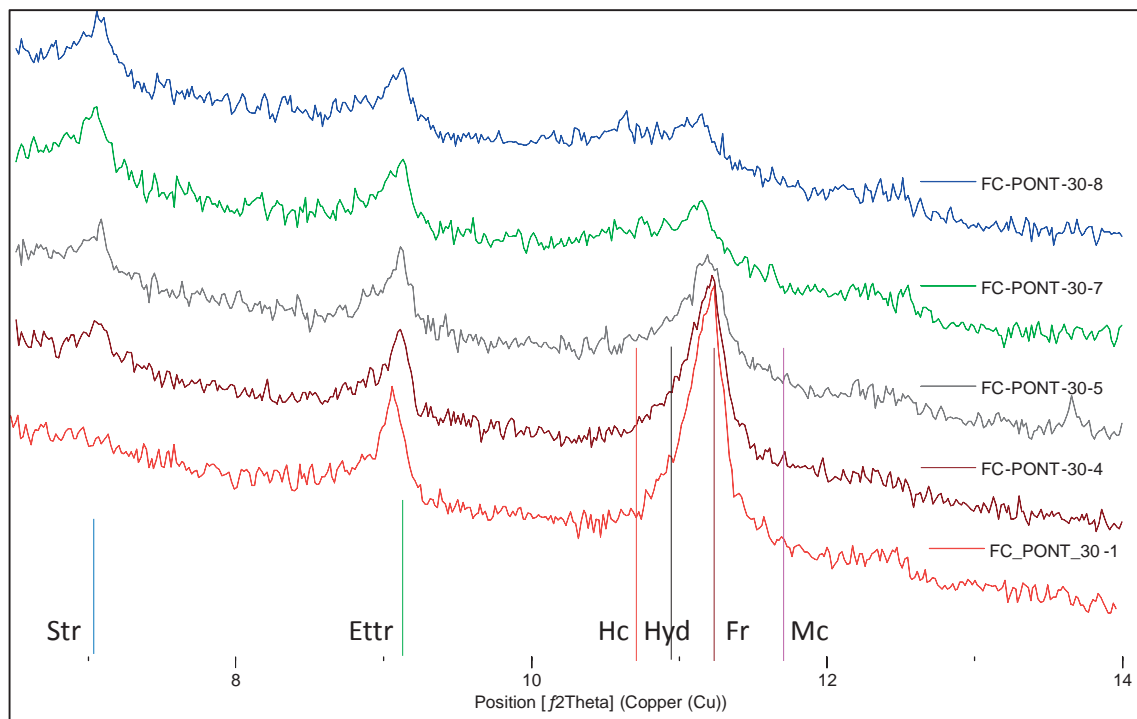
Depth [mm]	Total Cl, mg/g cement												
	PC	MK 30	MK B15	MK B22	MK B30	MK B45	Pont 30	Pont B15	Pont B22	Pont B30	Pont B45	Ar 30	Ar B45
L1-1.25	1.91	3.13	3.47	3.70	3.42	2.31	4.84	2.40	3.81	4.58	3.79	4.12	3.26
L2-3.75	2.05	2.94	3.56	3.75	3.00	2.38	3.86				3.36	4.98	3.57
L3-6.25		2.18	2.75	2.66	2.05	1.45	3.52	2.87	3.33	3.19	3.09	4.31	2.69
L4-8.75		2.30	2.28	2.08	1.10	0.53	2.62				2.49	4.20	2.05
L5-11.25	1.48	1.42	1.59	1.35	0.95	0.23	2.03	1.62	2.10	2.20	1.94	2.98	
L6-13.75		1.03	1.45	1.02	0.99	0.16	1.78		1.18	1.85	1.23	3.54	
L7-16.25		0.79	1.17	0.88	0.95	0.16	1.35	1.13	0.86	1.58	0.16	2.48	
L8-18.75		0.55		0.89	0.92		1.10	0.97	0.68	1.26	0.12		
L9-21.25	1.52	0.40					0.97				0.21	1.71	0.07

L14-33.75										0.84			
L15-36.25		0.29											
L16-38.75	1.52	0.37										1.21	0.11





Figures 10.1: X-Ray Diffractograms obtained after 2 years Ponding for MKB15, MKB22 and MKB30



Figures 10.2: X-Ray Diffractograms obtained after 2 years Ponding for Pont15 & Pont30

X-Ray Diffractograms for Pont30 show very high formation of Friedel's salt in the top layers, with decreasing intensity as we proceed to deeper layers. Strätlingite on the contrary is absent at the surface but its peak is growing with increasing depth. Ettringite seems stable throughout. It shows similar phase assemblage than MK30 but with increasing chloride binding in deeper layers.

PontB45 shows a similar phase assemblage as B45, but the relative intensity of the chloride bearing AFm phases compared with ettringite is considerably higher. Ettringite amounts stay constant over the depth. In the deepest layers, monocarboaluminate is clearly present as well as strätlingite, and this coincides with a decrease in intensity of the hydrocalumite peak. The same progressive shift observed in B45 from Friedel's salt on the surface to hydrocalumite and or hemicarboaluminate with increasing depth is seen in this sample.

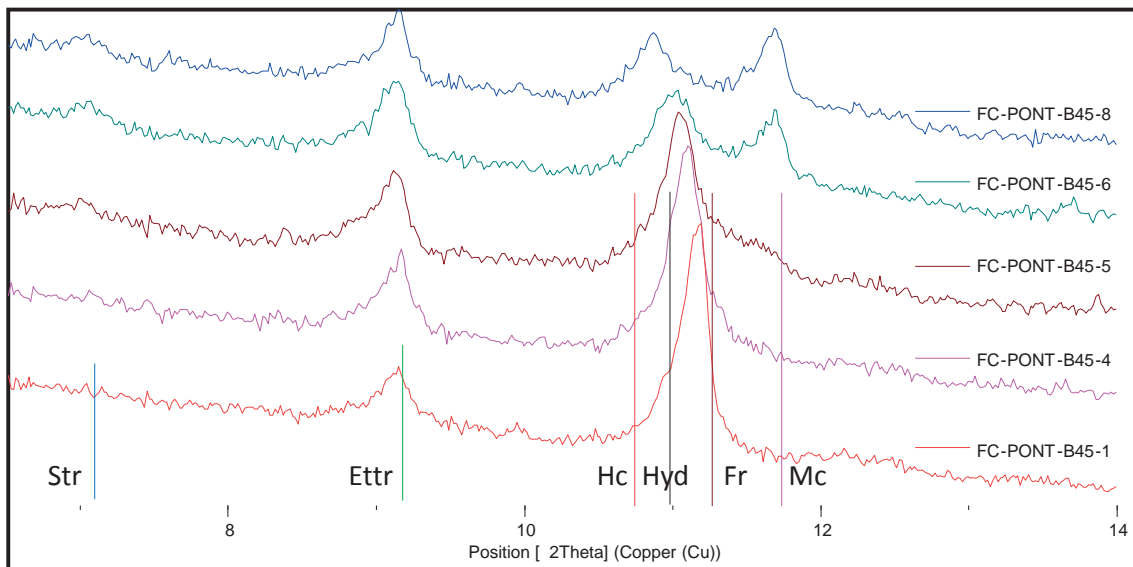
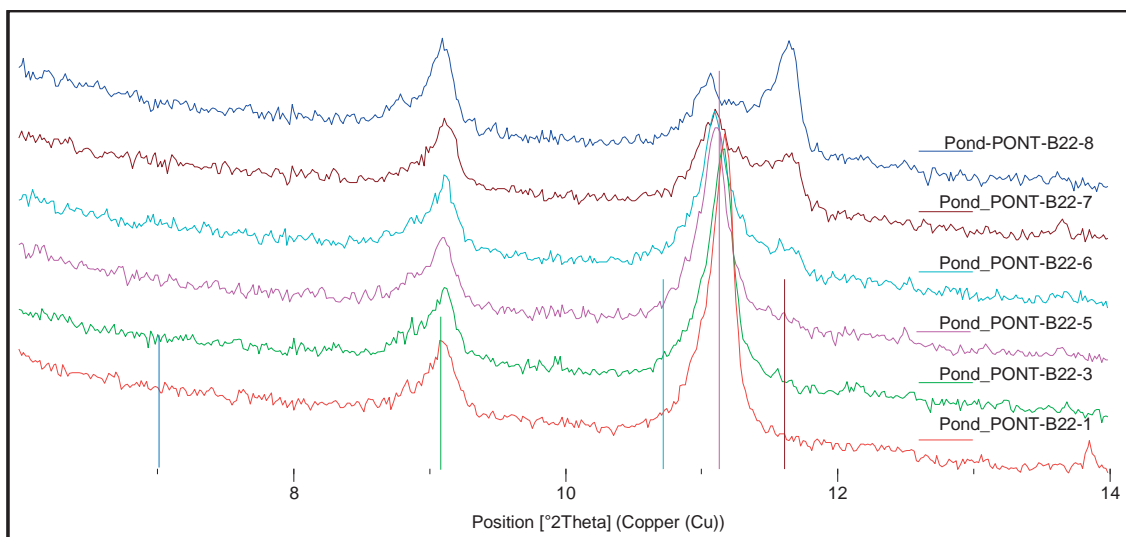
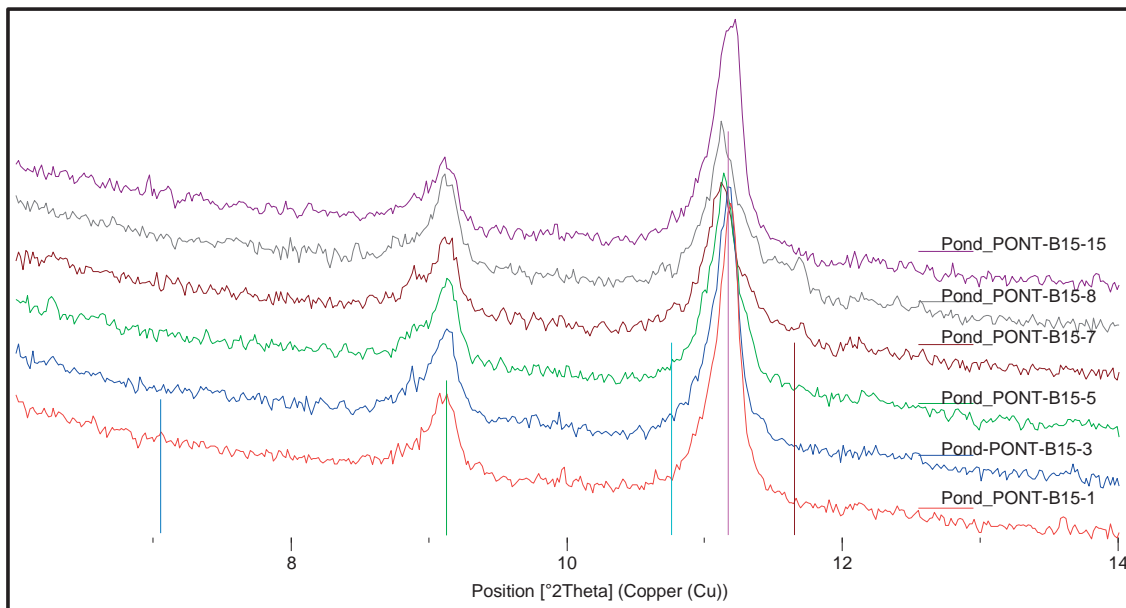
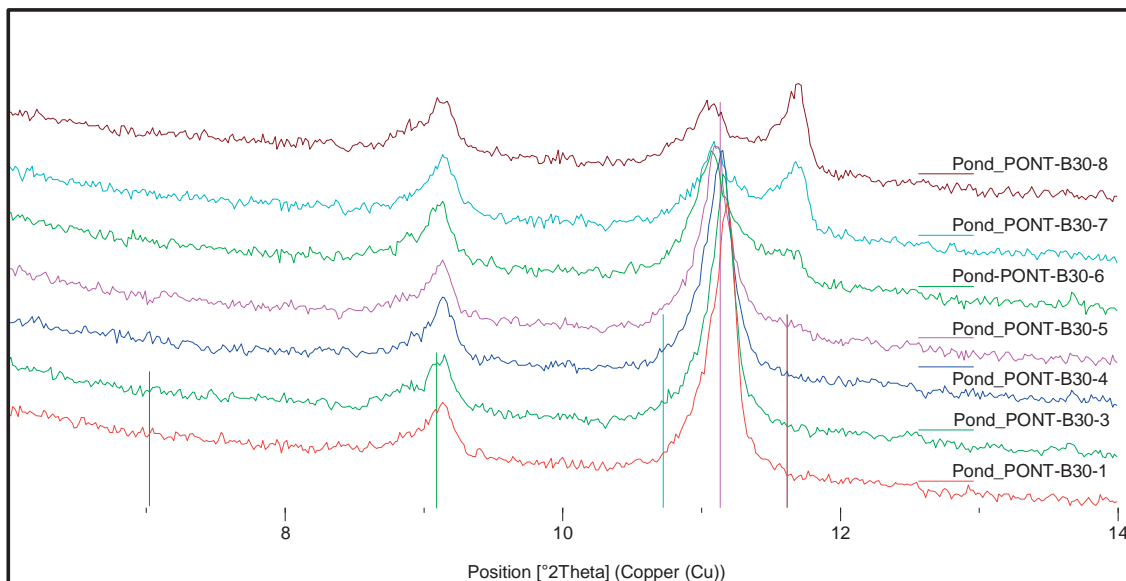


Figure 10.3: X-Ray Diffractograms obtained after 2 years Ponding for PontB45

For PontB15, the interpretation is not immediate because there was contamination from the bottom (Friedel salt peak is visible in layer 15, the real bottom). Even in the deepest layer that could be ground Friedel salt remains (though the amount is low).





Figures 10.4: X-Ray Diffractograms obtained after 2 years ponding for PontB15, PontB22 and PontB30

Ar30 contains 30% of calcined clay with only 40% kaolinite content. It shows almost constant phase assemblage in the 4 first layers with only Friedel salt in significant amount and some ettringite present (Figure 10.5). In the deeper layer, the intensity of Friedel salt seems to decrease and is intermixed with hydrocalumite, but both peaks are merged. No strätlingite is noticeable in any layer.

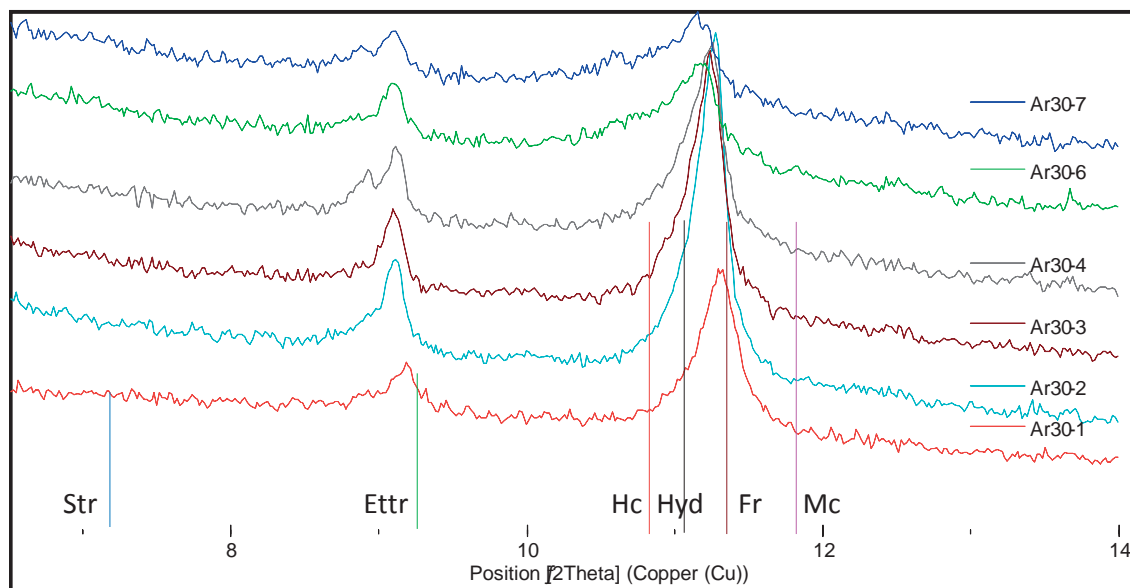


Figure 10.5: X-Ray Diffractograms obtained after 2 years Ponding for Ar30

Finally ArB45 (Figure 10.6) shows a phase assemblage similar to that of PontB45 (see Figure 10.3). The two deeper layers containing some hydrocalumite and also monocarboaluminate but no strätlingite. Peak intensity for Friedel salt is very high in the first surface layers in ArB45, correlating well with the high total chloride level found.

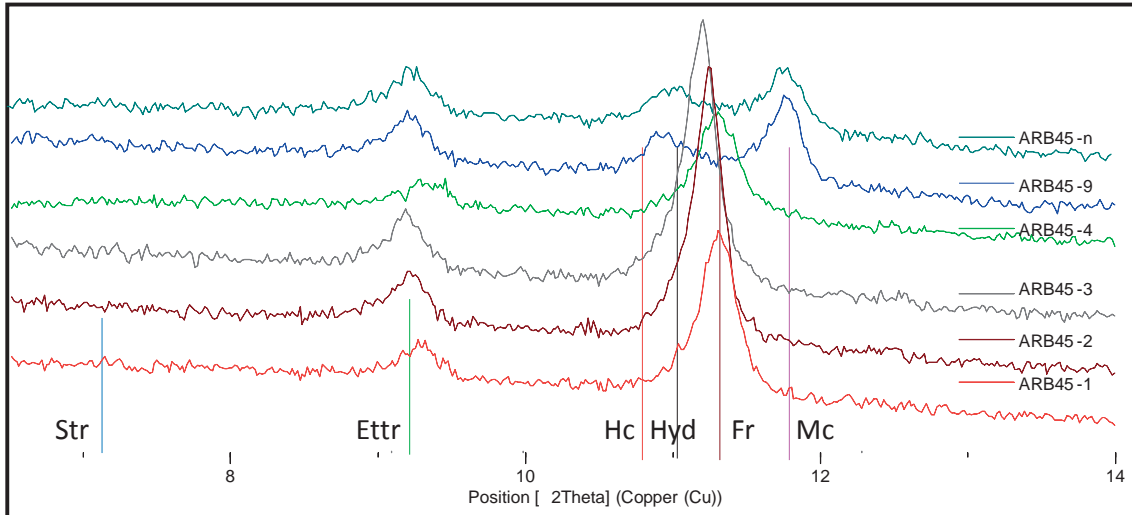


Figure 10.6: X-Ray Diffractograms obtained after 2 years Ponding for ArB45

10.2. FORMATION FACTOR, SNYDER

The formation factor Υ is defined as the ratio of the pore solution electrical conductivity σ_p to the bulk (solid and pore solution) conductivity σ_b (Equation 10-1):

$$\Upsilon = \frac{\sigma_p}{\sigma_b} \quad \text{Equation 10-1}$$

$$\sigma_b \text{ can be approximated to be } \sigma_b = \frac{U}{i} \cdot \frac{r^2}{l} \quad \text{Equation 10-2}$$

where U & i and the initial voltage at the electrodes and the current at the surface of the sample measured on the migration test respectively, while r and l are the radius and the thickness of the sample respectively.

For the calculation of the pore solution electrical conductivity σ_p , the contribution of each ionic specie has to be taken in account, in Equation 10-3:

$$\sigma_{p,calc} = \sum_i z_i c_i \lambda_i, \quad \text{Equation 10-3}$$

z is the valence of ion I, c its concentration and λ its equivalent ionic conductivity.

The equivalent ionic conductivity in high ionic strength solution such as pore solution is described with the following Equation 10-4 & 10-5:

$$\lambda_i = \frac{\lambda_i^0}{1 + G_i I_M^{1/2}} \quad \text{with} \quad I_M = \sum_i z_i^2 c_i \quad \text{Equation 10-4 \& Equation 10-5 respectively}$$

Where λ_i^0 is the equivalent conductivity of an ionic specie at infinite dilution and only function of temperature, I_M the ionic strength and the empirical coefficients G_i are chosen to best agree with published data for the electrical conductivity of solutions. In principle, the coefficient G_i will also depend upon temperature.

In pore solution of cementitious material, alkali and hydroxyls are present in much higher concentration than the other species and the bulk conductivity is calculated only considering Na^+ , K^+ and OH^- (SO_4^{2-} is the ionic specie with the next highest concentration and account for less than 2%, it can be neglected considering the variation on the pore solution measurement is around 5%).

Species	$z\lambda^0$ ($\text{cm}^2 \text{ S/mol}$)	G (mol/l) ^{-1/2}
OH^-	198	0.353
K^+	73.5	0.548
Na^+	50.1	0.733
Cl^-	76.4	0.548
Ca^{2+}	59	0.771
SO_4^{2-}	79	0.877

Finally the Diffusion coefficient can be calculated from the Formation factor by Equation 10-6:

$$D_{\text{OH}^-} = \frac{D_{\text{OH}^-}^0}{Y\phi}, \quad \text{Equation 10-6}$$

with $D_{\text{OH}^-}^0$ the diffusion coefficient in diluted solution and ϕ the water accessible porosity.

10.3. STADIUM

10.3.1. DESCRIPTION

STADIUM allows the interpretation of the results of migration tests using the Nernst-Planck-Poisson set of equation (Equation 10-9). The model allows step by step solution of the mass conservation equations for each ionic species as well as the chemical equilibrium relationships for the reactions between the pore solution and the hydrated cement paste.

The equations are first written at the microscopic scale. They are then integrated over a representative elementary volume using a homogenization technique, to yield the equations at the macroscopic scale. It allows a single coefficient τ to be determined characterizing the whole pore structure that applies to all ionic species. The coefficient is called “inversed tortuosity” and is defined in Equation 10-7:

$$\tau = \frac{D_i}{D_i^0} \quad \text{[Equation 10-7]}$$

The numerical extrapolation of the tortuosity, which is the parameter related to the refinement of the porous structure, is based on the expression of the total current as a function of the sum of the ionic flows [185], described here in Equation 10-8:

$$I = SF \sum_{i=1}^N z_i J_i \quad \text{[Equation 10-8]}$$

. Where S is the surface of the sample [m^2], z_i is the valence number of the species i , F is the Faraday constant [96488 C/mol] and J_i are the ionic fluxes [$mol/m^2/s$] described by the extended Nernst Planck equations in Equation 10-9 [180, 185]:

$$J_i = -\phi D_i \text{grad}(c_i) - \phi \frac{D_i z_i F}{RT} c_i \text{grad}(\psi) - \phi D_i c_i \text{grad}(\ln \gamma_i) \quad \text{Equation 10-9}$$

Where ϕ is the water accessible porosity (that is equivalent to the total water content because samples are saturated) [m^3/m^3], c_i is the molar concentration [mmol/l], D_i is the diffusion coefficient [m^2/s] of the species i , ψ is the electrodiffusion potential [V], R is the ideal gas constant, T is the

temperature [$^{\circ}\text{K}$], and γ_i is the activity coefficient of the specie i [-], according to a modified version of Davies equations[186].

For each ionic specie, the law of mass conservation can also be applied, Equation 10-10

$$\frac{\partial c}{\partial t} + \text{div}(J_i) = 0 \quad \text{Equation 10-10}$$

Finally both equations 10.9 and 10.10 can be merged into Equation 10-11:

$$\frac{\partial(\theta_s C_{si})}{\partial t} + \frac{\partial(wC_i)}{\partial t} - \text{div}(D_i \text{grad}(C_i)) + \frac{D_i z_i F}{RT} C_i \text{grad}(\Psi) + D_i C_i \text{grad}(\ln \gamma_i) + D_i C_i \text{grad}(\ln \gamma_i) T \text{grad}(T) - C_i V + R_i = 0$$

Equation 10-11

Note that the temperature dependency term has been included but is usually neglected because migration tests are carried out at constant temperature.

The values at 25°C of D_i^0 in diluted solutions (free water), are given here:

Table 10.3: Values at 25°C of D_i^0 in diluted solutions

OH^- :	$5.273 \times 10^{-9} \text{ m}^2/\text{s}$
Na^+ :	$1.334 \times 10^{-9} \text{ m}^2/\text{s}$
K^+ :	$1.957 \times 10^{-9} \text{ m}^2/\text{s}$
Cl^- :	$2.032 \times 10^{-9} \text{ m}^2/\text{s}$
SO_4^{2-} :	$1.065 \times 10^{-9} \text{ m}^2/\text{s}$
Ca^{2+} :	$0.792 \times 10^{-9} \text{ m}^2/\text{s}$

10.3.2. DISCUSSION

One of the limitations found with the model is the relatively poor modelling of the downstream chloride concentration (see Figure 10.7). If the onset of chloride passing through the sample is well captured, the chloride concentration was systematically overestimated.

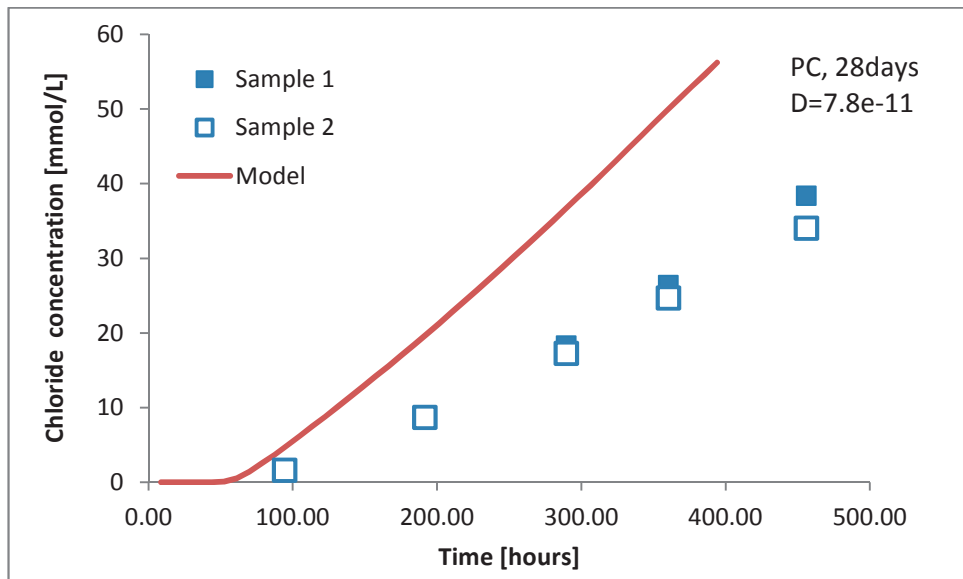


Figure 10.7: Chloride downstream concentration measured values and obtained for the model for the PC sample, 28 days old during migration test.

It could be related to the on-going chloride binding in the samples with time but also with some refinement of the microstructure with chloride binding. This latter point can be taken in account by Stadium via a module which takes in account the variation of the total solid volume, according to Equation 10-12 [187] but was not included during the modelling.

$$\tau = \frac{D_i}{D_i^0} \left(\frac{\phi}{\phi_0} \right)^3 \left(\frac{1-\phi_0}{1-\phi} \right)^2$$

Equation 10-12:

Implementation of a term for the porosity evolution to taken in account the changes of porosity and solid volume during the migration test.

With Series 2 it has indeed been observed that monosulfate and Kuzel's salt were present (during the chloride binding isotherm experiment). The release of sulfate upon conversion in Friedel's salt there can promote supplementary ettringite to precipitate. Similarly, carbonate release can also promote calcite precipitation. This latter is however less beneficial in term of volume gain.

These two last points mentioned above might explain for the large deviation between the model and the experimental points in Figures 7.33 b) for MK30. In this case, the formation of Friedel's salt by ionic exchange from strätlingite was essential in order to capture the current evolution during the migration test. But the chosen law was copied from the example of chloride interaction of

monosulfoaluminate and is visibly not accurate, since Friedel salt has been found in the various experiment only at the surface in the ponding experiment.

Overall the effect of the main parameters is briefly discussed below.

The initial pore solution composition will mostly affect the initial slope of the curve. As the voltage is imposed the chloride concentration at the upstream interface in the sample is increasing, but the hydroxyl concentration is decreasing faster because the hydroxyl ions are more mobile. In addition, at the downstream interface, 0.3 mol/L sodium ions are replacing the initial sodium and potassium concentration. But potassium ion has a greater mobility than sodium. Overall, the ionic strength at both interfaces of the sample will tend to decrease. This decrease is directly related to the total content of hydroxyls and alkali ions of the pore solution and causes the decrease of the overall conductivity and therefore directly affects the initial current reduction (see Figures 7.33). It clearly explains the difference in behaviour during the first hours between PC & B15's on one hand that show fast drop of current, while on the other hand MK30 and B45s, with much lower alkali concentration have almost no current decay. The effect of hydroxyls content is schematized in Figure 10.8.

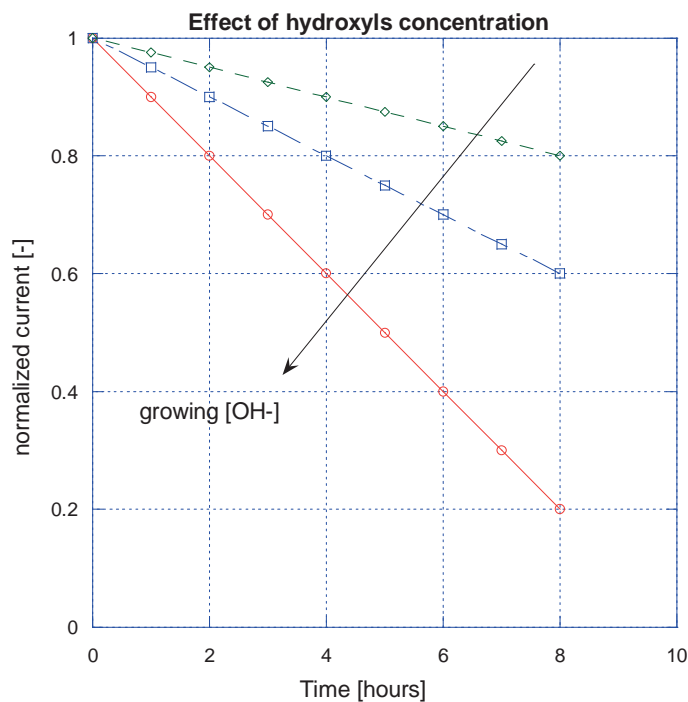


Figure 10.8: Effect of alkalinity and hydroxyls concentration on initial current slope during migration test.

Porosity level directly affects the level of the current but only marginally modifies much the onset of current increase (Figure 10.9).

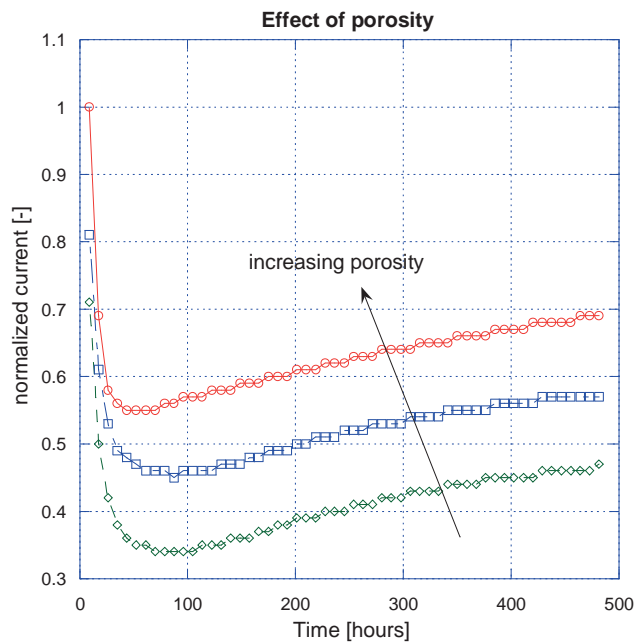


Figure 10.9: Effect of porosity on initial level of current during migration test

AFm initial content but also evolution during the test is the major unknown in the phase assemblage. It is also the parameter that affects the most the fit. By increasing AFm content chloride binding is increased and the time taken by chloride ions to diffuse through the sample can be significantly delayed (Figure 10.10).

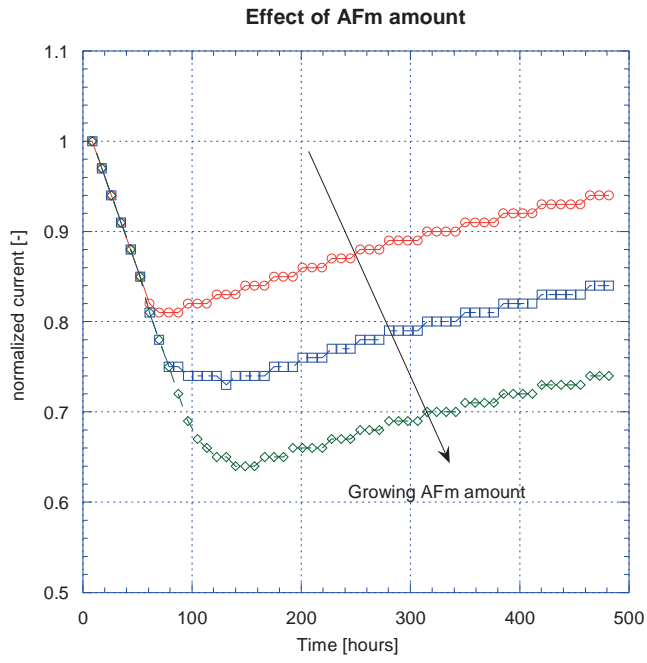


Figure 10.10: Effect of different AFm content on current evolution during migration test

10.3.1. ADDITIONAL FIGURES

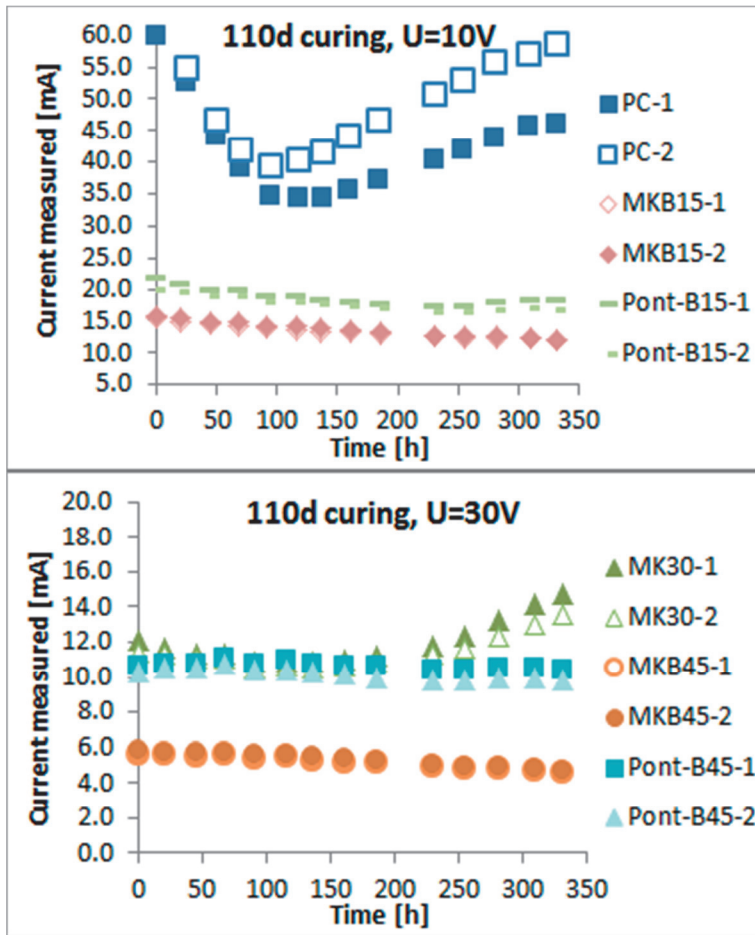
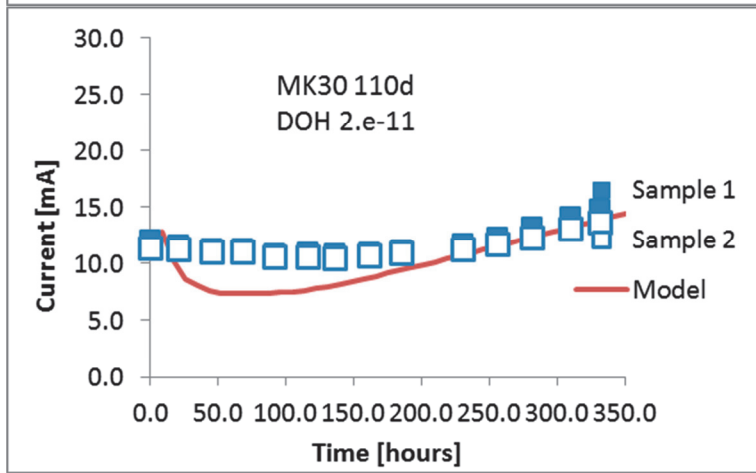
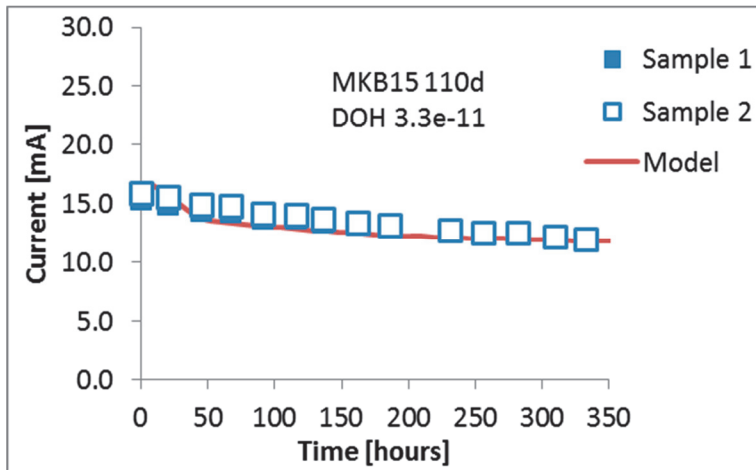


Figure 10.11: Current evolution monitored for series 2 and 110d curing during migration test



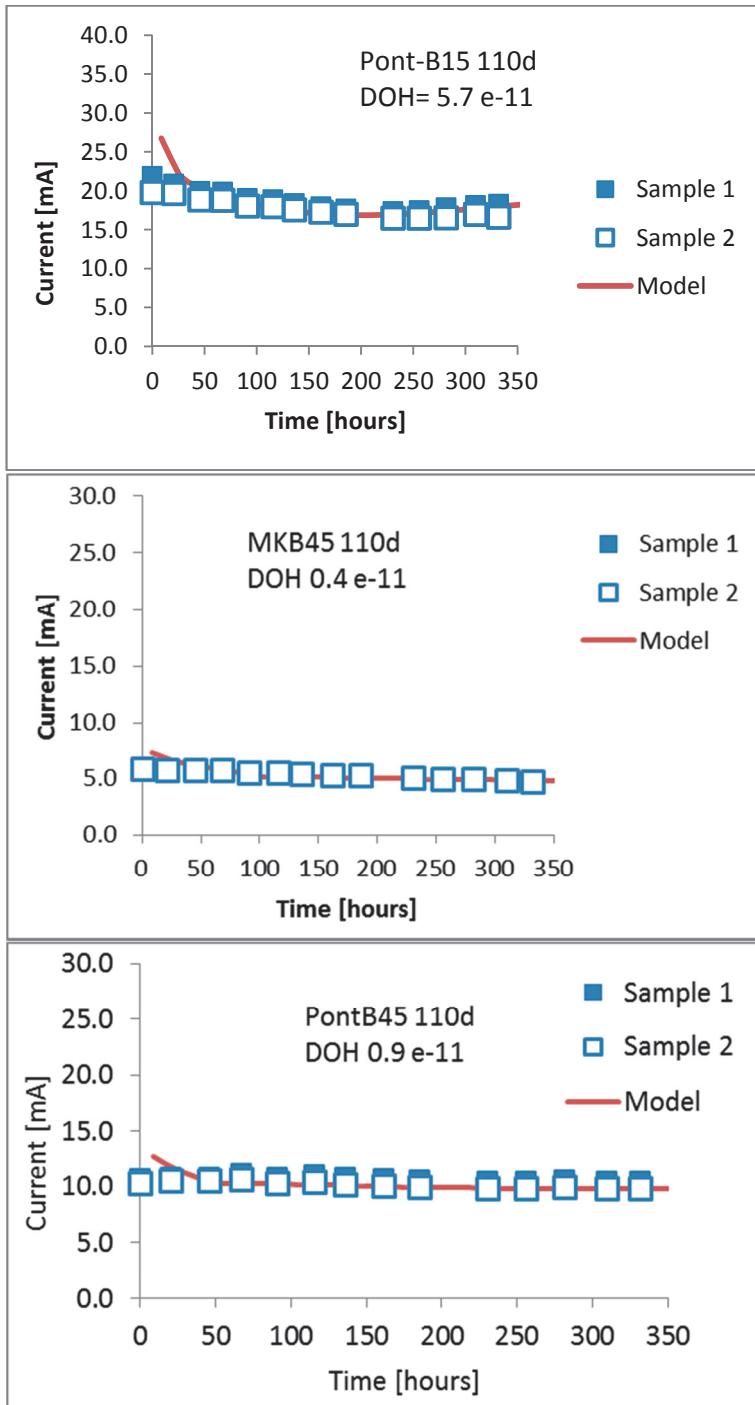


Figure 10.12: Current values with best model obtained by Stadium, migration tests at 110d

CURRICULUM VITAE

Antoni
Mathieu Georges
Rue de la Borde 27
CH- 1018 Lausanne Suisse
30 years old
++41 76 233 78 77
mathieu.antoni@gmail.com

- **EPFL Construction materials specialist**
- **PhD in cement chemistry and durability**
- **4 years experience in R & D**
- **Proficient in Fr/ Germ/Engl/ Spanish**

Education

2009-2013 **PhD:** Investigation of combined addition of calcined clays and limestone in **cement** – **Ecole Polytechnique Fédérale de Lausanne**

2000-2005 **Master** of Science in Material Science - **Ecole Polytechnique Fédérale de Lausanne**

1 year exchange at **ETH Zürich** (2003-2004)

Work experience

2005–2009 **Material Research & Development Engineer** in **Epcos, Deutschlandsberg, Austria**

-In charge of 3 different R&D Projects (**50 to 100 k€**) in the fields of Electronic Functional Ceramics. Domains investigated included: LTCC Materials & Product Development, Ferrite Cosintering, Ferroelectrics

-Development of a **new** LTCC dielectric material **compatible** with other existing LTCC materials, opening new perspectives and markets and reducing the **processing costs**

-Production troubleshooting for LTCC, resulting in improved production reliability and publication

Skills

General skills -Project Management

Technical skills

-Cement chemistry, Durability of construction materials, Blended cements,

-Electronic Microscopy, X-Ray Diffraction,

-Structural and Electronic ceramics

Computer skills

-MS-Office, Origin, Matlab, GEMS, PhreeqC, X'Pert Highscore

Academic Project

EPFL

-Development of a **novel** cementitious binder where up to 50% cement is replaced by combined addition of calcined clays and limestone. Natural inexpensive clays with average kaolinite content can be used.

-The potential benefit of this was a reduction by 32% of CO₂ emission per tonne of material for equivalent strength and improved durability.

-A trial (130 Tons) at **industrial scale** was carried out.

-Based on this work, a new project, funded by Swiss Development Cooperation Agency (4M CHF budget), was started to implement this technology at larger scale in India.

Publication

2012

Cement substitution by a combination of metakaolin and limestone, CCR 42 (2012) 1579-1589

Language skills

French

Native speaker

German

Proficiency level, C1 level (5 years in German speaking countries)

English

Proficiency level, C1 level

Spanish

Proficiency level, C1 level

Interests

-Plays national Swiss level Rugby for 10 years

-Training seven Austrian National Team (2 years) & Children in Rugby (4 years)

Personal information

Married

French citizen